AD-A103 556 MASSACHUSETTS INST OF TECH CAMBRIDGE DEPT OF CIVIL E--ETC F/G 8/13
CREEP BEHAVIOR OF FROZEN SAND.(U)
JUN 81 R T MARTIN, J M TING, C C LADD DAAG29-77-C-0016
UNCLASSIFIED R81-19 ARO-14725.3-GS NL

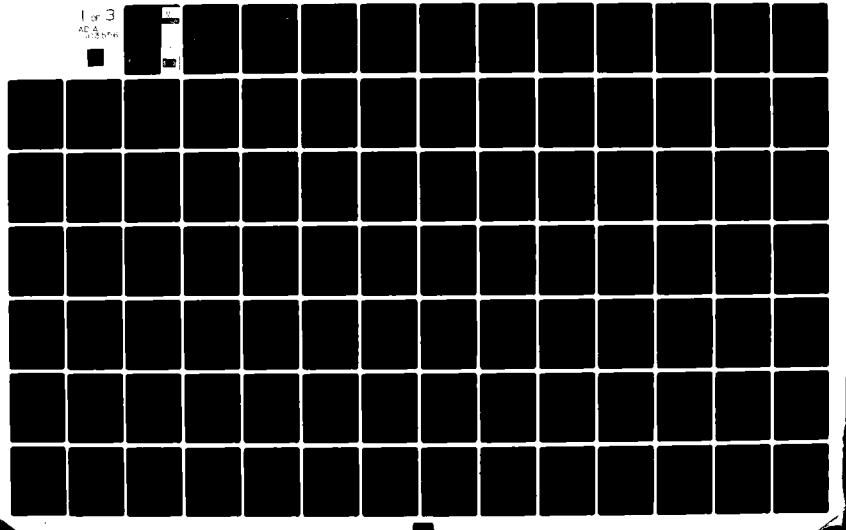

MIT

LEVEL III (12)

CREEP BEHAVIOR OF FROZEN SAND

FINAL REPORT PART I

by
R. Torrence Martin
John M. Ting
Charles C. Ladd

June 1981

DEPARTMENT
OF
CIVIL
ENGINEERING

SCHOOL OF ENGINEERING
MASSACHUSETTS INSTITUTE OF TECHNOLOGY
Cambridge, Massachusetts 02139

U.S. ARMY RESEARCH OFFICE
Contract Number
DAAG29-77-C-0016

Constructed Facilities Division
Geotechnical Order No. 703
Research Report No. R81-19

THE FINDINGS IN THIS REPORT ARE NOT TO BE CONSTRUED AS AN OFFICIAL DEPARTMENT OF THE ARMY POSITION, UNLESS SO DESIGNATED BY OTHER AUTHORIZED DOCUMENTS

(1) AD-A103 556 (11) 1 Nov 81 (12) 5.3-4 N

SECURITY CLASSIFICATION OF THIS PAGE (When Data Entered) - 1 -

REPORT DOCUMENTATION PAGE	READ INSTRUCTIONS BEFORE COMPLETING FORM
1. REPORT NUMBER (6)	2. GOVT ACCESSION NO. AD-A103556
3. RECIPIENT'S CATALOG NUMBER	
4. TITLE (and Subtitle) Creep Behavior of Frozen Sand	(9) 5. TYPE OF REPORT & PERIOD COVERED Final Report. (Part 1), Feb 1977 — Mar 1981
(4) 6. PERFORMING ORG. REPORT NUMBER R81-19	Order No. 703
7. AUTHOR(s) (10) R. Torrence Martin, John M. Ting, Charles C. Ladd	(15) 8. CONTRACT OR GRANT NUMBER(s) DAA G29-77-C-0016
9. PERFORMING ORGANIZATION NAME AND ADDRESS Massachusetts Institute of Technology, 77 Massachusetts Avenue, Cambridge, MA 02139	10. PROGRAM ELEMENT, PROJECT, TASK AREA & WORK UNIT NUMBERS (12)
11. CONTROLLING OFFICE NAME AND ADDRESS U.S. Army Research Office, P.O. Box 12211, Research Triangle, NC 27709	(11) 12. REPORT DATE Jun 1981
	13. NUMBER OF PAGES 237
14. MONITORING AGENCY NAME & ADDRESS(if different from Controlling Office)	15. SECURITY CLASS. (of this report) Unclassified
	15a. DECLASSIFICATION/DOWNGRADING SCHEDULE

16. DISTRIBUTION STATEMENT (of this Report)

Approved for public release; distribution unlimited

17. DISTRIBUTION STATEMENT (of the abstract entered in Block 20, if different from Report)

NA

18. SUPPLEMENTARY NOTES

The findings in this report are not to be construed as an official Department of the Army position, unless so designated by other authorized documents.

19. KEY WORDS (Continue on reverse side if necessary and identify by block number)

creep, creep tests, deformation, frozen sand, frozen soil, ice, shear strength, shear tests, rate process theory, temperature, unfrozen water

20. ABSTRACT (Continue on reverse side if necessary and identify by block number)

A total of 150 tests were run to evaluate the applicability of rate process theory, RPT, for frozen soil. Three creep test types: (1) constant load into tertiary creep, (2) temperature stage test under constant load, and (3) stress stage test under constant temperature were used to obtain the parameters in the RPT equation. The soil was Manchester Fine Sand, MFS, at ice saturation of 40 and 100% and a constant relative density

DD FORM 1 JAN 73 1473 EDITION OF 1 NOV 65 IS OBSOLETE

Unclassified

SECURITY CLASSIFICATION OF THIS PAGE (When Data Entered)

investigated over a temperature range -11 to -27°C with control of a given temperature to ± 0.02°C.

The creep data on frozen MFS show qualitative trends expected from RPT. Quantitative agreement with RPT was not very good because: (1) the free energy of activation was high, 320 to 480kJ $mol^{-1}°K^{-1}$, and (2) the cross-check on number of bonds $S_\alpha = S_\beta$ was very poor even where both S_α and S_β were for the same narrow temperature and stress range. Three possible explanations for the discrepancy are: (1) the creep of frozen MFS involves two or more mechanisms of approximately equal energy; (2) the basic RPT is wrong; (3) the assumption about X in order to obtain an operational equation from the basic theory has a flaw.

There was as much unfrozen water associated with the ice phase as there was associated with the soil phase based upon analysis of NMR data at different total water contents and temperatures.

ABSTRACT

A total of 150 tests were run to evaluate the applicability of rate process theory, RPT, for frozen soil. Three creep test types; (1) constant load into tertiary creep, 2) temperature stage test under constant load, and 3) stress stage test under constant temperature were used to obtain the parameters in the RPT equation. The soil was Manchester Fine Sand, MFS, at ice saturation of 40 and 100% and a constant relative density investigated over a temperature range -11 to -27°C with control of a given temperature to ± 0.02°C.

Plots of $\ell n \dot{\varepsilon}/T$ vs. 1/T were linear with negative slope as predicted by RPT. The coefficient of determination r^2 varied between 0.95 and 0.99 indicating reasonable agreement with RPT. For a given ice saturation and relative density the intercept term in the plots of $\ell n\ \dot{\varepsilon}/T$ vs. 1/T varied by a factor of 10^{60} which is not the constant implicit in the RPT equation for a given material. The experimental activation energy E was about the same whether obtained from the slope of $\ell n\ \dot{\varepsilon}/T$ vs. 1/T plot or from temperature stage test data. The plot of E vs. applied stress D at constant material had a negative slope as predicted by RPT. The r^2 for E vs. D plots were 0.86 and 0.91 for ice saturation of 40 and 100% respectively. The free energy of activation, ΔF which is the intercept term from the E vs. D plot was 480kJ $mole^{-1} \cdot K^{-1}$ for S_i = 40% and 320kJ $mol^{-1} \cdot K^{-1}$ for S_i = 100%.

The number of bonds S was obtained in two ways from the RPT equation. From the slope of E vs. D the number of bonds S_β was calculated. The quantity $\partial \ell n \dot{\varepsilon}/\partial D$ from stress stage test data permitted calculation of the number of bonds S_α . Mean value of S_α was a factor of ten larger than S_β for the same narrow temperature and stress range. There was a strong stress dependance to $S_\alpha (r^2=0.95)$ for saturated Manchester Fine Sand which does not agree with RPT. The calculated parameters in the RPT equation were essentially the same on a given material whether evaluated at the time of minimum creep rate or at 1/4 the time to minimum.

The creep data on frozen MFS show qualitative trends expected from RPT. Quantitative agreement with RPT was not very good because 1) the free energy of activation was high 320 to 480kJ $mol^{-1} \cdot K^{-1}$, and 2) the cross-check on number of bonds $S_\alpha = S_\beta$ was very poor even where both S_α and S_β were for the same narrow temperature and stress range. Three possible explanations for the discrepancy are: 1) the creep of frozen MFS involves two or more mechanisms of approximately equal energy; 2) the basic RPT is wrong; 3) the assumption about X in order to obtain an operational equation from the basic theory has a flaw.

Other significant observations based upon the data obtained from frozen MFS were:

1) The strain at minimum strain rate was essentially constant independent of temperature and stress.
2) The so-called "secondary strain rate" was in reality an inflection point in the strain rate-time plot.
3) There was a unique relation between the minimum strain rate and the time to reach that minimum for a given material. It was found that the time to reach minimum strain rate could be predicted to within a factor of three times the observed time to minima.

There was as much unfrozen water associated with the ice phase as there was associated with the soil phased based upon analysis of NMR data at different total water contents and temperatures.

CREEP BEHAVIOR OF FROZEN SAND

LIST OF FIGURES

LIST OF TABLES

LIST OF SYMBOLS

Symbols commonly used throughout this report are listed below:

Rate Process Theory:

h = Planck constant, 6.62×10^{34} joule-sec

k = Boltzmann constant, 1.38×10^{23} joule molecule^{-1}°K^{-1}

R = Molar gas constant, 8.3136 joule mol^{-1}°K^{-1}

N = Avagadro's number, 6.03×10^{23} molecules/mol^{-1}

T = Temperature, °K

θ = Temperature below 0°C(273.15°K), °C

f = Force on a flow unit

τ = Applied shear stress

D = (for σ_3=0) Deviator stress, MPa

$D_u=\sigma_i$ = Ultimate or instantaneous strength = maximum deviator stress at $\dot{\varepsilon} = 0.02 sec^{-1}$

λ = Jump distance, minimum value equals diameter of an oxygen atom 2.8×10^{-10}m.

X = Dimensionless quantity proportional to the combination of successive barrier crossings and λ such that $\dot{\varepsilon} = X(\underset{\rightarrow}{\nu}-\underset{\leftarrow}{\nu})$; i.e. an assumption to make RPT equation operational for experimental testing.

ΔF = Free energy of activation needed to cross over the energy barrier, kJ mol^{-1}°K^{-1}

E = Experimental activation energy = $\Delta F-(\lambda N/4S_\beta)D$, kJ mol^{-1}°K^{-1}

S = Number of bonds per m^2

Rate Process Theory (continued)

S_α = Number of bonds determined from stress dependance

S_β = Number of bonds determined from temperature dependance

$\beta = \lambda N/4S_\beta = \partial E/\partial D$, $m^3 mol^{-1}$

$\alpha = \lambda N/4S_\alpha RT = \partial \ell n \dot{\varepsilon}/\partial D$, $(MPa)^{-1}$

V_f = Volume of a flow unit = λ/S, m^3

Strain:

ε = Strain = change in length ÷ initial length, dimensionless; generally given as % of initial length

$\dot{\varepsilon}$ = Strain rate = $\partial\varepsilon/\partial t$, sec^{-1}

$\dot{\varepsilon}_m$ = Minimum strain rate during complete creep, $\partial\dot{\varepsilon}/\partial t = 0$, sec^{-1}

ε_m = Strain at minimum strain rate

t = Time, min

t_m = Time to reach minimum strain rate, min

m = $-\partial \ell n \dot{\varepsilon}/\partial \ell nt$, a constant in Singh-Mitchell creep model

$(\dot{\varepsilon}_{fit}/\dot{\varepsilon}_{act})_m$ = Ratio of fitted to actual strain rate at minimum strain rate

$(\dot{\varepsilon}_{pred}/\dot{\varepsilon}_{act})_m$ = Ratio of predicted to actual strain rate at minimum strain rate

Water Content:

w = Water content, g water/g dry soil usually expressed as percent

w_u = Unfrozen water content, g liquid water/g dry soil

S_i = Ice saturation, calculated from degree of pore voids filled with water times the specific volume of ice (1.093) expressed as percent.

General:

D_r = Relative density = $(\gamma_{max}/\gamma)(\gamma-\gamma_{min}/\gamma-_{max}\gamma_{min})$

γ = compacted dry density

γ_{max} = maximum achievable compacted dry density

γ_{min} = minimum achievable compacted dry density

$\bar{x}$ = Mean value of parameter x = $\Sigma x/n$

SD = Standard deviation = $\left[1/_{(n-1)} \ \Sigma(x_i-\bar{x})^2\right]^{1/2}$

CV = Coefficient of variation = $(SD/\bar{x})100$

r^2 = Coefficient of determination

I. INTRODUCTION

A. Background

The highly time and temperature dependent nature of the stress-strain-strength behavior of frozen soil has always posed great difficulties to engineers responsible for the design of facilities constructed in and/or on frozen ground. Oil exploration in cold regions and construction of the Alaskan pipeline attracted worldwide attention to this problem, along with greatly expanded research into the mechanical properties of both ice and frozen soil. Most of this research, of necessity, focused on development of empirical solutions to immediate engineering problems, with much less effort devoted to investigations of fundamental behavior.

The properties of frozen ground are also extremely complex compared to other construction materials such as steel and concrete, or even unfrozen soil, which have been extensively studied for a much longer time span. Hence very little data exist about the many factors that affect the mechanical behavior of frozen soil compared to other materials.

Results of "conventional" triaxial compression strength tests run on frozen and unfrozen soil show very different behavioral trends. For "drained" loading, the unfrozen strength increases more or less linearly with confining stress and is essentially unaffected by changes in temperature and strain rate and its behavior can be more or less uniquely

explained in terms of the effective stress principle, i.e. as a function of effective stress ($\bar{\sigma}$) = total stress (σ) minus pore water pressure (u). In contrast, the strength of frozen soil is highly temperature and strain rate dependent and varies in a complex fashion with changes in confining stress. It is difficult to explain this behavior due to lack of information concerning the mechanical properties of the pore ice, the magnitude of effective stress acting on the soil skeleton and the interaction between these two components. The same problems arise with interpreting and understanding data obtained from "creep tests", e.g. strain versus time under constant load conditions.

Finally, a wealth of data exist about the behavior of unfrozen soil as a function of soil type, its density and/or stress history, etc. such that significant progress has been made in developing constitutive relationships which can be used with some confidence to predict strength-deformation characteristics for various loading and drainage conditions. To develop a comparable knowledge for frozen soils, much further research is needed, both concerning basic behavioral trends and an understanding of the physical mechanisms controlling time dependent strength-deformation characteristics. In essence, the current state of knowledge about the mechanics of frozen soil is comparable to that which existed in soil mechanics about 30 years ago.

B. Scope and Objectives

The Army Research Office (ARO) initiated a three year research contract with the Massachusetts Institute of Technology (MIT) in February 1977 entitled "Mechanical Properties of Frozen Soil". The general objective of this cooperative research effort with the Cold Regions Research And Engineering Laboratory (CRREL) was to develop an improved understanding of the fundamentals governing the strength-deformation characteristics of frozen soils, with particular emphasis on creep behavior. Variations in basic parameters obtained from analysis of creep data in terms of RPT would then be used to infer the significance of the "structure" of the frozen soil. Finally, the research would attempt to measure certain components of structure, such as "pore water pressures" and the "fabric" of the solid phases (soil and ice) and the pores (unfrozen water associated with soil and with ice).

Based on a review and synthesis of the literature and available experimental data regarding the creep behavior of ice and frozen soil made during the first few months of the contract, MIT concluded that:

(1) The mechanical behavior of ice was poorly understood, at least compared to that of unfrozen saturated soils;

(2) The precise structure of ice had a significant, but ill-defined, effect on creep behavior and therefore had to be carefully controlled in any experimental program involving creep testing of frozen soil;

(3) Essentially all creep data on frozen soils were too limited and/or poorly controlled to enable a systematic analysis via Rate Process Theory.

Consequently, considerable effort was then devoted to a thorougn and carefully controlled experimental investigation of the creep and strength characteristics of frozen Manchester Fine Sand at varying temperature and ice saturation in cooperation with CRREL. This work eventually led to a comprehensive evaluation of Rate Process Theory, one of the principal research objectives, but pushed aside any attempts to measure components of the "structure" of frozen soil as originally planned (other than measurements of the amount of unfrozen water present in frozen soil).

Another change in the original scope and objectives occurred with the decision to conduct a very detailed synthesis and evaluation of theories and experiments reported in the

literature regarding the strength and creep properties of both ice and frozen soil. This effort, combined with a special creep testing program on glass beads, lead to new insights regarding the principal mechanisms controlling the time-dependent strength-deformation characteristics of frozen soil and improved capabilities for modelling creep behavior. It also caused a one year extension of the original three year contract.

Finally, at the request of CRREL, the project supported a laboratory study of the relationship between acoustic energy emission and the creep behavior of frozen sand. Results from this research, performed at CRREL under its supervision, are not contained in the MIT reports listed in Section D.

C. Staff and Facilities

Dr. R. Torrence Martin, Senior Research Associate and Dr. Charles C. Ladd, Professor of Civil Engineering, served as co-principal investigators throughout the four year project. Both are members of the Constructed Facilities Division in MIT's Department of Civil Engineering. Dr. Martin spent a major portion of his time during the first three years working at CRREL, which provided the physical facilities used for testing frozen soil and ice along with substantial support personnel. Dr. Martin developed the creep testing equipment, supervised the experimental program and analyzed the results in terms of Rate Processs Theory. Dr. Ladd administered

the contract, provided technical assistance and supervised parallel experimental work on unfrozen soil conducted in the Geotechnical Laboratory at MIT.

Mr. John M. Ting worked on the project for three and one-half years as a Graduate Research Assistant, dividing his time about equally between CRREL and MIT. He assisted Dr. Martin with the strength and creep testing of frozen Manchester Fine Sand (MFS), conducted a special test program on frozen glass beads and took major responsibility for evaluation of the literature. This work, which served as his doctoral thesis, led to a better understanding of the physical mechanisms controlling the behavior of frozen soil and improved modelling capabilities. Mr. Ting will receive his Ph.D. degree in June 1981.

Mr. Vincent J. Perrone developed the procedures used to prepare uniform samples of MFS and established its unfrozen strength-deformation characteristics. This work, partially funded by CRREL, was conducted at MIT and served as Mr. Perrone's S.M. thesis (degree awarded June 1978). Dr. Suzanne M. Lacasse, Lecturer in Civil Engineering at MIT, helped extend these techniques to obtain uniform frozen samples of MFS. Finally, Mr. Anatole Fish served as a Research Engineer in Civil Engineering at MIT for about 30 months in order to perform research at CRREL on the acoustic energy emission characteristics of frozen sand and to assist CRREL with some of its other projects.

It should be emphasized that CREEL provided substantial assistance throughout this research project in the form of physical facilities, funds and support personnel. It was truly a cooperative venture with very close technical interaction between CRREL and MIT staff at all levels. In addition, numerous seminars presented by Dr. Martin and Mr. Ting at both CRREL and MIT served as an excellent vehicle for disseminating information and facilitating interaction during the course of the research.

D. Publications and Reports

In addition to the usual Progress Reports submitted semi-annually to ARO, the project resulted in the following publications and technical reports:

(1) Perrone, V.J. (1977), "Strength-Deformation Characteristics of Unfrozen Manchester Fine Sand", Report submitted to CRREL under P.O. No. DAC89-78-0164.

(2) Ting, J.M. and Martin, R.T. (1979), "Application of the Andrade Equation to Creep Data for Ice and Frozen Soil", Cold Regions Science and Technology, Vol. 1, pp. 29-36.

(3) Martin, R.T., Sayles, F.H. and Ting, J.M. (1980), "MIT Creep Data on Manchester Fine Sand", CRREL-IR627 (internal report containing computerized data).

(4) Ting, J.M. (1981a), "The Creep of Frozen Sands: Qualitative and Quantitative Models", Research

Report R81-5, Order No. 692, Department of Civil Engineering, M.I.T., 4 p. (Also Sc.D. thesis).

(5) Ting, J.M. (1981b), "The Mechanics of Frozen Soil: A Review", CRREL Report

(6) Martin, R.T., Ting, J.M. and Ladd, C.C. (1981), "Creep Behavior of Frozen Sand", Research Report R81-19, No. 703, Department of Civil Engineering, M.I.T., 237 p. (This report).

E. Acknowledgements

Dr. Steven J. Mock, Geologist in the ARO Geosciences Division at Research Triangle Park, N.C., who served as technical monitor, was most understanding during the early stages of the project when its scope and objectives were being changed and cooperative in extending the contract for an additional year.

The authors are also deeply indebted to CRREL for its generous support in terms of funding, use of facilities and support staff. We particularly appreciated the cooperation of Fred Crory, Dr. Dean Fretag, William Quinn, Dr. Kay Sterritt and Al Waori. We also benefited greatly from the scientific interaction with Dr. Andrew Assur, Ron Atkins, Edwin Chamberlain, David Cole, Dr. Sam Colbeck, Dr. Don Haynes, Austin Kovacs, Richard McGraw, Dr. Malcolm Mellor, Dr. Donald Nevel, Frank Sayles, Dr. William St. Lawrence and Al Tice. Lastly, but definately not least importantly, we

wish to acknowledge the especially generous technical assistance provided by David Carbee, David Cole, Gary DeKoff, Greg Fellars, Frank Sayles and Al Tice.

II. BACKGROUND

A. Review of the Mechanics of Frozen Soil

A very extensive review of the mechanics of frozen soil, too voluminous and detailed for presentation herein, will be published as a CRREL Report (Ting 1981b). This section presents a synthesis of that literature review.

The aspects of mechanical behavior which constitute the bulk of engineering interest in frozen soils are strength and deformation under load. Due to the complexity in defining a generalized stress-strength-deformation-time temperature model, an arbitrary division is usually made between strength and deformation models. These include various models of instantaneous and long-term strength and elastic, pseudo-elastic and creep deformation models.

Traditional methods of analyzing the mechanics of frozen soil have focused on qualitative (descriptive), empirical (macro-analytical), and micro-mechanistic approaches. Each approach has its own advantages and disadvantages.

Various qualitative mechanistic explanations for the behavior of frozen soil have been proposed, notably by Vyalov (1973), Sayles (1968, 1974), Goughnour and Andersland (1968) and Chamberlain et al. (1972). These explanations aid greatly in the understanding of the mechanics of frozen soil, but are of little help in quantifying its strength-deformation behavior. Also, owing to the immense complexity of the

problem, these studies have generally tended to be less than completely thorough in describing the various mechanisms of strength and deformation of frozen soil.

Consequently, the empirical approach is by far the most popular one for frozen soils. Various quantitative models have been proposed, for example, by Vyalov (1959, 1962, 1963), Ladanyi (1972), Goughnour and Andersland (1968) and Sayles (1968, 1973). The advantages of these models involve their relative mathematical simplicity and the fact that the number of experimental parameters required are few and usually easy to determine. However, since the models are often formulated for a specific situation and soil, they are not generally applicable to other loading situations or soils. Usually, the problem is oversimplified, and important behavior is overlooked in the model. Most importantly, these models have little theoretical basis; consequently, it is difficult to understand what is actually happening within the frozen soil system using these models.

Quantitative mechanistic models, needless to say, are extremely difficult to formulate and generally have limited engineering value at the present time. Rate Process Theory (RPT) is a model which is based on statistical mechanics and has been applied with success in pure chemical systems. This model is considered to be a mechanistic model in that its parameters may be interpreted to have fundamental

physical significance. However, due to the complexity of the frozen soil system, the RPT model cannot adequately describe the actual mechanisms of strength and deformation in the frozen soil. Consequently, use of the RPT for frozen soil is really pseudo-mechanistic in nature. For soil and frozen soil systems, the physical significance of the model parameters remain unclear and attempts to apply this theory to soil, ice and frozen soil systems have met with varying degrees of success (Mitchell et al., 1968; Andersland and Al-Nouri, 1970; Andersland and Douglas, 1970).

The thrust of this research project has been an evaluation of the validity of RPT as a tentative working hypothesis for modelling the creep behavior of frozen soil.

This section first presents the nature and structure of frozen soil. Then, the various qualitative and empirical models for the mechanics of frozen soil are described. The bulk of the report presents the results of the evaluation of RPT as a working model for frozen soil.

1. Nature and Structure of Frozen Soil

Frozen soil is a complex multiphase system consisting of soil, ice, unfrozen water and air. In order to understand the nature and structure of the frozen soil system, it is necessary to understand the nature of unfrozen soil, ice, adsorbed water, and the nature of ice nucleation, growth and interaction with silicaceous particles. Pertinent facts

concerning each of these topics are presented and discussed in the following paragraphs.

The physico-chemical effective stress equation describes the various components of stress believed to act in unfrozen soil systems. As can be seen from Fig. II-1, the average effective (intergranular) stress, equal to the total stress minus the pore water pressure, may be expressed as the sum of contact stresses and double layer stresses. For coarse grained soils, the mass (contact) forces dominate and the surface (double layer) forces are negligible. For clays, however, the surface forces can control, or at least strongly influence, overall mechanical behavior.

For coarse grained soils under an applied load, grain to grain contact is assured due to the high contact stresses present. These contact stresses may be sufficient to crush quartz particles. For all but ideally dispersed clays, solid particle to particle contacts probably exist. Data by Hofmann (1952) on freeze-dried clay gels and indirect data by Mitchell et al. (1968) support this hypothesis.

The structure and location of the ice in frozen soil depend on many factors. These include the initial water content, soil permeability, freezing rate, freezing temperature, soil pore and grain size distributions, and initial water table location. The ice in frozen soil is polycrystalline (Gow 1975) and is probably limited in maximum

grain size by the pore size. Air bubbles and voids may exist within the ice and possibly between ice grains.

It has been shown that water is very strongly adsorbed by silicate particles. It requires in excess of 400MPa to squeeze the last molecular layer of adsorbed water away from a clay surface (Steinfink and Gebhart 1962, van Olphen 1963). The adsorbed water in unfrozen and frozen soils is continuous, completely surrounds the mineral surfaces, and is probably fairly mobile parallel to the mineral surfaces. The adsorbed water does not behave like bulk water, and is capable of significant freezing point depression. While the exact nature of this film is not clear, it probably exhibits Newtonian viscous flow parallel to the mineral surface (Mitchell, 1976).

Unfrozen water is also present in ice at least down to -25°C in a vapor saturated environment. This transitional water is probably located on the exterior ice surface and at the grain boundaries.

Based on these observations concerning soil, ice and adsorbed water, a structure for a frozen sand system may be postulated (Ting, 1981a). This is shown in Fig. II-2 and corresponds to a "fused" system according to the classification of Tsytovich (1975). Of interest are the following points:

(1) Effective solid contacts exist between soil grains;

(2) Probably no direct soil/ice contact exists;

(3) Unfrozen water exists at the soil/ice interface and at the ice grain boundaries.

For finer grained soil systems, no significant differences are anticipated from this soil model other than finer ice grains. However, when segregation freezing occurs, a significantly altered soil structure with horizontal ice lenses may result.

2. Mechanics of Ice and Unfrozen Soil

Ice Ih is a solid with a hexagonal crystallography. The crystal structure is distinctly planar, with water molecules forming puckered sheets consisting of hexagonal rings. The plane of the sheets is termed the basal plane, and the axis normal to the basal plane is the c-axis. Slip occurs most readily along the basal plane, and is called basal or easy glide. Slip not along these planes is termed nonbasal or hard slide, and can be induced only at stresses greater than ten times that required for easy glide (Higashi, 1969), One such nonbasal mechanism is dislocation climb, in which a line defect climbs from one glide plane to the next. However, it has been shown that when attempts are made to induce slip in nonbasal directions, the ice often fractures before slip can occur (Gold, 1962 and 1966, Weeks and Assur, 1969).

Ice exists in nature in polycrystalline form. One common form is granular, or snow, ice, which consists of approximately equidimensional ice grains. Mechanically, snow ice behaves isotropically, due to the random orientation of the individual ice grains.

A variety of deformational mechanisms exist for polycrystalline ice. The relative importance of each one depends upon the applied stress or strain rate, temperature and ice structure. These mechanisms may be loosely grouped into the following categories:

(1) Microcreep (movement of defects). At low temperatures, stress and strain rates, the movement of point and line defects are important mechanisms of deformation. These mechanisms include the diffusion of point vacancies and defects, and the dislocation of line defects along basal and nonbasal directions. These mechanisms dominate below about -10°C and 0.50MPa (Shoji and Higashi, 1978). At higher temperatures and stresses, these mechanisms are probably still present, but not as rate controlling processes.

(2) Microcracking. At stresses and strain rates slightly above those causing (1), microcracking can occur. This cracking occurs at dislocation pileups at the grain boundaries and stress concentrations within the crystal due to defects or impurities. This mechanism is essentially a brittle phenomenon, but can result in an overall mechanical behavior

which is ductile in appearance. This mechanism is considered to be the primary deformational mechanism in ice, and may be detected by its accompanying acoustical emissions.

(3) Grain boundary mechanisms. These include grain boundary sliding, formation of unfrozen water at the boundaries, grain boundary migration and growth, and pressure melting and surface regelation. In the region above -10°C, Barnes et al. (1971) suggest that the first four grain boundary mechanisms may occur. Above -3°C, pressure melting and surface regelation are also present at the grain boundaries.

Based on data from various sources, it is possible to construct deformational mechanism maps for a given ice type as a function of stress level, temperature and strain rate. Such a map is shown in Fig. II-3, as constructed by Goodman (1977) for polycrystalline ice.

For unfrozen soil, mechanisms of strength and deformation exist which are not normally encountered in continuous materials, due to its particulate nature. Some of these mechanisms involve: elastic deformations, both axially and flexurally; particle crushing at the contacts; sliding and rolling at the contacts; changes in interparticle spacings; and particle rearrangement and reorientation. Some of these mechanisms are reversible, such as the elastic deformations and the changes in spacing, while the others are not. Consequently, an altered structure results from shearing which can greatly affect future behavior.

Rowe (1962) proposed that the strength of a dry cohesionless particulate material consists of three basic components. Using the Mohr-Coulomb failure criterion,

$$\tau_{ff} = c + \sigma_f \tan\phi \qquad \text{(II-1)}$$

where τ_{ff} = shear stress at failure on the failure plane

σ_{ff} = normal stress at failure on the failure plane

ϕ = friction angle

c = apparent cohesion, equal to zero for cohesionless sands.

Rowe postulated that the total frictional resistance as measured in triaxial tests is composed of the following:

(1) Interparticle friction. This forms the bulk of the resistance, and is due to particle sliding friction at the contacts. It has since been proposed by Skinner (1969) that rolling friction should also be included within this category;

(2) Dilation effect. For soils which exhibit dilation, i.e. increased volume behavior during shear, such as dense sands and overconsolidated clays, additional work must be expended due to the expansion of the sample against its confining stress;

(3) Particle interference and reorientation. This occurs under all conditions except with very dense sands at small strains.

The three components of strength are shown in Fig. II-4 as a function of density. Quantitatively, Rowe presents:

$$\left(\frac{\sigma_1}{\sigma_3}\right)_{max} = \left(1 + \frac{dv}{d\varepsilon}\right) \tan^2\left(45 + \frac{\phi_f}{2}\right) = \frac{1+\sin\phi}{1-\sin\phi} \qquad \text{(II-2)}$$

where $\phi_u = \phi_{frictional}$

$\phi_f = \phi_u$ for very dense conditions

$\phi_f = \phi_{cv}$ for very loose conditions

$\frac{dv}{d\varepsilon}$ = rate of volume change with respect to strain.

When water is present, the mechanisms of strength as presented by Rowe are still applicable, provided the loading is drained, i.e. no excess pore water pressure develops during shear, and the stresses are expressed in terms of the effective stresses $\sigma' = \sigma - u$. With these constraints, equation (II-2) has been used by several workers to describe the drained strength of sands (e.g. Lee and Seed, 1967).

The effective stress principle and the Mohr-Coulomb failure criterion predict that additional strength will be generated in "wet" soils by the presence of negative pore water pressure. When a negative pore water pressure exists in soil, a positive effective (intergranular) stress results, even when the applied total stress is zero. This may occur due to capillarity (e.g. due to drying of the external soil surfaces) or due to dilation of the pore spaces during

undrained shear. Regardless, an "apparent cohesion" results. For example, moist beach sand exhibits some strength at zero total confining stress.

For fine-grained soils, slow shearing rates are required to prevent the generation of excess pore pressures due to the low permeability of clays and silts. When drained conditions prevail, the concepts presented in the previous paragraphs still apply, provided the stresses are expressed in terms of the effective stresses. However, additional strength can be generated due to "true cohesion" caused by physical cementation and/or the existence of net interparticle attractive stresses (e.g. A > R or $\sigma''_a > \sigma''_r$ in Fig. II-1). Also, the magnitude of the capillary tension that can be generated in clays and silts is far greater than in sands. Consequently, the magnitude of the apparent cohesion may be far greater in fine-grained soils than in sands.

For undrained loading, excess pore pressures develop during shear. This may occur in sands when drainage is not permitted, or in silts and clays due to their low permeability relative to usual rates of loading. The overall mechanical behavior of an undrained sample differs from a similarly loaded drained sample depending upon the magnitude of the excess pore pressures developed during shear. Thus, while the same basic mechanisms control deformation and strength in both cases, the resultant stress-strain-strength

characteristics vary due to differences in effective stress acting in the drained and undrained cases.

3. Qualitative Models for Frozen Soils

Various qualitative models have been advanced to provide mechanistic explanations for the strength and deformational behavior of frozen soils. Basically, frozen soil is a multi-phase composite material which exhibits considerable "short term" strength, generally several times stronger than conventionally tested ice and up to an order of magnitude stronger than unfrozen soil under the same testing conditions.

Frozen soil possesses a component of strength which is dependent upon the confining stress level ("frictional strength") and one which is independent of confining stress ("cohesive strength"). The "cohesive" component of strength in frozen soil is an order of magnitude larger than in unfrozen soil, and is of the same order of magnitude as that for polycrystalline ice alone. Frozen soil strength decreases with increasing time to failure, or decreasing applied strain rate. Typical strength data from unconfined (uniaxial) testing of frozen soil and ice, plotted in Fig. II-5, demonstrate its large time dependence. Analogously, frozen soils exhibit considerable time-dependent (creep) deformation under a fixed load. In addition, frozen soil behavior is very temperature sensitive. Other factors which influence the mechanical behavior include compositional factors, such as the degree of

ice saturation, soil type, and relative density of the soil.

Any valid qualitative model for frozen soil should encompass all aspects of frozen soil behavior. Specifically, it must address the question of why frozen soil is so strong relative to its components, ice and soil, and explain its stress, temperature, strain rate, time and compositional dependencies.

Sayles (1968) proposes that the strength of frozen soils depends upon the cohesion and internal friction of the component materials. The "ice cohesion" depends on the amount of ice, strength of the ice, and area of contact between the ice and soil, each of which depends on temperature. The internal friction is due primarily to the soil component, and is a function of the grain size, distribution, shape and arrangement. The "ice cohesion" is considered by Sayles to be the dominant strength factor in frozen soils, although internal friction is important in dense sands. Although not explicitly mentioned by Sayles, the magnitude of the intergranular stress between the soil particles is also important in determining the frictional component of strength of the frozen soil system.

Data by Sayles (1974) indicate that two peaks exist in the stress-strain curves of frozen soils at low confining stress levels. The first peak appears to correspond to a yielding within the ice matrix, while the second corresponds to mobilization of the internal friction. For larger confining

stress levels, the first peak disappears. This behavior would tend to confirm the concept of "cohesion" and "friction" components of strength. However, it does not completely clarify the nature of the "cohesive" or "frictional" components of strength, nor the nature of the interaction between the ice and soil.

According to Vyalov (1963), the cohesive component consists of: (1) intermolecular solid/solid attraction, (2) "structural" cohesion, and (3) ice cementation. Note that even though it is now known that the soil particles are completely surrounded by unfrozen water, ice/soil cementation is considered to exist. The existence of substantial ice cementation is confirmed, for example, by the adhesional experiments of Jellinek (1957, 1960, 1962). However, the exact nature of the "structural" cohesion is not specified.

Vyalov (1963) postulated the following schematic model for frozen soils: as an external load is applied to a frozen soil sample, stress concentrations exist at the contact points, resulting in plastic flow and pressure melting of the ice. The melted water migrates to zones of lower stress and refreezes. Simultaneously, structural and ice cementation bonds in weak locations yield and mineral particles slip. This is accompanied by ice crystal reorientations and mineral rearrangements and reorientations. The ice reorientations tend to weaken the system, as the crystals tend to realign

with their basal planes in the direction of slip. Soil rearrangements may serve to weaken or strengthen the system. Vyalov proposed that when the strengthening of the system exceeds the weakening during loading, damped creep behavior results.

Chamberlain et al. (1972) postulated that the triaxial compressive behavior of frozen soil is controlled by interparticle interlocking and friction, the unfrozen water content, pressure melting of the ice, and the ice/water phase change. By carrying out triaxial tests to very high levels of confining stress on sand and silt, Chamberlain et al. observed the behavior indicated in Fig. II-6. For both soils, three distinct zones were identified. In the low confining stress range, increasing strength is observed for the sand and essentially constant strength is observed for the nondilatant silt. In the intermediate stress range, strength decreases with increasing confining stress. Above about 110MPa, a complete phase change from ice to water is observed, and strength again increases with increasing confining stress. According to Chamberlain et al., the strength of the sand in Zone I is due to interparticle friction and interlocking. For the silt in this region, Chamberlain et al. postulate that the unfrozen water films surrounding the soil particles obscure the interparticle friction of the system, resulting in an essentially constant

strength. In the intermediate stress region, local pressure melting due to stress concentrations causes a decrease in the observed strength of the frozen soil systems. In Zone III, global pressure melting of the ice matrix results in essentially high-pressure triaxial testing of unfrozen soil. The observed strengths are essentially undrained shear strengths and therefore should be relatively unaffected by the confining stress level for Skempton's "B" parameter near unity.

Goughnour and Andersland (1968) carried out a sequence of unconfined and triaxial compression tests on ice with varying concentrations of Ottawa 20-30 sand. For a given strain rate and temperature, a slight increase in strength was observed with increasing sand concentration over that for pure ice. Above a critical sand concentration, 42% by volume in the case of Ottawa sand, a marked increase in strength was observed. This considerable strength increase is attributed to interparticle friction and dilatancy of the sand at the higher sand concentrations. This behavior is shown in Fig. II-7.

Goughnour and Andersland propose that the strengthening of sand-ice systems over pure ice may be due to three mechanisms. For the lower sand concentrations, deformation occurs primarily in the ice matrix. No continuous soil skeleton exists in this range, and all of the load must be carried by the ice. Since sand is much less deformable than ice, a larger deformation

rate is imposed upon the ice with increasing sand concentration. Since ice strength is very strain-rate sensitive, as indicated by Fig. II-5, an increase in strength is observed. This mechanism is mobilized in all strains, and depends only on the sand volume concentration. However, once a continuous sand skeleton is established at the higher sand concentrations, load is primarily carried by the sand. Consequently, this mechanism is probably not a significant factor at the higher sand concentrations.

The second mechanism is the result of interparticle friction at the contacts between sand particles. Goughnour and Andersland consider this mechanism to be function of the frictional characteristics of the solid material, "degree of suspension of the solids", and normal stress at the interparticle contacts.

The third mechanism is concerned with the sample volume change. Dilatancy of the sand structure during shear is impeded by the ice matrix. Adhesion between the sand particles and ice matrix may create an effect analogous to higher effective stress in unfrozen soil, and give high values of cohesion to the sand-ice mass. The strength increase due to dilatancy continues to increase until volume increase ceases, or until the limiting strength of the ice is exceeded.

This review has thus far presented the data and qualitative models which are available in the literature. The explanations

described here have been largely those of the individual researchers. However, a complete qualitative model for frozen soil behavior is not yet available.

By considering the various mechanisms of strength and deformation possible, it is hoped that a positive step can be made towards such a comprehensive model. Many of the mechanisms have been previously described; however, others are possible which have not been actively considered. Some of these are described in the following paragraphs.

The ice in frozen soil is probably significantly different from ice which is normally found in granular ice. While the granular or columnar grained polycrystalline ice normally tested in ice mechanics is on the order of 1mm in diameter, the ice in frozen soil is of necessity much finer. The grain size of ice in soils is constrained by the pore size within the soil skeleton. For most soils, this practically guarantees a grain size at least several orders of magnitude less than for normally tested ice. It is usually considered that a finer-grained material is stronger than a coarse grained one. However, some data by Baker (1978) appear to indicate that below about 1mm, a decreasing grain size results in a weaker (more creep susceptible) ice structure. These data are currently the subject of some controversy.

In addition, the loading of the ice matrix is much different from the loading of a pure ice sample. Rather than

a simple uniaxial or triaxial stress state, a complex multi-axial stress state exists in each pore with applied shear and normal stresses and stress concentrations. These complex stress states should affect the overall behavior, but it is not clear how these effects would be manifested.

Much of the problem in understanding frozen soil behavi[illegible] may involve the current inability to measure the effective stress. Thus all results to date have been analyzed using total stresses, an approach that certainly has proved to be entirely inadequate in understanding the undrained stress-strain-strength behavior of unfrozen soils. Also, the "drainage" conditions, of utmost concern in unfrozen soil, are not usually closely controlled or considered in frozen soil testing. While one would expect volume constancy during the shearing of saturated frozen soils, measurements of volume increase, for instance, suggests that voids are created in the frozen soil system, either by cleavage between the ice and soil particles (at or near the unfrozen water film) or within the ice matrix by accomodation cracking.

As already stated, it is necessary to have as complete and thorough an understanding of the various mechanisms of strength and deformation responsible for behavior as is possible in order to better understand the behavior of frozen soils. In this review, the various explanations for frozen soils behavior which exist in the literature have been

summarized. Some of the other possible mechanisms of strength in frozen soil have been described. This topic was the subject of the continuing MIT-ARO research project. Preliminary results are presented in the review of the mechanics of frozen soil in a CRREL Report (Ting, 1981b) and final results of the research are found in the doctoral thesis of John Ting (1981a) (Part II of this Final Report).

4. Empirical Models for Frozen Soils

From the previous discussion, it is obvious that difficulties exist in merely describing the behavior of frozen soils conceptually. Any attempts at mechanistically based quantitative modelling must of necessity be exceedingly complex. Consequently, empirical modelling is by far the most popular approach for frozen soils. Various empirical models proposed to describe the deformation and strength behavior of frozen soils have been summarized by Andersland and Anderson (1978) and are briefly described here.

Typical deformation-time behavior under constant stress loading for ice, soil and frozen soil is shown in Fig. II-8. Three phases are usually defined, during which the creep rate is (1) decreasing, (2) approximately constant, and (3) increasing. These phases are termed primary, secondary and tertiary, respectively. Numerous models have been proposed which can model the various phases of creep. Basically, these models demonstrate the types of deformation-time

behavior illustrated in Fig. II-9. These may be loosely classified as (i) primary, (ii) secondary, and (iii) tertiary creep models.

Vyalov (1962) proposed a primary creep model for frozen soils that has been successfully applied to a variety of frozen soil types by Sayles (1968) and Sayles and Haines (1974). In this model, strain is expressed as:

$\varepsilon = \varepsilon_o + \varepsilon(t)$, where for negligible initial strain ε_o,

$$\varepsilon = \varepsilon(t) = \left[\frac{\alpha t^{\lambda}}{\omega(\theta+\theta_o)^{\kappa}}\right]^{1/m} \qquad \text{(II-3)}$$

where

$\theta = -T(°C)$

θ_o = reference temperature, usually -1°C

σ = applied stress

$\omega, \kappa, \lambda, m$ = soil parameters

By differentiating (II-3) with respect to time, the strain rate may be obtained:

$$\dot{\varepsilon} = \frac{\lambda}{m}\left[\frac{\sigma}{\omega(\theta+\theta_o)^{\kappa}}\right] t^{\frac{1}{m}} t^{\frac{\lambda-m}{m}} \qquad \text{(II-4)}$$

Note that the strain rate $\dot{\varepsilon}$ continuously decreases with time, hence confirming the fact that (II-3) is a primary (strain hardening) creep model. In addition, note that by

taking logarithms of both sides of (II-4), a linear relation results between log $\dot{\varepsilon}$ and log t. In this respect, this model is similar in form to the three-parameter creep model proposed by Singh and Mitchell (1968) for unfrozen soils.

The parameters for the Vyalov model may be obtained by a series log-log curve fits. First $\dot{\varepsilon}$ and σ are plotted to yield the intercept $A(t) = t^{\lambda}/\omega(\theta+\theta_o)^{\kappa}$. Then, A(t) and t are plotted at different temperatures to yield the intercept R and slope λ, where $R = At^{\lambda}$. Finally, R and $(\theta+\theta_o)$ are plotted to yield the intercept ω and slope κ. Sayles (1968) determined the various parameters for Ottawa Sand 20-30 and Manchester Fine Sand 40-200 with some success. These are summarized in Table II-1.

A secondary creep model for frozen soils has been proposed by Ladanyi (1972) based on work in metals by Hult (1966). At constant temperature and stress, the strain may be expressed as:

$$\varepsilon = \varepsilon_i + \varepsilon_c \qquad \text{(II-5)}$$

where ε_i = pseudo-instantaneous strain = $F(\sigma,T)$ and can be expressed as the sum of a recoverable portion and an irrecoverable portion. The creep strain ε_c may be described from:

$$\frac{d\varepsilon_c}{dt} = G(\sigma,T) = \dot{\varepsilon}_c\left[\frac{\sigma}{\sigma_c(T)}\right]^{n(T)} \qquad \text{(II-6)}$$

where $\dot{\varepsilon}_c$ is a strain rate which corresponds to a specific stress level, $\sigma_c(T)$, and n is a constant. Then, for a given material at a constant temperature,

$$\varepsilon = \frac{\sigma}{E} + \varepsilon_\kappa \left(\frac{\sigma}{\sigma_c}\right)^\kappa + t\dot{\varepsilon}_c \left(\frac{\sigma}{\sigma_c}\right)^n \qquad \text{(II-7)}$$

For engineering applications, the third term in (II-7) gives good approximations of the total strain.

Care must be exercised in the use of these primary and secondary creep models, since they are applicable only in the time range for which they were formulated. For secondary creep models, for example, creep strain during primary creep is overestimated, while strain during tertiary creep is underestimated. Also, the potential of creep rupture is not accounted for in these models.

Goughnour and Andersland (1968) proposed a more sophisticated model which accounts for decelerating and accelerating creep. In this model, the plastic strain rate is composed of the sum of a strain hardening term and a softening term which is dependent on the absorbed strain energy. Since integration of their strain-energy based model is quite difficult, Goughnour and Andersland proposed a separate empirical equation in terms of time:

$$\dot{\varepsilon}_p = \frac{\kappa_1}{t^{1/2}} \exp\left(-n_1 t^{1/2}\right) + \kappa_2 \exp(n_2 t) \qquad \text{(II-8)}$$

where n_1, n_2 are soil parameters which are functions of temperature, and κ_1, κ_2 are functions of stress and temperature:

$$\kappa = \frac{C}{T^n} \left(\frac{\sigma}{\sigma_c}\right)^m \quad \text{is a normalizing constant}$$

Goughnour and Andersland (1968) report excellent agreement between their model and their data on Ottawa Sand 20-30.

While the deformation models which have been described can model a variety of creep behavior, including tertiary creep, the possibility of creep rupture is not accounted for. Separate strength models exist to describe this phenomenom. These models are described in the following paragraphs.

The strength of frozen soils may take on various meanings depending upon the nature of the loading problem. Short-term strength usually refers to the peak stress achieved during load or strain application. Limiting longterm or creep strength refers to the stress below which creep rupture or excessive creep deformations do not occur. For unconfined (uniaxial) compressive creep tests, failure is usually defined as the beginning of tertiary creep. When large deformations occur without creep rupture, an arbitrarily large strain, say 20%, is sometimes defined as the failure condition.

Vyalov (1959) suggests that the variation of longterm strength of frozen soil with time may be represented by:

$$\sigma_f = \frac{\sigma_o}{\ell n\left(\frac{t_f + t^*}{t_o}\right)} \cong \frac{\sigma_o}{\ell n\left(\frac{t_f}{t_o}\right)} \qquad \text{(II-9)}$$

where σ_o, t_o = soil parameters which are temperature dependent

t_f = failure time

σ_f = longterm strength

$t^* = t_o \exp(\sigma_o/\sigma_i)$

σ_i = instantaneous reference strength

For the temperature dependence of strength, power or exponential functions are typically employed.

For short-term strength analyses, various models based on the Mohr-Coulomb theory and plasticity have been proposed. Due to the difficulties in determining an actual effective stress in frozen soils, total stresses and quasi-single-phase models are used. For most frozen soils, considerable dependence on the confining stress is present. Consequently, these frozen soils are termed "frictional" soils. Based on a series of triaxial compression tests with different times to failure, a sequence of Mohr-Coulomb failure envelopes may be constructed. Triaxial data from Sayles (1973) and direct shear data from Roggensack and Morgenstern (1978) suggest that the failure envelope for the frozen soil at

large times to failure, expressed in terms of total stress, approaches that for the unfrozen condition under drained loading. In each case, the friction angles for the frozen and undrozen soils were approximately equal, while the apparent cohesion intercept for the frozen soil decreased with increasing time to failure.

These data suggest that the following failure model may be used:

$$\tau_f = c(T, t_f \text{ or } \dot{\varepsilon}) + \sigma_f \tan \phi \qquad \text{(II-10)}$$

where $c = C(T) \left(\frac{\dot{\varepsilon}}{\dot{\varepsilon}_o}\right)^{1/n}$

$\tan \phi$ = component of frictional strength

τ_f = shear strength

σ_f = normal stress at failure

A sequence of such envelopes is shown in Fig. II-10. Note, however, that since total stresses are used in this formulation, it is difficult to draw any conclusions from the relative magnitude of the parameters in (II-10).

For ice-rich fine-grained soils, Ladanyi (1972) assumes that the strength is relatively independent of total stress changes. Based on this concept, Ladanyi used the von Mises yield criteria and plasticity theory assuming volume constancy during shear to describe the strength of such a "nonfrictional"

soil. While relatively little experimental data exist to confirm the existence of such behavior, data by Chamberlain et al. (1968) on a nondilatant silt indicated that relatively little change in strength occurred for confining stresses up to about 0.2MPa. However, it has been shown that even clean polycrystalline ice demonstrates a strength increase with increasing confining stress (Smith and Cheatham, 1975; Jones, 1978).

For individual creep tests, predictions of "failure" usually involve predictions of the time to failure t_m as a function of the secondary strain rate, $\dot{\varepsilon}_m$, failure strain, ε_m, and loading conditions. The simplest model is based on the secondary creep model as proposed by Ladanyi (1972). Assuming a constant creep rate, the time to failure for a given temperature and stress is:

$$t_m = \frac{\varepsilon_m - \varepsilon_i}{\dot{\varepsilon}_m} \qquad \text{(II-11)}$$

For large time intervals and high ice content soils where the pseudo-instantaneous strain, ε_i, is small compared to the time-dependent strain,

$$t_m \cong \frac{\varepsilon_m}{\dot{\varepsilon}_m} \qquad \text{(II-12)}$$

Note that if the strain at failure ε_m is approximately constant, then: $t_m = C/\dot{\varepsilon}_m$.

Use of equation (II-12) still requires prediction of the minimum strain rate as a function of the testing conditions. Such predictions are described in Section V-C.

B. Rate Process Theory, RPT

The basis of rate process theory is that the rate of a reaction is thermally activated. The reaction may be most any time dependent rearrangement of matter, such as chemical reactions, viscosity, deformation and/or shear of soil. No detailed derivation of the theory will be given. The basic equations will be stated along with explicit indications of the assumptions involved.

The atoms, molecules, or particles participating in the time dependent reaction are termed flow units, these being constrained from movement relative to each other by a "fence" called the activation energy. For the viscous flow of water, the activation energy is about 17kJ/mol, which is just about equal to the energy of the hydrogen bond. For creep of ice single crystals, the activation energy is about 59kJ/mol, which is equal to the energy for self diffusion of either H or O atoms in ice. This last result strongly suggests that the motion of water molecules controls the thermally activated reaction.

For a material at rest, the frequence of activation is given by the Boltzmann distribution of the thermal energy and, in the absence of a directional potential, barriers are crossed with equal frequency in all directions. The frequency of activation, ν, is given by Mitchell (1976) as

$$\nu = (kT/h) \exp(-\Delta F/kT) \qquad \text{(II-15)}^*$$

where k = Blotzmann constant

T = Temperature, °K

h = Planck constant

and ΔF = the free energy of activation.

Eq. (II-15) is a correct formal relation from which it is impossible to evaluate any parameter by experiment because at rest barrier crossings occur with equal frequency in all directions, which produces no net result; i.e., at rest.

When a bias potential such as a directional shear force, f, is applied to a flow unit the energy barriers become distorted. The bias force f reduces the effective height of the energy barrier in the forward direction and increases the effective barrier height in the opposite direction, while the free energy of activation as defined in Eq. (II-15) remains unaffected. The net frequency in the direction of the applied bias force acting on a flow unit is

$$\underset{\rightarrow}{\nu} - \underset{\leftarrow}{\nu} = (2kT/h) \exp(-\Delta F/kT) \sinh(f\lambda/2kT) \qquad \text{(II-16)}$$

where λ equals the distance between successive equilibrium positions. Two implicit assumptions in Eq. (II-16) are that the reaction rate is controlled by a single mechanism and that the work expended to reach activation is given up entirely as heat when the flow unit drops from the energy barrier peak to

*Editing deleted Eq. II-13 and -14.

a new equilibrium position. It should be noted that if more than one mechanism of approximately equal reaction rate is involved in the process, then while ΔF is still a well defined quantity, it is virtually impossible to interpret the significance of the value obtained. That is, ΔF must be a single valued function to have fundamental physical significance, which means that the reaction rate must be controlled by a single mechanism. Again, Eq. (II-16) represents a correct formal relation, but with no way to evaluate any parameter from experimental data. Thus, to be able to experimentally test Eq. (II-16), it is necessary to make additional assumptions.

An operational equation that can be experimentally evaluated is the strain rate equation derived from (II-16) (Mitchell, 1976). Each flow unit that is successful in crossing the barrier will yield a displacement λ. The vector of λ in the direction of the applied bias force times the number of barrier crossings per unit time gives the rate of movement. When this movement rate is expressed on a per unit length basis, the result is a strain rate, $\dot{\varepsilon}$. Define a dimensionless quantity X which is proportional to the combination of successive barrier crossings and λ, such that

$$\dot{\varepsilon} = X \left(\underset{\rightarrow}{\nu} - \underset{\leftarrow}{\nu}\right) \qquad \text{(II-17)}$$

The parameter X may be dependent on time and structure, but is assumed to be independent of T and f. The definition of X as independent of T and f obviously simplifies the analytical treatment of data for evaluating the rate process theory. As will subsequently become apparent, the definition of X as implied by Eq. (II-17) really requires the implicit assumption that a fixed fraction of the activated flow units proceed forward independent of the bias force applied. This point will be discussed in some detail later. Substitution of Eq. (II-17) into Eq. (II-16) gives

$$\dot{\varepsilon} = (2XkT/h) \exp(-\Delta F/kT) \sinh (f\lambda/2kT) \quad \text{(II-18)}$$

In order to experimentally evaluate this strain rate equation, it is necessary to express f, the force on a flow unit, in terms of some measurable macroscopic variable, such as the applied shear stress. Assume that the applied shear stress, τ, is distributed uniformly over S flow units per unit area. Then $f = \tau/S$ with the direct consequence that the volume of a flow unit, V_f is λ/S. One then obtains

$$\dot{\varepsilon} = (2XkT/h) \exp(-\Delta F/kT) \sinh (\tau\lambda/2SkT) \quad \text{(II-19)}$$

Eq. (II-19) is the starting point for experimental evaluation of the rate process theory. The rest of this section discusses the deformation of two very simple systems using data from the literature. These examples will illustrate how Eq. (II-19)

can be evaluated experimentally and what one can deduce from the use of rate process theory (RPT).

1. Viscosity

For Newtonian flow where the stress τ is very small, the quantity $\tau\lambda/2SkT$ will be less than one so that the hyperbolic sine of the quantity becomes equal to the quantity. Vicosity, η by definition equals $\tau/\dot{\varepsilon}$ and R=kN, where N = Avogadro's number; thus Eq. (II-19) becomes

$$\eta = h/XV_f \exp (\Delta F/RT) \quad . \qquad \text{(II-20)}$$

Experimentally the viscosity, η, is measured as a function of temperature, T. Then a plot of $\ell n\ \eta$ vs. 1/T permits calculation of ΔF from the slope of the plot and the flow volume from the intercept. The viscosity of water is often cited as verification of RPT and certainly the first line of Table II-2 confirms a good fit of $\ell n\ \eta$ vs. 1/T. Further, the ΔF of 16kJ/mol is just about the hydrogen bond energy. Assuming X=1 yields a flow volume of $4.22 \times 10^{-28} m^3$ which represents a sphere 0.93nm(9.3A°) in diameter, or about three water molecules across.

The fit of $\ell n\ \eta$ vs. 1/T can be improved by using a shorter temperature range, as shown in Table II-2. Table II-2 also reveals that neither ΔF nor (h/XV_f) are constant. Going from a mean temperature of 15°C to 45°C reduces ΔF by 17% and decreases the flow volume sphere diameter from 1.33nm at 15°C

to 0.84nm at 45°C. Recall that X=1 was assumed in the flow volume calculation; however, the change in flow volume size with temperature cannot be attributed to X because X was defined to be independent of temperature. Viewing the flow volume parameters as describing the structure of water, its decrease with increase of temperature is reasonable, but raises a question about the definition of X. Increasing the temperature decreases the number of hydrogen bonds. The decrease in ΔF with increase of temperature cannot be explained by the argument of fewer hydrogen bonds (as is frequently done) because ΔF is per mole of bonds.

Andersland and Douglas (1970) measured the viscosity for some homoionic illitic clay slurries which can be used to show what happens to the water structure from the addition of clay particles and their associated ions. The results summarized in Table II-3 were computed from the data given in Fig. 6,7 and 8 of Andersland and Douglas (1970) for Li, Na and K clay respectively. There was no variation in ΔF between the different homoionic clays or for a tenfold clay concentration change. However, there was a 14% decrease in ΔF compared to the ΔF of pure water evaluated over the same temperature range. The presence of clay in the water at 10g/ℓ decreased the flow unit diameter by 30% and increasing the clay concentration to 100g/ℓ gave a further decrease in flow unit diameter of 13% to a value nearly one half the diameter for pure water.

Since the volume of a flow unit in the clay slurry is as a maximum one millionth the minimum volume of a clay particle, the flow units must involve only water. Through the use of RPT it has been shown that the presence of the clay has disrupted the water structure by decreasing the size of the flow unit and decreasing the free energy of activation.

2. Creep

For the creep of ice or frozen soil, the shear stress will be fairly large so that the quantity $(\tau\lambda/2SkT)$ in Eq. (II-19) exceeds 1.5. Thus, replacement of the hyperbolic sine with one half exp is justified. For the sake of clarity and continuity all the necessary equations in operational form are given, then applied to creep data for ice single crystals. Assume that the shear stress equals one half the deviator stress; i.e., $\tau = D/2$. Then, Eq. (II-19) becomes

$$\dot{\varepsilon} = (XkT/h) \quad \exp(-\Delta F/RT) \quad \exp(\lambda ND/4SRT) \; . \qquad \text{(II-21)}$$

Experimentally, the temperature dependence is evaluted from a rearrangement of Eq. (II-21)

$$\ell n \; (\dot{\varepsilon}/T)_{t,s,D} = \ell n \; (Xk/h) - E/R(1/T) \qquad \text{(II-22)}$$

where E is the experimentally determined activation energy defined by $E = \Delta F - (\lambda N/4S)D$. Following Mitchell (1976), it is assumed that the number of flow units equals the number of

bonds, S. The subscripts on the right hand side of Eq. (II-22) have been added as a reminder that from the assumptions made the temperature dependence must be evaluated at constant deviator stress, D, constant structure, s, and constant time, t. Note that the experimental activation energy is explicitly a function of stress. The theory predicts that E should decrease as D increases. Data at two stress values permit calculation of ΔF by extrapolation to D = 0 of the E vs. D data and the slope $\beta = \lambda N/4S$ allows computation of the number of bonds S per square meter. The problem parameter is structure which requires the assumption that X is constant to permit an evaluation of E from (II-22). The intercept, the first term on the right side of Eq. (II-22), allows a determination of X to ascertain the variability of X; ideally X should remain constant.

Experimentally, it is difficult to obtain identical samples so that even if the plot of $\ell n\ (\dot{\varepsilon}/T)_{t,s,D}$ vs. 1/T were linear, one cannot exclude the possibility that the observed linearity resulted from sample variability. This dilemma can be circumvented by running what is called a stage test after a general method usually attributed to Tietz and Dorn (1956). For a temperature stage the sample is allowed to creep under constant load for some time t, then the temperature T is rapidly changed to a new temperature T_2 where creep continues for some further time period under the same applied

load. When the time required to change the temperature can be kept short, extrapolation of creep rate at temperature T_2 back to the time t of the temperature change comes as close to constant t and s as are experimentally possible. Thus for a temperature stage test at stress D_1, Eq. (II-22) becomes

$$E_1 = RT_2T_1/(T_2-T_1)\ \ell n\ (\dot{\varepsilon}_2T_1/\dot{\varepsilon}_1T_2)_{t_1,s,D} = 1 \quad (11-23)$$

During the experiment D_1 is constant, temperature T_1 is constant up to t_1, and after t_1 temperature T_2 is constant. The strain rates $\dot{\varepsilon}_1$ and $\dot{\varepsilon}_2$ are for T_1 and T_2 respectively, both at time t_1, which assures constant structure because the strain rates are taken on one sample at one point in time for the two temperatures. Note that this one test yields an experimental activation energy E, not the free energy of activation ΔF, and also does not permit computation of S the number of bonds (or V_f if preferred).

A second temperature stage test at D_2 on a second sample yields a second value of E.

$$E_2 = RT_2T_1/(T_2-T_1)\ \ell n\ (\dot{\varepsilon}_4T_1/\dot{\varepsilon}_3T_2)_{t_1,s,D_2} \quad (II-24)$$

Just as described for the first stage test, the nature of the test assures constant structure, but provides no assurance that the structure in samples 1 and 2 was identical. It is necessary to assume constant structure so that ΔF and β can

be calculated from these two temperature stage tests. The slope of the plot E vs. D yields β and subsequently S_β because

$$S_\beta = \lambda N/4\beta$$

at the average temperature $(T_2 + T_1)/2$ and average stress $(D_1 + D_2)/2$. The intercept on the E axis at D = 0 yields ΔF.

Stress dependence can be evaluated from a rearrangement of Eq. (II-21) and the definition of $\alpha = \lambda N/4SRT$.

$$\ell n\ (\dot{\varepsilon})_{t,s,T} = [\ell n(XkT/h) - \Delta F/RT] + \alpha D \qquad \text{(II-25)}$$

A plot of $\ell n(\dot{\varepsilon})_{t,s,T}$ vs. D for a series of samples should be linear with a positive slope α provided that the samples are sufficiently identical to have the same structure.

Stage tests for stress can be run analogous to the temperature stage tests described above. From Eq. (II-25)

$$\alpha_1 = \ell n\ (\dot{\varepsilon}_1/\dot{\varepsilon}_2)_{t_1,s,T_1} / (D_1-D_2) \qquad \text{(II-26)}$$

from which $S_\alpha = \lambda N/4RT\alpha_1$. A partial confirmation of the theory would be the cross check $S_\alpha = S_\beta$; however, such a comparison requires a second stress stage test in order to obtain an average S_α for the mean temperature $(T_2 + T_1)/2$ corresponding to the same condition as for S_β.

As straightforward as the above procedures appear to be for evaluation of RPT, the authors know of no investigation

that has examined this cross correlation $S_\alpha = S_\beta$ on the same material under the same experimental conditions. The theory is not proved completely when $S_\alpha = S_\beta$; nevertheless, one's confidence in applying the theory is greatly increased, because of the demonstrated strong internal consistency, if $S_\alpha = S_\beta$.

Mitchell et al. (1968) and others have shown that the temperature and stress dependency qualitatively fit RPT predictions and that the values of S and ΔF are reasonable for unfrozen soils. Andersland and coworkers (1968, 1970), among others, have applied RPT to frozen soil and obtained a very large experimental activation energy. There are no soil data available in the literature for a comparison of $S_\alpha = S_\beta$.

Referring back to Eq. (II-25) it is noted that once α has been determined, which implies some assumption about the constancy of X, ΔF can be computed directly without any experimental data for the effect of temperature. In fact, numerous authors have used this procedure to obtain ΔF; i.e. solve Eq. (II-25) for ΔF

$$\Delta F = RT[\ell n(kT/h) + \alpha D + \ell n(X/\dot{\varepsilon})] \qquad \text{(II-27)}$$

Although mathematically permissible, ΔF calculated from Eq. (II-27) is very sensitive to the experimental variables, as shown by the following numerical example, and all authors

have implicitly assumed X = 1.

For frozen saturated Manchester Fine Sand at -15°C, the lowest measured strain rate at $\dot{\varepsilon}_{min}$ was $10^{-10}sec^{-1}$ for a D = 3.45MPa, and the largest measured strain rate at $\dot{\varepsilon}_{min}$ was $10^{-4}sec^{-1}$ for a D = 17.24MPa. The experimentally determined α was $1.02 \pm 0.44(MPa)^{-1}$. Substituting these numbers into Eq. (II-27), along with the constants R = 8.3136 J/mole°K, k = 1.38×10^{23}J/molecule°K, and h = 6.62×10^{-34}J-sec gave the following results:

		ΔF for X=1 (kJ/mole)		
D	$\dot{\varepsilon}$	α=0.58	α=1.02	α=1.46
3.45	10^{-10}	116.59	119.82	123.04
17.24	10^{-4}	104.12	120.24	136.31

The extremes of experimental conditions gave a ΔF range from 104 to 136 kJ/mole, but these computations assumed X = 1, as explicitly stated. Now one can go back and check the X = 1 assumption. Solve Eq. (II-27) for X

$$X = \exp\left(\ell n\dot{\varepsilon} - \ell n(kT/h) + \Delta F/RT - \alpha D\right) \qquad \text{(II-28)}$$

For input data use the mean value of ΔF at a given α from above, then for all other parameters the same as above the calculated values of X are:

		X for ΔF mean value		
D	$\dot{\varepsilon}$	α=0.58	α=1.02	α=1.46
3.45	10^{-10}	0.06	1.1	22.0
17.24	10^{-4}	18.3	0.9	0.05

Clearly, X is a sensitive parameter to small changes in ΔF and/or α.

Two final comments about Eq. (II-27) are in order. If one says that a ΔF of about 85 to 125kJ/mol is an "expected reasonable value", then computation via Eq. (II-27) is guaranteed to yield the correct answer. On the other hand, ΔF is the temperature dependent parameter in RPT and as such it might be suggested that somehow a temperature change should be involved in the determination of ΔF, as for example by a temperature stage test.

Now, examine RPT as applied to ice single crystals from data obtained by Ramseier (1971) on a series of ice single crystals oriented at 45° to the c axis and covering a temperature range -10°C to -35°C and a stress range from 0.2MPa to 19MPA. Further, all tests were carried into tertiary creep so that the minimum strain rate was experimentally measured. Ramseier's objective was not testing RPT; however, his data were summarized in tabular form so that by selecting tests at different temperatures and stress constant to within

0.6% for a given test set, the temperature dependence of RPT can be evaluated.

Input data for use in Eq. (II-22) and the results obtained were:

Input Data *			Calculated for mean Θ= 28.13°C		
D(MPa)	Θ(°C)	$\dot{\varepsilon}(s^{-1})$	Mean D(MPa)	E(kJ/mol)	$X \cdot 10^{-7}$
1.188	35.10	1.33×10^{-6}	1.195	54.73	2.74
1.203	21.45	6.30×10^{-6}			
3.568	34.28	1.50×10^{-5}	3.589	50.25	2.94
3.611	21.70	5.60×10^{-5}			

* Ramseier (1971)

Note that while X was reasonably constant, it certainly was far less than unity. From the values of E and mean D, ΔF = 56.97kJ/mol and $\beta = 1.87 \times 10^{-3} m^3$/mol were calculated. A major conclusion of Ramseier's work was that for ice single crystals all the temperature dependence of strain rate could be accounted for using the self diffusion coefficient of a water molecule in ice. Thus, the expected theoretical value of ΔF is 59.76kJ/mol (the free energy of activation for self diffusion of water in ice) which is only 4.7% larger than the value of ΔF computed from RPT. The number of bonds per square meter, S_β is equal to $\lambda N/4\beta$. Making the assumption

that the minimum value of λ, the jump distance, is the diameter of a water molecule (0.28nm) one obtains S_β at -28.13°C of 2.257×10^{16} bonds/m^2. A physical concept for this number of bonds is difficult to visualize, so it can be converted into an equivalent spherical diameter of the flow unit, D_f, from the definition of $V_f = \lambda/S$ and that $D_f = (6V_f/\pi)^{1/3}$. The resultant spherical diameter of the flow unit D_f for ice single crystals was 2.87nm, which is a diameter of only ten water molecules. The flow unit diameter obtained from data on viscosity of liquid water at -7°C was D_f = 2.74nm. It should be mentioned that the flow unit diameter does not involve any assumption about the jump distance λ because it cancels out.

Fortunately, Ramseier's data are sufficient to provide a reasonable evaluation of the stress dependence for this same ice single crystal material. Input data for use in Eq. (II-25) and the results obtained were:

Input Data			Calculated			
Θ(C°)	D(MPa)	$\dot{\varepsilon}(s^{-1})$	Mean Θ(C°)	$\alpha(MPa)^{-1}$	Intercept A**	ΔF X=1.0 (kJ/mol)
10.50	0.927	1.52×10^{-5}	10.47	0.9162	7.176×10^{-6}	89.2
10.45	3.010	1.40×10^{-4}				
10.47	4.810	5.25×10^{-4}				
—	—	—	—	—	—	—
21.45*	1.203	6.30×10^{-6}				
21.51	1.905	1.50×10^{-5}				
21.51	2.035	1.50×10^{-5}	21.57	0.9168	2.311×10^{-6}	88.4
21.70	3.374	5.60×10^{-5}				
21.70*	3.611	5.60×10^{-5}				

* Data points also used for temperature dependence
**A = ($\ell n(XkT/h) - \Delta F/RT$)

The number of bonds/m^2, S_α, can be computed from α with the following results: at -10.47°C, S_α is 2.11×10^{16} bonds/m^2; and at -21.57°C, S_α is 2.20×10^{16} bonds/m^2, which agree reasonably well with S_β of 2.26×10^{16} bonds/m^2 at -28.13°C. However, since S_α is explicitly a function of temperature, it is reasonable to calculate S_α at -28.13°C, the temperature for S_β. The cross check $S_\alpha = S_\beta$ at -28.13°C for ice single crystals shows rather good agreement.

bonds/m^2 x 10^{16}	
S_α	S_β
2.262	
	2.257
2.260	

The free energy of activation, ΔF, calculated from the stress dependence using the usual implicit (explicitly stated here) assumption that X = 1 are given in the last column above. The values at -10 and -21°C are close together and yield a mean of 89.2kJ/mol which is 49% above the expected theoretical value; however, it is well within the 85 to 125kJ/mol range. This computation again proves that Eq. (II-25) or Eq. (II-27) are unreliable equations for computation of ΔF unless X is known. Finally, using the theoretical value of ΔF for self diffusion of water molecules in ice and Eq. (II-28) one can calculate X, the fraction of activated flow units that proceed forward. The resultant X is $1.08 \pm .07 \times 10^{-6}$, which again emphasizes that one cannot summarily neglect X or make the common assumption that X equals equity.

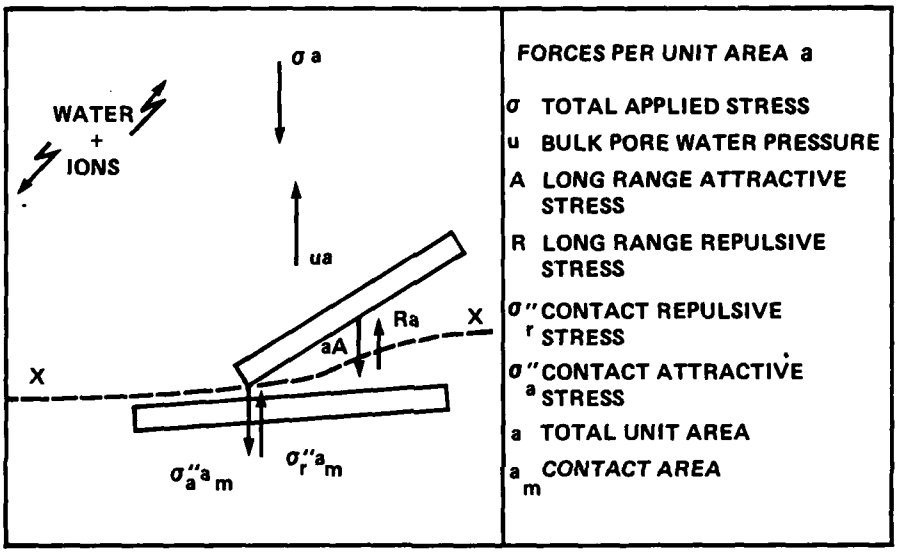

PHYSICO-CHEMICAL EFFECTIVE STRESS EQUATION:

$$\sigma' = \sigma - u = (R-A) + (\sigma''_r - \sigma''_a)\frac{a_m}{a}$$

DOUBLE LAYER STRESS	CONTACT STRESSES

Fig. II-1 The Physio-chemical Effective Stress Equation

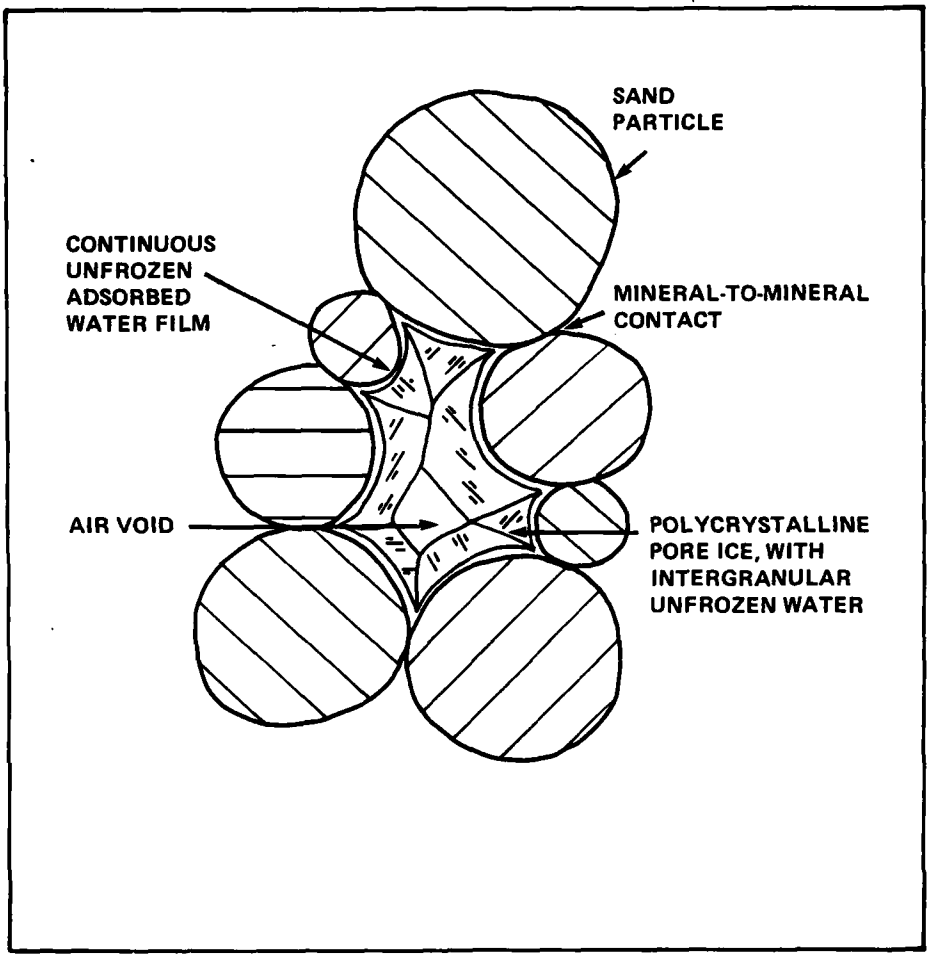

Fig. II-2 Proposed Two Dimensional Schematic Model for Structure of Frozen Soil

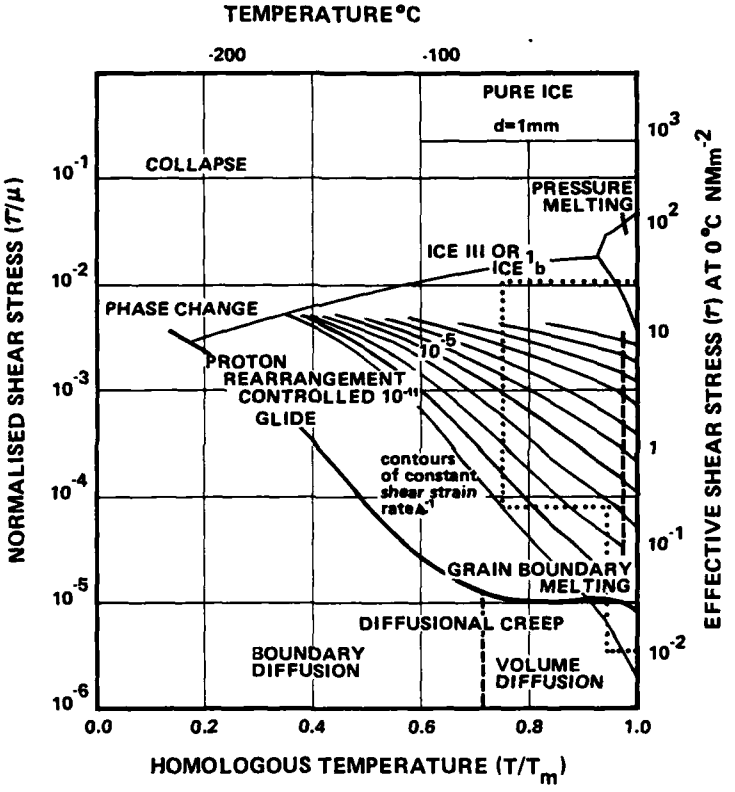

Fig. II-3 Deformation Mechanism Map for Polycrystalline Ice of 1mm Grain Size (from Goodman, 1977)

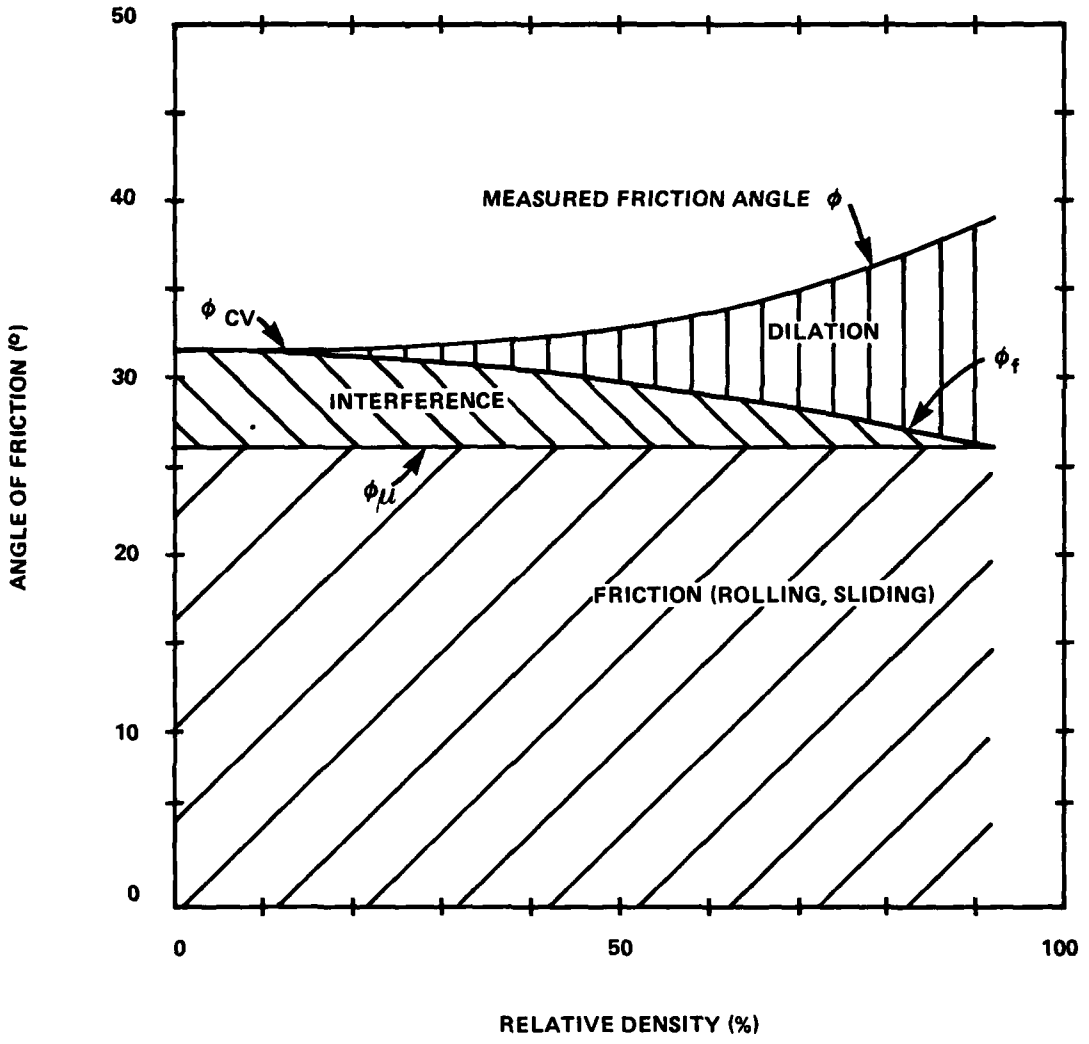

Fig. II-4 Components of Sand Strength after Rowe (1962)

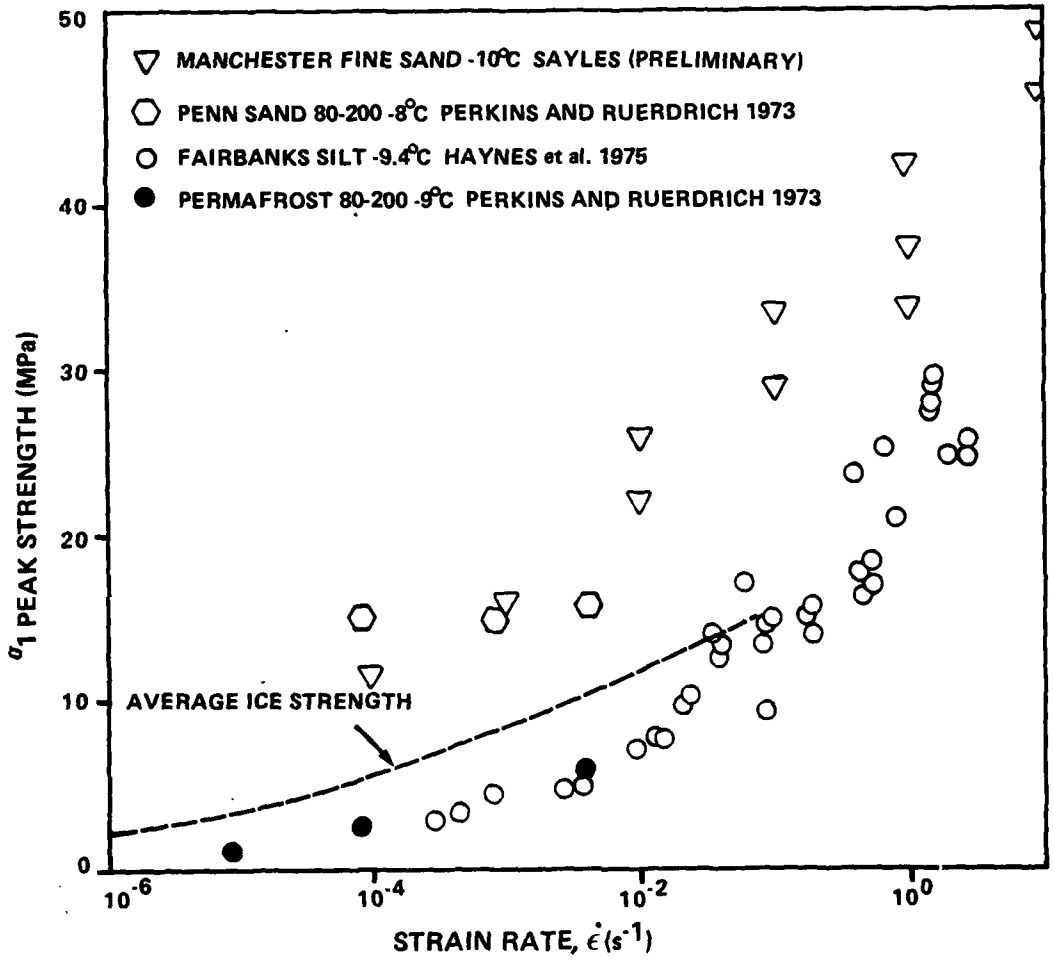

Fig. II-5 Uniaxial Compressive Strength of Frozen Soil at -10°C

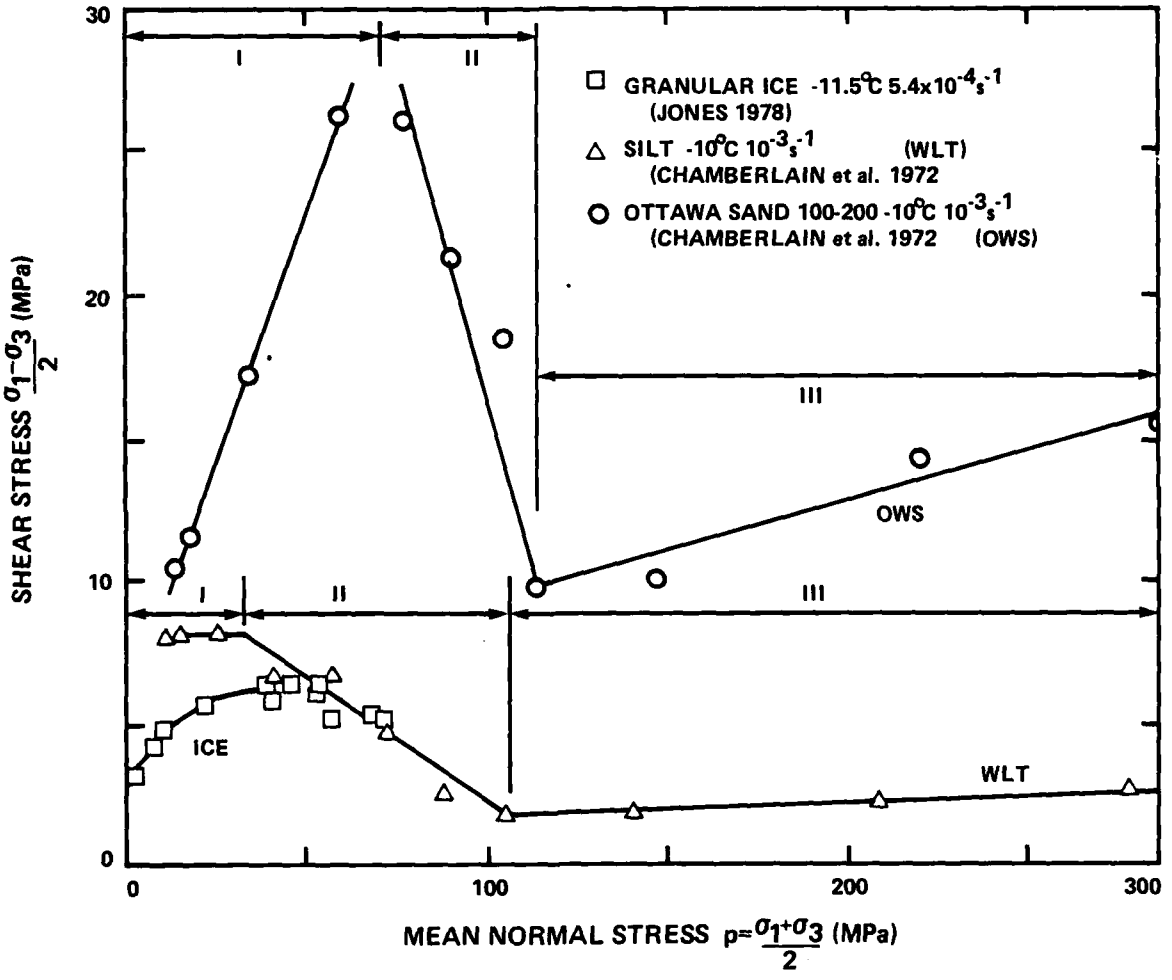

Fig. II-6 Triaxial Strength of Ice and Frozen Soil

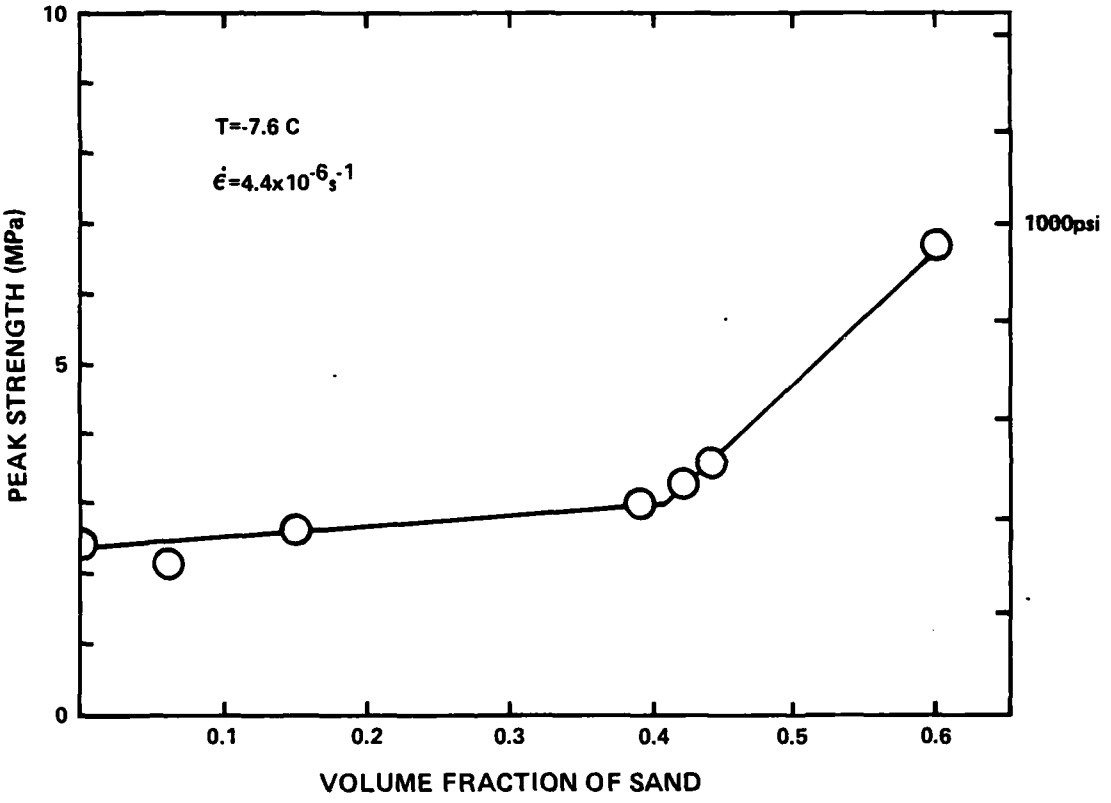

Fig. II-7 Effect of Sand Concentration on the Uniaxial Strength of a Sand-Ice System (from Goughnour & Andersland, 1968)

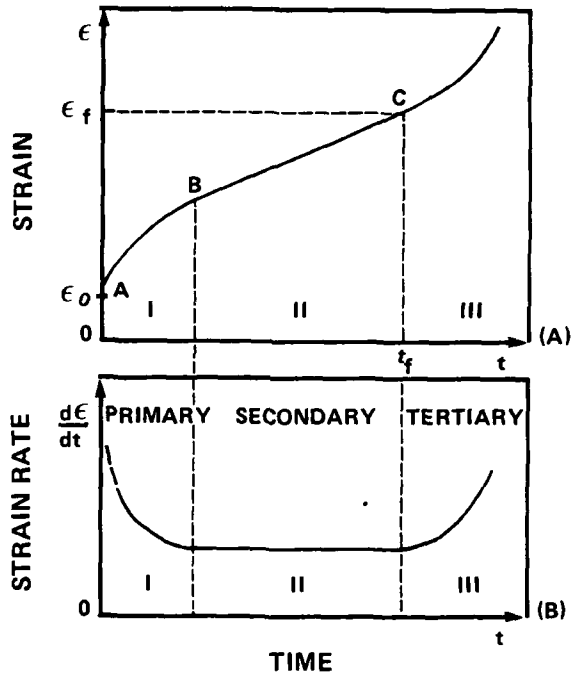

Fig. II-8 Strain and Strain Rate in Constant Stress Creep Test

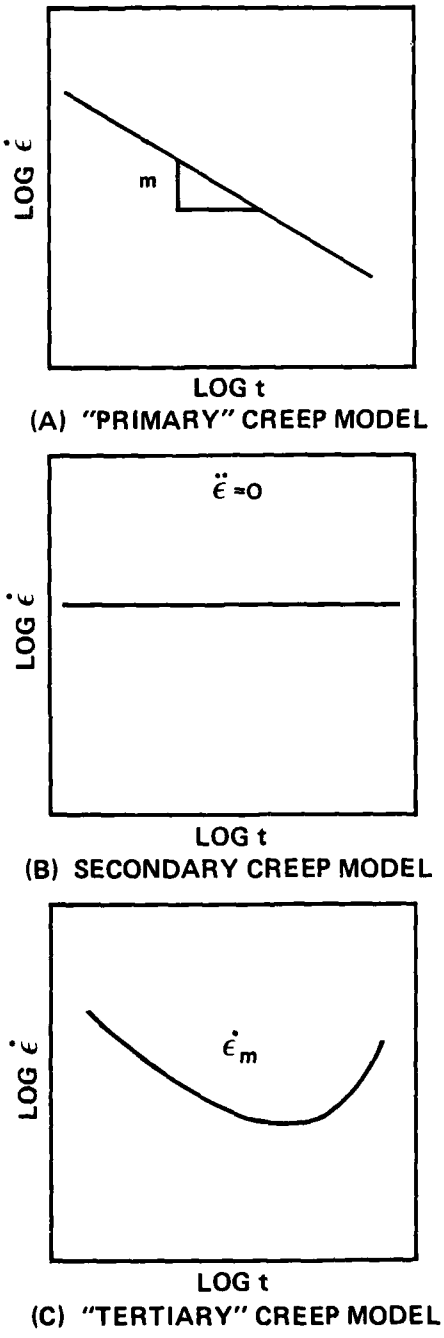

Fig. II-9 Basic Types of Creep Models Used in Frozen Soils

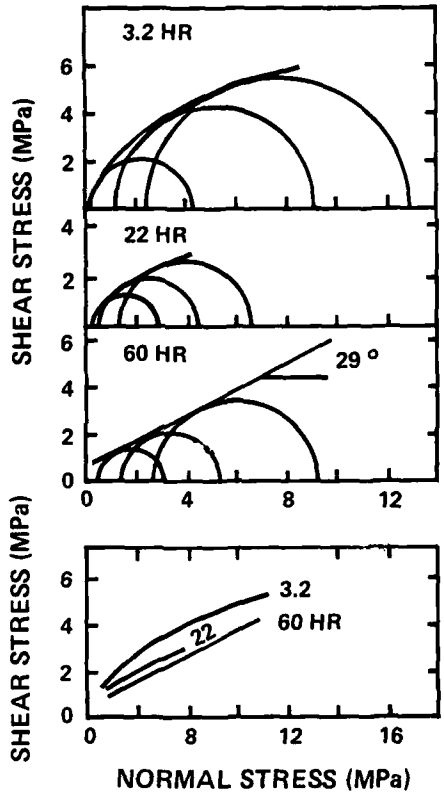

Fig. II-10 Mohr Envelopes for Creep Strength of Ottawa Sand (from Sayles, 1974b)

Table II-1

Parameters for Vyalov's Model*

Material	m	λ	w**	k
OWS 20-30	0.78	0.35	456	1.0
MFS 40-200	0.38	0.24	234	1.0

* After Sayles (1968)

** for θ = 1°C in $kg/cm^2(hr)^{\lambda}/(°C)^k$

Table II-2

Rate Process Parameters for Water

Temp Range (°C)	Coefficient of Determination (r^2)	ΔF (kJ/mol)	$(h/XV_f).10^{-7}$ (j-sec/m^3)
22-48	0.99951	15.82	15.73
12-18	0.99993	18.12	5.38
22-28	0.99995	16.78	10.30
42-48	0.99997	14.94	21.18

Table II-3

Rate Process Parameters for Clay Slurries*

Illitic Clay Concentration (g/l)	Ion	ΔF (kJ/mol)	Diameter Flow Volume (nm)
0	Water	15.82	0.93
10	Li	13.81	0.65
10	Na	13.22	0.61
10	K	13.89	0.68
100	Li	13.89	0.54
100	Na	13.39	0.54
100	K	13.39	0.52

* Data from Andersland & Douglas (1970) recomputed.

III. EXPERIMENTAL PROCEDURES

A. Scope and Objectives

The program's major objective is to evaluate rate process theory under experimental conditions that hopefully will satisfy the boundary conditions for the theory. The types of creep data needed are: (1) a series of single stage creep tests at constant stress, but different temperatures; (2) a series of single stage creep tests at constant temperature, but a different stress levels; (3) a series of temperature stage creep tests at different stress levels; and (4) a series of stress stage creep tests at different temperatures. Data also have been obtained for "instantaneous strength" and unfrozen water content.

Meeting the above objective imposed a number of restrictions in the experimental design. The temperature range investigated was kept below -10°C in order to minimize the effect of unfrozen water. In so doing, it was recognized that this low temperature may not be of prime engineering interest but was dictated from the major objective for evaluation of the rate process theory. Temperature stage tests require that the sample temperature be changed as rapidly as possible; therefore, a liquid constant temperature environment was preferable to air to enable more rapid heat transfer. Also, a small sample size was used to achieve more rapid equilibration during temperature changes. An air pressure system for load

application ensures that the load can be changed rapidly with minimum distrubance of the system during a stress stage test. Finally, Manchester Fine Sand, (MFS), was chosen as an appropriate soil because it is near the lower limit for a natural, truly cohesionless material, which hopefully will simplify the number of parameters influencing the creep behavior.

Preliminary experiments using the equipment readily available in the CRREL soils lab indicated that: (1) trimming of frozen samples did not yield reproducible samples; and (2) temperature control was not adequate (± 0.2°C). It was further determined that both the pressure and displacement transducers were sensitive to temperature transients arising from the cold room defrost cycle. Based upon the preliminary testing and considerations cited above, a constant load creep cell was designed and built for use in the main testing program described below.

B. Materials

1. Manchester Fine Sand

Particle size distribution data obtained from wet sieving of the sand were:

µm	% Finer by Wgt.
420	0.4
420 - 250	6.9
250 - 149	49.9
149 - 74	30.8
74	12.0

Eighty percent of the sand particles fall between 74 and 250µm size. The specific gravity of the sand was 2.67g/cm^3.

The mineralogy of the sand material was predominantly quartz and feldspars. Potash feldspar was the most abundant feldspar species. The clay minerals present were mica, illite, vermiculite and chlorite with considerable interstratification evident in the X-ray diffraction data because of the non-rational series of basal reflections that changed position depending upon the hydration state. The sand contained 0.48% magnetics, primarily magnetite. The electrical conductivity of a 5:1 water: soil slurry was 14µmhos. Assigning this electrical conductivity to salt present in the unfrozen water associated with the soil (0.85%), the salt concentration in the unfrozen soil would be 0.06M. The actual salt concentration would be lower because there is also unfrozen water associated with the ice phase.

Scanning electron photomicrographs for different size fractions are shown in Figs. III-1 through III-4. The specimens for scanning electron microscopy were prepared by dry sieving in order to observe possible variations in surface coatings between size fractions and/or different mineral grains. General grain shape and degree of rounding are shown for the three coarser size fractions in Fig. III-1 to -3. Except for the micaceous flakes, the grains are about equidimensional. All size fractions contained micaceous flakes that, from the visible split edges, suggest considerable weathering, probably due to hydrobiotite and/or vermiculite which would be consistent with the X-ray diffraction data. At low magnification, the mineral grains appear to be reasonably clean; however, at 5000X (Fig. III-4) surface coatings were observed in all size fractions and on all mineral types. The chemical composition of the surface coatings determined from energy dispersive analysis by X-rays suggest clay coatings. Visually there is an increase in grain roughness, excluding the clay coatings, from mica to quartz to feldspar.

The maximum grain size for ice in frozen soil will be limited to the voids between packed mineral grains, unless one postulates that ice grows as a single grain from pore to pore through the pore constrictions. The probability for continuous ice grain growth is considered to be very small. It is much more likely that individual ice

grain growth is confined to a single pore space. With this hypothesis in mind, examine the possible maximum grain size for ice in the frozen soil. The ice grain diameter can be calculated from simple geometry of equal sized spherical particles (diameter = d) in loose or in dense packing. For dense packing, the pore diameter, $\phi_d = d[\tan 60° - (1 + \tan 30°)]$, and for loose packing the pore diameter, $\phi_l = (2\ d^2)^{1/2} - d$. Using a particle diameter d of 200μm, which is the mean diameter for 50% of the sand, the calculated maximum ice grain diameter will be between 31μm and 83μm. In other words, the absolute maximum possible ice grain size in frozen Manchester Fine Sand will be very fine grained ice compared to normal polycrystalline ice where the usual grain size is 1000μm or larger.

Relative density, D_r, is defined by the equation $D_r = (\gamma_{max}/\gamma)(\gamma-\gamma_{min})/(\gamma_{max}-\gamma_{min})$, where the γ values refer to dry bulk densities. Experimentally the maximum and minimum dry density that could be achieved for Manchester Find Sand were 1707kg/m^3 and 1370kg/m^3 respectively. For Manchester Fine Sand, the relative density equation reduces to $D_r = 5.0653 - 6939.4/\gamma$. Most of the creep tests were run on samples prepared at a relative density of 0.55. Ice saturation of voids for a given compacted relative density requires only 0.916 as much water as needed for water saturation.

2. Ice

The ice samples were prepared after the method described by Cole (1979), who provided the samples tested herein. The ice specimens produced were fine grained equidimensional crystals exhibiting random c-axis orientation. Average grain size was 1.2mm. The density was 917 ± 2kg/m^3. The ice was visually clear with some fine microscopic bubbles in a narrow column along the central axis of the specimens. As frozen, the ice samples were 50.8mm diameter and 216mm long. Right cylinders were machined to have parallel ends that were exactly perpendicular to the axis of the cylinder. Final dimensions of the ice specimens were identical to the frozen soil specimens, 35.69mm diameter by 81.38mm long. The electrical conductivity of the melt water from specimens thus prepared was 4μmhos.

C. Sample Preparation

Ideally one would like to have identical isotropic samples; however, freezing guarantees some anisotropy in the water (ice) distribution. Therefore, the most one can hope for are reproducible samples. The sample size chosen, 35.7mm (1.405 in.) diameter by 81.3mm (3.20 in.) long, represents a compromise of small diameter to speed thermal equilibration vs. a large sample to average out local inhomogeneities. A schematic of the compaction-freezing mold is shown in Fig. III-5. The sample cylinder (1001 + 1002) is rigidly clamped to the base during compaction by four bolts through the clamp ring and is not disturbed when the compaction collar is removed to attach the top plate. This top plate is also secured by four bolts to the clamp ring. The mold provides a fixed total volume that also assures parallel and flat ends to the sample. Seals are provided so that the sample can be deaired by evacuation prior to wetting with thoroughly deaired water. The inner split sleeve permits extrusion of the frozen sample from the confining cylinder with minimum stressing of the sample.

Compaction was by the under-compaction method (developed by R.S. Ladd as reported in Silver, 1976) in five separate layers each containing an equal weight of soil, but compacted into progressively smaller volumes from bottom to top in order to allow for additional compaction of the lower layers by the compactive effort on upper layers. The molding water content

was 10% for samples to be frozen at w = 10% and at w = 25% (saturated). Some samples were compacted and frozen at w = 5% and w = 3%. Samples were prepared at relative density, D_r, between 20% and 95%, although most of the testing was done at a fixed relative density of 55%.

Partially saturated samples were frozen confined and sealed in the compaction mold by placing the mold in a freezing cabinet at between -30°C and -50°C. To determine the freezing rate a thermocouple was buried at the center of a sample and another thermocouple attached to one of the end caps. Figure III-6 shows that the sample completely froze in 0.5 hour. The freezing occurred from all around toward the center because the end caps were metal and the sample clyinder was Lucite. Freezing proceeded faster from the ends because of the low rate of heat extraction through the Lucite cylinder. The data in Fig. III-7 show the results from five samples cut into thirds and then each third cored so that the volume of the center core was about equal to the volume of the outer shell. The relative moisture distribution gives the ratio of water content for a particular specimen to the average water content for that entire sample. Moisture migration away from the center is obvious. While the moisture distribution was not homogeneous through the sample, the distribution was reproducible as shown by the two times standard deviation bars in Fig. III-7. Also shown in Fig. III-7 is the average

moisture distribution for 86 samples cut into five cylindrical sections.

Saturated samples were frozen inverted so that during freezing the bottom was the upper cold surface and the top (now the bottom) was open to a water resevoir outside the freezing cabinet with the liquid level set about 10cm above the sample cold surface. The freezing rate for a saturated sample is shown in Fig. III-8. Nine hours was about the minimum time required to freeze saturated samples. Moisture distribution for saturated samples (nominal w = 25%) are shown in Fig. III-9, along with data for partially saturated samples. On the assumption that the coefficient of variation $(\frac{S.D.x100}{Mean})$ is a measure of homogeneity, the w = 5% slices have the greatest moisture heterogeneity, the w = 10% samples are slightly more homogeneous than the w = 25% samples, and the center of sample water content was more uniform than the ends regardless of water content. However, as shown in Fig. III-7, the center section of partially saturated samples was really not homogeneous. In Fig. III-9 the number of each bar is the average water content and the number in brackets is the coefficient of variation.

Further data about sample homogeneity are given by the radiographs in Fig. III-10. These data indicate a higher density of the sand at the bottom of each compacted lift, but that successive lifts appear to be remarkably similar.

The anisotropy introduced from compaction of sand by various methods has been examined in some detail by Mahmood (1973) and Oda (1972).

Some samples were tested for continuity of air voids. Air permeability was readily observed in frozen samples until the total water content exceeded 21%, which corresponds to an ice saturation of about 85%.

The sample mold was designed so that the frozen sample could be removed from the mold without stressing the frozen soil. Upon removal from the mold, the total sample weight was recorded, the sample double wrapped with Saran Wrap, labeled, and stored in a sealed container which had a layer of chipped ice at -8.5 ± 0.5°C. Storage for as long as 120 days showed no weight loss, indicating that significant sublimation did not occur. The creep behavior was the same for samples stored 90 to 120 days compared to samples tested immediately after preparation. This constant creep behavior suggests that no change in the ice occurs within the frozen soil resulting from up to 120 days of storage.

AD-A103 556 MASSACHUSETTS INST OF TECH CAMBRIDGE DEPT OF CIVIL E--ETC F/G 8/13
CREEP BEHAVIOR OF FROZEN SAND.(U)
JUN 81 R T MARTIN, J M TING, C C LADD DAAG29-77-C-0016
UNCLASSIFIED R81-19 ARO-14725.3-GS NL

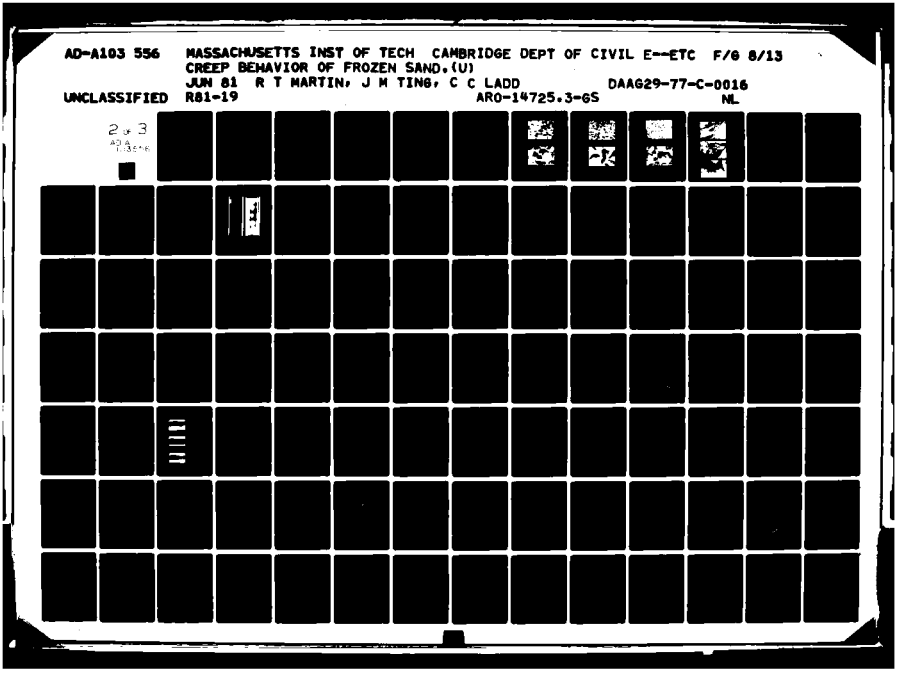

D. Creep Testing

Unconfined constant load creep tests were run in the cell shown schematically in Fig. III-11. The equipment operated in a cold room at -8 ± 2°C. A rubber membrane around the sample was secured to the end caps with O-rings which sealed the sample from the circulating constant temperature fluid (glycol-water). Pressure, deformation and temperature were measured with electrical transducers and recorded as a function of time by a data acquisition system that permitted computer manipulation of the data.

Load application was with an air jack equipped with a frictionless rolling diaphram and a linear ball bushing. Control of air pressure to the jack was with a pressure regulator which resulted in load variability on the sample of about 0.002MPa. It should be mentioned that the equipment provided constant load not constant stress. Periodically it was necessary to remove ice from the air lines because the air supply pressure was not thoroughly dry. Occasionally, a test was lost because the air supply system failed.

A Lauda refrigerated circulator gave temperature control to the circulating fluid around the sample. When the constant temperature circulator was functioning properly, a mean temperature over several hundred minutes would have a standard deviation, SD, of 0.006°C and a SD of 0.01°C for up to 10,000

minutes. Less precise control resulted when either the coolant flow rate through the creep cell was too slow, or when the cooling coil in the circulator itself would ice up. These control problems increased the SD of the mean temperature to as much as 0.08°C. Therefore, periodically between tests the temperature of the circulator was routinely raised to above freezing for several hours to ensure good temperature control during creep testing. The degree of temperature control and time required to achieve equilibration following a temperature stage are shown in Figs. III-12 and III-13. The thermal conductivity of ice is greater than of soil so a sample at a low water content, w = 10%, was prepared with a thermistor at its center in order to measure the temperature lag between a change of surface temperature and the temperature at the sample center. Figure III-12 shows that the lag was about 5 minutes. The warming stage was done by adjusting the thermal regulator on the circulator and plugging in an auxiliary heater. A 200 watt heater was used for the data shown in Fig. III-12. When the heater was changed to 1000 watts, a much more rapid temperature change was effected as shown in Fig. III-13. For the readout equipment employed a temperature change of 0.005°C was detectable with the thermistors. The thermistors were calibrated against a reference thermistor from the CRREL calibration lab.

The magnitude of room temperature transient effects on

two displacement transducers are shown in Fig. III-14. The Collins displacement transducer was superior not only in having a greater tolerance for temperature transients but also had about 2.5 times the sensitivity of an HP transducer of equivalent stroke. The basic stability of the length measurement system associated with the creep cell was obtained from a test on a 304S/S cylinder 38mm diameter and 82mm long. Over a time period of 9720 minutes, 1106 measurements of length change were taken while the steel cylinder was under a small constant load of 0.27 ± 0.002MPa and at a constant temperature of -18.81 ± 0.02°C. The average of all length readings was 1265.8mv with a standard deviation, SD, of 0.12mv. Omitting data for a 20 minute period during each room defrost cycle, the SD was reduced to 0.10mv. The length reading data for the first and last 540 minute time periods gave mean values of 1265.73mv and 1265.75mv respectively with SD of 0.062mv and 0.050mv. The long term stability of the displacement transducers was evaluated on three separate occasions over a period of 5 to 7 days. To minimize temperature transients, the defrost cycle for the cold room was changed from 180 minutes to 560 minutes and has worked very satisfactorily for over two years.

It should be mentioned that using a readout module in the data acquisition system that permitted reading to 0.01mv did not reduce the error in the long term stability of the displacement transducer below 0.1mv. Thus, a strain rate

number good to within 10% of its value requires a one millivolt change in displacement transducer reading. If one allows one day (1440 minutes) for this 1mv deformation, then the lower bound or strain rate measurement would be about $6 \times 10^{-11} sec^{-1}$.

The alignment pin on the base of the load frame assured precise alignment of the sample cell. The alignment of the sample and top cap was done by visual inspection as the loading piston was slowly lowered into contact with the steel ball sitting on the top cap. If needed, adjustments were made until the sample was visually perfectly aligned. A small seating load of about 0.1MPa was applied to the sample during the thermal equilibration period of 12 to 72 hours. Data recorded during the thermal equilibration established that: (1) temperature control was adequate; and (2) strain and strain rate were sufficiently small that a coolant leak into the sample was unlikely. Generally, samples were equilibrated overnight, which produced a net strain of <0.005%; even samples left for 3 days only strained 0.008%. Strain that occurred during equilibration was not included in sample strain computations. Zero strain was based upon the average displacement transducer reading the hour before application of the test load. The seating load was included as part of the test load or deviator stress.

To initiate a creep test, the valve between the loading

piston and the air pressure regulator was closed, the regulator adjusted to the desired pressure, and the valve to the loading piston opened. Data were generally recorded every minute during the start of the tests. The opening of the valve to apply the load was done five seconds prior to the time when the deformation transducer would be read automatically. The first deformation reading after the valve opening was defined as time zero. Figure III-15 shows a continuous record from load and deformation transducers when the valve was opened at -5 seconds. Time equal zero in Fig. III-15 corresponds to the above definition of t = 0. The blip on the strain curve at -0.5 sec is an artifact which occurred at the time the data acquisition system read the deformation transducer. While this determination for t = 0 was not ideal, it did provide a t = 0 time that was at most 5 to 10 seconds after the start of load application. Any error from this timing procedure was not considered important because initial modulus data were not taken.

The load recorded in Fig. III-15 was the load measured by the load transducer at the air regulator, not in the cylinder for the loading piston. Thus, at time -5 sec the load on the sample was the seating load. The sample loading from time -4.5 to 0 sec probably is given by the curve shown in Fig. III-15, while at time -5 sec the load was 0.05MPa and increased to 3.1MPa at -4.5 sec. This interpretation would be consistent

with the strain curve. From the several continuous recordings made several months apart on different samples, it was concluded that it took between 2.5 and 4 seconds to achieve a stable load condition. Once established, this stable load was constant to within 0.002MPa except when the supply air pressure dropped excessively or ice accumulated in the air supply line.

200μm

200μm

Fig. III-1 Scanning Electron Photomicrographs of +250μm Fraction of MFS

200μm

100μm

Fig. III-2 Scanning Electron Photomicrographs of 250-150μm Fraction of MFS

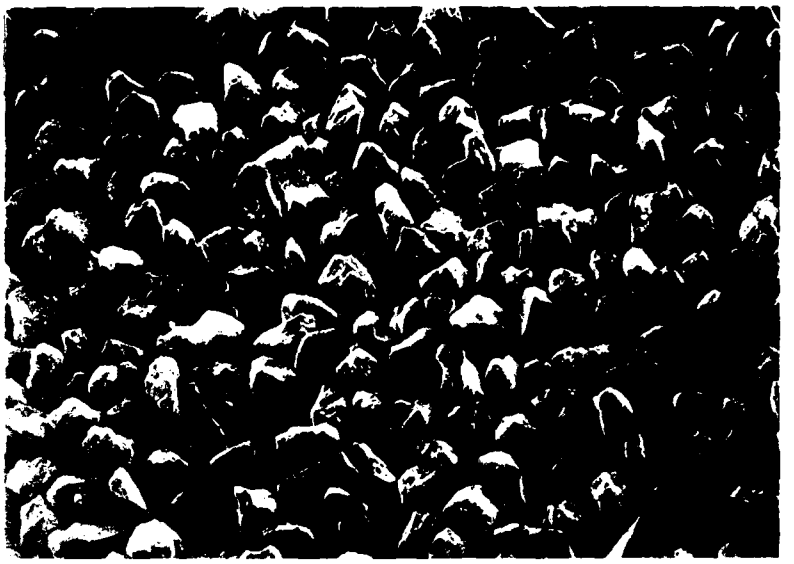

200μm

100μm

Fig. III-3 Scanning Electron Photomicrographs of 150-74μm Fraction of MFS

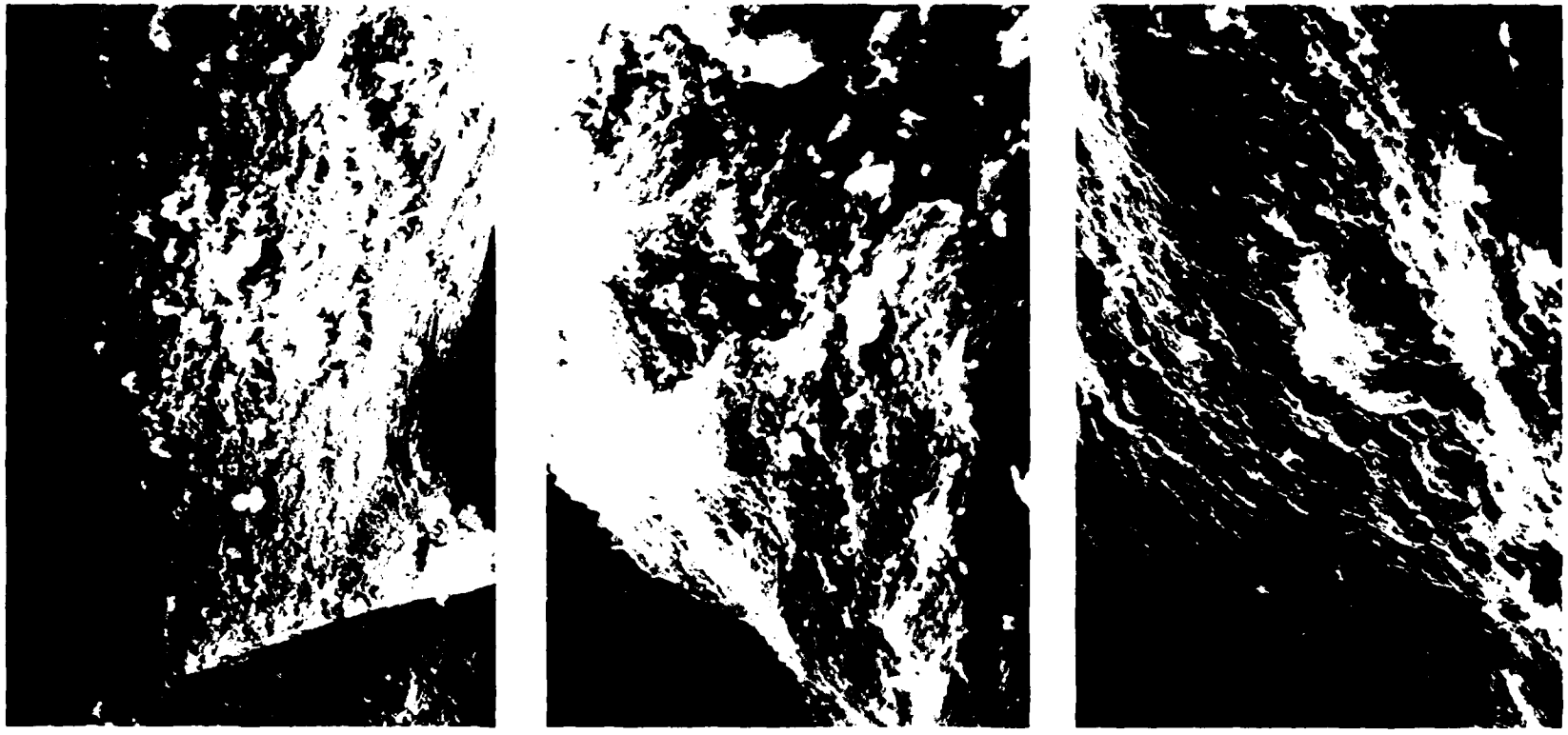

Fig. III-4 Scanning Electron Photomicrographs of MTS Mineral Grain Surfaces at 5000X; a) Mica, b) Feldspar, c) Quartz

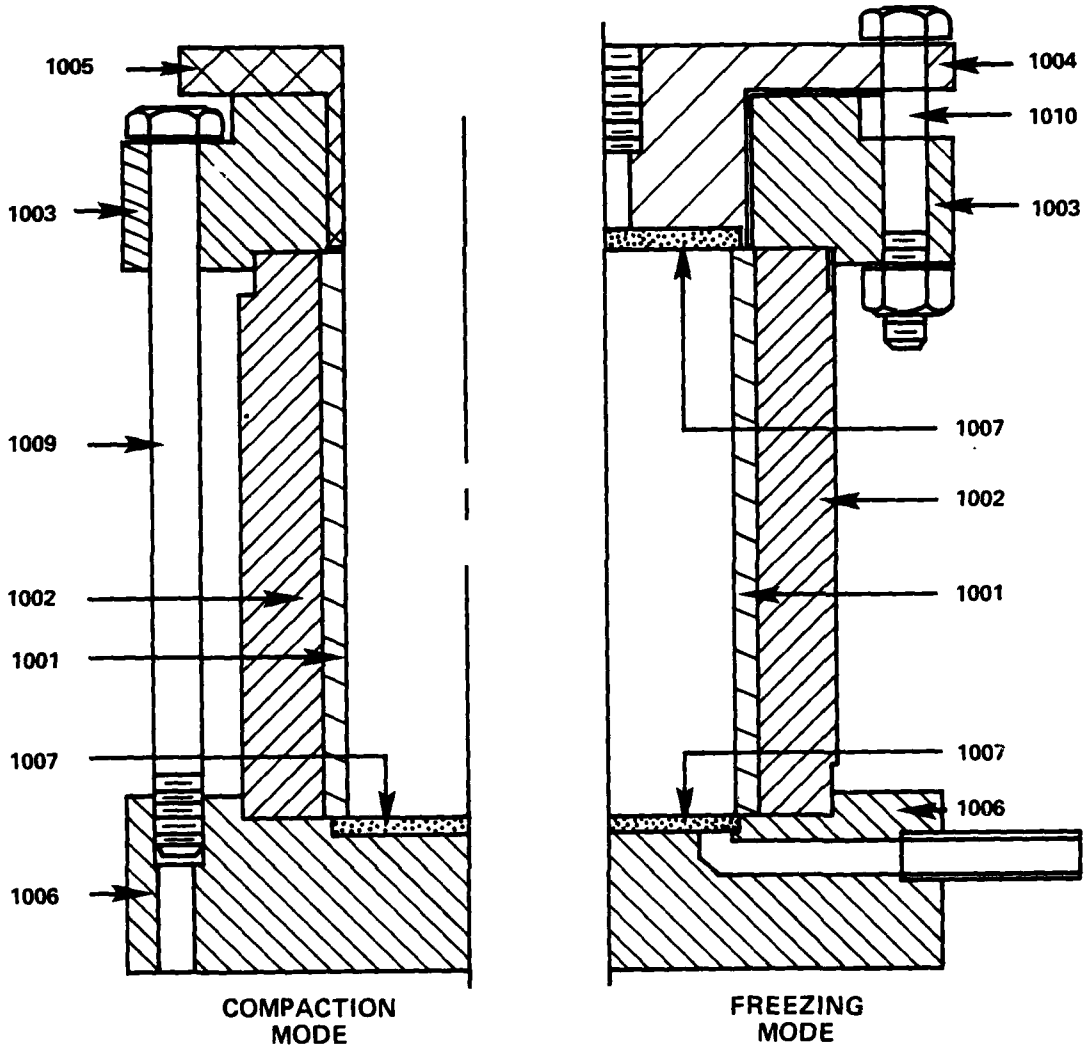

Fig. III-5 Compaction - Freezing Mold

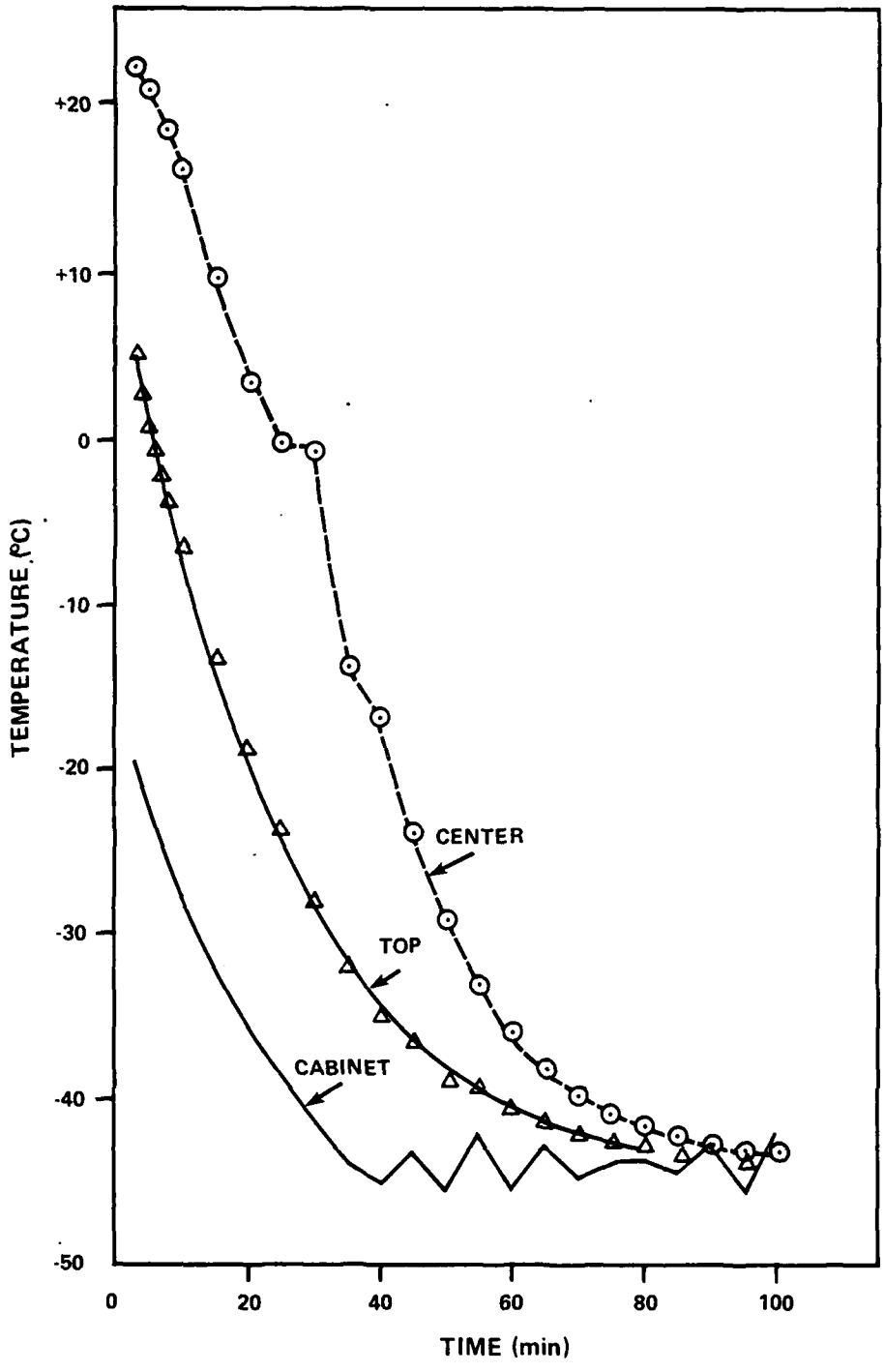

Fig. III-6 Cooling Curve for Partially Saturated MFS

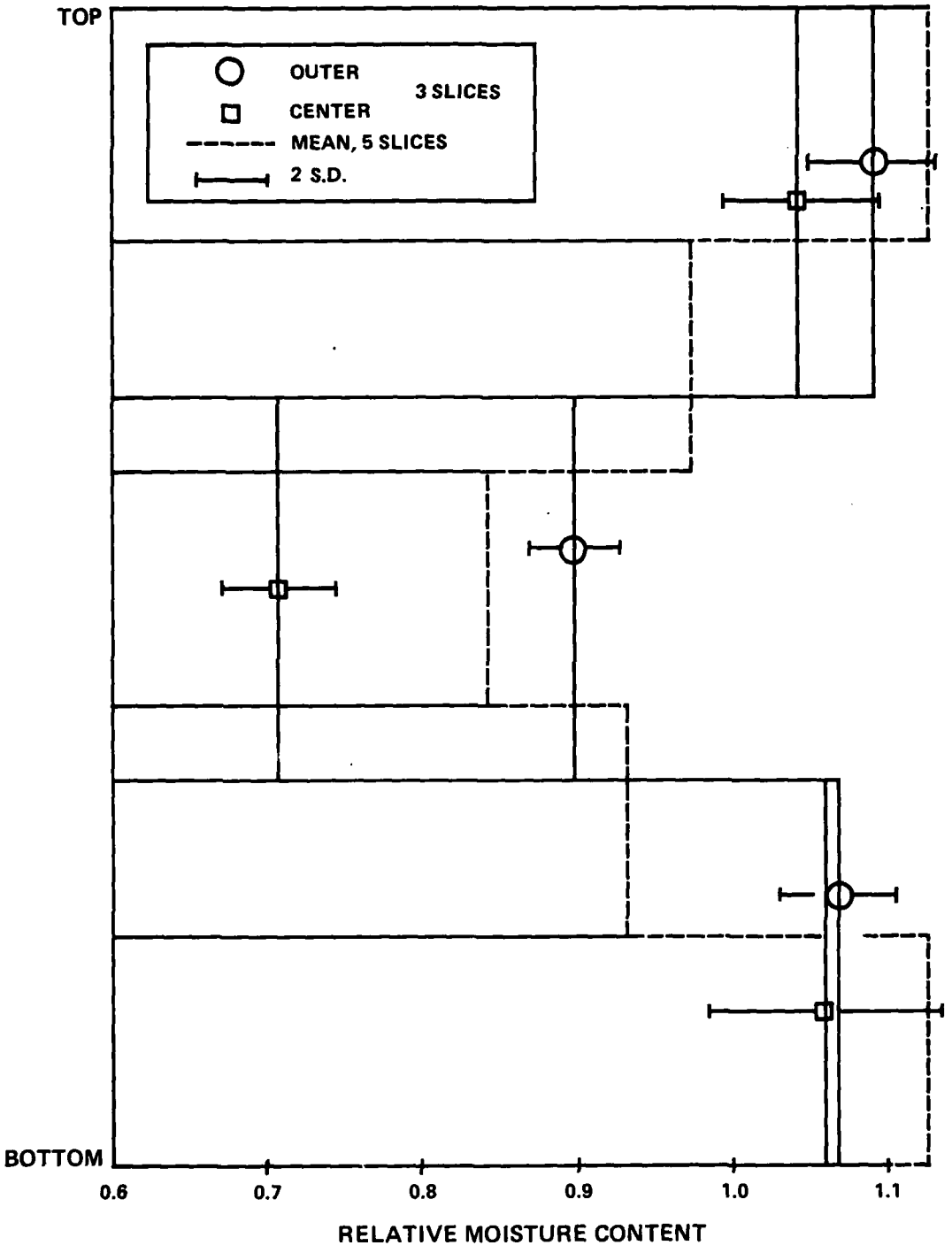

Fig. III-7 Moisture Distribution in Frozen Partially Saturated MFS

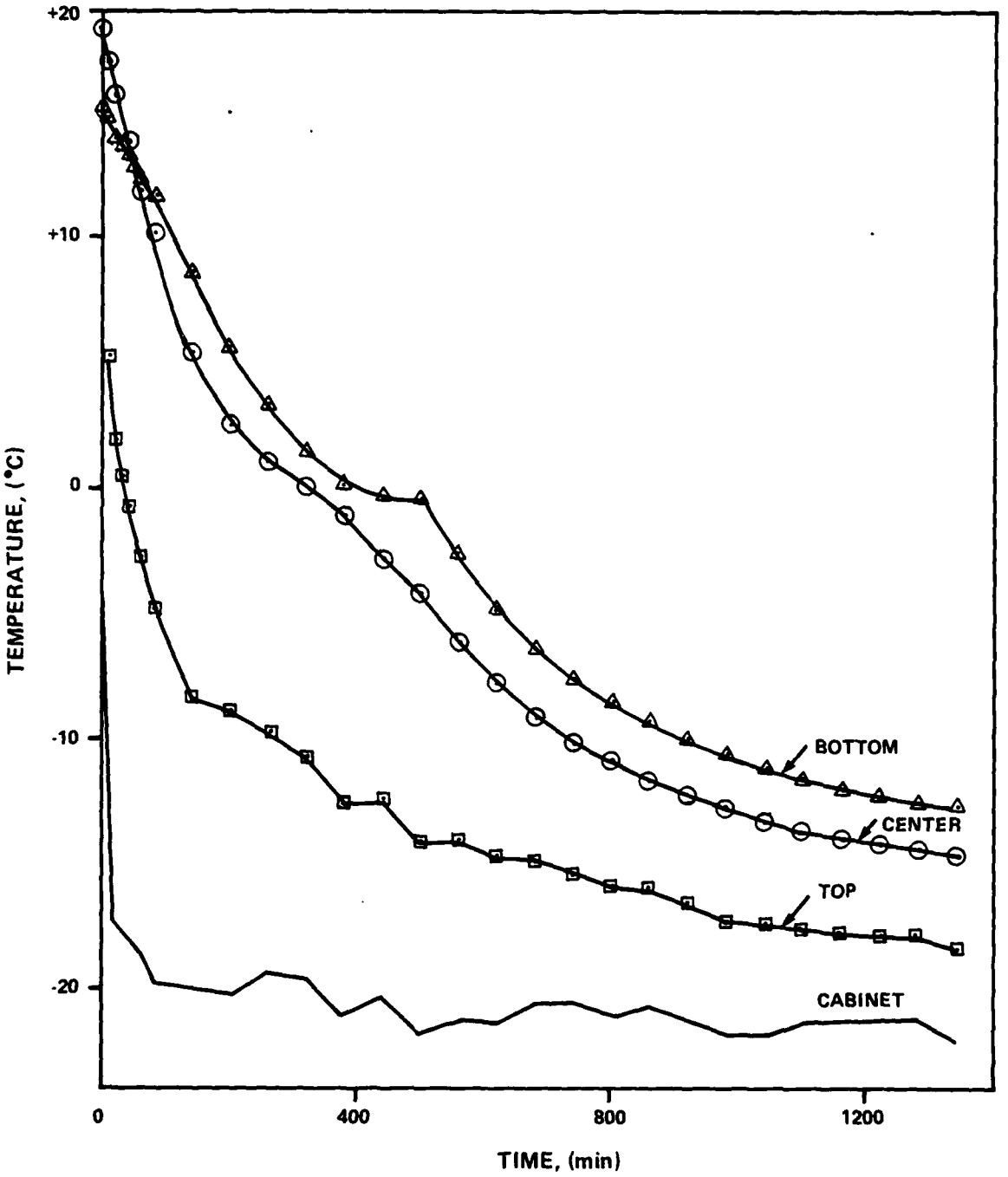

Fig. III-8 Cooling Curve for Saturated MFS

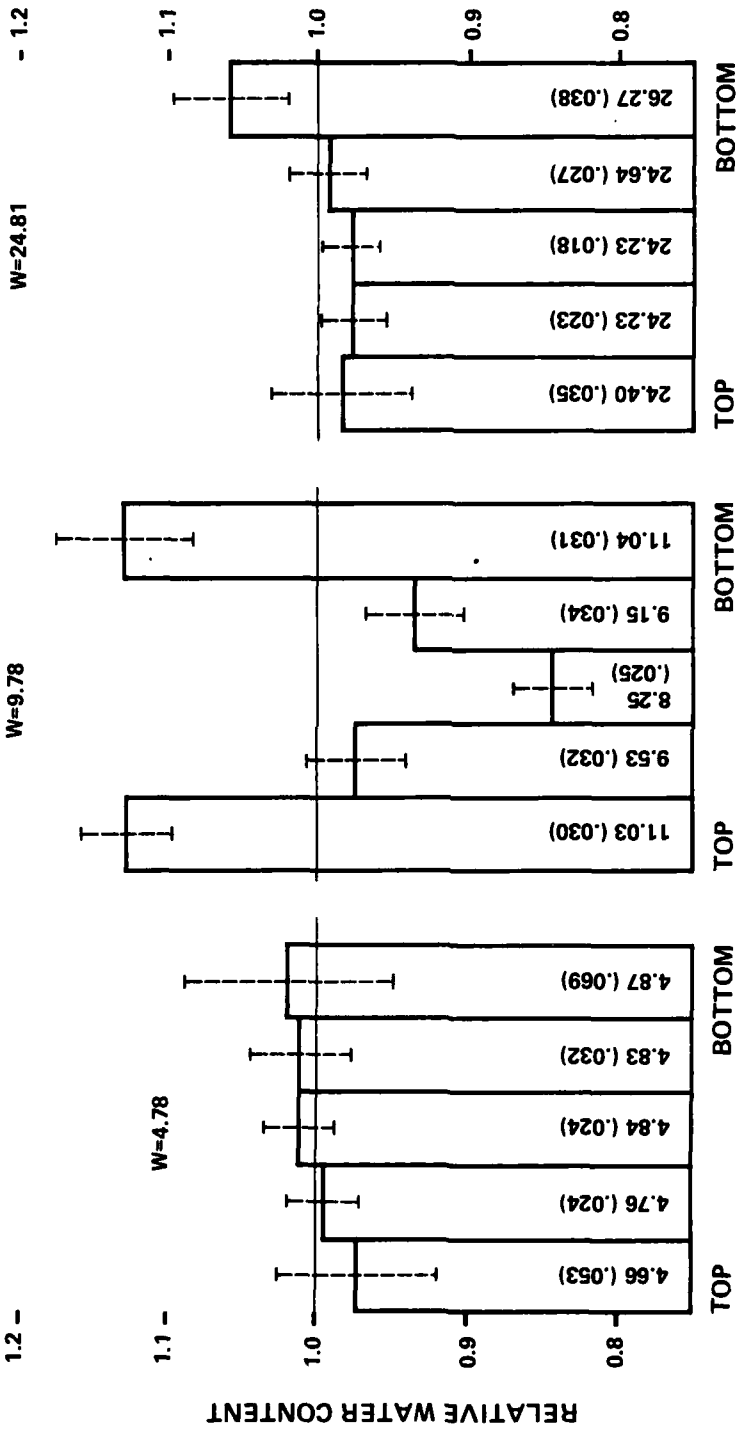

Fig. III-9 Moisture Distribution in Frozen MFS at Different Average Water Content

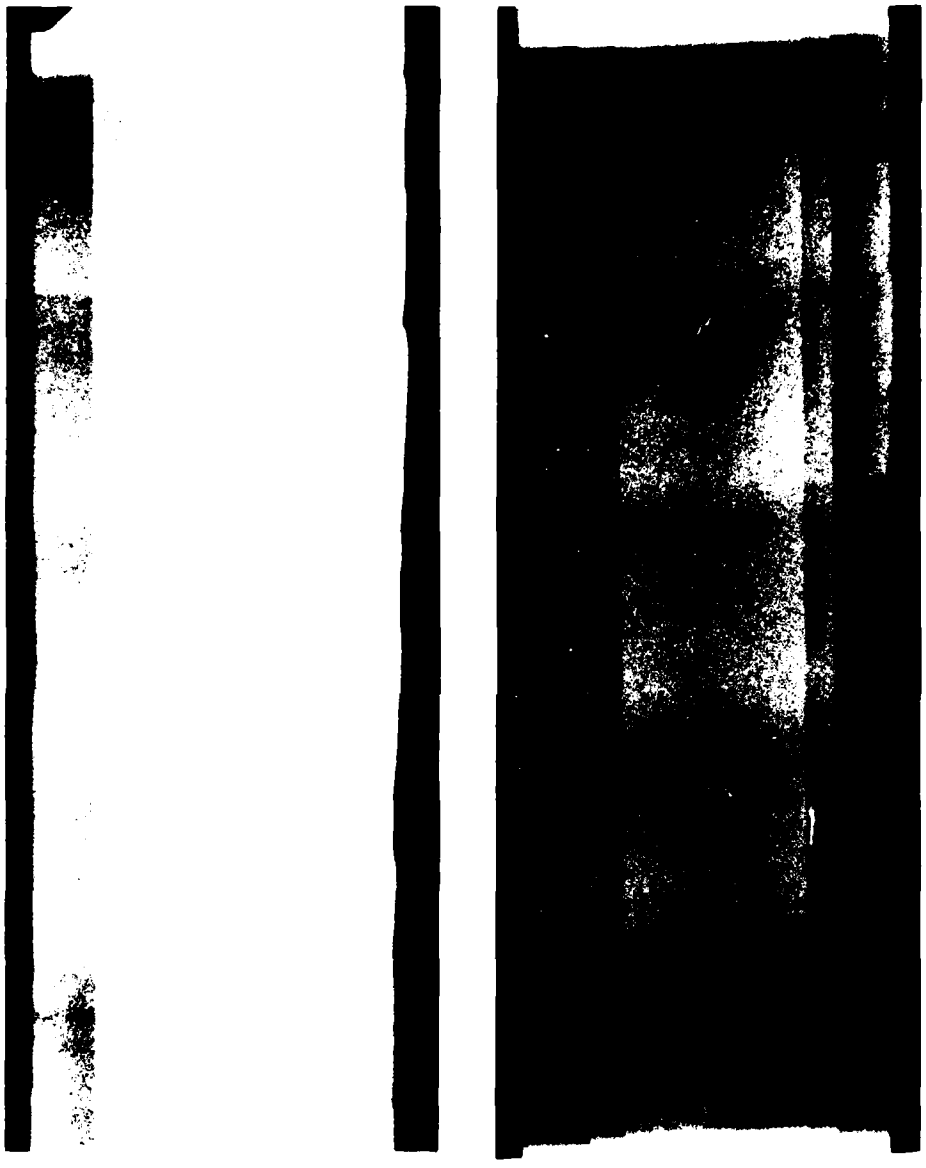

a) b)

Fig. III-10 Radiographs of Compacted and Frozen Manchester Fine Sand
a) Sample S9-52 (w = 10%)
b) Sample S9-153 (w = 25%)

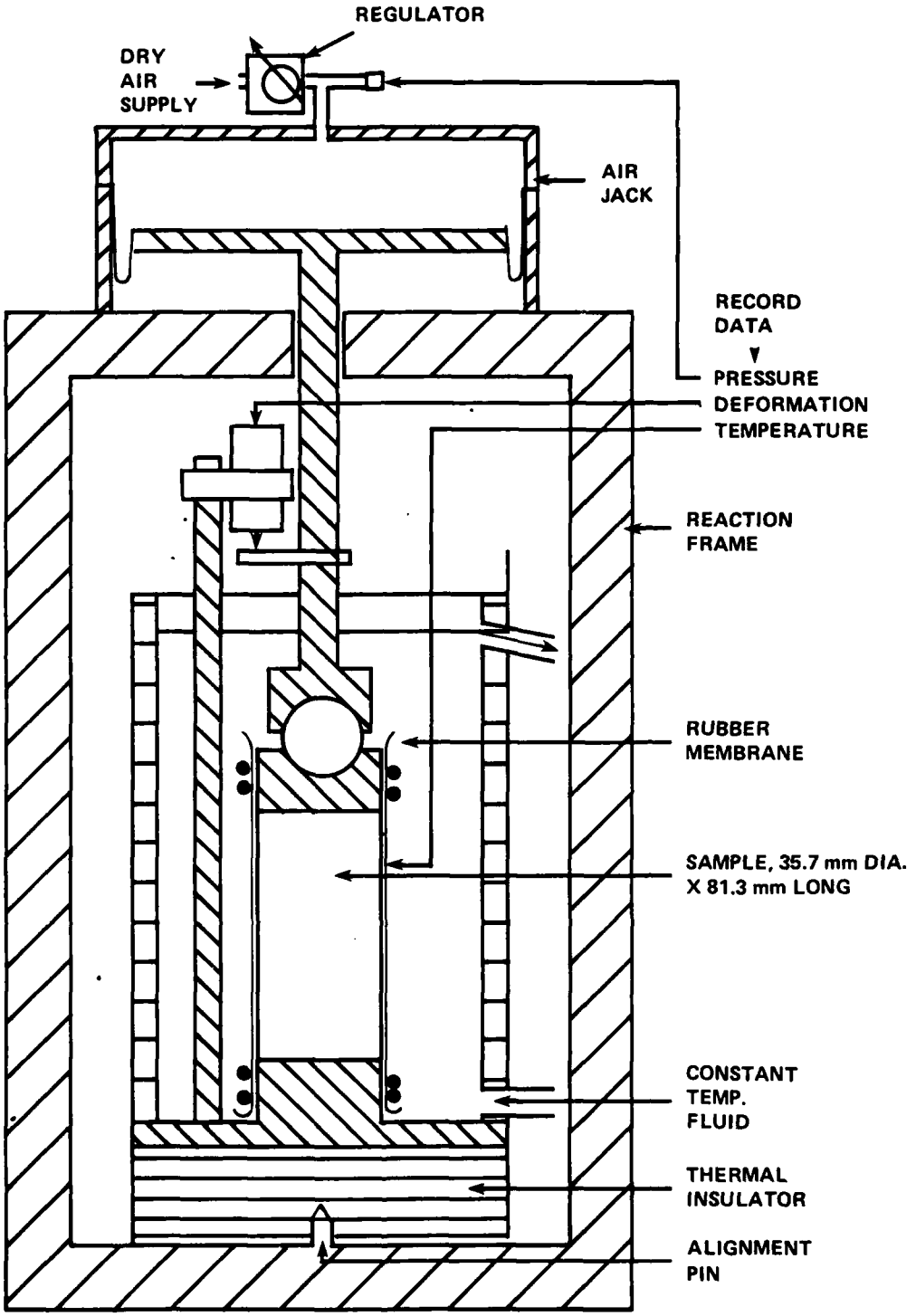

Fig. III-11 Schematic for Constant Load Creep Cell

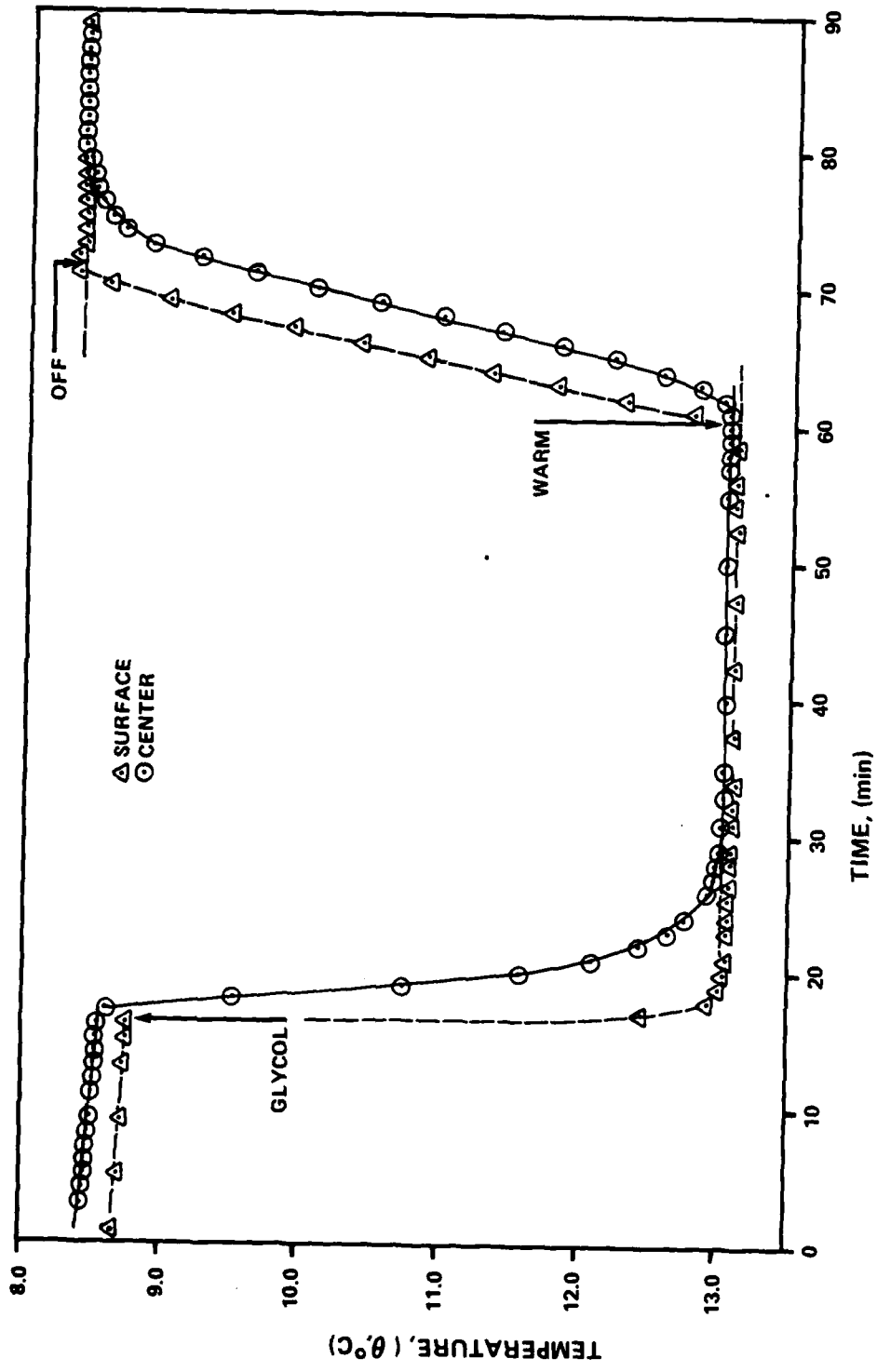

Fig. III-12 Temperature Equilibration after a Temperature Change: Slow Heating

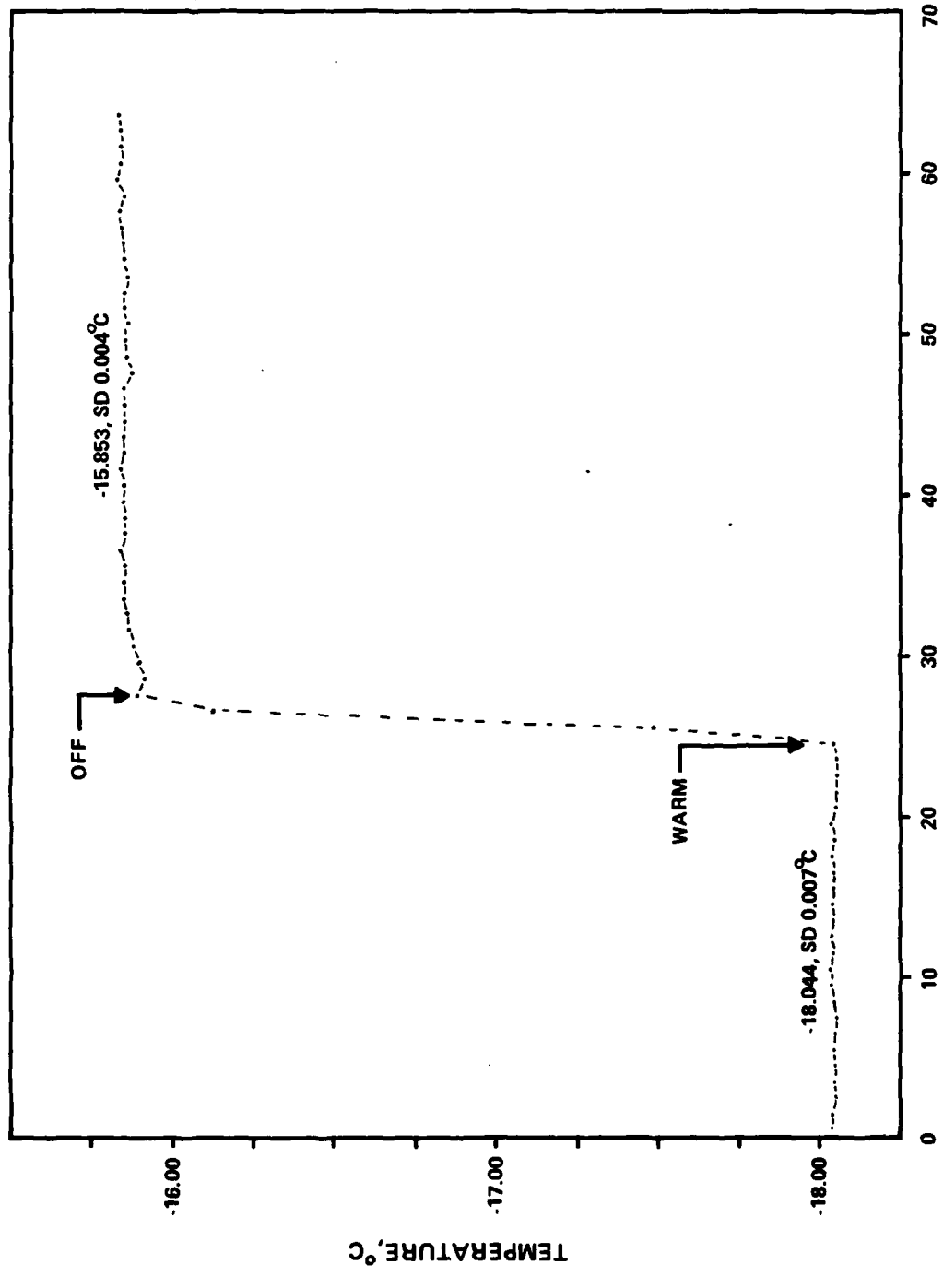

Fig. III-13 Temperature Equilibration after a Temperature Change: Rapid Heating

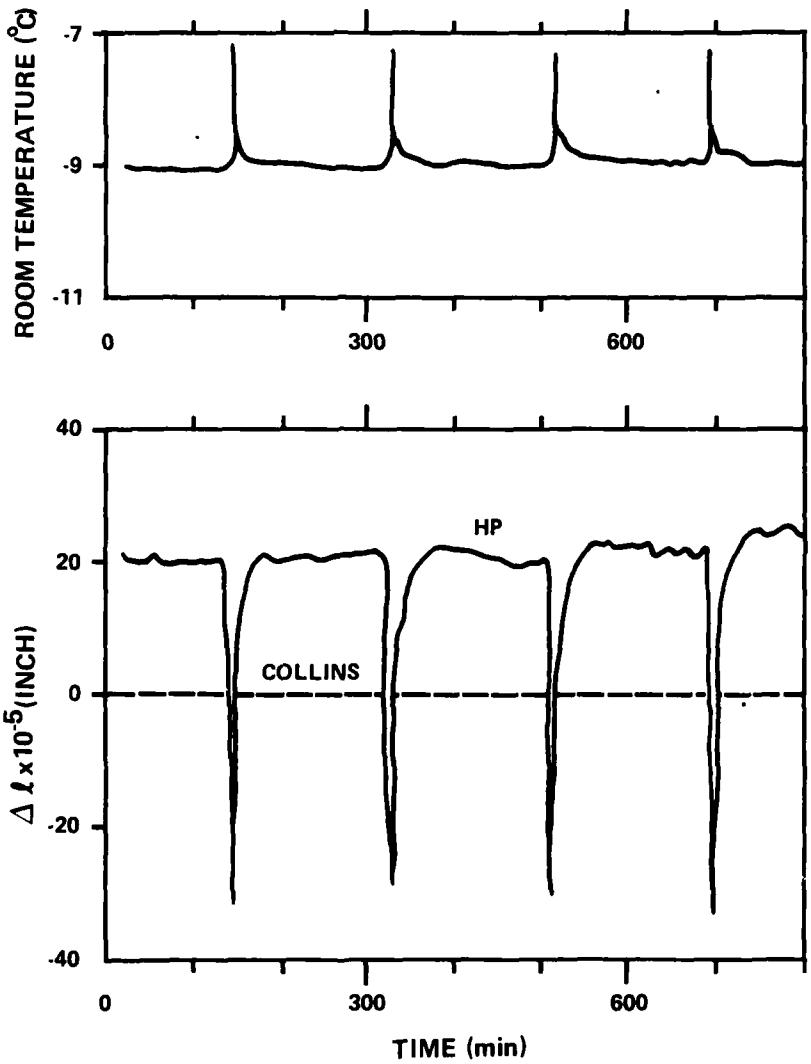

Fig. III-14 Effect of Temperature Change on Displacement Transducers

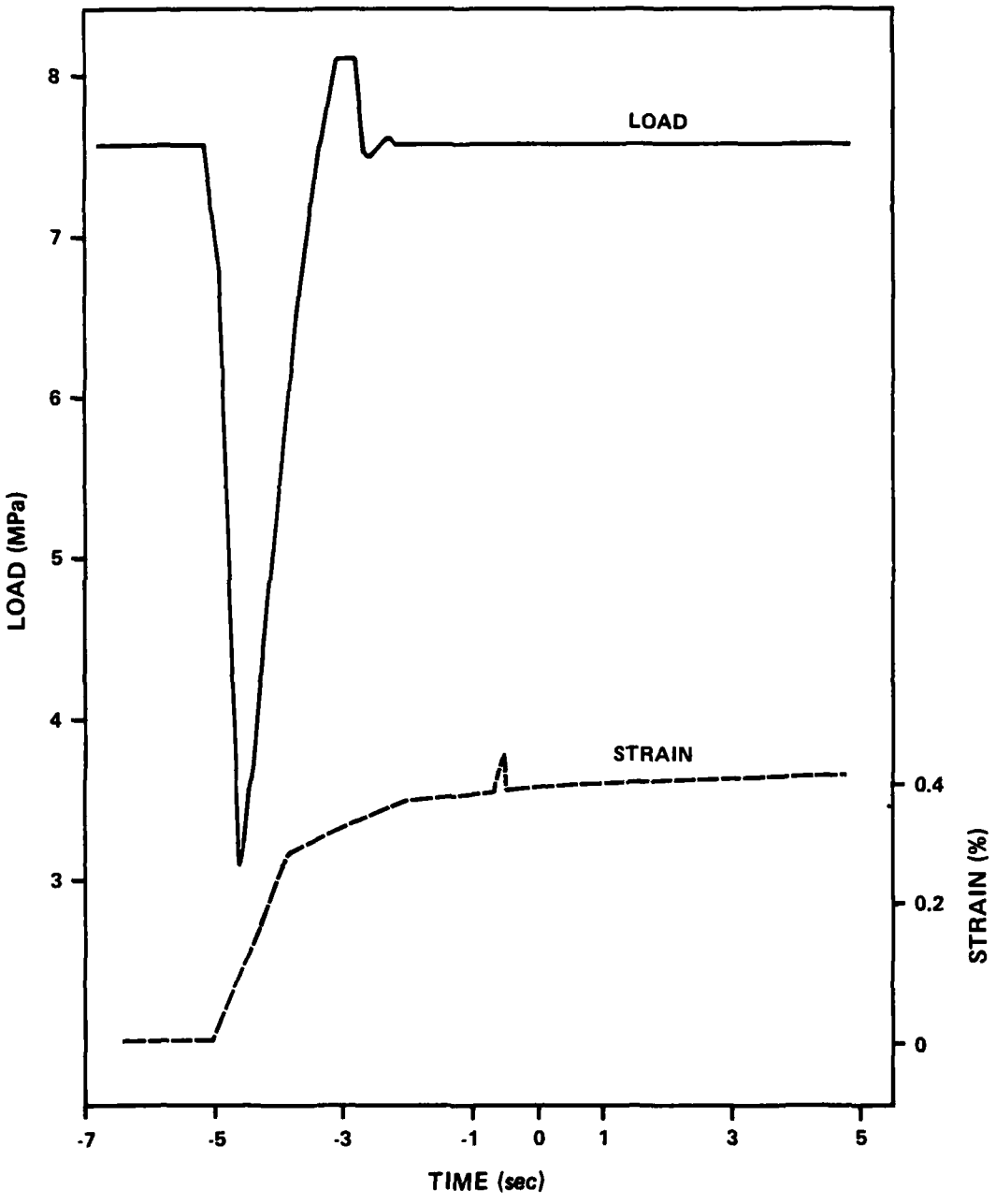

Fig. III-15 Time Required for Load Application

IV. RESULTS

The detailed results for each sample, as well as the actual creep data, are available on magnetic tape at CRREL (Martin, Sayles, and Ting [1981]). Before discussing the results, a brief consideration of the errors involved in material properties, control parameters, and strain are presented. Strength data are reported first in order to establish a possible upper bound for applied deviator stress. After illustrating various ways for representing creep data, the results in a form appropriate for RPT analysis are given. This Chapter ends with brief reports of miscellaneous test results that were obtained on creep of ice, on unfrozen water content for MFS and on specific heat of MFS.

A. Errors

The samples as prepared introduce unavoidable errors to the material properties. A large batch of the starting material Manchester Fine Sand, MFS, was thoroughly mixed in an attempt to ensure that all subsamples would be identical. Measured properties of the material were water content, w, and relative density, D_r. From the weighing error associated with the balance used to measure water content, the error in water content will be ± 0.1g water/100g soil irrespective of w. Thus, the percent error in water content is 1.7 when w = 5% and decreases to 0.3% error when w = 25%. The error in

relative density, D_r, involves measurement of sample weight and sample volume. Even with the coarse balance used to measure sample weight, the error in sample weight would not exceed 0.1%. Nominal sample volume was set by the compaction-freezing mold; however, the extruded samples, especially partially saturated ones, showed some variation in volume. The error in sample volume was about 0.3%. The error in relative density was to a good first approximation the same as the percent error in water content. For the nominal D_r at which most samples were prepared this yields $D_r = 55 \pm 1\%$ for $w = 5\%$ and $D_r = 55 \pm 0.2\%$ for $w = 25\%$ as the expected errors. Heterogeneity of the water content within a sample has been discussed under sample preparation. Efforts to measure heterogeneity of D_r within samples were completely unsuccessful because the available methods and equipment caused excessive experimental errors in the measurements.

The magnitude of the deviator stress was calculated using the load applied to the loading piston as measured by the pressure transducer and the area ratio between the loading piston and a nominal sample area of $1000mm^2$. As already noted, when the equipment was functioning properly, the applied load converted to deviator stress, D, was constant within 0.002MPa, which even for a small load of 3.5MPa amounts to an error of only 0.06%. The initial sample area was not constant but had an inherent error of 0.3%, so that the error

in D was controlled by the error in sample area. Further, as the sample strains the area will increase and the deviator stress must decrease since the applied load was constant. Assuming constant volume and uniform strain, the decrease in deviator stress would be directly proportional to the increase in strain. Any correction for the area effect would be artibrary and was not made. In this report, the deviator stress, D, was based on the nominal initial sample area; therefore, D may be in error by several percent and will vary during a test even though the load was constant. Load fluctuations of less than 1% have a marked effect on strain rate as shown in Fig. IV-1. Moisture (ice) in the air supply line was the cause of these load fluctuations. The rapidity of response to small load changes is evident in Fig. IV-2, which is a detail from Fig. IV-1.

When experimental control of the adjustable variables, temperature and load, was good the strain rate gave a fairly smooth curve as shown in Fig. IV-3. The influence of poor temperature control on strain rate is illustrated in Figs. IV-4 and IV-5. During test S8-43, the cooling coil for the constant temperature circulator started to ice up and the mean temperature change of 0.12°C clearly was reflected in the strain rate plot, Fig. IV-4. A numerical estimate for the influence of temperature fluctuations on strain rate over the observed range of temperature fluctuations is given

in Table IV-1. The coefficient of variation, CV, is defined as 100 times the standard deviation divided by the mean value. The next to last column in Table IV-1 gives CV observed during a particular test with temperature variations as shown. From the experimental error in measuring deformation one expects the coefficient of variation to decrease if a larger deformation increment (longer time) is used for calculation. The last column in Table IV-1 gives the CV calculated assuming that the only error in strain rate was from the expected error in the deformation increment. It should be noted that there was good load control for the tests given in Table IV-1. Good temperature and load control gave strain rates that were within the expected error from the deformation transducer. For frozen MFS, temperature control to 0.10°C gave a strain rate variation that was dependent upon the error in the deformation increment. A temperature fluctuation of 0.04°C gave a strain rate variation three times larger than could be attributed to error in the deformation increment.

B. Strength

1. Testing

The so-called "instantaneous strength" of frozen soil is an ill-defined quantity which is very strongly dependent on strain rate. Rapid strain rate controlled unconfined (uniaxial) compression strength tests were run in an effort to determine the strength at the strain rate corresponding to the ductile-brittle transition. The tests were run on the MTS testing facility at CREEL at strain rates between 1.6 and 0.01 sec^{-1}. The first set of strength tests were run using visual sample alignment. The strength variation for presumed identical samples was 50 to 100%. It was assumed that the highest strength resulted from better sample alignment and was more likely the correct value for that strain rate. A special set of alignment jigs were then prepared and the variation in strength on identical samples was reduced to less than 5%, with the mean value being the highest strength observed in the original tests.

Samples were equilibrated for 24 hours in a cold room set at the desired test temperature between -10°C and -20°C. Samples were transported to the MTS testing facility in a well insulated box containing a large quantity of ice at the test temperature. Each sample was quickly transferred (about 1 min.) to the environmental test chamber on the MTS machine

and allowed to equilibrate for 15 to 20 minutes before the strength test was performed. Temperature control in the MTS environmental chamber was about 0.2°C.

2. Results

Strength data are summarized in Table IV-2 where D is the peak deviator stress = applied load divided by initial sample cross section area. The samples numbered 7- are for the highest strength measured at each temperature because of the alignment problem discussed under test method. For the partially saturated samples, nominal strain rates of 1.6 and $0.18s^{-1}$ gave essentially the same strength, suggesting that a strain rate was reached where strength was no longer dependent on strain rate. At very high strain rates, inertia affects the strength results. According to Whitman (1979) inertia effects will be negligible as long as the product of compressional wave velocity, C, times the failure time, t, is greater than ten times the sample length, L; i.e. $Ct > 10L$. Nakano et al. (1972) gave dilational wave velocity for frozen soils at -10°C from 4.4×10^6mm/sec on Ottawa Sand down to 3.5×10^6mm/sec on clay. The shortest time to failure for the strength data in Table lV-2 was 4.68msec. Thus Ct was greater than 16.4m, which is very much larger than 10L of 0.8m. Therefore, even if the time to failure were 0.25msec, there would still be no inertia effect.

Figure IV-6 shows the effect of temperature on the unconfined strength of partially saturated and saturated samples. The saturated samples gave an average increase in strength of 1.5MPa/°C, while the partially saturated samples increased 0.65MPa/°C. In contrast to the partially saturated samples, the strength of saturated samples was strongly dependent on strain rate, as illustrated in Fig. IV-7. Visual observation of the fracture on saturated samples indicated that the two higher strain rates definitely failed by brittle fracture, while for the lowest strain rate the sample bulged at failure indicating ductile fracture. The nature of the visual observations are evident from the photos in Fig. IV-8. However, the strength-strain rate plot showed no change in slope at the ductile-brittle transition, which was visually observed to be approximately at a strain rate of $0.02s^{-1}$.

Based upon the available data, the recommended estimates for instantaneous uniaxial or compression strength of Manchester Fine Sand as prepared herein are:

$$\text{saturated; } D_u(\text{MPa}) = 10.1 + 1.5\theta$$

$$\text{partially saturated; } D_u(\text{MPa}) = 0.65 + 0.65\theta$$

where θ is °C below 0°C.

C. Basic Creep Behavior

The usual way of plotting time dependent deformation from a constant load in uniaxial compression is from a strain-time plot. Experimental data points of strain, ε, vs. time, t, are given in Fig. IV-9 for MFS which show the usual creep states: (1) an initial instantaneous elastic deformation, (2) a stage of decelerating creep, (3) a stage in which strain rate appears to become constant for a time, and (4) a stage of accelerating creep. The terms primary, secondary, and tertiary creep are usually applied to stages two through four respectively. Secondary creep has often been referred to as "steady state creep" but in general secondary creep should be regarded as the transition zone from decelerating to accelerating stages of creep. Herein the secondary creep rate is defined as the minimum strain rate, $\dot{\varepsilon}_m$, for this transition zone. The location of $\dot{\varepsilon}_m$ is much clearer from the ℓn-ℓn graphical presentation in Fig. IV-10, which used the same data given in Fig. IV-9. In order to avoid any ambiguity, two other terms associated with the minimum strain rate are defined:

t_m = time from load application to minimum strain rate

ε_m = total strain at the time of $\dot{\varepsilon}_m$

Individual data points make up the curves in Figs. IV-9 and IV-10 from which it is apparent that drawing a smoothed curve through the data points would not introduce any large

uncertainty. A series of creep curves at different temperatures and constant applied deviator stress are given in Fig. IV-11 for MFS at w = 10%. Again, the same data are plotted in Fig. IV-12 as $\ell n\dot{\varepsilon}$ vs. ℓnt where the position of minimum strain rate, $\dot{\varepsilon}_m$ is more clearly evident that in the ε-t plot of Fig. IV-11. It would appear that there is a unique relation between $\ell n\dot{\varepsilon}_m$ and ℓnt_m with a negative slope slightly greater than one. The data in Fig. IV-12 indicate that during the major portion of primary creep (stage 2) the $\ell n\dot{\varepsilon}$ - ℓnt plots are approximately parallel. The constant applied stress; D = 4.78MPa, for the tests shown in Figs. IV-11 and IV-12 gave a variable stress ratio, (D/D_u), from 0.34 to 0.58 because of the variable instantaneous strength, D_u, with temperature.

Detailed plots of $\ell n\dot{\varepsilon}$ vs. ℓnt for a series of different applied stresses at constant temperature for MFS at w = 10% in Fig. IV-13 indicate that the same type of behavior is evident whether θ or D was the variable. The stress ratio covered by Fig. IV-13 was about the same as for Fig. IV-12. Fig. IV-14 shows that ice saturated, w = 25%, MFS samples have the same general trend as partially saturated samples. The plot of $\ell n\dot{\varepsilon}_m$ vs. ℓnt_m yields a good linear relation for w = 10% and for w = 25%, as shown in Fig. IV-15 which summarizes data for a range of temperature and deviator stress. The scatter about the regression line was less for w = 10%, and

the partially saturated MFS also gave a slightly greater slope. Data for all single stage creep tests are summarized in Tables IV-3, IV-4, and IV-5.

The regression lines in Fig. IV-15 fit the data fairly well, which implies that ε_m is a constant (Ting, 1981a) However, inspection of the ε_m data in Tables IV-3 to IV-5 indicates that for a given water content, the strain at minimum creep rate, ε_m, showed a good deal of scatter with a coefficient of variation, CV, of 17.0% and 21.6% for w = 10% and w = 25% respectively. In Fig. IV-15, data points to the right of a given regression line generally had a high ε_m, while points to the left had low ε_m. Therefore, regressions of $\ell n\varepsilon_m$ vs. ℓnt_m were computed for data points of approximately constant ε_m. The results in Table IV-6 for w = 25% indicate that the slope was approximately independent of ε_m, but with a significant improvement in the regression fit as shown by the higher values of r^2. For w = 10%, the trend with ε_m also was evident; however, the $\dot{\varepsilon}_m$ range for a given ε_m was rather narrow for the w = 10% data. These few data suggest ε_m is a material property that is independent of stress and temperature.

In Fig. IV-15, the creep rate minima point only was plotted because the complete $\dot{\varepsilon}$-t curve for all samples would have obscured the trend. However, all $\dot{\varepsilon}$-t curves were not as ideal as those shown in Figs. IV-10, -12, -13, and -14. The worst four such curves for w = 25% MFS are given in Fig. IV-16.

Details of total available data on each sample provide evidence that could explain the shape of these plots. Sample S9-86 was the first specimen prepared by a new technician, where from the notes made on the sample preparation sheet it is extremely doubtful if the sample was saturated. The fact that the sample completely "crushed" at 6.48% strain would suggest an unsaturated sample because "good" saturated samples strained to 10 to 13% did not "crush". Further, at time 210 minutes during creep of sample S9-86, the applied load increased 0.1% for 10 minutes, then decreased to a value 0.06% above the earlier stable value. Sample S9-53 at the end of test was very badly cracked at one end, rather than the usual bulging that resulted from deformation. The reason for the end being cracked was the very low water content at that end. Sample S9-114 was also dry at one end, but not as extreme as sample S9-53. There were load fluctuations up to 0.05% during creep of S9-114. The collar on the mold broke during the freezing of sample S8-68, which must have produced unusual stresses in the sample. It should be noted that these really fairly small perturbations evident in the $\ell n\dot{\varepsilon}$ - ℓnt plots were not visible in the ε-t plots. The detail shape of the $\ell n\dot{\varepsilon}$ - ℓnt plot is suggested as a possible indicator of even fairly small experimental variability.

The data considered so far have all been for tests where the strain rate minima, $\dot{\varepsilon}_m$, was greater than 10^{-8} sec^{-1}.

The shape of the $\ell n\dot{\varepsilon}$ - ℓnt plot changes for test conditions that lead to $\dot{\varepsilon}_m$ less than $10^{-8}sec^{-1}$, as shown in Figs. IV-17 and IV-18. There appears to be a critical stress ratio, D/D_u, below which a pronounced slowdown in creep rate occurs. Possibly the change in curve shape is not a change in mechanism but merely reflects that the stress ratio is sufficiently small to permit secondary creep (3rd stage) to fully develop. For the sample at $D/D_u = 0.291$ in Fig. IV-17, a creep rate minima was reached at about 10^4 minutes, and based upon the projection of the regression line ($\ell n\dot{\varepsilon}_m$ - ℓnt_m) one would not expect the creep rate to increase until $t = 1.5 \pm 0.3 \times 10^5$ minutes. At D/D_u greater than 0.3 for MFS at w = 10%, the start and end of secondary creep are masked, most probably by the increasing stage four to such an extent that one only observes an inflection point $\dot{\varepsilon}_m$ in the $\ell n\dot{\varepsilon}$ - ℓnt plot. Since no test that reached very low creep rate was carried into clear tertiary creep (stage 4) means that the regression lines in Fig. IV-15 may be valid to $\dot{\varepsilon}_m$ of $10^{-10}sec^{-1}$ where $\dot{\varepsilon}_m$ now represents the end of secondary creep. In fact, Jacka (in Lile, 1979) has run tests on ice where it took over two years to reach tertiary creep. His data show the same general trend as shown in Fig. IV-15 for frozen MFS.

The spikes in the $\dot{\varepsilon}$-t plot in Fig. IV-17 lasted from one to three days under constant applied load and temperature. To check for possible friction in the loading system, a load

cell was installed in the sample position that gave constant load for the 1.44×10^5 minutes of the test during which there were no measured deformation. The spikes appear to be valid data which suggests a "slip-stick" creep behavior perhaps analogous to glacier surging. Secondary creep appears to be anything but "steady state". It is interesting that the creep rate after a surge returned to about the same value. Deformation observed is the summation of individual motions in the sand skeleton and in the ice matrix. Thus, the observed slip-stick may be a function of the finite number of individaul motions. If true, the strain rate at which the slip-stick phenomenon would be observed should increase with decreasing sample size. This phenomenon deserves further study.

Both Figs. IV-17 and IV-18 contain $\dot{\varepsilon}$-t data for a pair of samples that had nearly the same temperature and load and which show good reproducibility in the $\dot{\varepsilon}$-t data under fixed conditions. Figure IV-19 contains data for a pair of nearly identical samples at a D/D_u of 0.505, which again indicate reasonable reproducibility.

The relation between strain rate at minima, $\dot{\varepsilon}_m$, and stress ratio, D/D_u, for MFS at w = 10% and w = 25% is given in Fig. IV-20. The band of data is broader for w = 10% than for w = 25%. The scatter appears to be to the left, high $\dot{\varepsilon}_m$ for given D/D_u, for w = 25% and in the opposite direction for w = 10%. The solid data points for each nominal water content

were omitted from the repression calculation based solely upon visual inspection. For w = 25%, the four solid circle data points arbitrarily omitted from the regression turn out to be the anomalous four samples shown in Fig. IV-16. The temperature range covered in Fig. IV-20 was from -11 to -21°C and from -11 to -27°C for w = 10% and w = 25% respectively. Two thirds of the data for w = 10% were at $\theta = 18 \pm 0.5$°C, for which the goodness of fit showed some improvement, r^2 increased to 0.953 with no significant change in the regression coefficients. For w = 25%, only one quarter of the data points were at constant θ of 18 ± 0.5°C and there was no change in r^2. Apparently for ice saturated MFS the temperature dependent stress ratio accounts for nearly all the experimental temperature variation in $\dot{\varepsilon}_m$.

The instantaneous strength, D_u, was for a strain rate of 0.02sec^{-1} based upon the available data. The regression equation for w = 10% in Fig. IV-20 gives $\dot{\varepsilon}_m = 0.026\text{sec}^{-1}$ at $D/D_u = 1.0$. Data points at the high end of the regression line for w = 25% all fall below the line; therefore, the regression was recalculated using data for $\dot{\varepsilon}_m > 10^{-6}\text{sec}^{-1}$ only, which then gave $\dot{\varepsilon}_m = 0.035\text{sec}^{-1}$ at $D/D_u = 1.0$. Since D_u was for a strain rate $\dot{\varepsilon}$ of 0.02sec^{-1}, the mean strain rate of 0.035sec^{-1} at $D/D_u = 1.0$ only confirms that the $\dot{\varepsilon}_m$ vs. D/D_u data in Fig. IV-20 constitute a consistent pattern. At a given D/D_u, the material with the higher ice content (w = 25%)

always gave a higher $\dot{\varepsilon}_m$. Data at very low ice content, w = 5%, could not be plotted because no D_u data were available.

The data thus far were all nominally at a relative density, D_r, of 55% although there were variations as shown in Tables IV-3 through IV-5. A brief investigation of deliberately varying D_r was made and the results summarized in Fig. IV-21. The strong effect indicated for D_r on $\dot{\varepsilon}_m$ on MFS at w = 10% may help explain the larger scatter in Fig. IV-20 for partially saturated samples. The shape of the $\dot{\varepsilon}_m$ - D_r curve for w = 25% is the same shape curve observed by Mellor and Smith (1966) for compacted snow samples.

D. Rate Process Theory

In order to understand how the parameters derived from rate process theory (RPT) were obtained, a detailed example for each type of analysis will be presented along with tables and graphs summarizing results for each of the analyses. The sequence of presentation for each nominal water content will be temperature stage, $\Delta\theta$, and $\dot{\varepsilon}_m$ data leading to ΔF and S_β followed by stress stage, ΔD, and $\dot{\varepsilon}$-D at constant time leading to S_α.

1. Saturated MFS (w = 25%)

The basis for temperature stage analysis to compute the experimental activation energy, E, is Eq. (II-23), given below

in general form:

$$E = \frac{RT_2T_1}{T_2-T_1} \ln \left[\frac{\dot{\varepsilon}_2 T_1}{\dot{\varepsilon}_1 T_2}\right]_{t,s,D} \qquad \text{(IV-1)}$$

The applied load, D, was constant throughout any particular test. The test starts at temperature T_1 and at some time the temperature is changed to T_2. Strain was recorded at frequent intervals during the test so that strain rate, $\dot{\varepsilon}$, at any time could be computed. Strain rates for use in Eq. (IV-1) were obtained graphically from either $\dot{\varepsilon}$-t or $\dot{\varepsilon}$-ε plots as shown in Fig. IV-22. For consistency the strain rates at the two temperatures were taken at the time when the temperature change was started. The strain rate, $\dot{\varepsilon}_1$, was essentially the same whether evaluated graphically at time t as indicated in Fig. IV-22 or analytically from the strain time data. Strain rate $\dot{\varepsilon}_2$ at temperature T_2 was obtained by extrapolation back to time t. The first data point used for determining the slope of the line after the start of the temperature change was ten minutes minimum. As discussed earlier, ten minutes was adequate for the center of the test specimen to attain essentially all of the imposed $\Delta\theta$. Very frequently data points at time less than t+10 would fall on the line of $\dot{\varepsilon}$-t or $\dot{\varepsilon}$-ε but were not used to establish the position of the line. In Fig. IV-22 the t+9 data point falls on the line. Generally, the linear fit was better on the $\dot{\varepsilon}$-t plot, but there were times when a better fit was

obtained on the $\dot{\varepsilon}$-ε plot; however, the computed E was essentially constant using either method as shown by the data in Fig. IV-22. Refinement using a least squares fit to the data for determination of $\dot{\varepsilon}_1$ and $\dot{\varepsilon}_2$ had an insignificant effect on E.

As many as four temperature changes were imposed on a single sample. The data summarized in Table IV-7 include data from successive temperature stages on a number of samples. There appears to be no pattern to the direction or magnitude of the change in E for successive temperature stages. The time of temperature change in Table IV-7 is expressed as a fraction of the time to minima, t_m. The value of t_m was calculated based upon the applied load and temperature for the first stage of the test. These input data and the regression line equation for $\dot{\varepsilon}_m$ vs. D/D_u gave a calculated value of $\dot{\varepsilon}_m$, which was then inserted into the regression line equation for $\dot{\varepsilon}_m$ vs. t_m to give the value of t_m used to calculate t/t_m.

The dependence of the experimental activation energy, E, on stress is evident in Fig. IV-23. Although the data plotted in Fig. IV-23 show considerable scatter, the best least squares fit was for a linear relation between E and D, as predicted by RPT.

Recalling that $E = \Delta F - \beta D$, one obtains $\Delta F = 316 kJ/mol$ and $\beta = 0.014 m^3/mol$. The number of bonds per m^2, $S_\beta = \lambda N/4\beta$.

The jump distance λ was taken as 2.8×10^{-10}m, which represents the diameter of a water molecule or the diameter of an oxygen atom in a silicate structure. Avogadro's number N equals 6.0×10^{23}. Since the units of β are m^3/mol, the number of bonds/m^2 S_β equals $4.22 \times 10^{16}/\beta$ or $S_\beta = 3 \times 10^{15}$ bonds/m^2.

The more conventional approach to obtaining experimental activation energy is through the use of Eq. (II-22) applied to a series of constant stress creep tests at various temperatures.

$$\ell n(\dot{\varepsilon}/T)_{t,s,D} = \ell n(Xk/h) - E/R(1/T) \qquad \text{(IV-2)}$$

Thus a plot of $\ell n(\dot{\varepsilon}/T)$ vs. 1/T for the just mentioned test series should give a linear plot with a negative slope equal to E/R. Figure IV-24 gives the results for two nearly constant stress levels where the strain rate was taken as the minimum strain rate $\dot{\varepsilon}_m$ from Table IV-4. At the mean stress of D = 10.61MPa, the range was from 10.57 to 10.64MPa, and for a mean D = 16.69MPa, the range was from 16.54 to 16.81 MPa. Therefore, strictly speaking the stress was not constant. The least squares regression lines give a reasonable fit to the experimental data at each mean stress. The data in Fig. IV-24 are for experimental times equal to $t/t_m = 1.0$. Computations were also made for three other arbitrary time ratios. The experimental activation energy E obtained for different times are tabulated in Table IV-8. For each time ratio in Table IV-8 the values of ΔF and S_β calculated

indicate that ΔF and S_β are not very sensitive to time. The results for saturated MFS show there was no large difference in either ΔF or S_β whether calculated from temperature stage tests, Eq. (IV-1) or from a series of constant stress tests at varying temperature, Eq. (IV-2). It should be noted that the intercept term in Eq. (IV-2) was not constant as shown by "a", the intercept term in the regression equation in Fig. IV-24, where "a" equals $\ell n(Xk/h)$. The possible meaning obtained from the temperature dependence is considered in the discussion section.

Turning now to the stress dependance as shown by RPT, the generalized form of Eq. (II-26) was used for the stress stage, ΔD, analysis and Eq. (II-25) at various constant times for the conventional analysis procedure for obtaining α. Stress stage tests were run at constant temperature and the stress changed to determine α as follows:

$$\alpha = \ell n(\dot{\varepsilon}_1/\dot{\varepsilon}_2)_{t,s,T} \; / \; (D_1 - D_2) \qquad \text{(IV-3)}$$

From which $S_\alpha = \lambda N/4RT\alpha$ reduces to $S_\alpha = 5.077 \times 10^{18}/T\alpha$ using the same argument as applied to S_β from the temperature stage test data.

The shape of $\ell n\dot{\varepsilon}$ vs. ℓnt or $\ell n\dot{\varepsilon}$ vs. ε from ΔD tests is about the same as for $\Delta\theta$ tests, except that the new slope after ΔD generally was established within two to three minutes. Figure IV-25 shows an example of stress stage test data at

constant temperature. The strain rates to be used in Eq. (IV-3) were obtained in an analogous manner to the determination used for $\Delta\theta$ tests, except there was no fixed time to start the fit for the slope of $\ell n\dot{\varepsilon}$ vs. ℓnt or ε after the stress change. Again more than one stress stage was made on a particular sample. The results are given in Table IV-9.

The number of bonds/m^2, S_α, appears to be a function of stress. Using the 14 data points for a mean temperature of -18.3°C gave a power fit regression line, S_α vs. D, with a coefficient of determination, r^2, equal to 0.910. Including the four data points from other temperatures improved the fit to $r^2 = 0.953$. Stress dependance of S_α was strong. The r^2 term was the same whether one used the mean stress or the stress for the first stage. The relation between S_α and stress ratio D/D_u was very poor. Table IV-9 indicates that S_α was independent of time.

A comparison of S_α obtained from application of Eq. (II-25) and Eq. (IV-3) are given in Table IV-10. The largest discrepancy was at -12°C where the S_α from ΔD was at a stress level which was below the "knee" in the $\ell n\dot{\varepsilon}$ - D plot for any given time t (see Fig. IV-30). The low S_α means a high α, which would be expected for data below the knee in the $\ell n\dot{\varepsilon}$ - D plot. Mitchell's procedure for analyzing stress stage data to obtain α gave values consistently low by a factor of 2 to 4. The RPT indicates that α should increase slightly for

decreasing temperature in order that S_α be independent of temperature. The data for frozen MFS in Table IV-9 indicate that the direction of the temperature dependance of α is the wrong direction, which shows up in Table IV-10 as a temperature dependancy for S_α. At -18°C, S_α equals $5 \pm 1 \times 10^{16}$ bonds/m^2, which is a factor of ten larger than S_β for the same temperature and stress conditions. Possible reasons for this apparent internal discrepancy in RPT will be discussed later.

Most of the temperature and stress stage tests were continued for sufficient time to pass through the minimum strain rate. Figure IV-26 shows a comparison of $\dot{\varepsilon}_m$ from a temperature stage test with a conventional creep test. The twenty-nine data points for $\dot{\varepsilon}_m$ after stage tests fit the regression equation:

$$\dot{\varepsilon}_m = 7.78 \times 10^{-4} (t_m)^{-1.046}$$

with an $r^2 = 0.946$, which may be compared to the single load, single temperature data in Fig. IV-15 which gave

$$\dot{\varepsilon}_m = 8.21 \times 10^{-4} (t_m)^{-1.13} \text{ with } r^2 = 0.989).$$

The similarity of $\dot{\varepsilon}_m - t_m$ data from single and multiple stage tests suggests that there may be an unique equation of state that would describe the creep behavior of frozen MFS up to $\dot{\varepsilon}_m$.

2. Partially Saturated Samples

The analysis procedures for determining RPT parameters on partially saturated samples was the same as described for saturated samples. The results from temperature stage tests are summarized in Table IV-11. Temperature stage tests at ice saturation as low as 15% were successfully carried out, as illustrated in Fig. IV-27. The band of data points for E vs. D was rather broad, as shown in Fig. IV-28, even when the three extreme values in Table IV-11 were omitted. The data showed no clear pattern with time or with temperature. The solid lines in Fig. IV-28 represent the least squares fit to the data. The dashed lines are eyeball lines at the upper and lower bounds for the band of data points at w = 10%. The average value parameters from the eyeball fit were $\Delta F = 406 \pm 50$kJ/mol and $\beta = 0.042 \pm 0.001 m^3$/mol. Thus, the eyeball fit gave lower ΔF and β than the least squares fit for w = 10% data on frozen MFS. The number of bonds calculated from β would be 0.7 to 1 x 10^{15} depending upon which value of β was used. Plotting experimental activation energy, E, against stress ratio, D/D_u, gave a lower coefficient of determination, r^2, than the plot of E vs. D in Fig. IV-28.

Application of Eq. (II-22) to creep data for frozen MFS at w = 10% is illustrated in Fig. IV-29. The three stress levels shown in Fig. IV-29 used minimum strain rates, i.e. $t/t_m = 1.0$. The experimental activation energy changed less

than 1% when evaluated at t/t_m = 0.75, 0.5 or 0.25 rather than at t/t_m = 1.0, which was an even smaller change than observed for saturated samples. Again as with the ice saturated samples E calculated from Eq. (II-22) for different values of $\varepsilon/\varepsilon_m$ on partially saturated samples showed small variations. The data in Fig. IV-29 gave ΔF = 242kJ/mol and $S_\beta = 1.3 \times 10^{-15}$ bonds/m^2 that agree reasonably well with ΔF and S_β from temperature stage tests.

Stress stage tests results on frozen MFS at w = 10% are summarized in Table IV-12. The variation in S_α was small. No stress stage tests were run at w = 5%. Plots of $\ell n\dot{\varepsilon}$ - D at various times in Fig. IV-30 show the use of Eq. (II-25) for the determination of α. The dashed curve in Fig. IV-30 is for $\dot{\varepsilon}_m$ calculated from the regression line in Fig. IV-20 at w = 10%. The evaluation of $\alpha (=d\ell n\dot{\varepsilon}/dD)$ from data such as given in Fig. IV-30 is considerably more subjective than from stress stage test data. From the rather large variation in α evident in Fig. IV-30 it is doubtful if there is a significant difference between S_α computed from $(\ell n\dot{\varepsilon}\text{-}D)_t$ data compared to S_α from stress stage test data.

Data from temperature stage, stress stage, and constant temperature-stress at three different water contents for evaluation of RPT discussed above are summarized in Table IV-13. In general, the number of bonds decreased and the free energy of activation ΔF increased as the ice content

decreased. The different methods of analysis gave about the same ΔF; however, there was a consistent tenfold discrepancy between the number of bonds calculated from β vs. the number of bonds calculated from α for the same range in stress and temperature.

E. Ice

In order to supplement the data available for the evaluation of the Rate Process Theory, a series of creep tests was conducted on polycrystalline snow ice. The test results were also used to provide information for Ting's (1981a) study of the mechanisms of strength and deformation of frozen sand. The ice samples were prepared by the method of Cole (1979) and stored in a cold room set at -30°C. Prior to sample setup, the samples were allowed to equilibrate at -10°C for more than 8 hours. The samples were then trimmed to size on a lathe, and the ends squared using a squaring jig. The final sample dimensions were similar to those for the MFS samples, but varied due to the trimming process and the nature and location of any imperfections in the original ice samples. The final ice sample dimensions averaged 35.8mm in diameter and 82.2mm in height. The trimmed samples were then set up in the creep test apparatus previously described. The test procedures which were followed for the ice samples were the same as for the creep testing of the MFS samples.

The measured density of the ice samples was 916kg/m^3. Initial average ice grain diameter prior to creep testing

was 0.4 to 0.6mm as measured on thin sections obtained during the cutting of samples to length. The average ice grain diameter increased about 25% as a results of creep testing.

Three basic types of unconfined compressive creep tests were carried out: single stage constant load tests, temperature stage tests and stress stage tests. The results of the tests on the ice samples are summarized in Table IV-14. Qualitatively, the data indicate that the ice samples are much more creep susceptible and weaker than frozen MFS. For the range of test conditions imposed, the data indicate that the strain at minimum strain rate, $\dot{\varepsilon}_{min}$, is between 1 and 2% for ice. Polycrystalline ice gave a free energy of activation ΔF 1.5 times that for ice single crystals and about one-quarter that for frozen MFS. The number of bonds computed from α was about the same for polycrystalline as for single crystal ice. The number of bonds calculated from β for polycrystalline ice was one-sixth that obtained from α.

F. Miscellaneous

1. Unfrozen Water Content

Unfrozen water content was determined by nuclear magnetic resonance (NMR) using a Praxis model PR103 pulsed NMR analyzer operated in the 90° mode with a 0.1 sec clock. Unfrozen water was determined from the first-pulse amplitude. The method and sample preparation details have been described

by Tice et al. (1978). Different size fractions and the whole soil Manchester Fine Sand were used. The only pretreatment was to remove magnetics (0.45%) using a strong magnet. Samples were mixed at various water contents and taken through two freeze-thaw cycles before the NMR experiments.

No evidence for hysteresis between cooling and warming curves was observed on any of the samples, as shown in Fig. IV-31 - IV-33. The change in unfrozen water content for different size fractions at constant total water content are shown in Fig. IV-32. The high unfrozen water content for the +176μm fraction is tentatively attributed to the mica content. At any given temperature, there was a rather large change in unfrozen water as a function of the total water content, as evidenced by the data in Fig. IV-33. The lines in Fig. IV-33 are the best least squares fit of the experimental data expressed as $w_u = A + B \ln\theta$ with a coefficient of correlation (r^2) between 0.945 and 0.994. Experimental points have been omitted for $w_t = 24.8$ and $w_t = 9.8$ in order to more clearly show the trends. The ice content (I) is defined as the total water content minus the unfrozen water content. The use of this relation for ice content permits the determination of unfrozen water associated with the soil phase only (I=0) at any selected temperature as shown in Fig. IV-34. The significant point to be made from Fig. IV-34 is that the unfrozen water

content was remarkably independent of temperature between -1°C and -9.4°C.

The slope of any w_u-I curve at constant temperature and a chosen ice content yields the unfrozen water for the ice phase only expressed as water (liquid) per 100g ice. Figure IV-35 summarized results for some computations of the unfrozen water at different ice contents, each as a function of temperature. Note that the unfrozen water for the soil only and for the mixture soil plus ice are per 100g soil, while the unfrozen water with the ice phase is given per 100g ice (solid).

It would appear that the unfrozen water associated with ice is very temperature sensitive compared to unfrozen water associated with the soil phase. The increase in unfrozen water in ice per unit weight of ice as the ice content of the sample increases requires further research. An interesting point is that the unfrozen water/100g ice at all ice contents above 10g ice/100g soil extrapolate to zero unfrozen water on the temperature axis at -22 ± 1°C, which is the temperature at which experiments, Hosler et al. (1957), have shown that ice spheres no longer adhere to each other. That is, there is no longer any unfrozen water in ice colder than about -22°C.

2. Specific Heat

A Perkin-Elmer differential scanning calorimeter was used to measure specific heat after the method of Kay and Goit (1975). Details of the specific method have been reported

by Haynes et al. (1980). The data are given in Table IV-15 and Fig. IV-36. There is no significant difference between the specific heat at w_t = 0 and w_t = 1.2 for any given temperature, suggesting that the water remains unfrozen. The variations in slope below freezing at the other water contents probably are related to unfrozen water content.

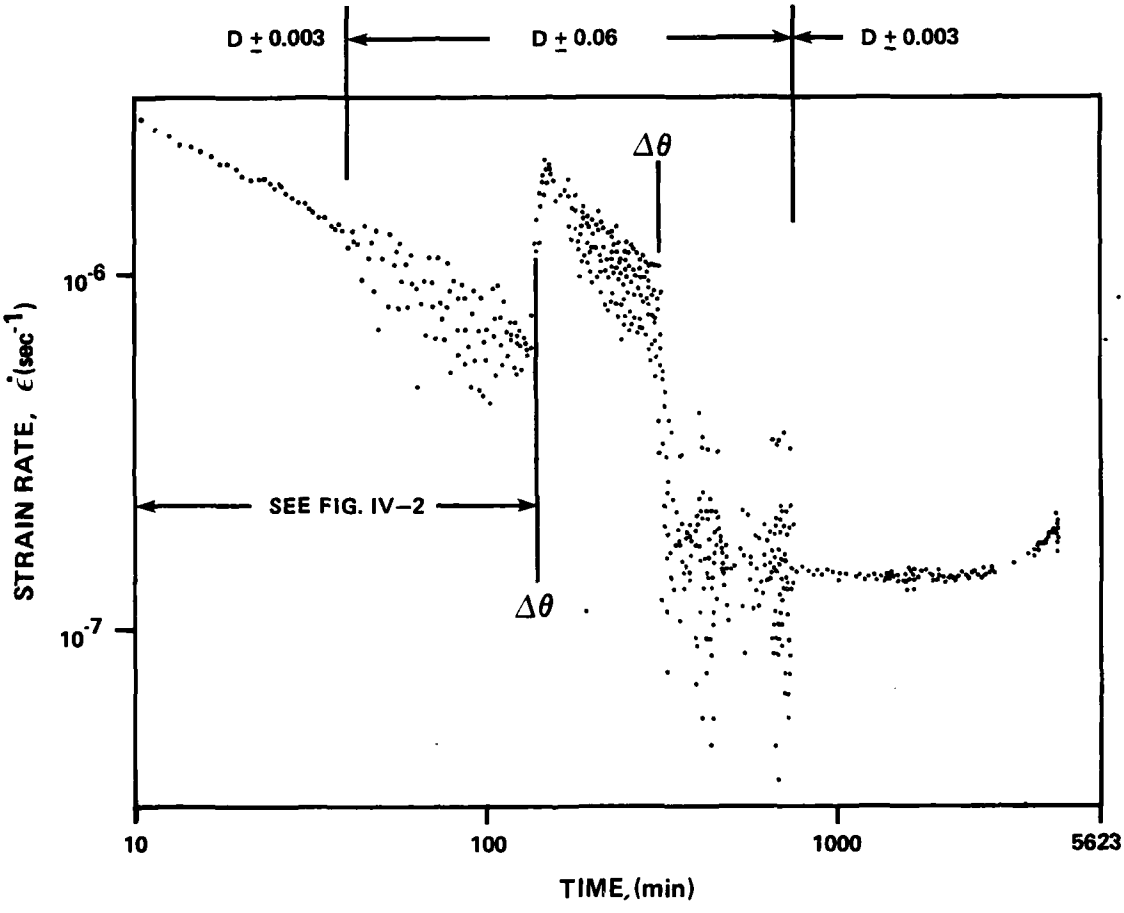

Fig. IV-1 Effect of Load Fluctuation on Strain Rate

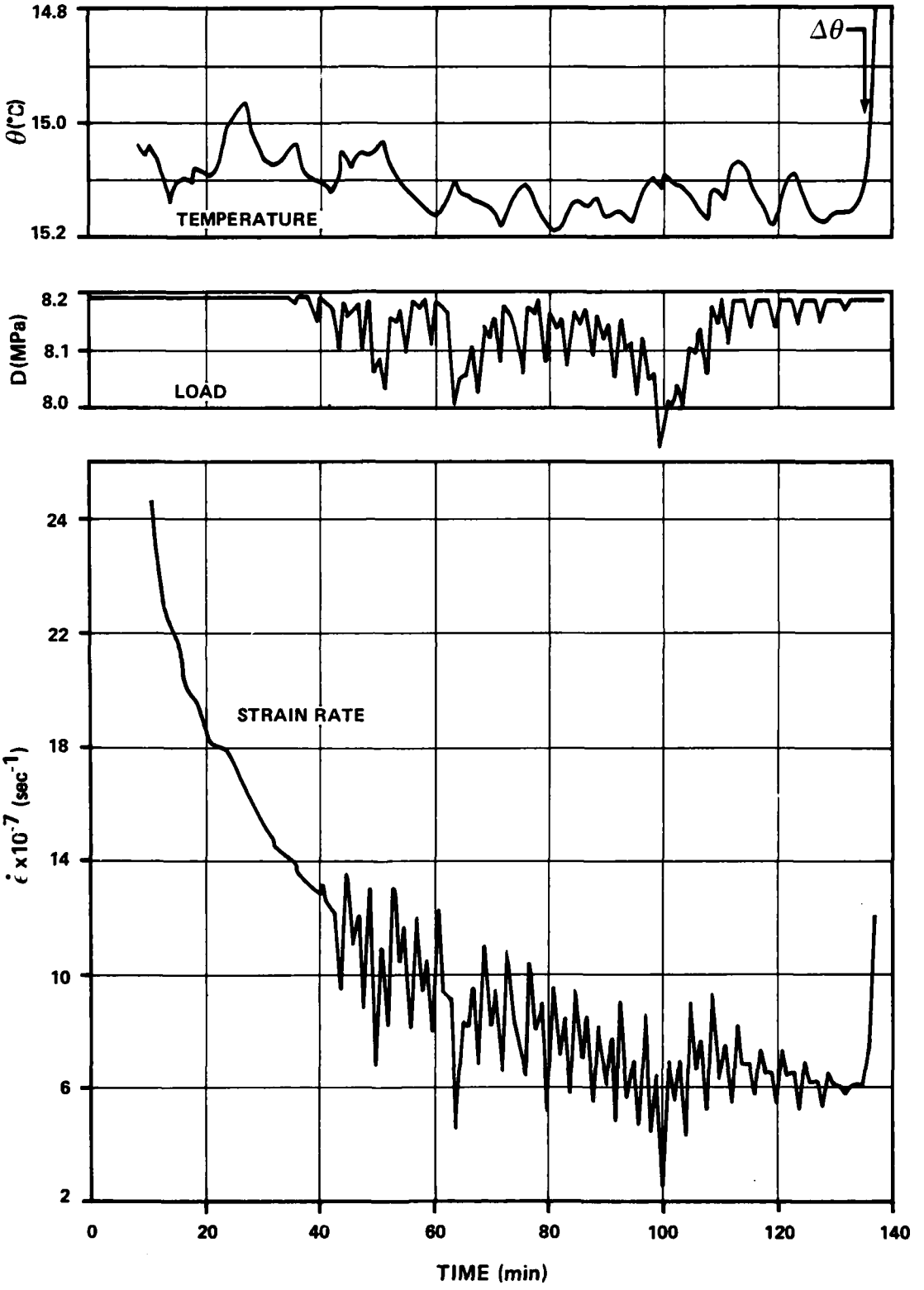

Fig. IV-2 Detail from Fig. IV-1

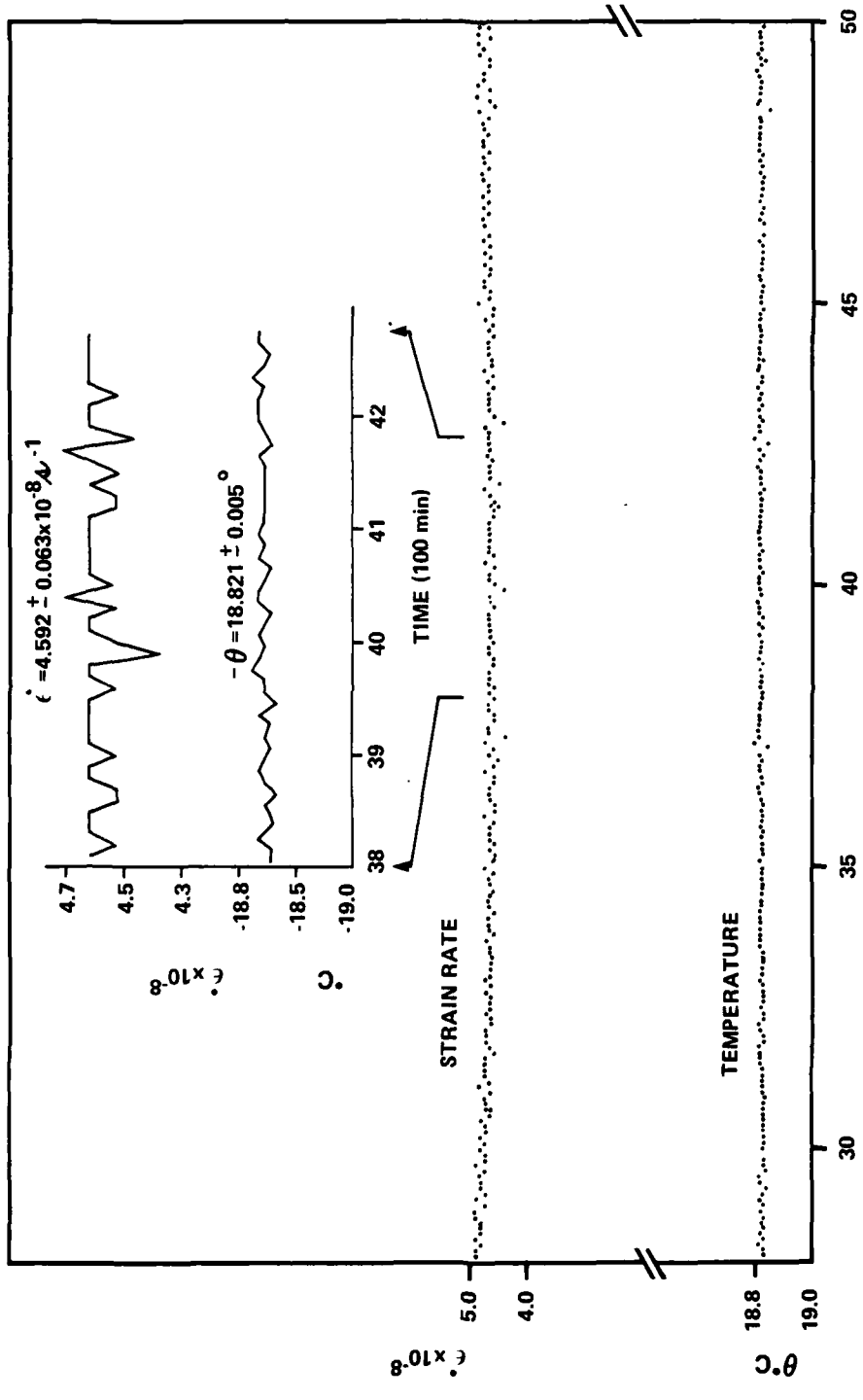

Fig. IV-3 Creep Rate Fluctuation under Excellent Temperature Control during Test S8-2

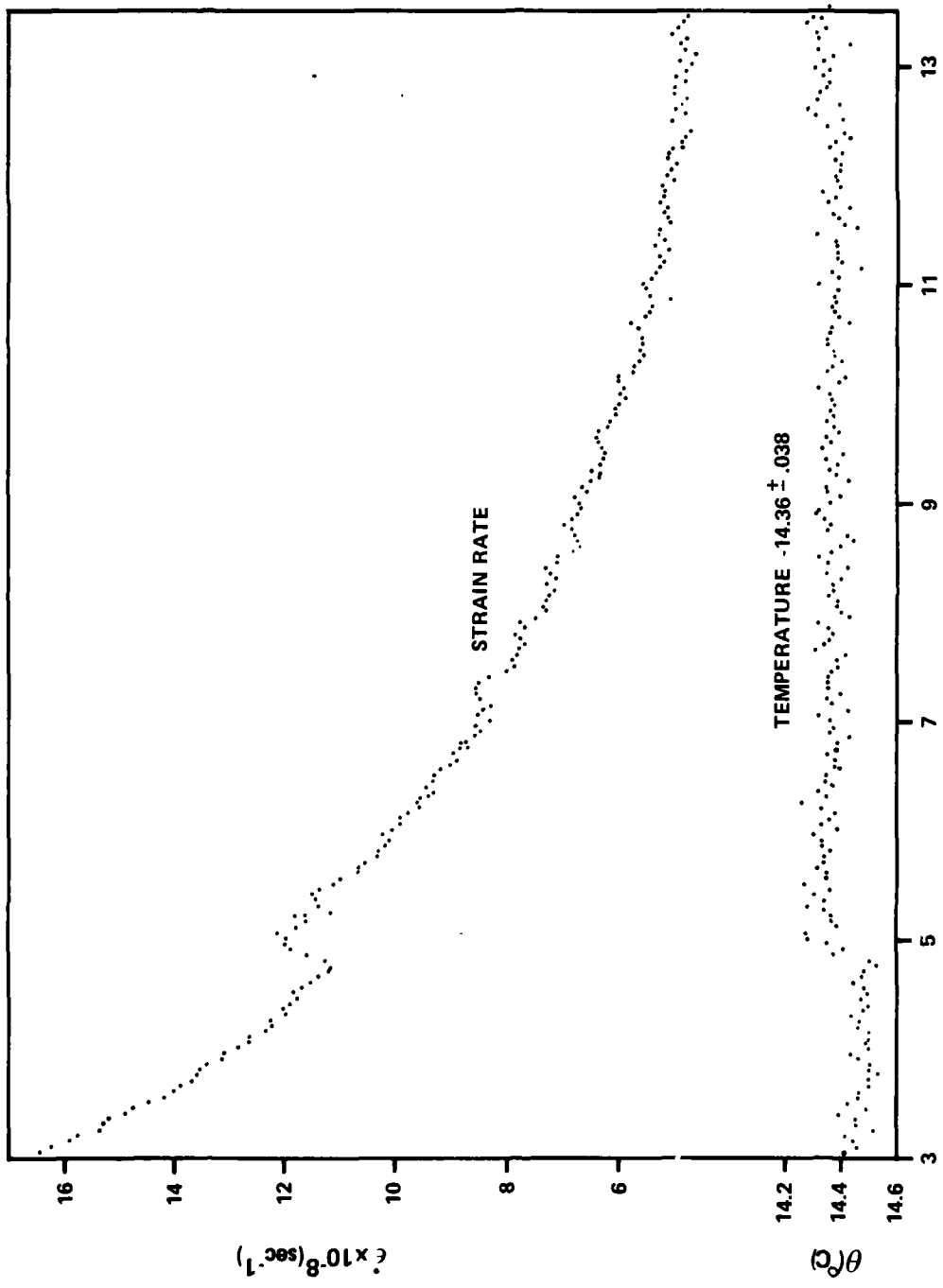

Fig. IV-4 Creep Rate Fluctuation under Fair Temperature Control During Test S8-43

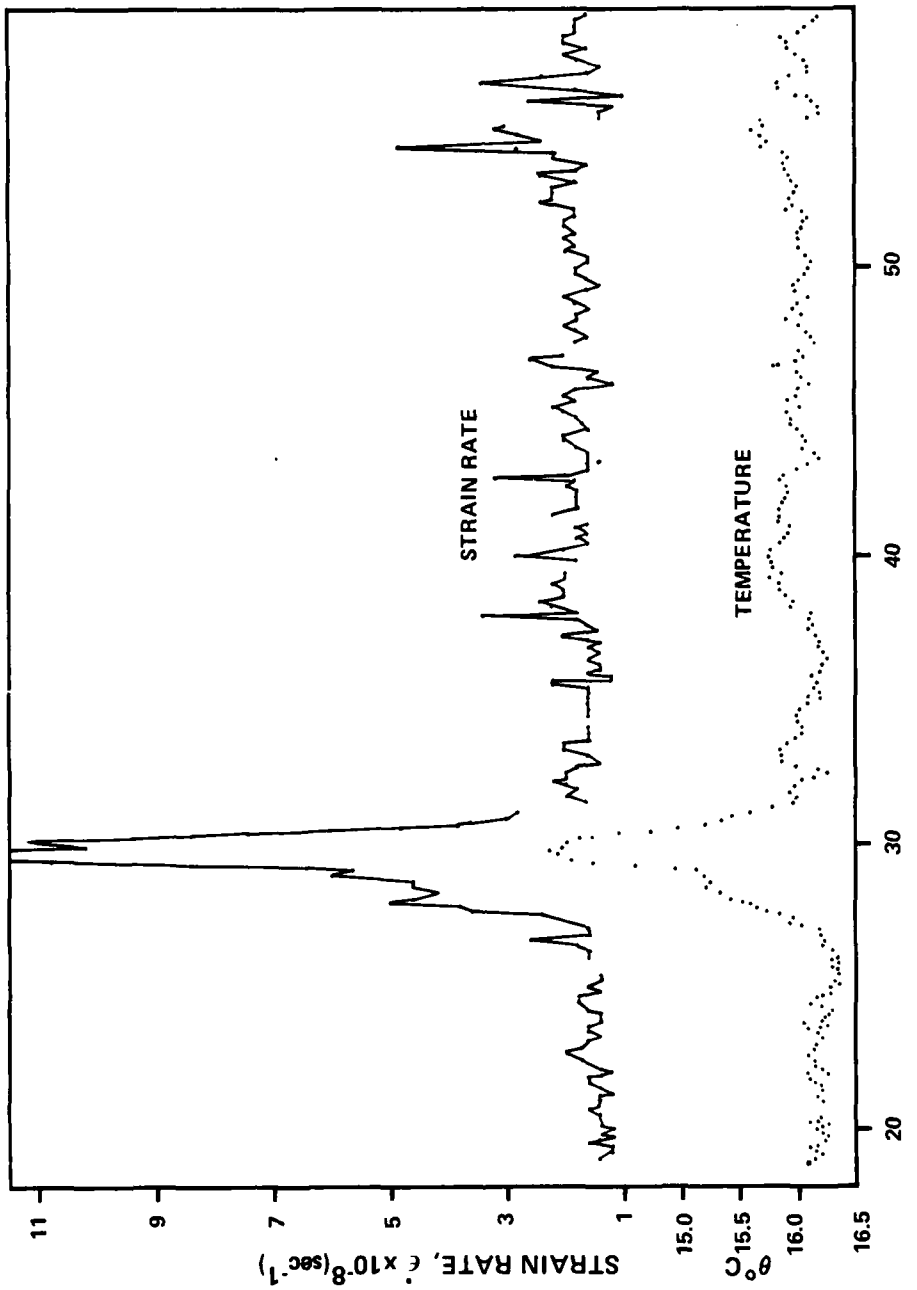

Fig. IV-5 Creep Rate Fluctuation under Poor Temperature Control During Test S4

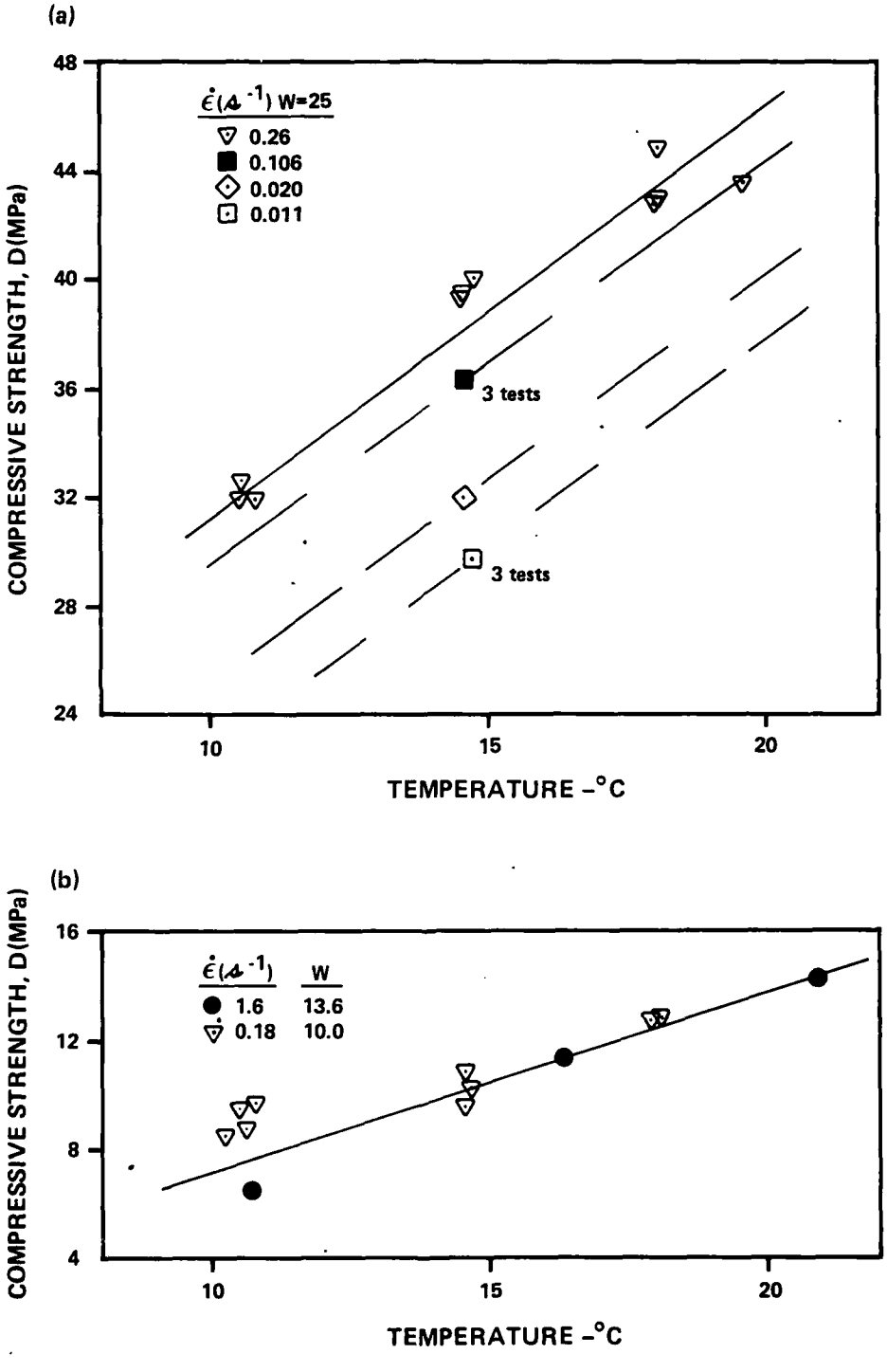

Fig. IV-6 Unconfined Compression Instantaneous Strength for Frozen MFS: a) Saturated b) Partially Saturated

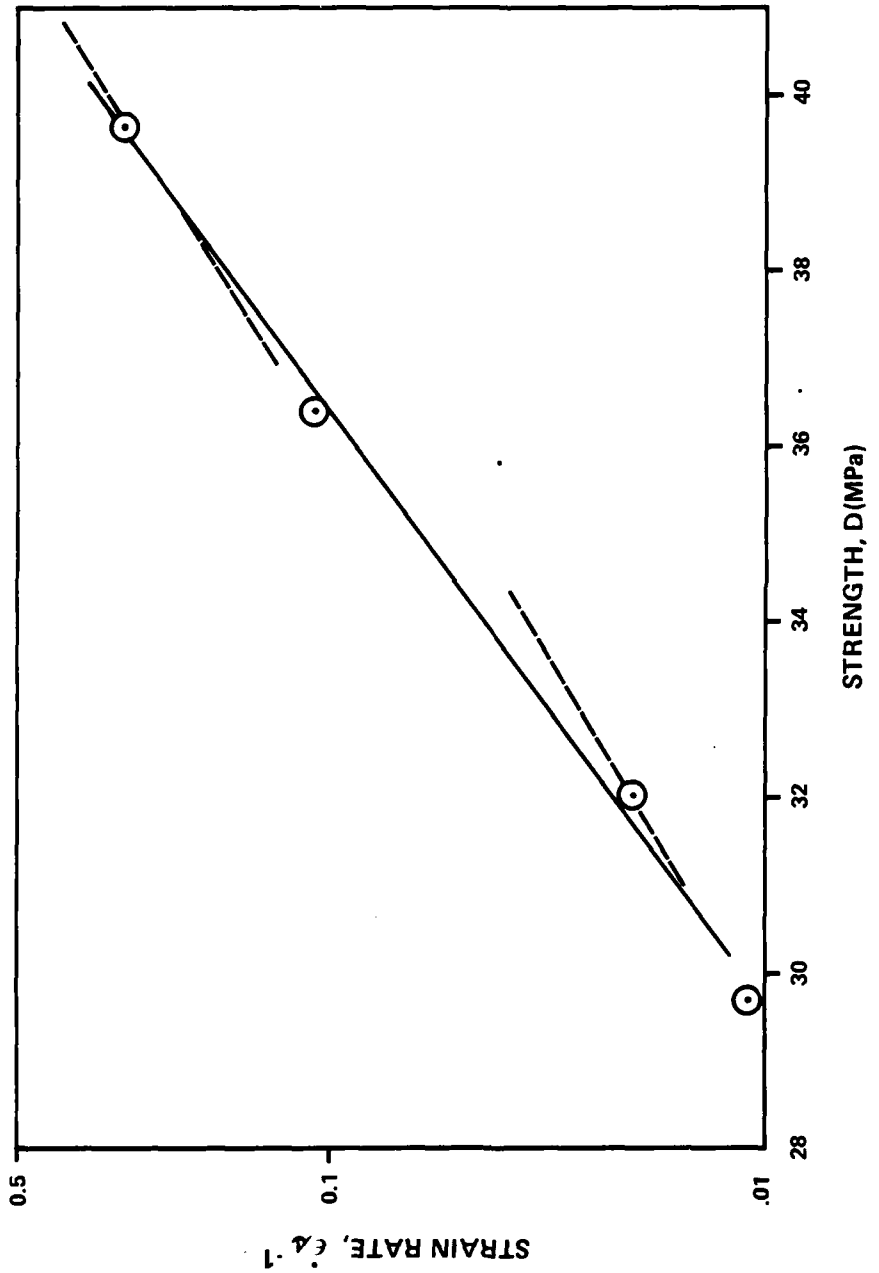

Fig. IV-7 Strain Rate Effect on Strength for Saturated MFS at θ = 14.6°C

a) DUCTILE b) B-D TRANSITION c) BRITTLE

Fig. IV-8 *Photos of MFS Samples Failed at Different Strain Rates:*
a) $\dot{\varepsilon} = 0.01\ sec^{-1}$, b) $\dot{\varepsilon} = 0.02\ sec^{-1}$,
c) $\dot{\varepsilon} = 0.1\ sec^{-1}$

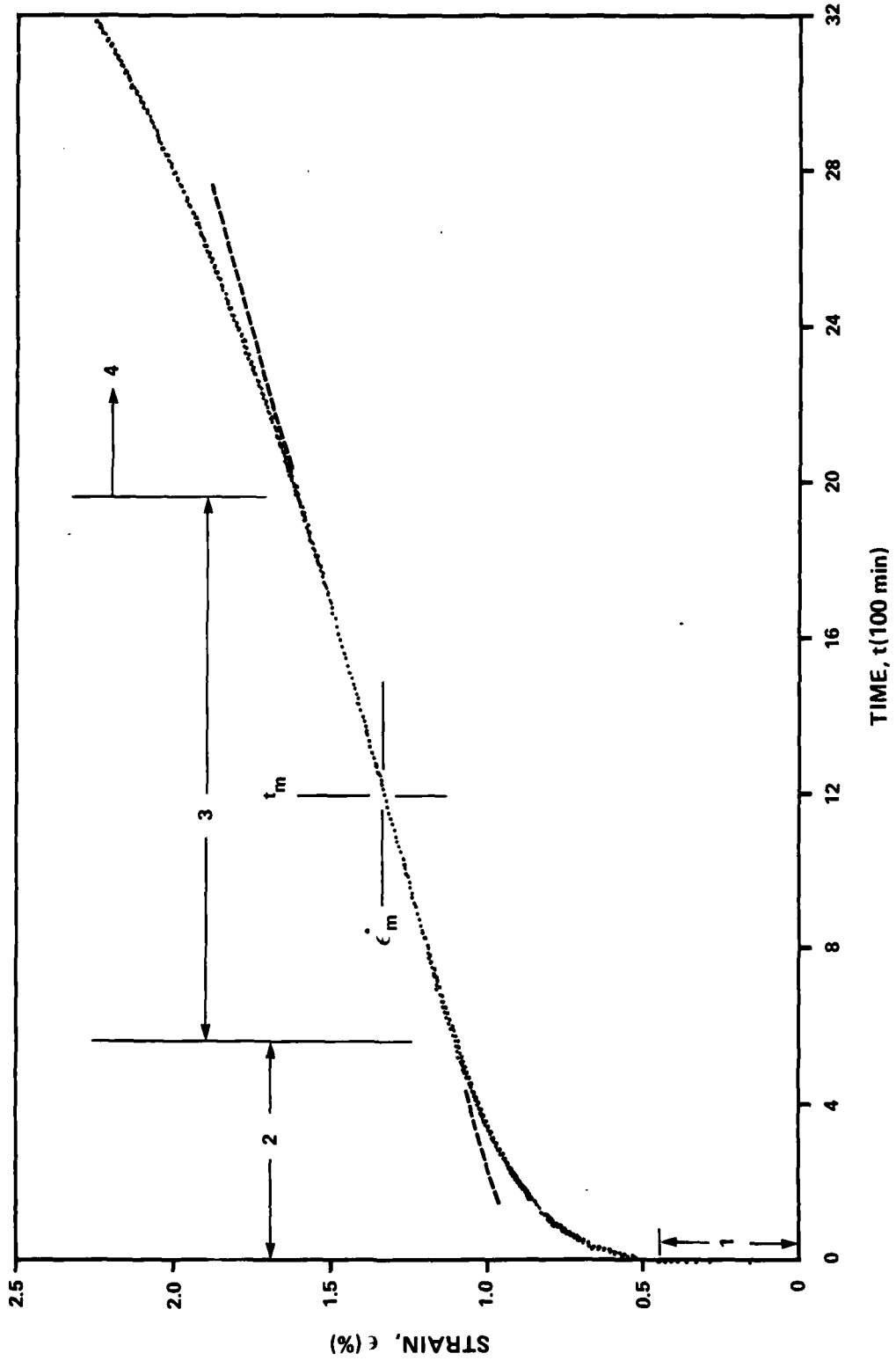

Fig. IV-9 Strain-Time Data from Creep of Frozen MFS at w = 10%, D = 3.98MPa, θ = 18.79°C

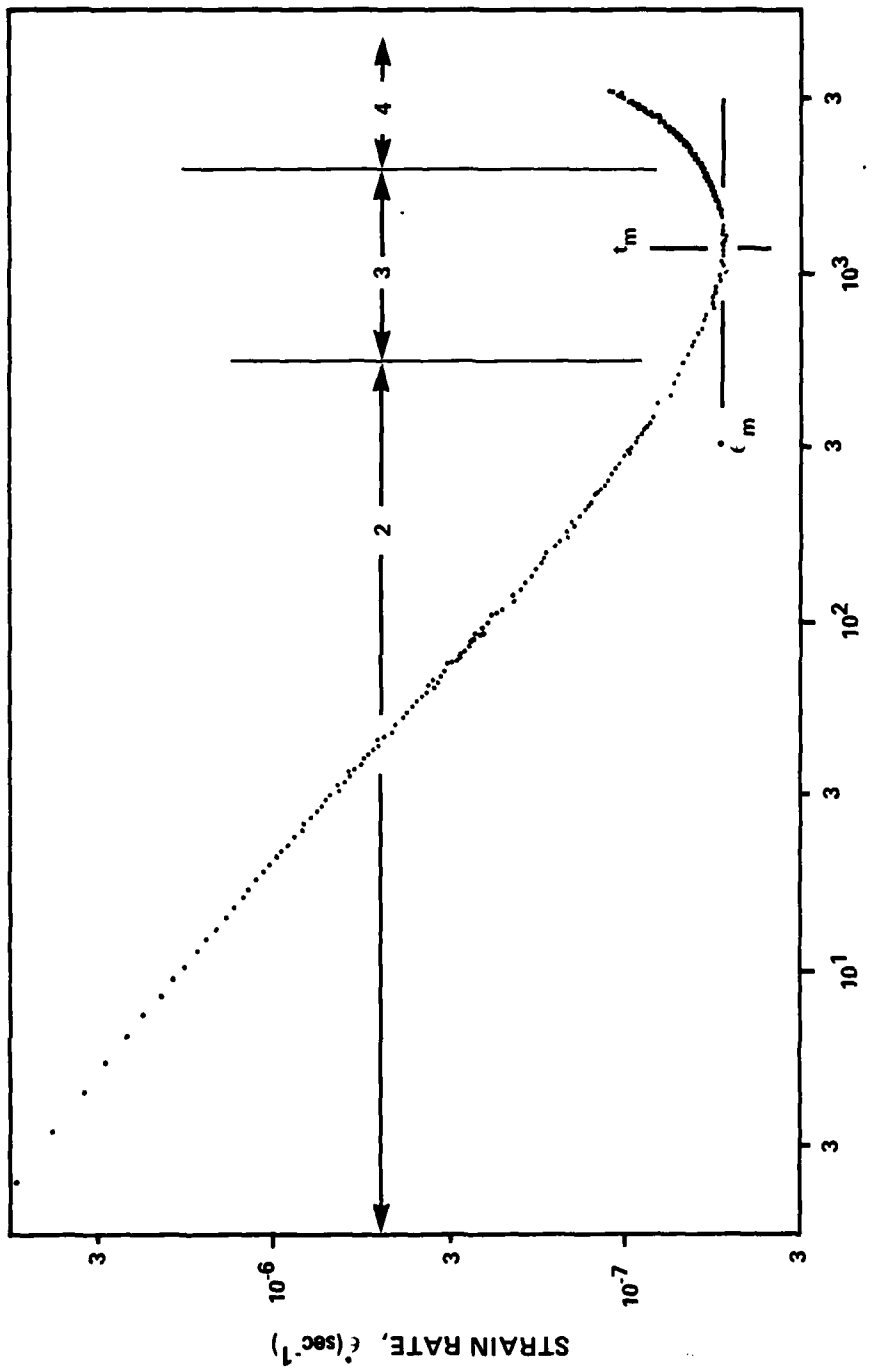

Fig. IV-10 Log Strain Rate - Log Time Data from Creep of Frozen MFS at w = 10%, D = 3.98MPa, θ = 18.79°C

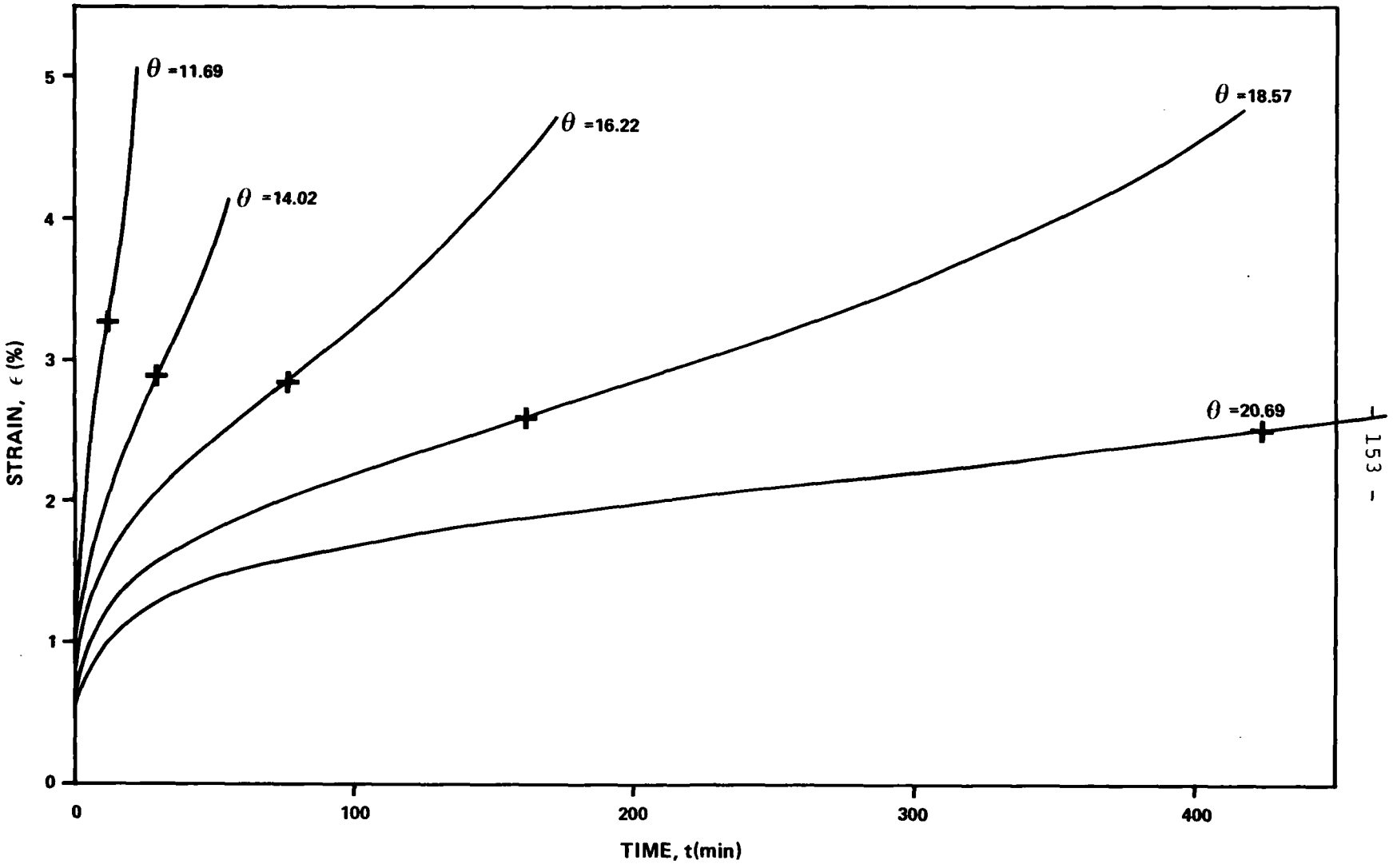

Fig. IV-11 Creep Curves under Constant Load D = 4.78MPa on Frozen MFS at w = 10。 for Various Temperatures, + = ($\dot{\varepsilon}_m$, t_m)

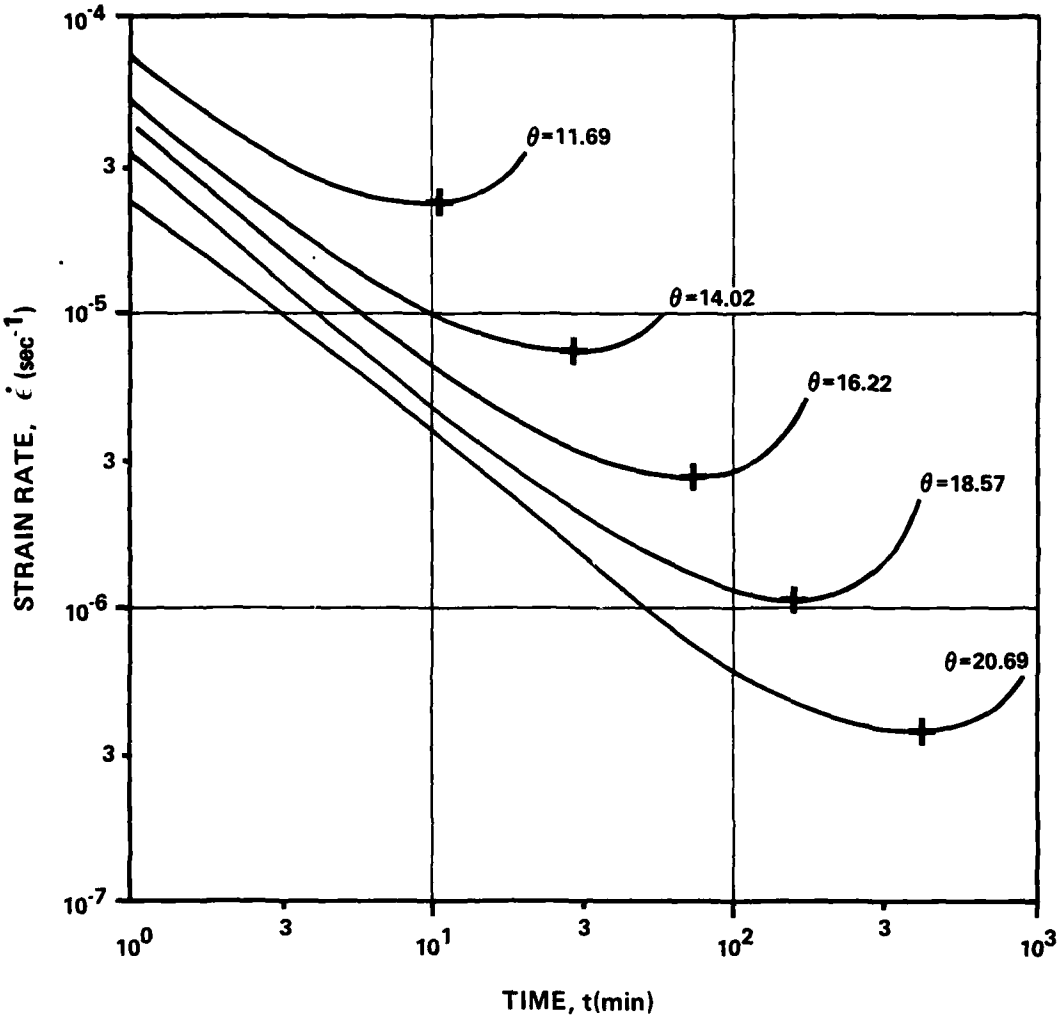

Fig. IV-12 Log Strain Rate - Log Time Curves for Frozen MFS at w = 10% Constant Load, D = 4.78MPa, Temperature Varied

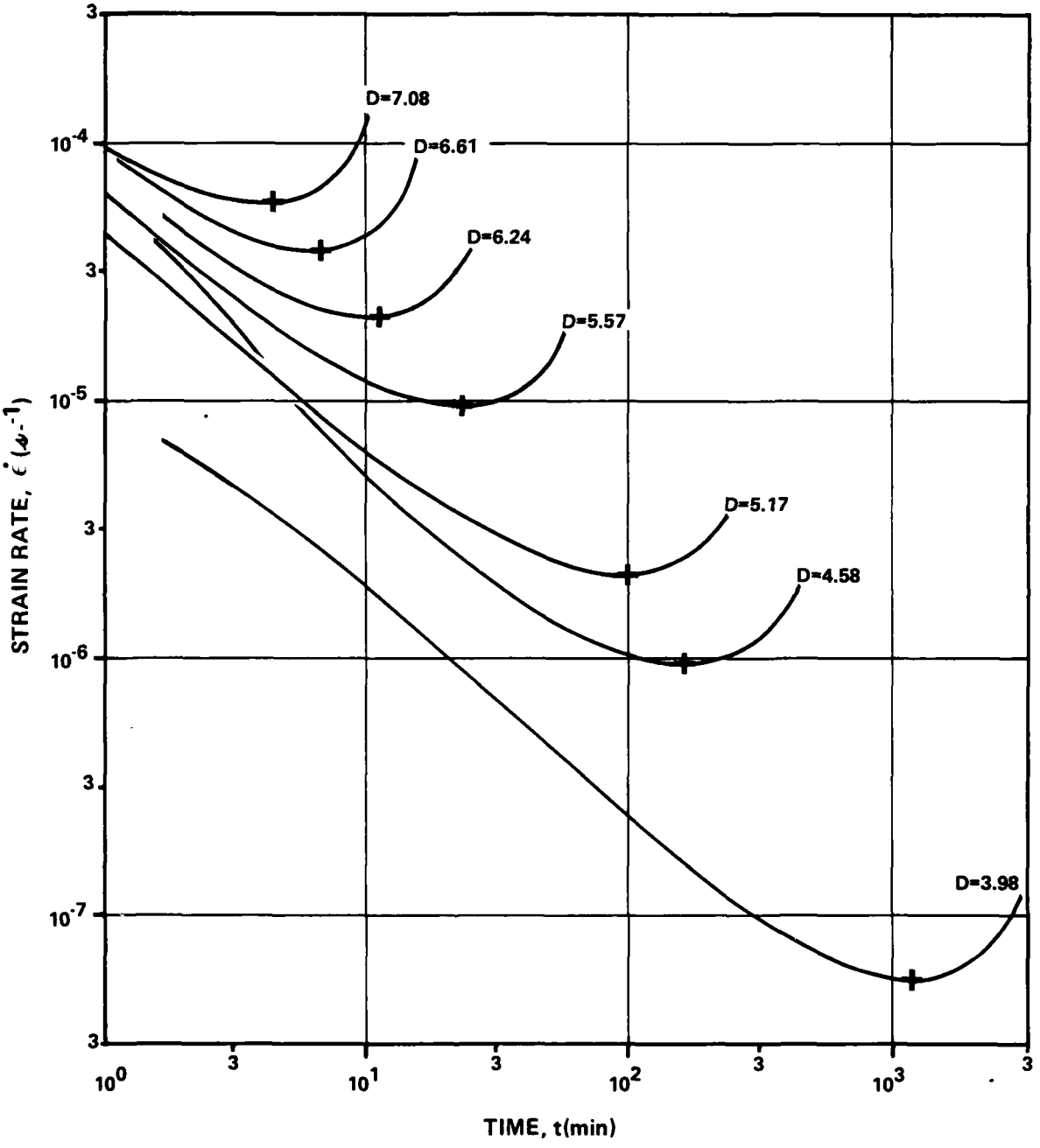

Fig. IV-13 Log Strain Rate - Log Time Curves for Frozen MFS at w = 10% under Constant Temperature θ = 18.78 and Various Loads (MPa), + = $(\dot{\epsilon}_m, t_m)$

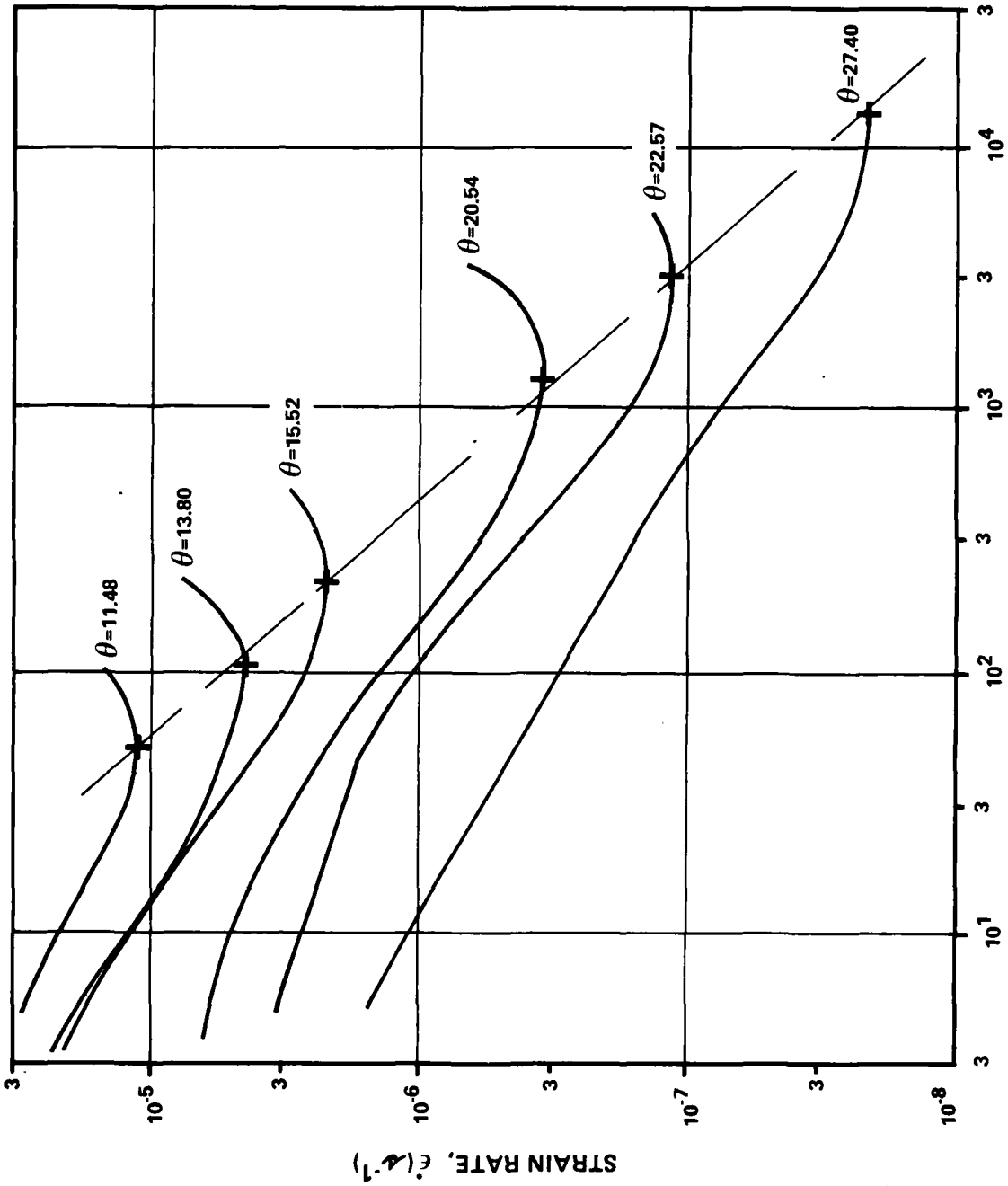

Fig. IV-14 Log Strain Rate - Log Time Curves for Saturated Frozen MFS under Constant Load D = 10.6 MPa and Various Temperatures, θ

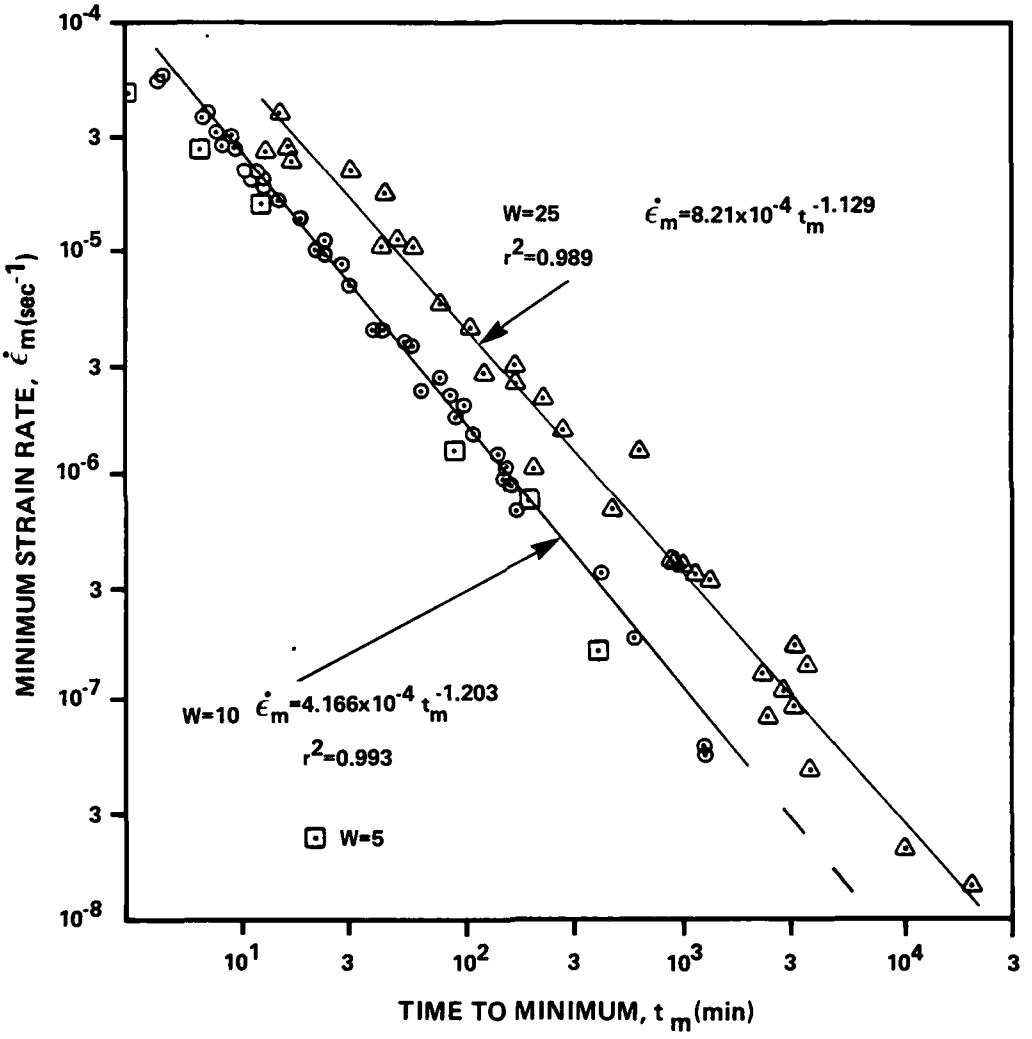

Fig. IV-15 Minimum Strain Rate vs. Time to Minima for Frozen MFS

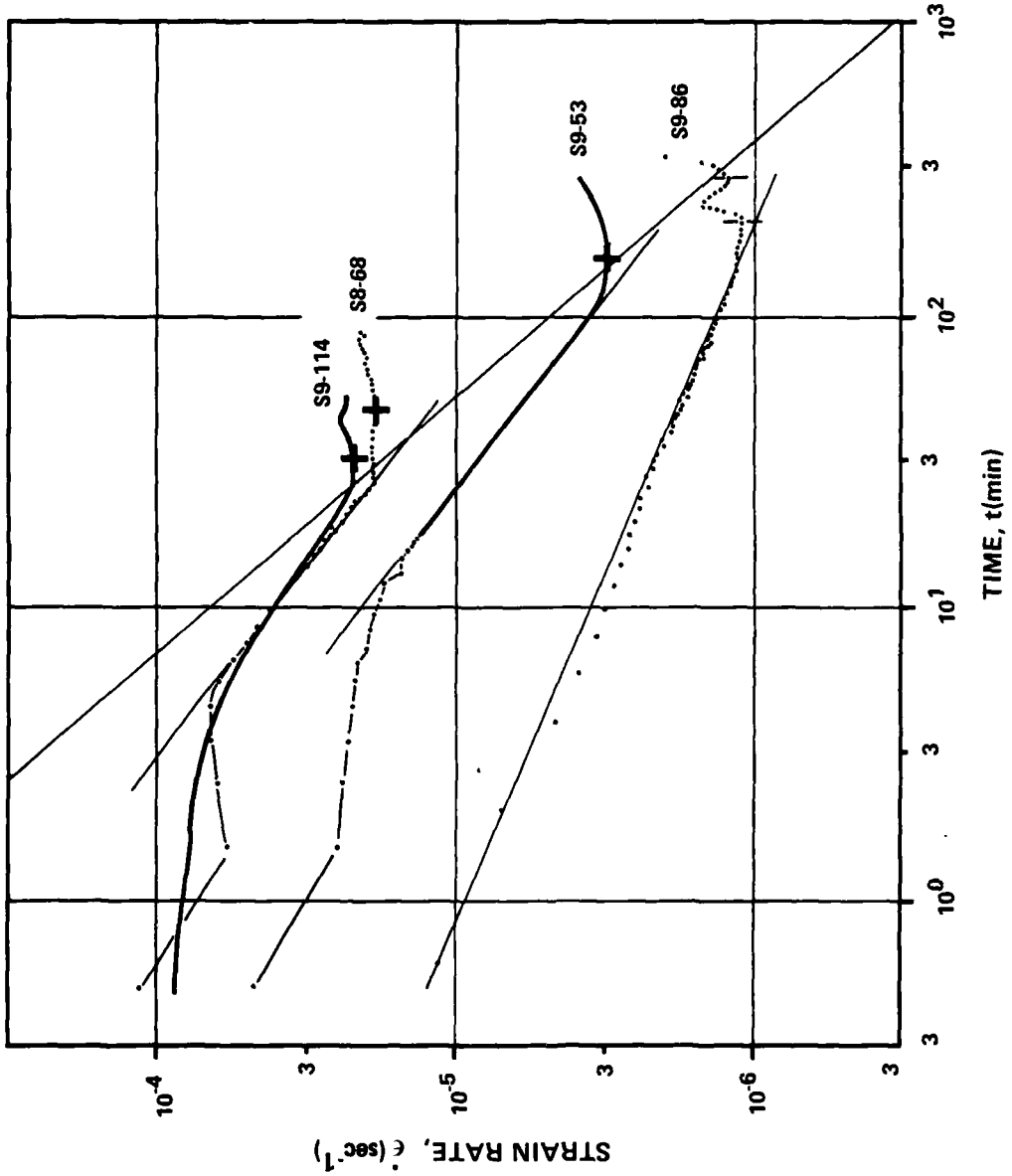

Fig. IV-16 Worst Case Strain Rate - Time Plots

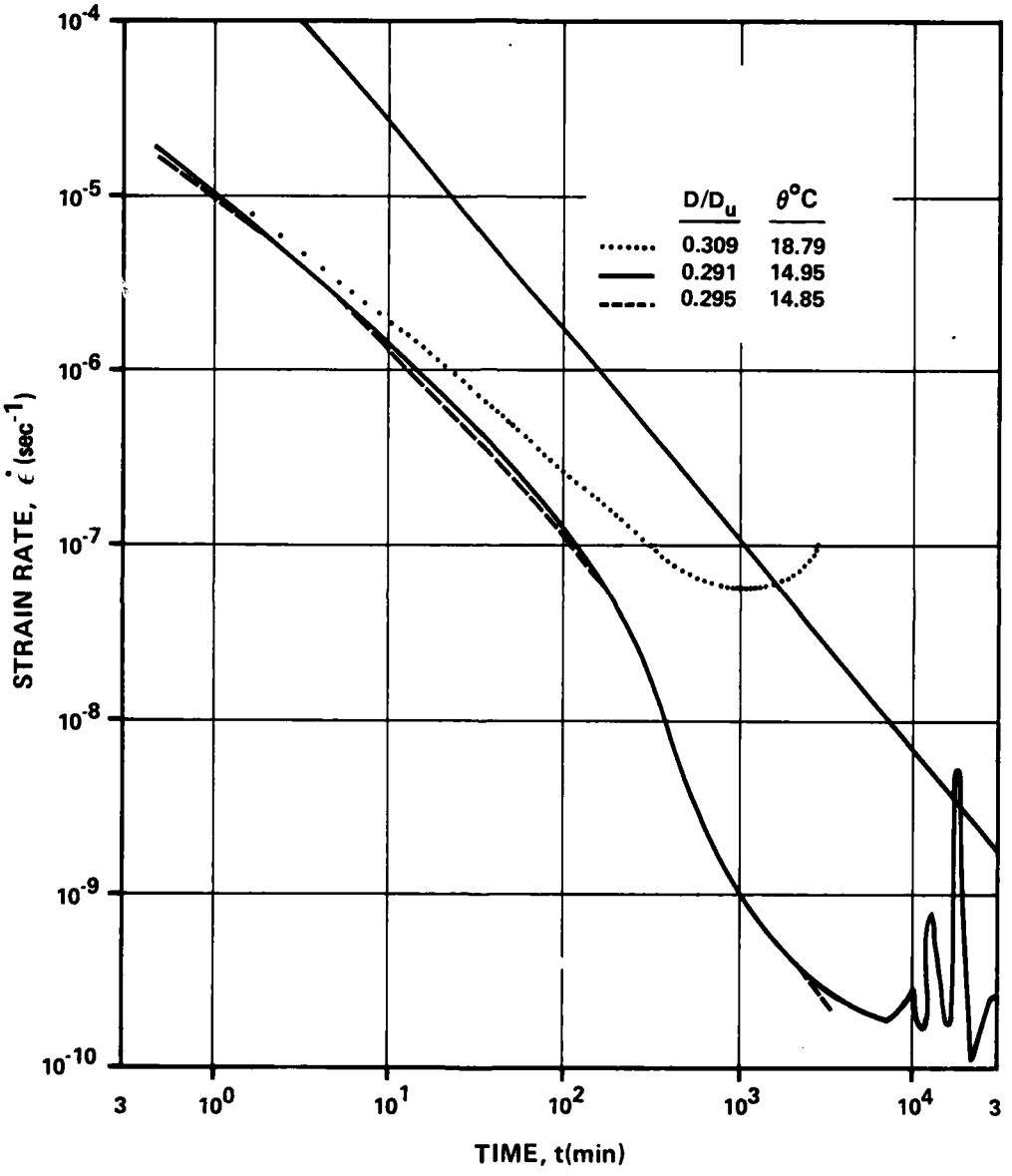

Fig. IV-17 Strain Rate - Time Curves at Low Stress Ratio for Frozen MFS at w = 10%

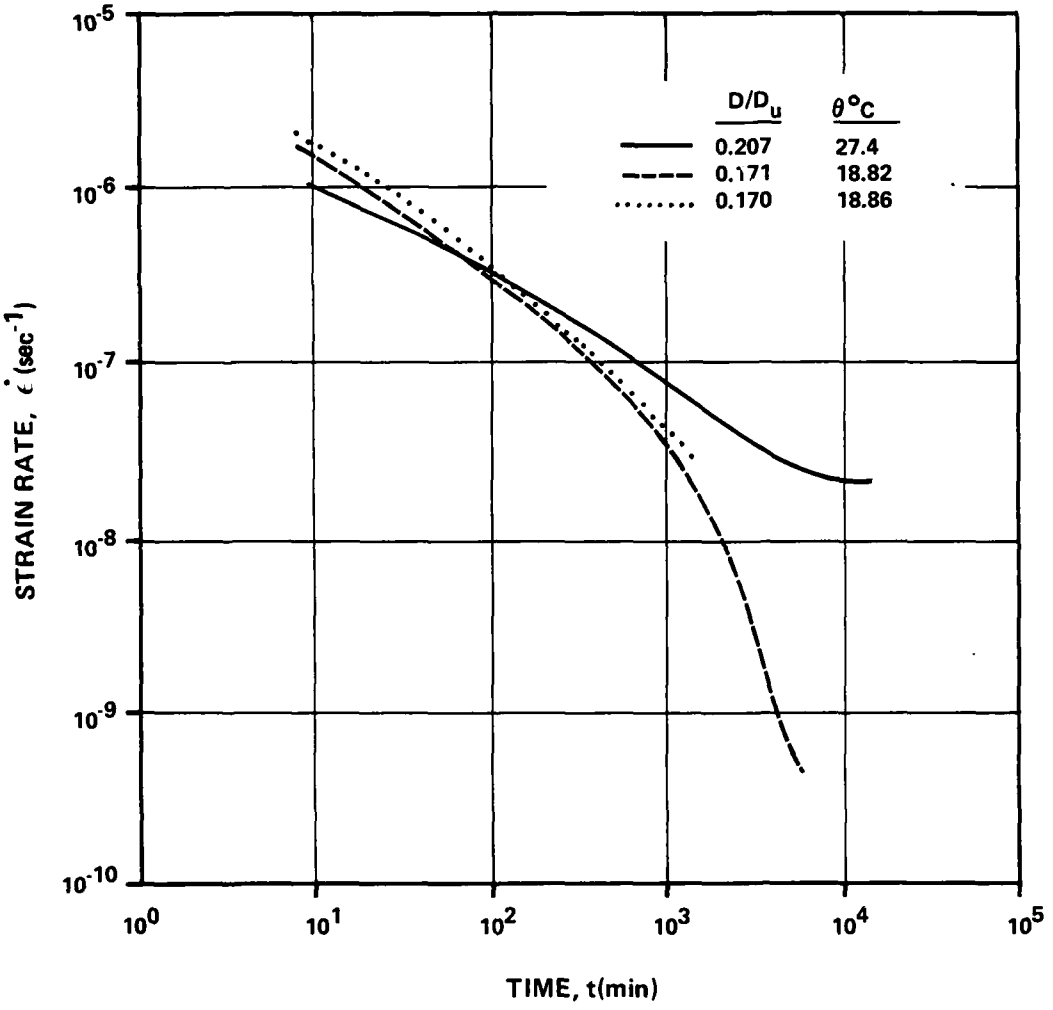

Fig. IV-18 Strain Rate - Time Curves at Low Stress Ratio for Frozen MFS at w = 25%

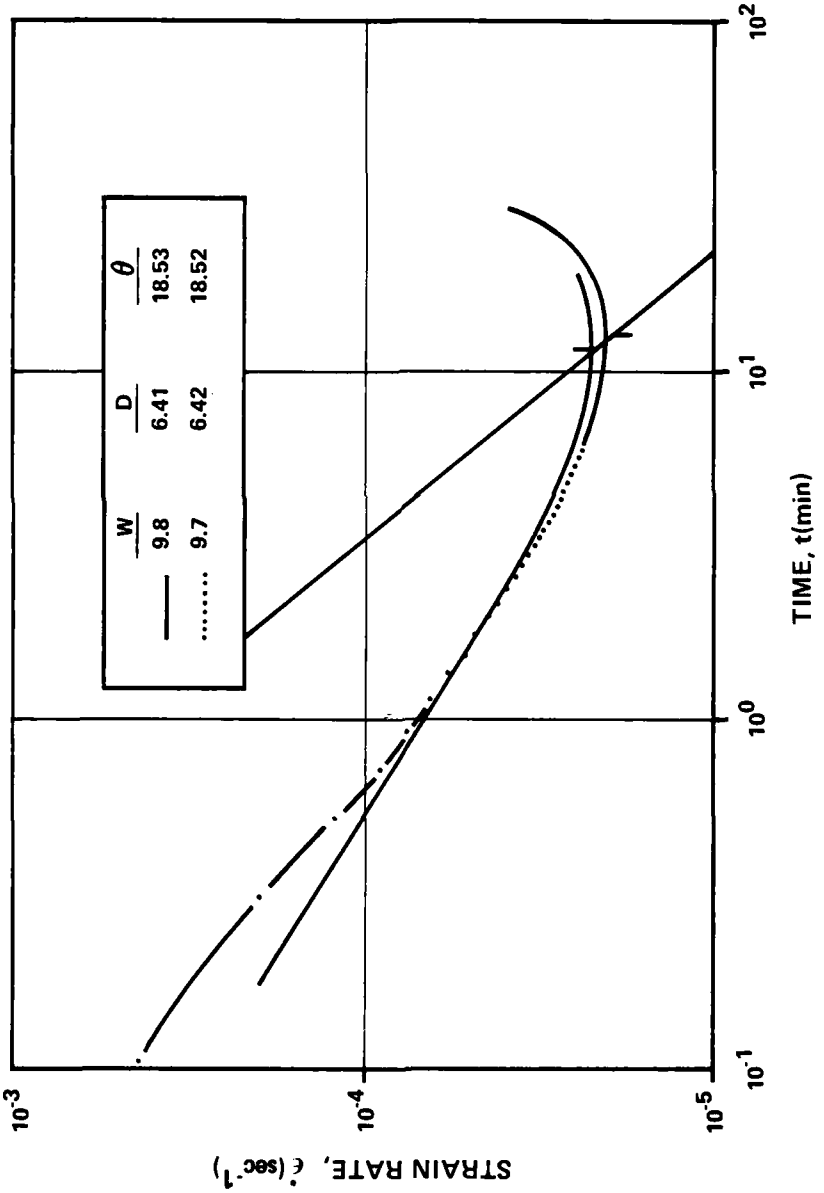

Fig. IV-19 Strain Rate - Time Curves at High Stress Ratio D/D_u = 0.505 for Frozen MFS at w = 10%

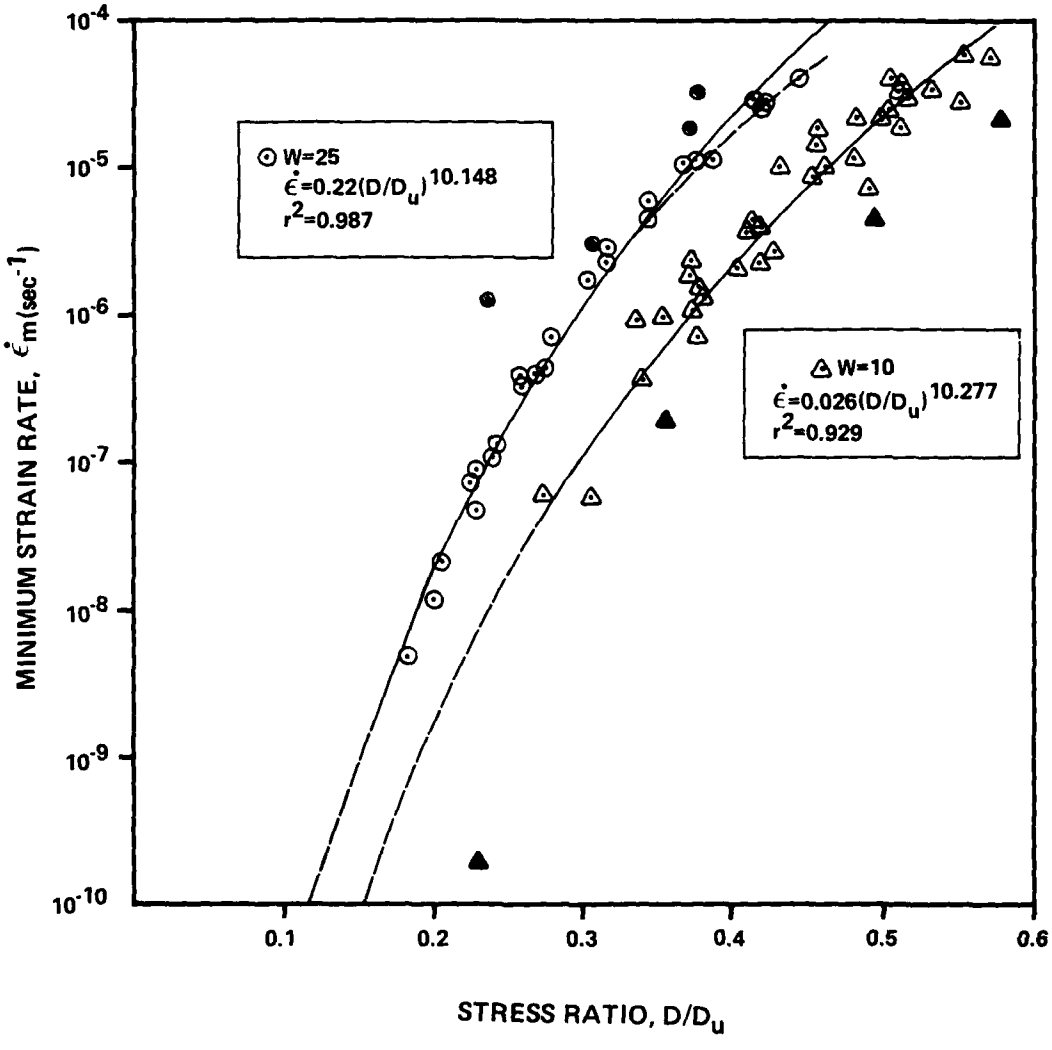

Fig. IV-20 Minimum Strain Rate Dependance on Stress Ratio for Frozen MFS

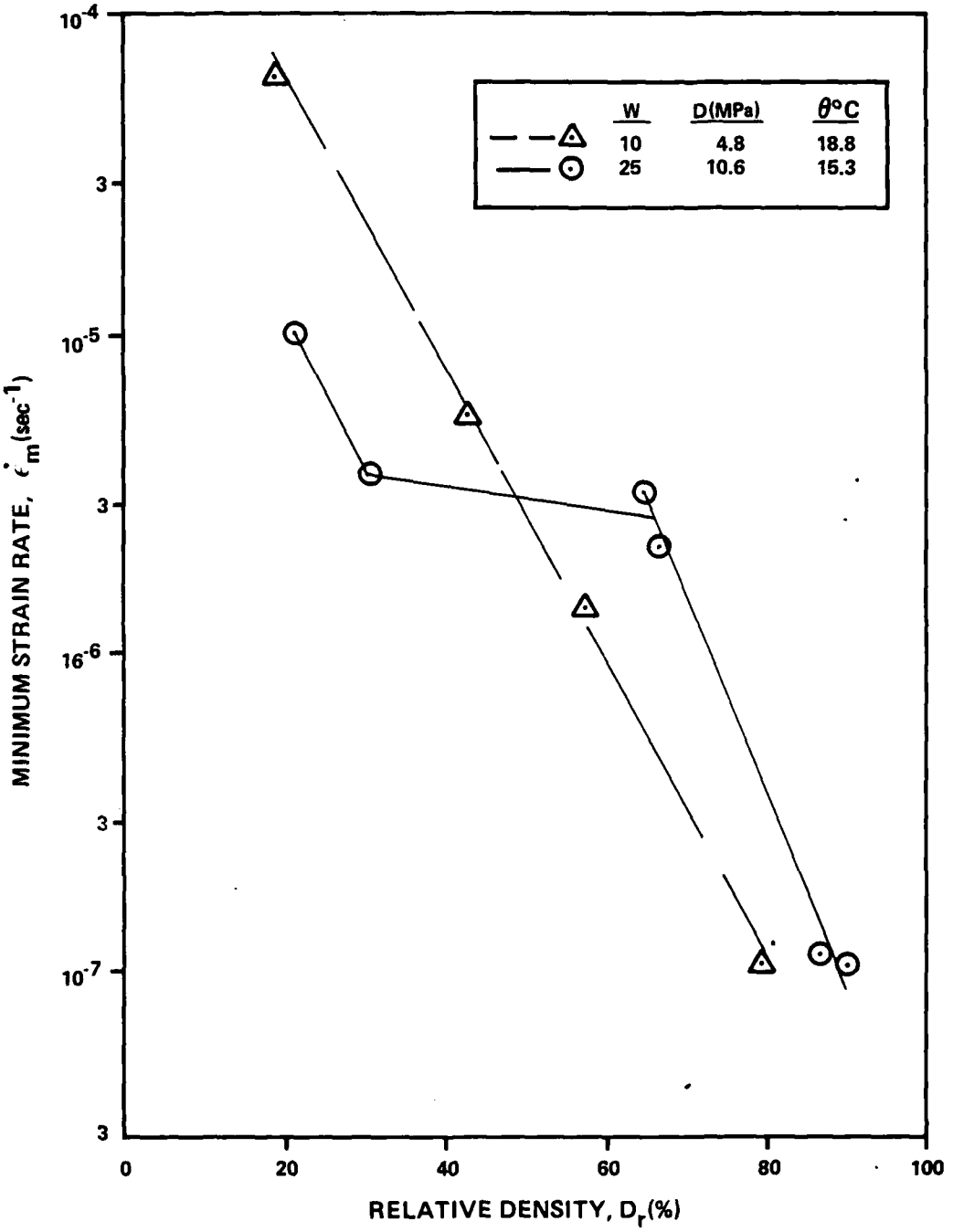

Fig. IV-21 Minimum Strain Rate Dependence on Relative Density for Frozen MFS

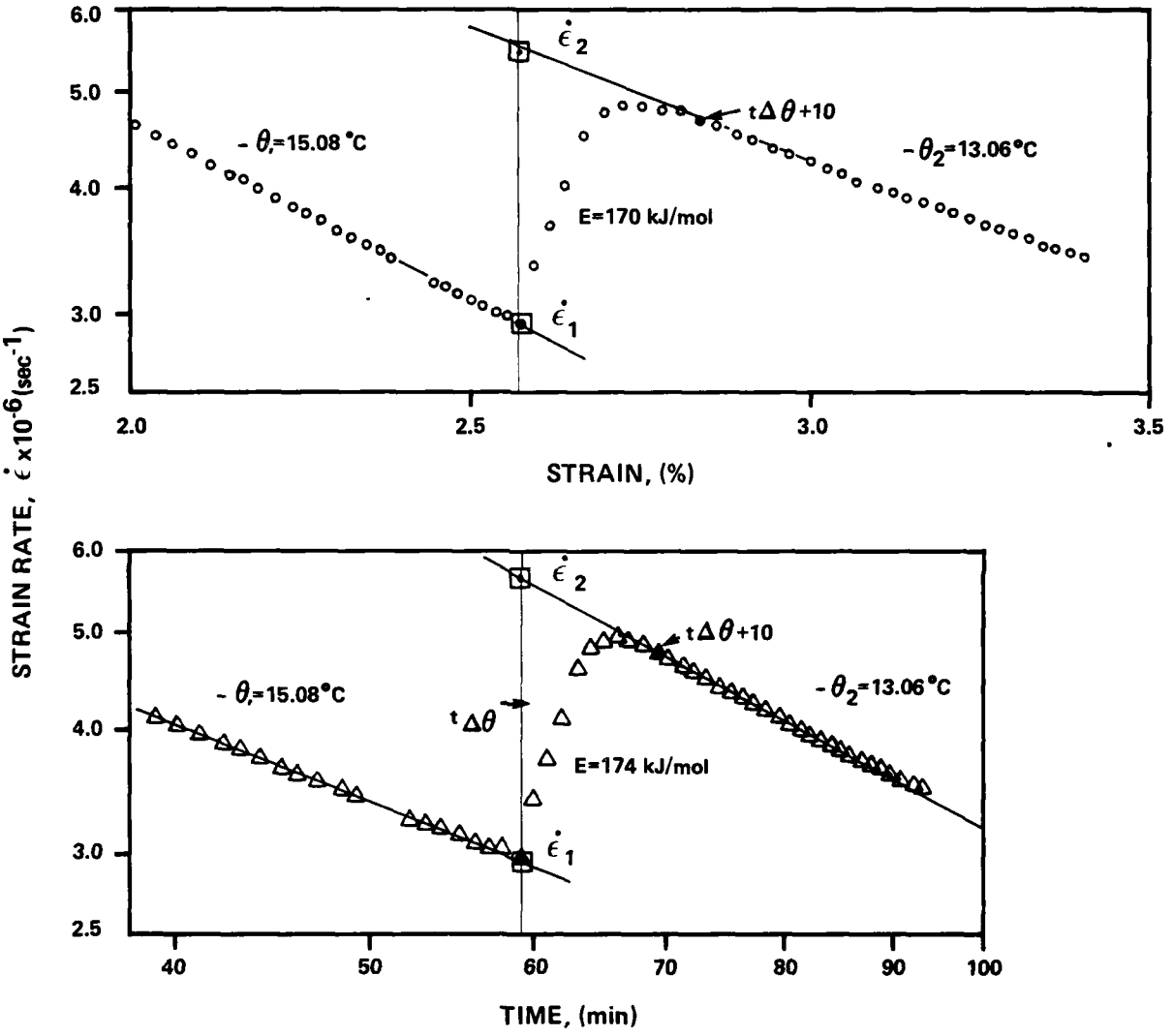

Fig. IV-22 Temperature Stage Test on Frozen Saturated MFS under a Load of D = 9.24MPa

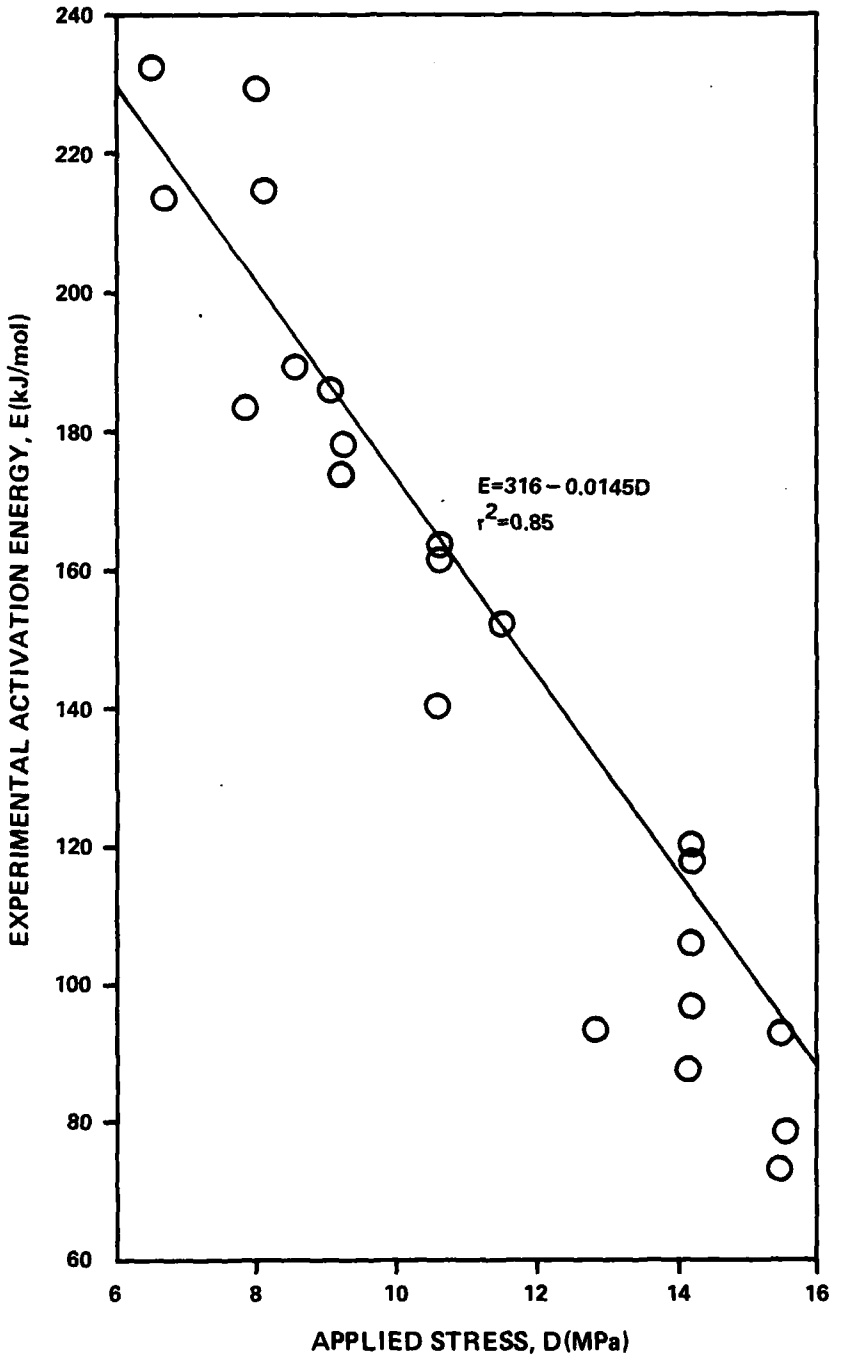

Fig. IV-23 Experimental Activation Energy from Temperature Stage Tests as a Function of Applied Load for Frozen Saturated MFS

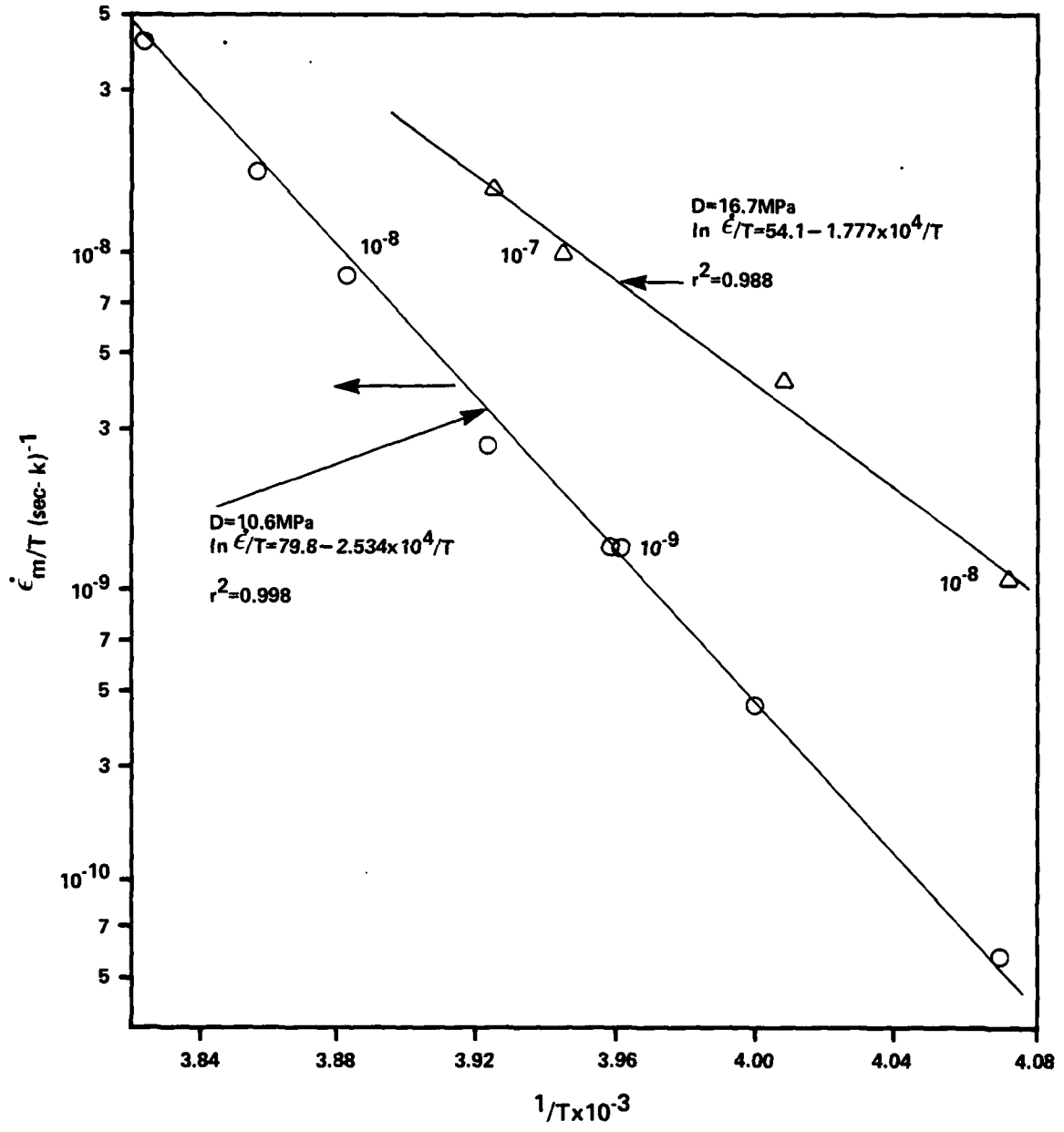

Fig. IV-24 Minimum Strain Rate as a Function of Temperature for Frozen Saturated MFS

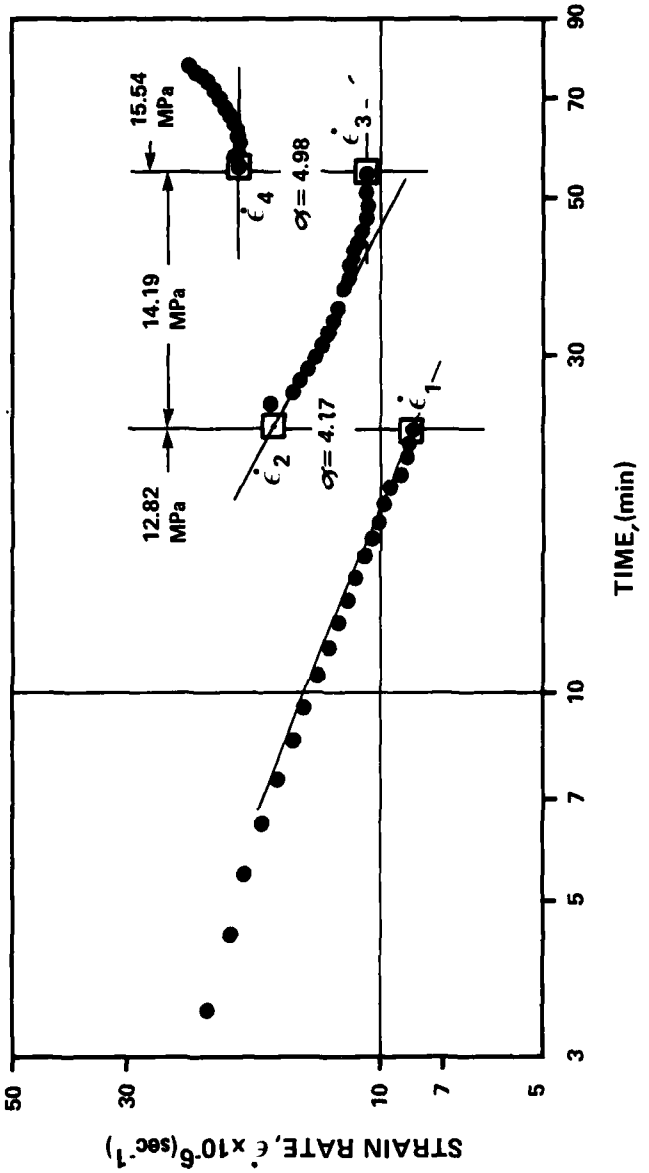

Fig. IV-25 Stress Stage Test on Frozen Saturated MFS at θ = 18.16°C

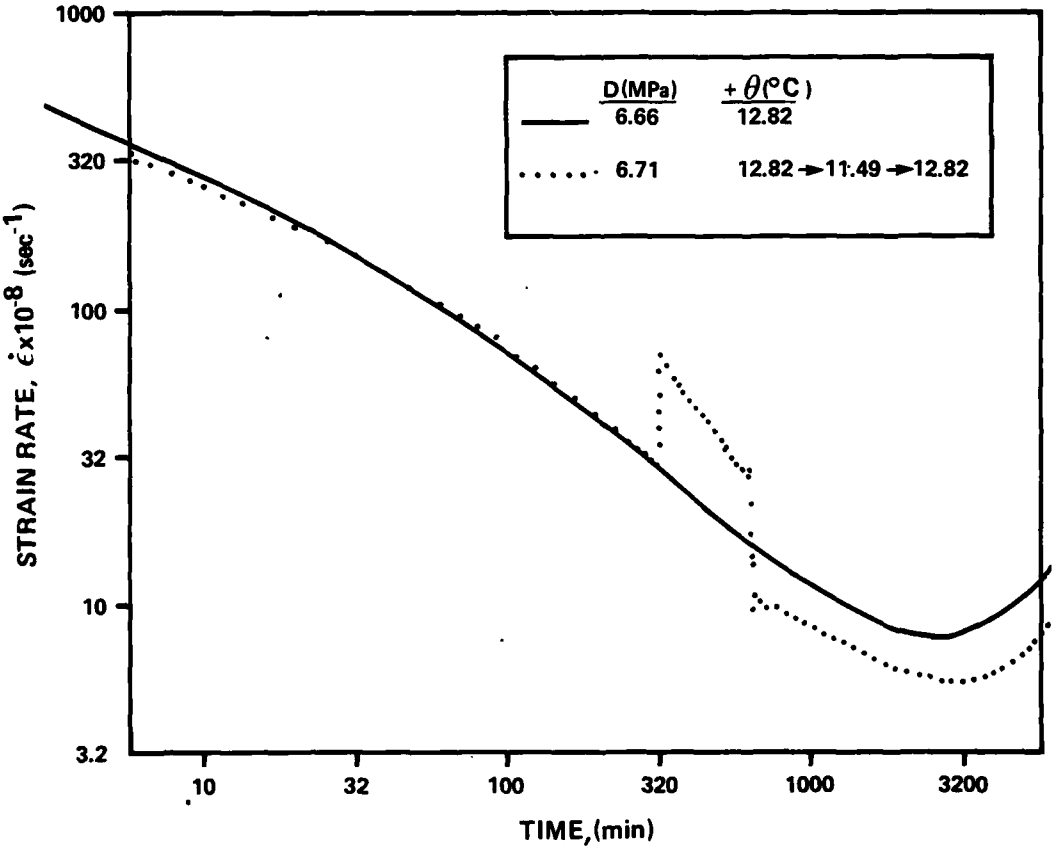

Fig. IV-26 Comparison of Single Temperature Creep Test with Temperature Stage Creep Test for Frozen Saturated MFS

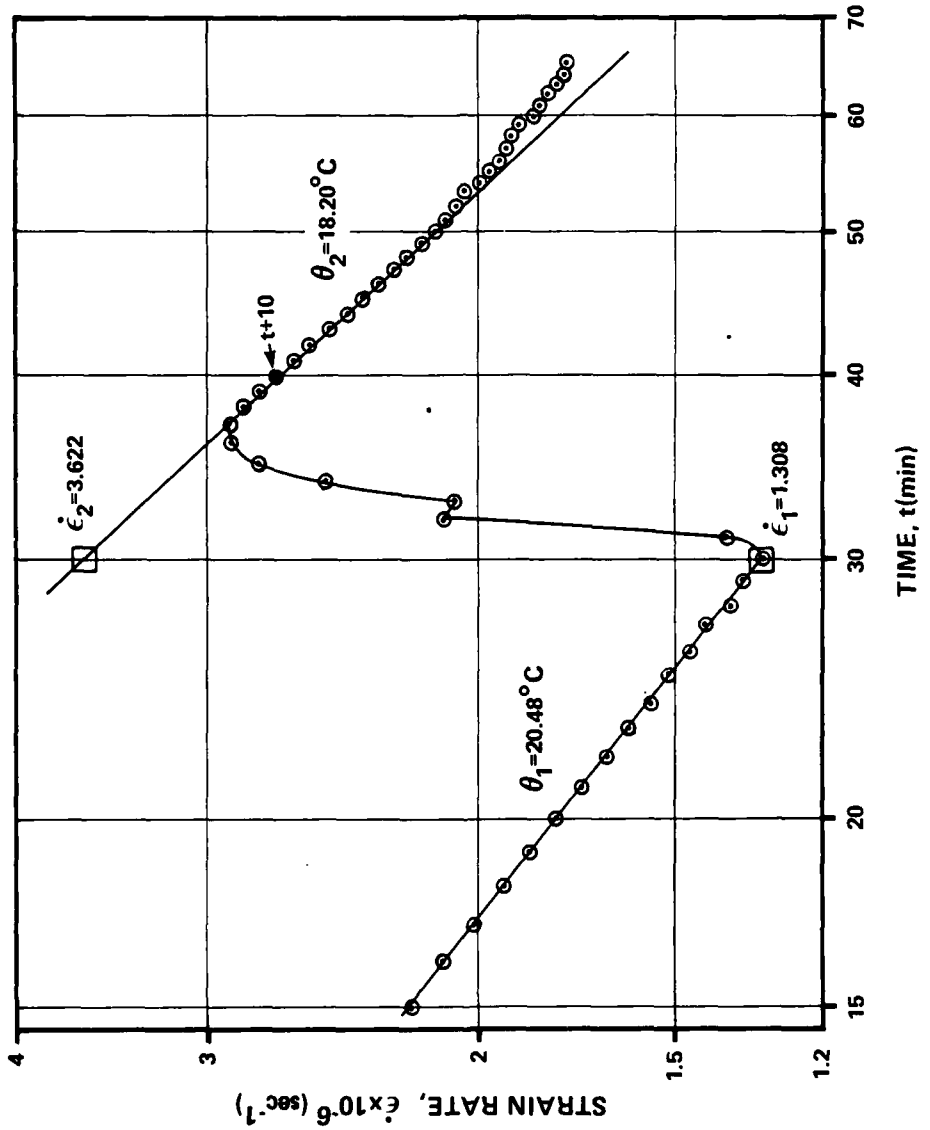

Fig. IV-27 Temperature Stage Test on Frozen MFS at w = 5% under a Load of D = 2.17MPa

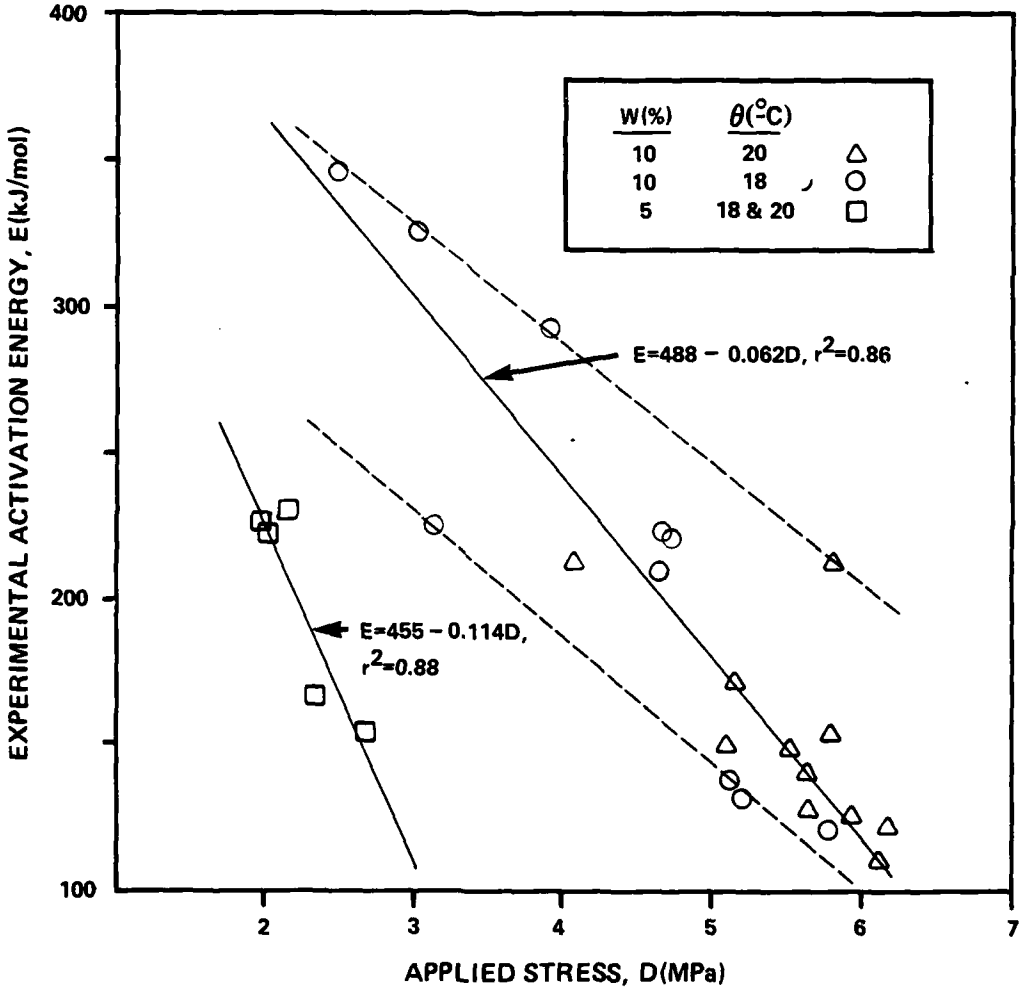

Fig. IV-28 Experimental Activation Energy from Temperature Stage Tests as a Function on Applied Load for Frozen Partially Saturated MFS

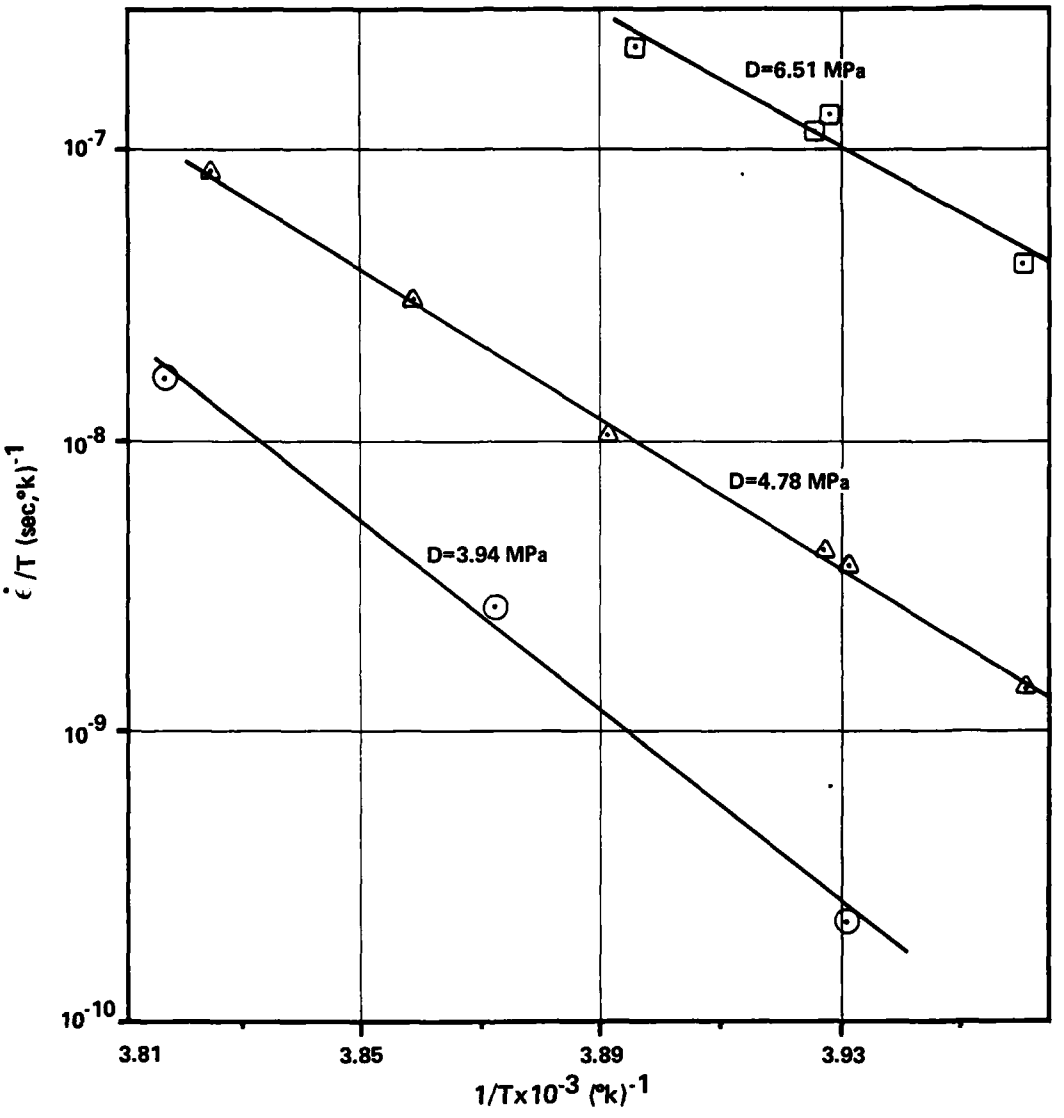

Fig. IV-29 Minimum Strain Rate as a Function of Temperature for Frozen MFS at w = 10%

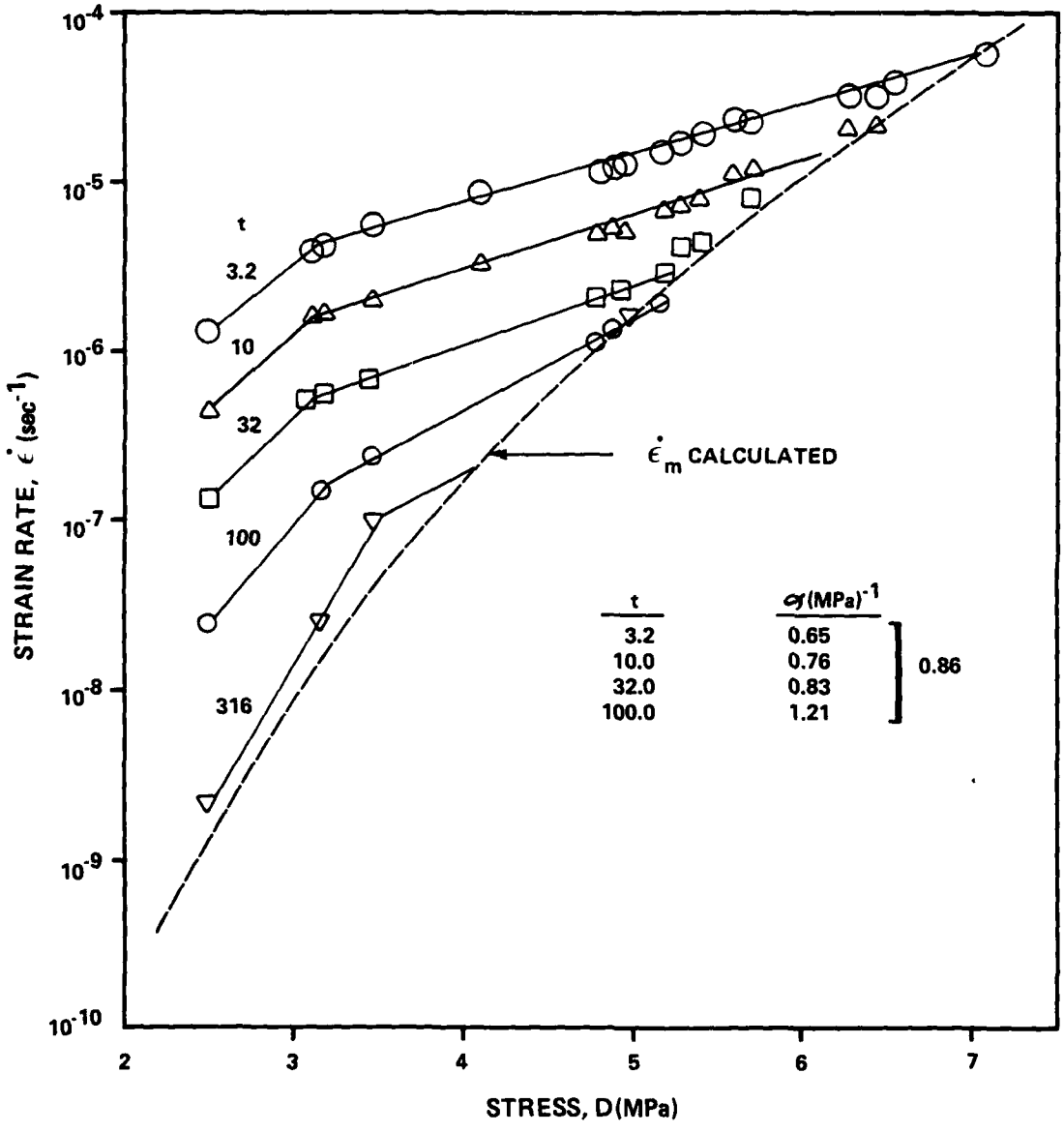

Fig. IV-30 Strain Rate at Constant Time as a Function of Stress for Frozen MFS at w = 10% and θ = 18.6°C

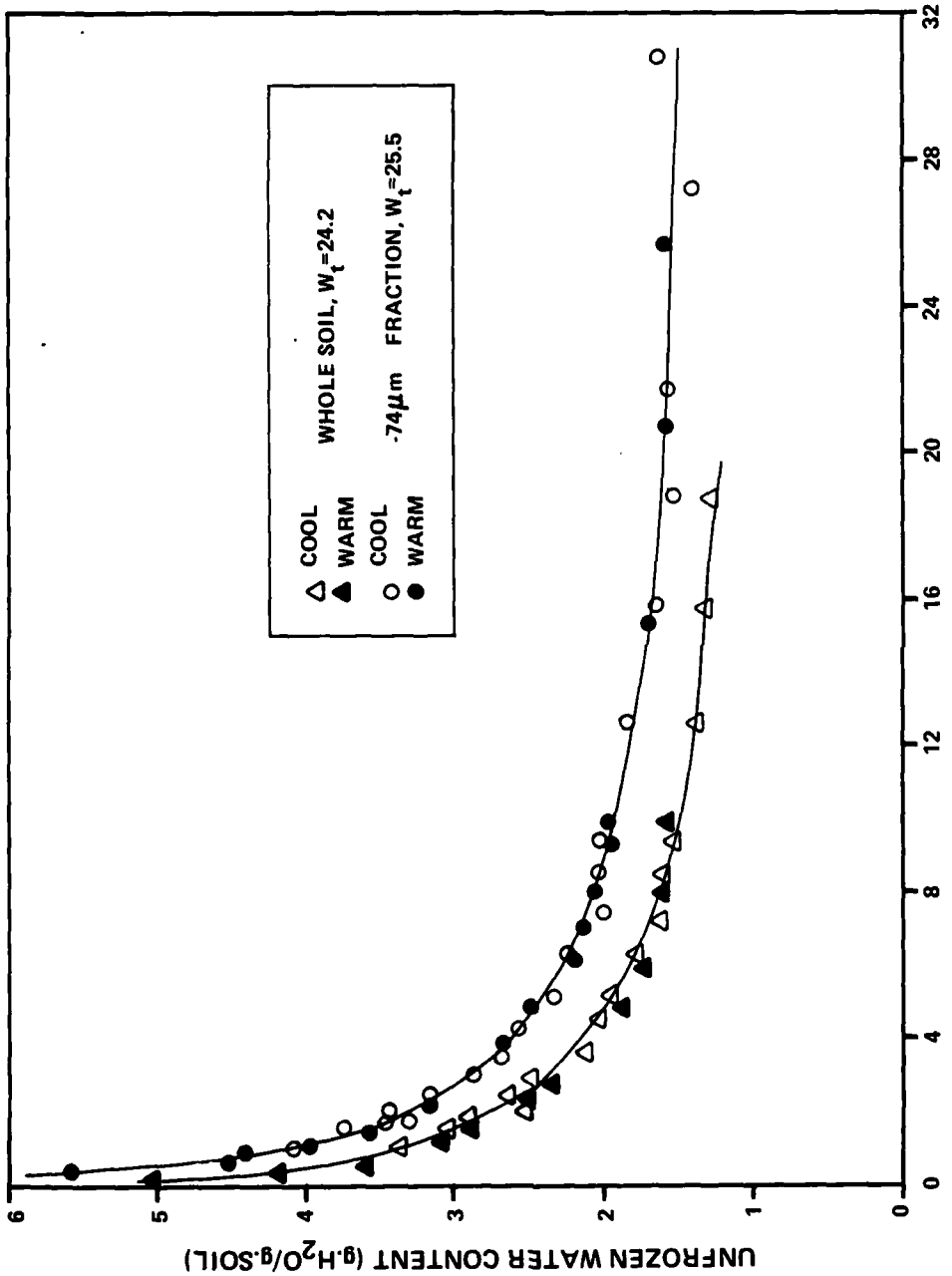

Fig. IV-31 Unfrozen Water Content in Frozen MFS

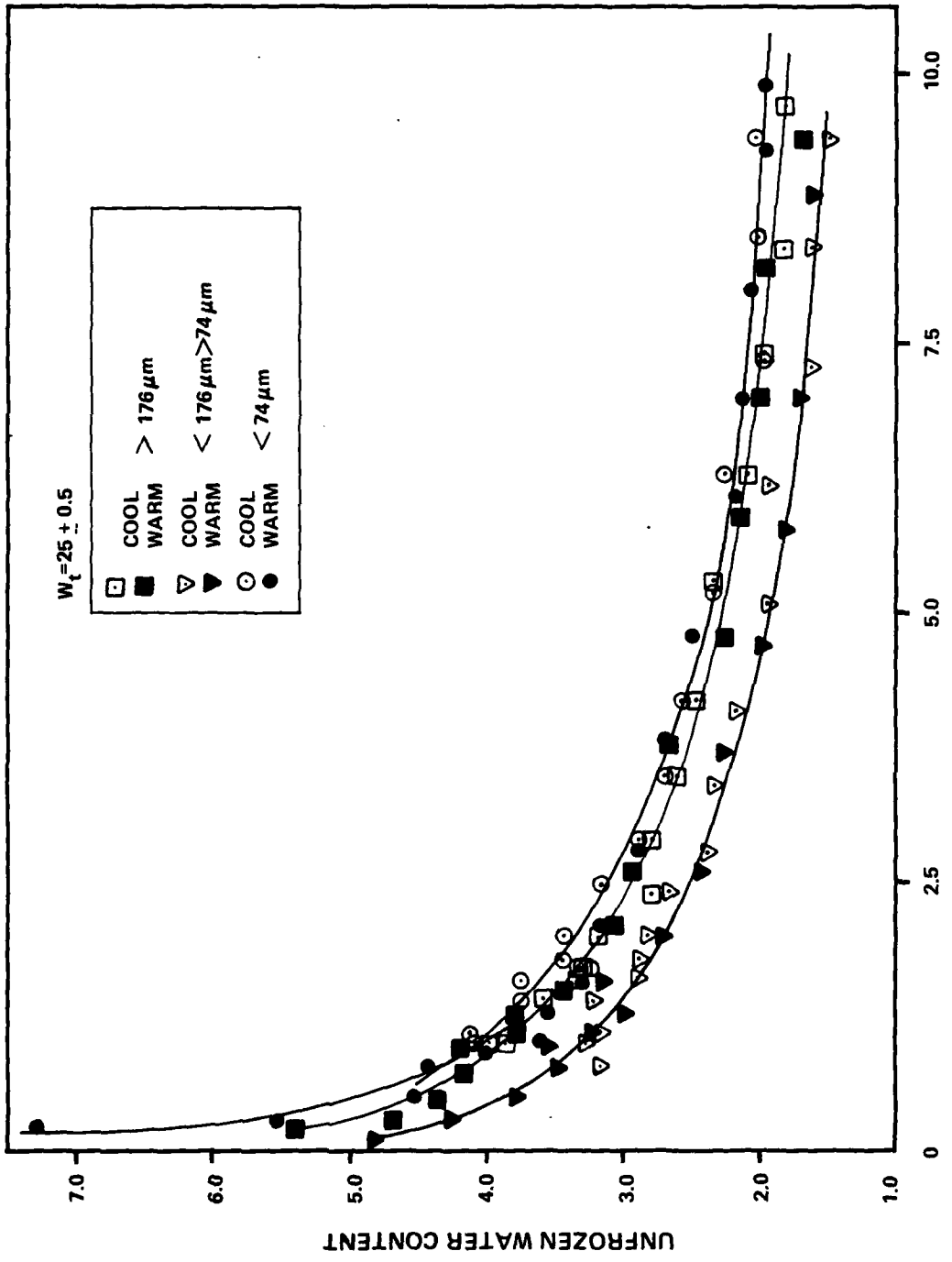

Fig. IV-32 Unfrozen Water Content in Various Size Fractions of Frozen MFS at Total Water Content of 25%

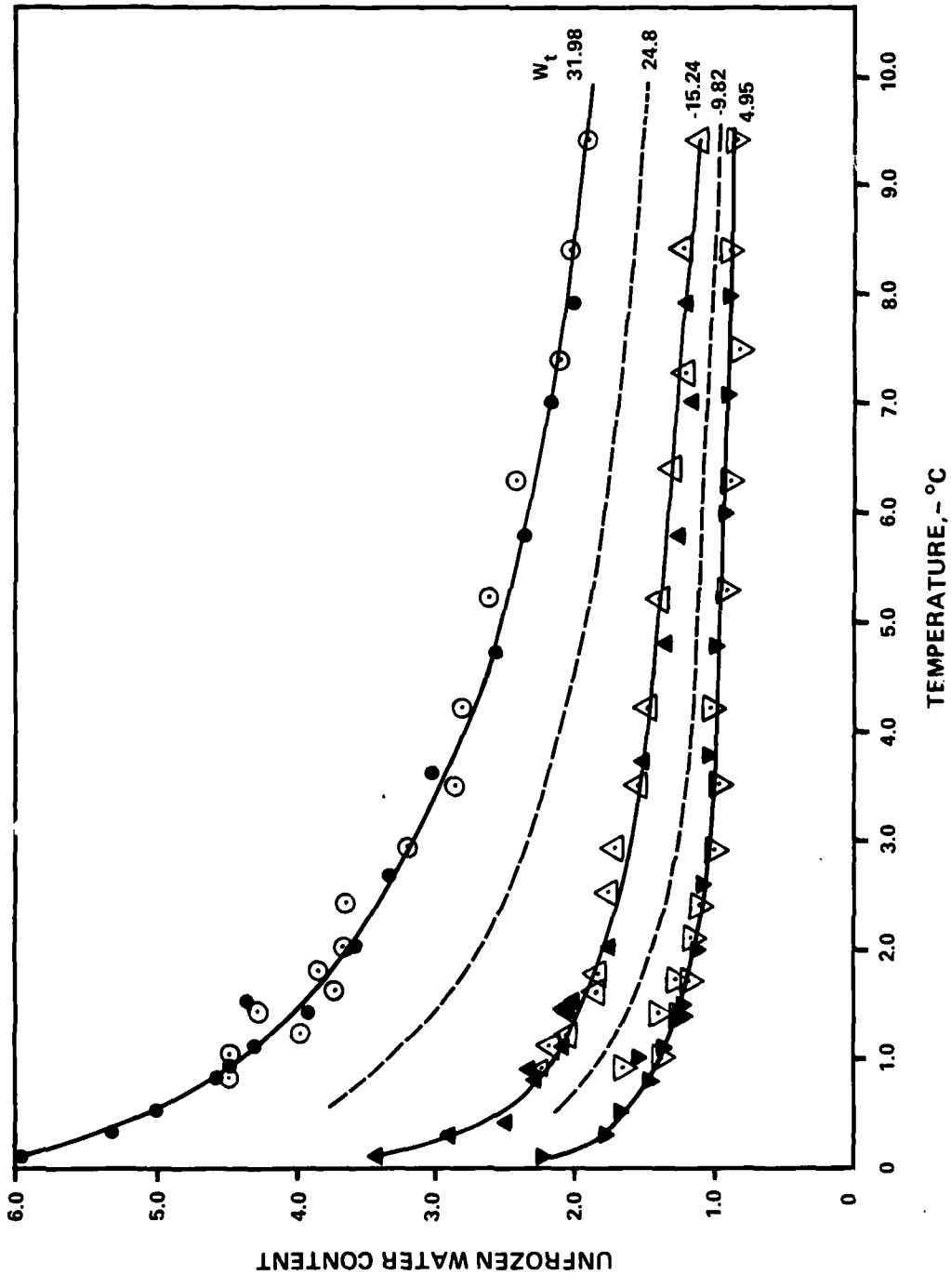

Fig. IV-33 Unfrozen Water Content in Frozen MFS at Different Total Water Contents

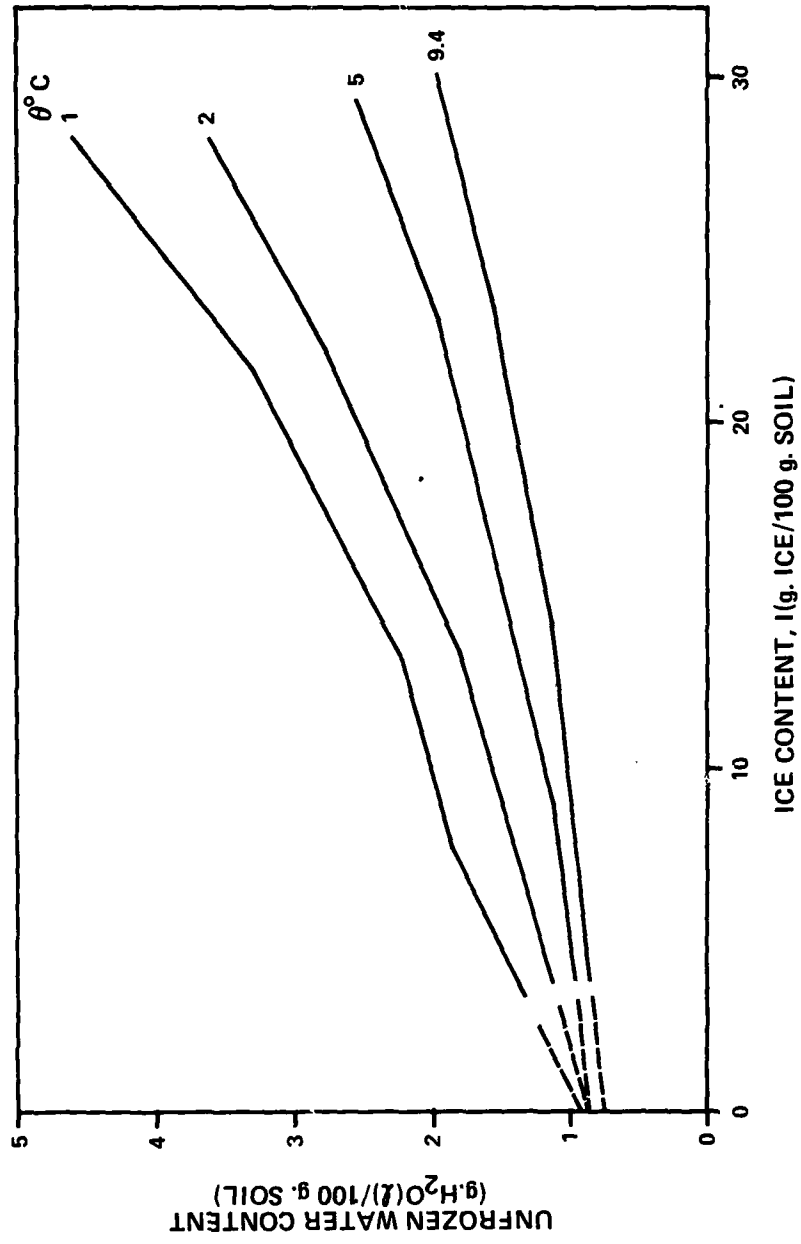

Fig. IV-34 Variation in Unfrozen WAter Content in MFS with Ice Content and Temperature

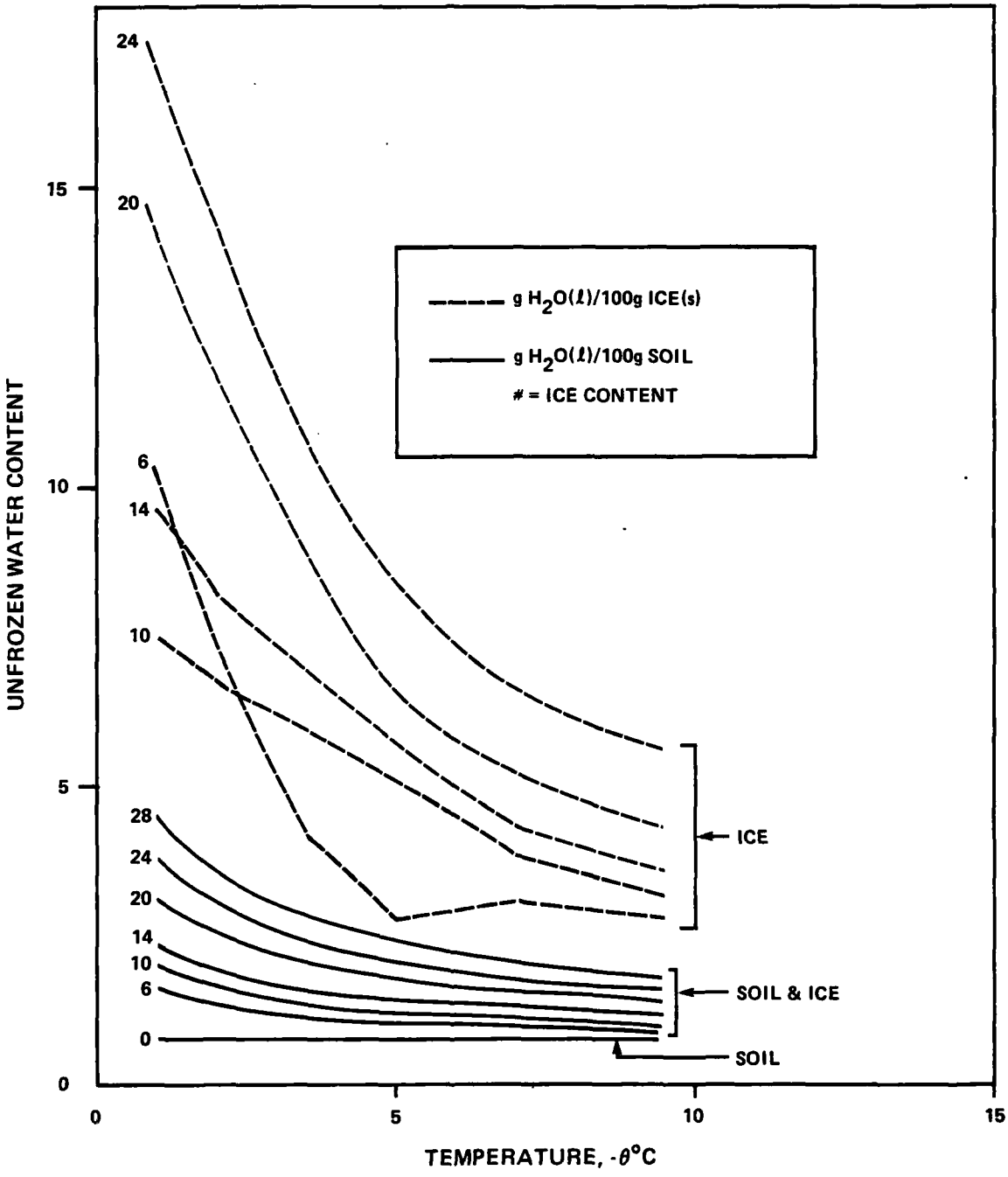

Fig. IV-35 Unfrozen Water Content Attributed to Different Soild Phases in the Frozen MFS System

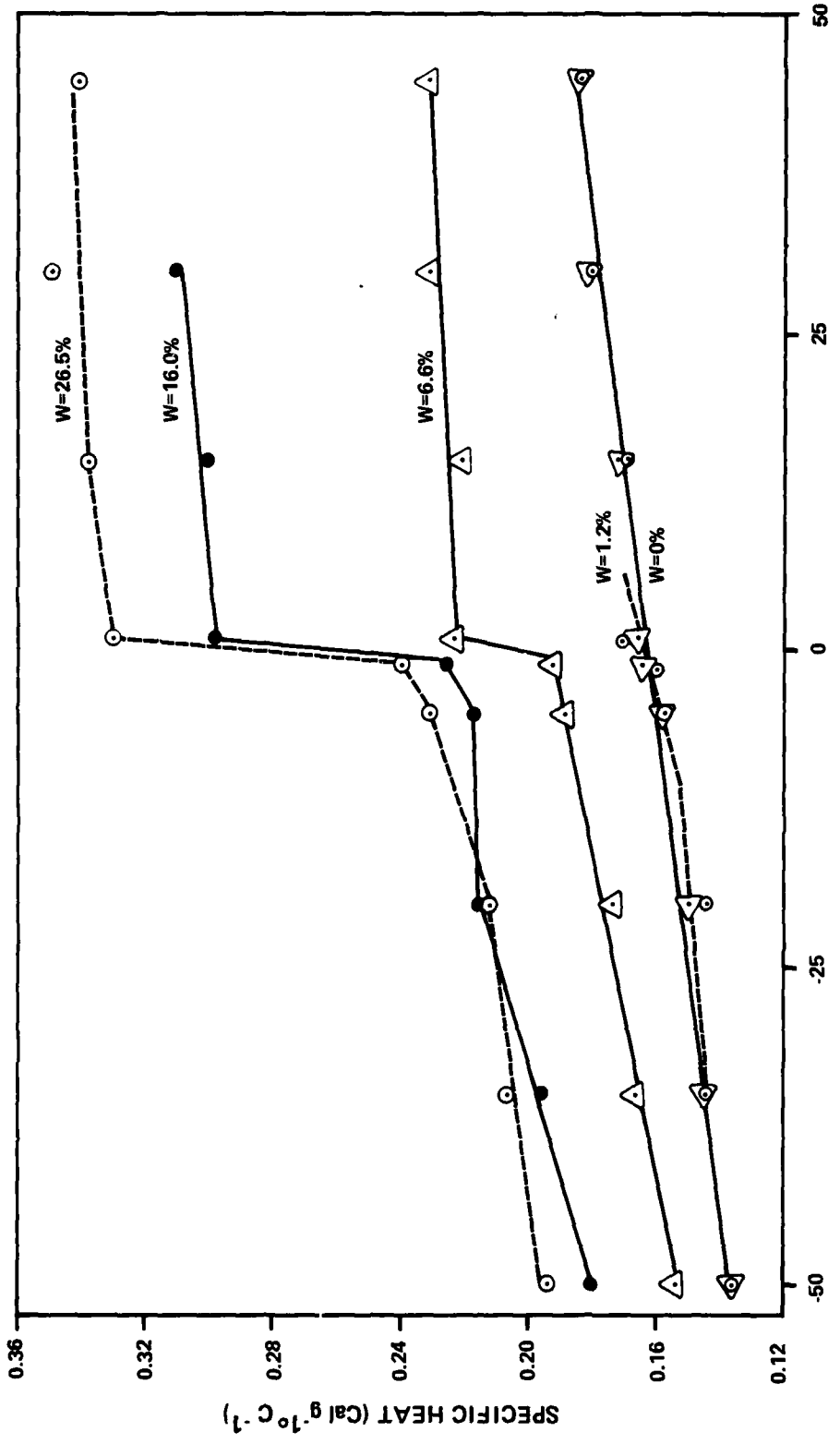

Fig. IV-36 Specific Heat of MFS as a Function of Temperature

Table IV-1

Effect of Temperature Fluctuation on Strain Rate

Sample Number	Temperature θ* Mean(°C)	CV(%)	Time** (Δt)	Strain Rate Mean ($\dot{\varepsilon}$x10^{-8}sec^{-1})	CV(%) Obs.	Expected
S4	16.20	0.44	20	1.56	14.7	6.2
	16.20	0.49	20	1.84	13.0	5.5
	16.20	0.49	60	1.86	11.3	1.9
	16.20	0.49	180	1.86	7.5	0.6
S8-43	14.36	0.29	5	4.86	8.4	3.8
	14.36	0.29	20	4.86	3.1	1.0
	14.79	0.08	20	1.19	3.0	3.8
S8-2	18.82	0.03	10	4.59	1.24	2.0
	18.82	0.03	40	4.59	0.06	0.05

* θ defined as °C below zero.

** time interval (min.) used for calculation of $\dot{\varepsilon}$

Table IV-2

Instantaneous Strength of Frozen Manchester Fine Sand

Sample Number	Average Water Content w (%)	Dry Density γ (kg/m^3)	Test Temp. θ (°C)	Peak Stress D (MPa)	Strain at Peak ε_f (%)	Strain Rate $\dot{\varepsilon}$ (sec^{-1})
7-13	14.8	1510	10.7	6.31	1.04	1.44
7-2	13.2	1563	16.3	11.18	1.25	2.06
7-1	12.9	1563	20.9	14.29	1.22	1.56
8-11	10.07	1539	18.0	12.73	1.03	0.16
8-12	10.01	1540	18.1	12.73	1.28	0.19
8-5	9.84	1542	14.6	10.74	1.03	0.14
8-17	9.91	1541	14.6	9.72	1.44	0.19
8-18	10.10	1539	14.7	10.34	0.85	0.13
8-6	9.77	1543	10.8	9.76	2.06	0.15
8-7	10.06	1539	10.6	8.88	1.40	0.23
8-9	10.24	1546	10.5	9.50	1.76	0.24
8-10	10.03	1550	10.3	8.61	1.50	0.16
S8-8	25*	--	19.6	43.49	1.85	0.22
S8-14	24.78	--	18.1	42.82	3.52	0.29
S8-15	25.20	--	18.1	42.96	2.70	0.22
S8-16	24.98	--	18.1	44.83	3.18	0.27
S8-7	25*	--	14.8	40.05	--	0.3*
S8-11	25*	--	14.6	39.60	--	0.3*
S8-19	25*	1545	14.6	39.36	3.81	0.29
S8-13	25.18	--	10.6	31.99	3.81	0.28
S8-21	25.09	--	10.6	32.52	--	0.3*
S8-22	24.65	--	10.8	31.95	2.42	0.24
S8-32	25*	1533	14.5	36.40	1.22	0.109
S8-33	25.26	1539	14.5	36.29	1.18	0.105
S8-34	25.19	1534	14.6	36.36	1.17	0.105
S8-35	25.21	1540	14.8	29.55	1.32	0.0113
S8-36	24.45	1529	14.7	29.84	1.17	0.0109
S8-37	24.74	1550	14.6	29.59	1.12	0.0104
S8-38	25.48	1529	14.6	31.95	1.17	0.0200

* nominal values

Table IV-3

Creep Data on Frozen Partially Saturated MFS

Sample No.	Average Water Content w (%)	Relative Density D_r (%)	Applied Stress D (MPa)	Temp Θ (°C)	Minimum Strain Rate $\dot{\varepsilon}_m$ (s^{-1})	Time to Minima t_m (min.)	Strain at Minima ε_m (%)
8-29	10.0	56	2.62	10.93	$8.91E^{-7}$	168	2.30
9-53	10.1	72	3.45	13.91	$1.90E^{-7}$	570	1.83
9-48	9.8	64	3.45	18.43	$6.2\ E^{-8}$	1200	1.60
8-22	9.7	56	3.91	11.13	$4.36E^{-6}$	42	2.18
8-26	9.9	55	3.92	14.92	$7.0\ E^{-7}$	182	1.88
8-14	10.0	54	4.02	15.52	$2.42E^{-6}$	65	2.02
8-21	9.6	54	3.98	18.79	$5.62E^{-8}$	1190	1.33
8-73	9.9	56	4.58	18.81	$9.52E^{-7}$	159	2.31
9-35	9.7	56	4.78	11.69	$2.26E^{-5}$	10.5	3.20
9-36	9.7	56	4.78	14.02	$7.28E^{-6}$	29.5	2.85
9-39	9.7	58	4.78	16.22	$2.66E^{-6}$	76	2.85
9-40	9.7	57	4.78	18.57	$1.07E^{-6}$	159	2.60
9-34	9.9	55	4.78	20.69	$3.52E^{-7}$	422	2.55
9-12	9.5	57	4.87	18.65	$1.26E^{-6}$	145	2.71
9-8	9.6	57	4.88	19.20	$1.84E^{-6}$	95	2.53
8-64	9.7	56	4.92	18.85	$1.54E^{-6}$	113	2.48
9-13	9.6	55	5.17	18.70	$2.02E^{-6}$	100	2.96
8-42	9.6	66	5.22	16.51	$1.39E^{-5}$	18.5	3.50
8-58	9.7	55	5.27	18.62	$4.26E^{-6}$	42	2.50
8-66	9.5	58	5.26	18.69	$3.80E^{-6}$	60	2.96
8-54	10.0	55	5.34	18.55	$3.89E^{-6}$	58	2.88
8-53	9.6	55	5.57	18.84	$9.97E^{-6}$	23	2.78
8-51	10.1	60	5.69	18.23	$8.62E^{-6}$	29	3.10
8-65	10.0	55	5.91	18.83	$1.85E^{-5}$	13	2.84
8-52	9.9	55	6.03	18.28	$1.12E^{-5}$	24	2.80
8-49	9.8	58	5.79	20.21	$2.26E^{-6}$	87	2.70
8-50	9.9	57	6.24	18.84	$2.04E^{-5}$	11	2.80
8-56	9.8	54	6.41	18.53	$2.17E^{-5}$	11.6	3.03
8-67	9.7	55	6.42	18.52	$2.03E^{-5}$	13	3.07
8-69	9.7	56	6.50	20.68	$1.0\ E^{-5}$	22	2.93
8-48	9.8	61	6.51	16.52	$5.62E^{-5}$	4.2	2.90
8-47	9.9	62	6.50	18.59	$3.28E^{-5}$	7.5	3.02
8-39	10.0	59	6.52	18.47	$2.89E^{-5}$	8.4	3.00
8-19	10	52	6.55	18.88	$3.98E^{-5}$	7	3.00
8-31	9.9	58	6.57	18.8	$1.64E^{-5}$	15	2.86
8-63	9.7	56	6.61	18.84	$3.83E^{-5}$	6.5	3.04
8-57	9.8	56	6.70	18.36	$3.25E^{-5}$	9	2.97
8-70	9.8	54	7.02	18.58	$2.76E^{-5}$	9.3	3.18
8-40	10.1	59	7.03	20.59	$2.19E^{-5}$	11.2	2.97
9-1	9.6	57	7.08	18.66	$5.89E^{-5}$	4.3	2.63

Table IV-4

Creep Data on Frozen Saturated MFS

Sample No.	Average Water Content w (%)	Relative Density D_r (%)	Applied Stress D (MPa)	Temp Θ (°C)	Minimum Strain Rate $\dot{\varepsilon}_m$ (s^{-1})	Time to Minima t_m (min.)	Strain at Minima ε_m (%)
S8-45	24.8	57	6.66	12.82	$7.80E^{-8}$	2330	3.04
S8-30	24.9	57	7.54	12.65	$3.99E^{-7}$	900	4.18
S8-28	24.7	58	7.87	14.88	$1.29E^{-7}$	2195	4.33
S8-46	24.7	58	7.87	12.62	$4.0\ E^{-7}$	970	4.88
S8-76	24.7	58	8.75	18.67	$9.1\ E^{-8}$	3200	4.8
S8-2	24.2	58	8.87	18.82	$4.73E^{-8}$	3800	3.0
S8-58	24.8	59	9.06	15.27	$4.10E^{-7}$	884	4.61
S8-59	25.2	56	9.08	12.31	$2.81E^{-6}$	120	3.88
S9-1	---*	56	10.57	18.50	$6.87E^{-7}$	465	4.3
S9-86	---*	60	10.61	22.92	$1.25E^{-6}$	300	2.8
S9-31	24.4	62	10.61	20.54	$3.41E^{-7}$	1290	4.6
S9-45	24.0	65	10.61	20.49	$3.50E^{-7}$	1140	4.9
S9-53	24.3	63	10.61	16.12	$3.08E^{-6}$	165	6.6
S9-39	24.1	65	10.62	22.57	$1.13E^{-7}$	3100	4.7
S9-137	25.0	55	10.62	27.40	$2.10E^{-8}$	10,000	2.9
S9-42	23.3	67	10.63	15.52	$2.18E^{-6}$	225	4.8
S8-80	24.9	55	10.63	11.48	$1.12E^{-5}$	51.5	5.5
S9-64	---*	63	10.64	13.80	$4.53E^{-6}$	110	4.8
S9-126	24.4	61	11.35	18.24	$1.62E^{-6}$	283	4.95
S8-68	25.2	53	14.07	18.35	$1.84E^{-5}$	45	6.37
S9-102	24.7	58	14.17	20.57	$5.96E^{-6}$	75	5.0
S9-41	24.6	62	14.22	18.46	$1.06E^{-5}$	60	5.8
S9-10	24.6	59	15.45	18.07	$2.85E^{-5}$	16.5	4.5
S9-114	24.2	62	15.51	20.55	$2.24E^{-5}$	30	6.61
S9-134	24.2	55	16.54	27.56	$2.55E^{-6}$	165	4.29
S9-138	25.1	54	16.64	19.63	$2.47E^{-5}$	17	3.70
S8-79	24.8	54	16.69	18.37	$3.98E^{-5}$	14.4	5.0
S9-135	25.1	58	16.81	23.63	$1.05E^{-5}$	42	3.73
S9-136	24.3	56	17.53	20.73	$2.65E^{-5}$	13	3.29

* Nominal w = 25%

Table IV-5

Creep Data on Frozen Partially Saturated MFS

Sample No.	Average Water Content w (%)	Relative Density D_r (%)	Applied Stress D (MPa)	Temp Θ (°C)	Minimum Strain Rate $\dot{\varepsilon}_m$ (s^{-1})	Time to Minima t_m (min.)	Strain at Minima ε_m (%)
8-05-3	5.0	57	1.382	19.09	$1.63E^{-7}$	390	1.29
9-05-2	4.6	57	2.166	20.09	6.34^{-7}	200	2.52
9-05-1	4.7	56	2.168	18.78	$1.27E^{-6}$	100	1.90
8-05-2	5.1	55	3.064	19.14	$2.74E^{-5}$	6.5	2.18
9-05-5	4.9	54	3.146	18.56	$4.92E^{-5}$	3.2	1.98
9-05-3	4.9	54	3.149	20.42	$1.64E^{-5}$	13	2.51
8-05-1	4.9	56	4.348	19.02	$2\ E^{-4}$	1.5	2.5

Table IV-6

Evaluation of $\dot{\varepsilon}_m - t_m$ at Different ε_m

(For w = 25%)

		Total	High	Medium	Low
Strain at Minima, ε_m(%)					
	Mean	4.7	6.4	4.79	3.0
	S.D.	1.0	0.3	0.17	0.2
Strain Rate Range		$4\ E^{-5}$	$1\ E^{-5}$	$4\ E^{-5}$	$2.7\ E^{-5}$
		$1\ E^{-8}$	$1\ E^{-8}$	$1\ E^{-7}$	$2\ E^{-8}$
Regression Coefficients*	$A.E^{-4}$	8.21	10.15	6.83	3.99
	B	-1.129	-1.137	-1.082	-1.089
	r^2	0.989	0.999	0.997	0.998

* $\dot{\varepsilon}_m = A(t_m)^B$

Table IV-7

Experimental Activation Energy from Temperature Stage Tests on Saturated MFS

Sample Number	Applied Stress D (MPa)	Experimental Activation Energy (kJ/mol)	Temperature of Stages (°C) θ_1	θ_2	Time* Ratio t/tm	Strain at Temp. Change $\varepsilon_{\Delta\theta}$ (%)
S8-51	5.33	460	19.17	17.84	0.0003	0.31
		344	20.39	18.53	0.003	0.36
S8-49	6.54	233	18.76	17.40	0.002	0.72
		227	17.40	18.82	0.008	1.09
S8-26	6.72	214	14.87	11.87	0.005	1.38
S8-50	7.86	183	18.46	17.24	0.01	1.12
		284	17.28	18.39	0.17	3.84
S8-55	8.02	230	14.86	13.04	0.06	1.42
S8-56	8.15	216	15.11	12.03	0.07	1.28
		271	12.03	15.15	0.62	2.53
S8-66	8.61	190	18.59	16.07	0.31	6.38
S8-52	9.04	186	19.70	18.37	0.03	0.53
		219	18.37	19.66	0.13	2.44
		228	19.66	18.23	0.29	3.61
		219	18.23	19.67	0.52	3.90
S8-57	9.24	174	15.08	13.06	0.09	2.58
		188	13.06	15.13	0.63	4.58
S8-60	9.25	178	15.07	13.07	0.10	2.70
		216	13.07	15.06	0.30	4.82
		220	15.06	13.05	0.46	5.44
S8-70	10.61	140	18.66	16.29	0.13	4.02
S8-73	10.61	164	16.28	18.65	0.14	3.95
S8-74	10.61	162	18.62	16.28	0.15	2.47
S9-127	11.52	153	18.19	15.59	0.42	2.94
S9-112	12.83	93.2	19.29	15.64	0.13	2.25
S9-22	14.15	120	18.04	15.85	0.32	2.75
S9-19	14.17	88.2	18.18	15.93	0.26	2.07
S9-67	14.20	134	18.51	16.14	0.96	5.75
S9-8	14.20	119	18.32	16.11	0.78	4.16
S9-33	14.20	106	18.17	16.01	0.51	3.3
S9-68	14.22	97.2	18.10	15.93	0.28	1.85
S9-5	14.24	72.9	18.02	15.84	0.45	3.62
S9-27	15.46	137	18.35	20.51	0.20	1.65
S9-128	15.50	93.0	24.66	22.88	0.19	1.86
S9-113	15.50	73.2	22.82	20.54	0.17	2.81
S9-111	15.53	78.4	20.52	18.21	0.29	4.15

* The fractional time toward minimum strain rate.

Table IV-8

RPT Parameters from Temperature Dependance at Various Time Fractions of t_m on Saturated MFS

Time Ratio t/tm	Experimental Activation Energy E(kJ/mol) D = 10.61 (MPa)	D = 16.69 (MPa)	Free Energy of Activation ΔF (kJ/mol)	Number of Bonds $S_\beta \times 10^{15}$ (bonds/m^2)
1.0	147.7	210.7	321	4.1
0.75	152.4	212.9	319	4.2
0.50	150.8	212.1	319	4.2
0.25	143.5	212.2	332	3.7
	From Δθ Stage		316	3.1

Table IV-9

Number of Bonds S_α from Stress Stage Tests on Saturated MFS

Sample No.	Temp. θ (°C)	Stress Stage α (MPa^{-1})	Number of Bonds $S_\alpha \times 10^{15}$ ($\#/m^2$)	Stresses for Stages (MPa) D_1	D_2	Time* Ratio t/t_m	Strain at Stress Change $\varepsilon\Delta D$(%)
S9-99	18.62	0.856	23.3	8.17	9.54	0.004	0.6
		0.803	24.8	9.54	10.90	0.08	1.74
S9-9	18.82	0.627	31.8	9.69	11.14	0.04	1.47
		0.619	32.2	11.14	11.97	0.31	2.80
S9-115	18.22	0.729	27.3	10.06	11.48	0.06	2.40
		0.578	34.4	11.48	12.81	0.40	3.95
S9-129	18.07	0.524	38.0	11.43	12.80	0.15	2.31
		0.510	39.0	12.80	14.15	0.85	3.97
S9-105	18.29	0.560	35.6	11.49	12.86	0.26	3.09
		0.481	41.4	12.86	14.20	1	5.3
S9-118	18.16	0.477	41.7	12.82	14.19	0.23	2.64
		0.399	49.9	14.19	15.54	1	4.8
S9-14	18.23	0.325	61.3	14.21	15.52	0.36	3.05
		0.325	61.2	15.52	16.89	1	5.6
S8-41	12.81	1.356	14.4	7.05	6.53	0.02	1.05
		1.825	10.7	6.53	7.29	0.79	3.14
S9-24	26.58	0.466	44.2	13.67	15.06	0.02	0.81
	27.83	0.377	54.9	15.06	16.23	0.11	1.38

$$S_\alpha = 0.0437 D_1^{1.799} \qquad r^2 = 0.953$$

* The fractional time toward minimum strain rate.

Table IV-10

Number of Bonds S_α Determined from Different Analysis Methods on Saturated MFS

Temperature θ	$S_\alpha \times 10^{15}$ (bonds/m^2) from ΔD Eq. IV-3	$S_\alpha \times 10^{15}$ (bonds/m^2) from $(\ell n \hat{\epsilon} - D)t$ Eq. II-25
12.5	-	38
12.8	13	-
15.0	-	41
18.3	39	-
18.5	-	56
20.5	-	60
27	50	-

Table IV-11

Experimental Activation Energy from Temperature Stage Tests on Partially Saturated MFS

Sample Number	Applied Stress D (MPa)	Experimental Activation Energy (kJ/mol)	Temperature of Stages (°C) θ_1	θ_2	Time* Ratio t/t_m	Strain at Temp. Change $\varepsilon_{\Delta\theta}$ (%)
w = 10%						
9-18	6.18	122	20.43	18.20	0.23	1.86
8-71	6.14	110	20.41	18.26	0.56	1.65
9-4	5.94	126	20.46	18.26	0.42	2.57
8-62	5.79	154	20.71	18.34	0.46	2.35
8-37	5.78	216	20.63	18.19	0.48	1.43
9-6	5.63	128	20.69	18.32	0.12	1.70
9-2	5.63	140	20.67	18.22	0.24	1.98
9-14	5.14	172	20.44	18.26	0.12	1.03
9-16	5.08	150	20.40	18.24	0.14	1.50
9-28	4.09	216	20.60	18.25	0.05	1.05
9-20	5.49	149	20.31	18.18	0.16	1.53
8-38	5.78	123	18.38	16.29	0.75	2.33
8-46	5.21	131	18.60	16.56	0.19	1.49
9-24	5.12	139	18.70	16.39	0.15	1.48
9-45	4.73	222	18.39	16.14	0.85	1.96
9-42	4.67	224	18.09	15.89	0.58	2.00
9-43	4.67	211	18.31	16.18	0.27	1.77
8-35	3.91	294	18.85	14.53	0.43	1.62
9-25	3.15	225	18.71	16.29	0.007	0.63
9-37	3.15	456	18.72	16.22	0.07	0.75
9-44	3.13	402	18.56	16.15	0.04	0.62
9-41	3.10	326	18.48	16.04	0.02	0.65
9-38	2.49	347	18.73	16.32	0.008	0.26
w = 5%						
9-05-8	1.99	211	20.43	18.26	0.05	0.81
9-05-10	2.01	222	18.24	15.90	0.09	0.46
9-05-7	2.17	231	20.48	18.20	0.15	0.78
9-05-9	2.32	166	20.42	18.25	0.13	1.27
9-05-11	2.68	154	20.86	18.83	0.38	1.52

AD-A103 556 MASSACHUSETTS INST OF TECH CAMBRIDGE DEPT OF CIVIL E--ETC F/G 8/13
CREEP BEHAVIOR OF FROZEN SAND.(U)
JUN 81 R T MARTIN, J M TING, C C LADD DAAG29-77-C-0016
UNCLASSIFIED R81-19 ARO-14725.3-GS NL

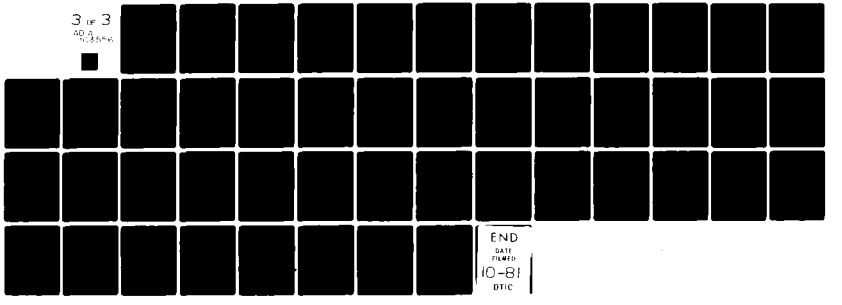

Table IV-12

Number of Bonds, S_α, from Stress Stage Tests on Partially Saturated MFS

Sample Number	Temp. θ (°C)	Stress Stage α (MPa^{-1})	Number of Bonds $S_\alpha \times 10^{15}$ ($\#/m^2$)	Stresses for Stages (MPa) D_1	D_2	Time Ratio t/t_m	Strain at Stress Change $\varepsilon\Delta D$(%)
9-7	18.36	1.88	10.6	4.09	4.76	0.06	0.82
		1.76	11.3	4.76	4.08	0.57	1.52
		1.91	10.4	4.08	5.11	0.21	1.58
		2.25	8.9	5.11	4.08	1.9	2.11
		2.54	7.9	4.08	5.10	.4	2.17
9-19	18.66	1.52	13.2	5.47	4.78	.28	1.69
9-17	18.61	1.76	11.4	4.78	5.47	0.171	1.50
		1.72	11.6	5.47	4.78	0.98	2.15
9-21	18.68	1.35	14.8	5.47	6.16	.30	1.82
		1.39	14.4	6.16	5.47	1.4	2.55
9-15	18.51	1.43	14.0	4.77	5.46	0.14	1.35
		1.62	12.3	5.46	4.78	1.2	2.36
9-23	18.68	1.44	13.9	4.78	5.47	0.06	-
		1.64	12.2	5.47	4.78	0.85	-
9-26	18.44	1.34	14.9	6.16	4.78	0.09	1.2
		1.48	13.5	4.78	6.16	0.18	1.76
9-27	18.76	1.32	15.2	4.78	6.16	0.013	0.86
		1.41	14.2	6.16	4.78	0.57	2.07

Table IV-13

Summary of RPT Parameters on Frozen MFS

Water Content (%)	Free Energy of Activation, ΔF (kJ/mol) from		Number of Bonds per m^2 $S_\beta \times 10^{15}$ from		$S_\alpha \times 10^{15}$ from	
	$\Delta\theta$	$\dot{\varepsilon}_m$	$\Delta\theta$	$\dot{\varepsilon}_m$	ΔD	$(\ell n \dot{\varepsilon} - D)_t$
25	316	320	3	4.2	39	56
10	488	424	0.7	1.3	13	23
	406*		1.0*			
5	455	-	0.4	-	-	23

* From average eyeball slope of E vs. D.

Table IV-14

Summary of Ice Creep Data

Sample Number	Applied Stress D (MPa)	Temperature θ (°C)	Minimum Strain Rate $\dot{\varepsilon}_m$ $(sec)^{-1}$	Time at minima t_m (min)	Strain at minima t_m (%)
SINGLE STAGE:					
I9-1	3.45	15.93	2.44^{E-6}	82	1.89
I9-4	3.70	13.71	3.31^{E-6}	41	1.34

E = 74.1 kJ/mol

TEMPERATURE STAGE:

			Activation Energy E(kJ/mol)	Δθ	Δθ
I9-2	3.53 3.53	15.90 13.50	37.6	20	0.95
I9-4	3.46 3.46	15.72 13.41	40.2	16	0.66
I9-6	2.67 2.67	15.84 13.33	50.9	31	0.65

$E = \Delta F - \beta D = 90.1 - 14.67D$

STRESS STAGE:

			Slope $d\ell n\dot{\varepsilon}/dD$ $(MPa)^{-1}$	ΔD	ΔD
I9-3	2.80 3.48	15.90 15.90	1.23	19	0.58
	3.48 4.15	15.90 15.90	0.98	42	1.19

$S_\alpha = 18 \pm 2 \times 10^{-15}$ bonds/m^2

$S_\beta = 3 \times 10^{15}$ bonds/m^2

Table IV-15

Specific Heat for Manchester Fine Sand

Temp. °C	Water Content	Specific Heat (Cal g^{-1} $°C^{-1}$)				
		0	1.2	6.6	16.0	26.5
+45		0.185	0.185	0.231	-	0.341
+30		0.181	0.182	0.231	0.310	0.349
+15		0.168	0.172	0.221	0.301	0.338
+ 1		0.171	0.167	0.224	0.299	0.330
- 1		0.162	0.166	0.193	0.226	0.240
- 5		0.157	0.159	0.189	0.217	0.231
-20		0.145	0.150	0.174	0.216	0.213
-35		0.144	0.146	0.167	0.196	0.207
-50		0.137	0.137	0.154	0.180	0.194

* from Haynes et al. (1980)

V. DISCUSSION

A. Rate Process Theory

It should be mentioned that most of the experiments described in this report were undertaken explicitly to determine the internal consistency of the rate process theory (RPT) in its entirety. To the authors knowledge this is the first time that a verification of this cross-check for RPT has been undertaken.

The rate process theory (RPT) parameters for frozen MFS given in Table IV-13 do not agree very well with the preconceived values one might have expected based upon inferences from the literature. However, the data may still provide clues to the creep behavior of frozen MFS. For a given ice content the free energy of activation ΔF was fairly consistent whether determined from a temperature stage test or at any time from t/t_m of 0.25 to 1.0 from a series of constant stress tests at various temperatures. The high value of ΔF may simply reflect that rate control is governed by multiple mechanisms over the time range from t/t_m = 0.25 to 1.0.

Most authors calculate an experimental activation energy E which, as the RPT shows, must always be less than ΔF so that values of E without specifying the applied stress have no significance. Mitchell (1976) explicitly defines $E = \Delta F - \beta D$, but presents values for E with D unspecified which are then referred to as free energy of activation. The

positive values of β mean a negative slope to the E-D plot as expected from RPT. From what can be pieced together from Mitchell's data, ΔF for unfrozen soil appears to be 335 ± 40kj/mol, which is similar to frozen MFS.

In the frozen sand, the higher the ice content the lower the free energy of activation. However, even for ice saturated frozen MFS, ΔF is about four times that for polycrystalline ice, which is about 1.5 times larger than for ice monocrystals. As noted in Section II-B, the ΔF for ice monocrystals was close to the ΔF for diffusion of water molecules in ice. Hence even for polycrystalline ice there must be some additional mechanism or a completely different mechanism controlling creep. The high ΔF for frozen MFS suggests either extremely strong bonds, about twice the energy required for diffusion of an oxygen atom in silicates, or that the creep rate is controlled by multiple mechanisms of nearly equal importance.

The RPT implicitly assumes X is a constant. The equation $\ell n(\dot{\varepsilon}/T)_{t,s,D} = \ell n(Xk/h) - E/R(1/T)$ (II-22) allows experimental testing for this condition. For ice monocrystals X was constant and a very small number ($\approx 3 \times 10^{-7}$). Polycrystalline ice gave a small nearly constant value for X. For frozen MFS, X was anything but constant, ranging from 10^{-3} to 10^{60}! The data from Fig. IV-24 and IV-29 strongly suggest X to be a function of D. That is, the fraction of successful barrier

crossings from the activated state is a function of the applied bias, which actually seems a more reasonable probability than that the fraction is a constant. The coefficient of determination, r^2, for ℓnX vs. D using data from Fig. IV-24 and IV-29 was 0.89; however, X is more strongly correlated with E. Using the same data set ℓnX vs. E gave $r^2 = 0.995$.

The data set for examination of the dependance of X on D and on E was expanded to sixty data points by using data from temperature stage tests with Eq. II-22 rather than Eq. IV-1. The best fit for X vs. D was the exponential (ℓnX vs. D) which gave $r^2 = 0.68$ and 0.79 for w = 10 w = 25% respectively. On the other hand, ℓnX vs. E gave $r^2 = 0.99$ which included all data. Thus X is very strongly correlated with E and is independent of water content, time, and strain. The fact that X correlates much better to E than to D suggests that X is a function of temperature.

Since the apparent activation energy E was strongly related to X, values for ΔF and β computed for approximately constant X are given in Table V-1. At a water content of 10% there appears to be a maximum in both ΔF and β for $X = 10^{15}$. For saturated frozen MFS neither ΔF or β are smooth functions of X. Unfortunately, the meaning of the quantity X is obscure other than that it is a "constant" in the RPT operational equation (which is assumed to be a function

of structure). Application of RPT to data for monocrystal or polycrystalline ice give approximately constant X, while for frozen MFS X is a variable. It is suggested that the variation in X may account for the 10 fold descrepancy between S_β and S_α found for frozen MFS.

The plots in Fig. IV-24 and IV-29 conform to Eq. II-22; however, this does not prove the validity of RPT because a slightly higher value of r^2 can be obtained for any particular data set from a plot of $\ell n\dot{\varepsilon}$ vs. $\frac{1}{T}$. Thus, while the data are consistent with RPT they do not exclude other possibilities. This same argument applies to the E vs. D data sets. While a plot of E vs. D is reasonably consistent with RPT, one can obtain an improved fit by plotting ℓnE vs. D. The range of a given data set may be too narrow to adequately test the theory; however, the fact remains that while the available data can be analyzed by RPT, the internal consistency varies between excellent for ice monocrystals to exceedingly poor for frozen sand. The physical significance of the parameters obtained from the operational equations derived from RPT likewise range from reasonable for ice monocrystals to ridiculous for frozen soil (unfrozen soil appears to be no better). It would seem to be self evident that the simplifying assumptions introduced in order to obtain operational equations are not well satisfied for frozen sand but were satisfied for ice monocrystals. The simpliest assumption that permits a coherent

concept for all the data is that there are multiple mechanisms of approximately equal importance operating during creep deformation of frozen sand. It is clear that the parameter X should not be ignored. The approximate equal magnitude multiple mechanism hypothesis is given as a tentative explanation for the consistent discrepancy between S_β and S_α observed for frozen MFS.

Polycrystalline ice gave a free energy of activation ΔF 1.5 times that for ice single crystals and about one quarter that for frozen MFS. The number of bonds computed from α was about the same for polycrystalline as for single crystal ice. The number of bonds calculated from β for polycrystalline ice was one sixth that obtained from α.

B. Nature of the Linear log $\dot{\varepsilon}_m$-log t_m Correlation

As noted in Section IV-D, a linear relation between the log $\dot{\varepsilon}_m$-log t_m data exists for 10% water content (S_i = 40%) and saturated MFS samples (see Fig. IV-15). This behavior has also been observed for ice and unfrozen soil, as shown in Fig. V-1. The nature of this relation will be examined via various simple creep models.

A secondary creep model such as proposed by Ladanyi (1972) is plotted in Fig. V-2. According to this model,

$$\varepsilon = \dot{\varepsilon}_m t + \varepsilon_i \qquad \text{(V-1)}$$

where for $\varepsilon_m >> \varepsilon_i$,

$$t_m \cong \frac{\varepsilon_m}{\dot{\varepsilon}_m} \qquad \text{(V-2)}$$

The lines of constant strain based on this model are given by:

$$\log t = \log \varepsilon(t) - \log \dot{\varepsilon}_m(t) \qquad \text{(V-3)}$$

and

$$\frac{d \log \dot{\varepsilon}_m}{d \log \varepsilon_t} = -1 \qquad \text{(V-4)}$$

These equations describe a family of straight lines with slope -1, as seen in Fig. V-3. Notice that as the strain increases, progressively less separation exists between the strain contours.

Since the data for the materials plotted in Fig. V-1 have a slope between -0.8 and -1.2, this suggests that the strain at the minimum strain rate is approximately a constant for each material. This concept has been advanced recently (Assur, 1979) after various discussions at CRREL. However, the slope of the actual log $\dot{\varepsilon}_m$ - log t_m line is not usually exactly -1, nor is the actual strain at the $\dot{\varepsilon}_m$ absolutely constant. For the frozen MFS, the slope is between -1.1 and -1.2 for the three degrees of ice saturation, S_i, plotted, and the strain at $\dot{\varepsilon}_m$ typically decreases with decreasing minimum strain rate. For unfrozen Haney clay, with a slope

between -0.8 and -0.9, the strain at $\dot{\varepsilon}_m$ increases slightly with decreasing minimum strain rate. These trends of decreasing ε_m with decreasing $\dot{\varepsilon}_m$ for slopes less than -1 and vice versa for slopes greater than -1 are consistent with the simple secondary creep model. However, since the actual shape of the log $\dot{\varepsilon}$ - log t creep curve for each test greatly differs from the secondary creep model, the $\dot{\varepsilon}_m$ - t_m data points for actual tests do not fit within the strain contours predicted by this model.

The more sophisticated three-parameter creep model proposed by Singh and Mitchell (1968), shown in Fig. V-2, is similar to that proposed by Vyalov (1962) in that each is based on a linear log $\dot{\varepsilon}$ - log t relation. According to the Singh-Mitchell model,

$$\dot{\varepsilon} = A\, e^{\alpha D}\, (\frac{t_1}{t})^m \qquad \text{(V-5)}$$

where D = some measure of shear stress

t_1 = some initial time

A, α, m = experimentally determined constants

with $m = -d\log \dot{\varepsilon}/d\log t$ of the creep curve,

and

$$\varepsilon = \varepsilon_1 + \frac{A}{1-m}\, e^{\alpha D}\, (t^{1-m}-1) \qquad \text{(V-6)}$$

for $m \neq 1$, $t_1 = 1$ and $\varepsilon = \varepsilon_1$ at $t = t_1$.

Combining these equations, the strain contours may be found

from

$$\varepsilon = \varepsilon_1 + \frac{\dot{\varepsilon}}{1-m} (t-t^m) \qquad \text{(V-7)}$$

where $\dot{\varepsilon}$ is the strain rate at the strain ε. For $\varepsilon >> \varepsilon_1$, $t >> t_1$, and $m \leq 0.7$,

$$\varepsilon \cong \frac{\dot{\varepsilon}}{1-m} t \qquad \text{(V-8)}$$

From this equation, the contours of constant strain may be plotted for any m. This has been done for m = 0.6 in Fig. V-4. The slope of the strain contours may be obtained by manipulating equation (V-7) to obtain:

$$\frac{\alpha \log \dot{\varepsilon}}{\alpha \log t} = -1 - \frac{d\log(1-t^{m-1})}{d\log t} \qquad \text{(V-9)}$$

For $m < 1$ and large times, t^{m-1} approaches zero and consequently the slope approaches -1. As before, progressively less separation exists between the strain contours at increasing strains. However, the actual locations of the strain contours differ from those predicted by the secondary creep model.

Actual creep data for 10% w(40%S_i)MFS are plotted in Fig. V-5 together with the strain contours from the Singh-Mitchell model. Most of the data fall within the contours predicted by the model for m = 0.6. However, at the higher strain rates, the strains predicted by the model are slightly higher than actual. This is probably due to two factors. Firstly, the actual log $\dot{\varepsilon}_m$ - log t_m data are not truly linear for the

higher strain rates, but exhibit concave downward curvature, as shown in Fig. IV-15. Consequently, the intersection of the fitted log $\dot{\varepsilon}_m$ - log t_m line with the strain contours results in a higher predicted ε_m. The second reason is due to a change in the value of m with varying $\dot{\varepsilon}_m$. Although the original Singh-Mitchell model is a fit of the creep curve during primary creep, the value of m = 0.6 used for computing the strain contours in Fig. V-5 was selected to represent an average slope of the log $\dot{\varepsilon}$ - log t data over the time interval from t_1 to t_m. However, at the higher strain rates, an m closer to 0.5 would be much more appropriate. The use of an m value which is too high also results in an overestimation of the strain at the minimum strain rate.

From this presentation, it can be seen that the linear log $\dot{\varepsilon}_m$ - log t_m correlation for the creep of engineering materials is primarily due to the existence of an approximately constant strain at the minimum strain rate, and the relative insensitivity of the log $\dot{\varepsilon}_m$ - log t_m correlation to small deviations from the constant ε_m. For materials with a fairly high ε_m, this insensitivity to small deviations is increased. Deviations from linearity at the high strain rates and trends in the strain with varying strain rate are consistent with the predictions of simple creep models, such as the secondary creep and Singh-Mitchell creep models.

C. Prediction of $\dot{\varepsilon}_m$ and t_m for Manchester Fine Sand

The point at which the creep rate of a system starts to accelerate has great practical significance. Quantities of specific interest in defining this point are the minimum strain rate, $\dot{\varepsilon}_m$, and the time to the minimum strain rate, t_m. This section summarizes the problem of fitting and predicting the minimum strain rate as a function of the loading conditions and sample structure parameters that is discussed in detail in Ting, 1981a.

The various methods used for fitting and predicting the minimum strain rate for the creep of Manchester Fine Sand (MFS) can be categorized into two groups, one which is loosely based on Rate Process Theory (RPT), and requires only creep test data for parameter evaluation, and another which uses stress ratios which requires both creep test data and the ultimate strength data determined in Section IV-B.

1. Prediction of $\dot{\varepsilon}_m$ using the "Modified RPT Method"

As presented in Section II-A, RPT states that:

$$\dot{\varepsilon}_m = \frac{2XkT}{h} \exp\left(-\frac{\Delta F}{RT}\right) \sinh\left(\frac{f\lambda}{2kT}\right) \qquad \text{(V-10)}$$

where for sufficiently large stresses,

$$\dot{\varepsilon}_m = XkT \exp\left(-\frac{E}{RT}\right) \qquad \text{(V-11)}$$

where E is the apparent activation energy, and is described by:

$$E = \Delta F - \frac{f\lambda N}{2} = \Delta F - \beta D \qquad \text{(V-12)}$$

E may be determined from single stage creep tests at constant deviator stress, D, and varying temperature, or temperature stage tests. In each case, however, some assumptions about the constancy of X need to be made, as previously emphasized.

According to RPT, the stress dependence of the creep should be completely accounted for through the variation of the apparent activation energy E. From stress stage tests, this stress dependence may be independently assessed:

$$\alpha = \frac{d\ell n\dot{\varepsilon}}{dD} \qquad \text{(V-13)}$$

According to RPT, the parameters α and β should therefore be related by:

$$\frac{\alpha}{\beta} = \frac{1}{RT} \qquad \text{(V-14)}$$

As already discussed in Section V-A, this is not the case, with α being almost ten times the magnitude of β. In addition, computed values of the structure parameter, X, often assumed to be constant or even equal to unity, actually varied from 10^{-3} to 10^{+60} for the various test conditions and sample types involved in the current testing program on MFS.

An empirical equation of the same general form as the Rate Process Theory was used for fitting the minimum strain rate, with the temperature dependence given by a constant

times Texp(-Q/T) where Q is assumed independent of stress level for all of the data at a given degree of ice saturation and relative density. At a given temperature, the fitted $\dot{\varepsilon}_m/T$ was evaluated for each level of stress for all of the 40% S_i (10%w) 55% relative density (D_r) MFS data. The accompanying least squares exponential and power fits of these data yield equations of the form:

$$\dot{\varepsilon}_m = A_1 T \exp(\gamma D) \exp(-Q/T) \qquad \text{(V-15)}$$

and

$$\dot{\varepsilon}_m = A_2 T D^n \exp(-Q/T) \qquad \text{(V-16)}$$

where the values of A_1 and A_2 are obtained from fitting the observed data at a given stress and temperature. Based on this procedure, the values of these parameters were evaluated for all of the 40% S_i 55% D_r MFS data:

$$\dot{\varepsilon}_m = 1.47 \times 10^{38} T \exp(2.03D) \exp\left(-\frac{29781}{T}\right) \qquad \text{(V-17)}$$

and

$$\dot{\varepsilon}_m = 2.03 \times 10^{35} T D^{10.4} \exp\left(-\frac{29781}{T}\right) \qquad \text{(V-18)}$$

A comparison of the logarithm of the actual minimum strain rate with the fitted $\dot{\varepsilon}_m$ gives a measure of the reliability of the two equations. The resulting frequency histograms are plotted in Fig. V-6, and indicate that both methods yielded reasonably centered fits with approximately 95% of the data within ± 4X the actual $\dot{\varepsilon}_m$.

Similar fitting carried out on 100% S_i 55% D_r MFS also

yielded fairly well centered fits with 95% of the data within ± 2X for the power fit compared with ± 4X for the exponential fit. Consequently, the power fit for stress was used for all subsequent fits. Note that the form of the power fit is similar to that used by a variety of workers in ice, notably Glen (1955), Weertman (1973), Langdon (1973), Gold (1973) and Homer and Glen (1978).

A similar procedure was performed on the rather limited 20% S_i 55% D_r MFS data. The resulting coefficients for this fit, together with the coefficients from the fits at other levels of ice saturation are summarized in Table V-2 along with the pertinent data on the quality of each fit.

Using a single value of n and Q, new "A" parameters were computed by fitting the actual data for a given stress and temperature, as tabulated in Table V-3. Then, a three-parameter exponential equation was used to fit the variation of A with respect to the degree of ice saturation:

$$\dot{\varepsilon}_m = 1.54 \times 10^{28} \exp\left(\frac{12.54}{S_i + 0.30}\right) T\, D^{10.0} \exp\left(-\frac{30000}{T}\right) \qquad \text{(V-19)}$$

Note that iteration was required to obtain the three parameters in the degree of saturation term.

To account for the variation of $\dot{\varepsilon}_m$ with relative density, the rather limited data at varying D_r at 50 and 100% S_i were used. Noting the similarity in the change in log strain rate

with relative density in the medium to dense range for both the 40 and 100% ice saturated samples (> 60% D_r), a single exponential term was introduced into equation (V-19). The resulting equation which fits the MFS data at all degrees of ice saturation, relative density, stress level and temperature is:

$$\dot{\varepsilon}_m = A \exp(\gamma D_r) \exp\left(\frac{\beta}{S_i + \alpha}\right) T D^n \exp\left(-\frac{Q}{T}\right) \quad \text{(V-20)}$$

for Dr > 60%, where

$A = 1.85 \times 10^{31}/s$

$\gamma = -12.4$

$\beta = 12.54$

$\alpha = 0.30$

$Q = +30000$ (°K)

$n = 10.0$

The resulting comparison of the fitted and actual minimum strain rates is plotted in Fig. V-7. Again, equation (V-20) yields a reasonably centered fit with 95% of the data within ± 5X of the mean predicted strain rate, which is +4X and -6X the actual. While the fit is not too bad, insufficient data exist at varying D_r to thoroughly test the validity of equation (V-20) with respect to this parameter. Note that this equation assumes the separability of the individual parameters, D_r, S_i, T and D.

The fits presented thus far were made using the entire data sets available. In order to see whether an equation of the form given by equation (V-20) is useful as a predictor of minimum strain rates, an arbitrary set of data was taken from the overall data set to determine the values of the parameters in the equation. The resulting equation based on 25 tests is:

$$\dot{\varepsilon}_m = 8.33 \times 10^{33} \exp(-10.5 D_r) \exp\left(\frac{8.28}{S_i + 0.15}\right) TD^{9.94} \exp\left(\frac{-31189}{T}\right) \quad \text{(V-21)}$$

The histogram of the reliability of the fit is plotted in Fig. V-8 and indicates that this fit, based on about one-third of the total data base, is as reliable as the fit using all of the data.

The fits have thus far assumed a constant value of Q. Since the effect on the predicted creep rate due to a variation in Q with stress is small compared to the effect of the stress alone, this assumption is reasonable. Modification of equation (V-20) to include variations in Q with degree of ice saturation yielded only slight improvement in reliability not considered worth the additional effort and complication.

Attempts were also made at using temperature stage and stress stage data for assessing the temperature and stress dependence of the minimum strain rate. However, the stage tests tended to uniformly and significantly underestimate

both the temperature and stress dependence of the $\dot{\varepsilon}_m$. Consequently, the data from the stage tests were not used in further attempts at fitting the minimum strain rate.

2. Prediction of $\dot{\varepsilon}_m$ with the "Stress Ratio Method"

The second method for predicting the minimum strain rate uses stress ratios based on the ultimate strength determined in Section IV-B. Here, a more empirical and more simple approach was used in attempting to fit the creep data:

$$\dot{\varepsilon}_m = A\left(\frac{D}{D_u}\right)^n \qquad \text{(V-22)}$$

where

$D_u = D(\theta)$ and

$D_u = 10.1 + 1.5\theta(\text{MPa})$ for 100% S_i,

$D_u = 2.38 + 0.46\theta(\text{MPa})$ for 40% S_i.

Note that the D_u for the 40% S_i samples is different from that in Section IV-B; the D_u here is based on only 10% w data, and is adjusted for an assumed ductile-to-brittle transition at an applied strain rate of 0.02/s. The temperature dependence of the creep rate was assumed to be accounted for by the variation in the ultimate strength with temperature. The resulting linear least squares fits for 40% and 100% S_i 55% D_r MFS creep data are shown in Fig. V-9.

By combining the equations for the 40% and 100% S_i fits with a common n and an exponential term to account for the

variation in S_i, the following equation results:

$$\dot{\varepsilon}_m = 3.49 \times 10^{-4} \exp(6.10 S_i) \left(\frac{D}{D_u}\right)^{9.74} \qquad \text{(V-23)}$$

where D_u may be expressed as:

$$D = -2.767 + 12.867 S_i - 0.233\theta + 1.733\theta\, S_i \ \text{(MPa)} \qquad \text{(V-24)}$$

Since data are available from only two different levels of saturation, equation (V-24) is "exact".

The quality of this fit is shown in Fig. V-10, and indicates a well-centered fit with 95% of the data within ± 2.5X of the actual. While this is much better than the fit shown in Fig. V-7 using the modified RPT method, note that this fit uses data from only one relative density and two S_i. Regardless of that fact, however, it can be seen that this method, based on stress ratios, is slightly better than the previous fitting method, and certainly employs a simpler empirical relationship.

As with the first method, this second method was checked to determine whether it could be effective as a predictive tool. Using the same eighteen 40 and 100% S_i 55% D_r MFS tests as before, and the ultimate strengths determined from a series of unconfined strength tests as in Appendix A.5 of Ting (1981a), gave the following equation:

$$\dot{\varepsilon}_m = 2.41 \times 10^{-4} \exp(6.74 S_i) \left(\frac{D}{D_u}\right)^{10.0} \qquad \text{(V-25)}$$

where D_u is as in equation (V-24).

Figure V-10 plots the resulting histogram, which show that the use this equation based on about one-third of the entire data base yields predictions which are just as good as when all of the data are used and fitted.

3. Models for Predicting t_m

Two methods were developed to predict the time to minimum strain rate for constant load creep tests on MFS. The first method uses the linear log $\dot{\varepsilon}_m$ - log t_m correlation which has been observed to be quite common in engineering materials, in conjunction with some of the predictive methods previously used for the minimum strain rate. The second method in effect replaces the $\dot{\varepsilon}_m$ - t_m correlation with a ε_m - log $\dot{\varepsilon}_m$ correlation and a creep model.

Figure IV-15 presents the coefficients describing the linear correlation between log $\dot{\varepsilon}_m$ and log t_m for 40, and 100% ice saturated MFS. The value of t_m may be estimated by using this relationship in conjunction with a prediction method for $\dot{\varepsilon}_m$. This was done for 40% S_i 55% D_r MFS using the constant Q modified RPT method, and the stress-ratio based fits. For this material,

$$\dot{\varepsilon}_m = 4.20 \times 10^{-4} \, t_m^{-1.21} \qquad \text{(V-26)}$$

from Fig. V-1. From equation (V-18),

$$\dot{\varepsilon}_m = 2.03 \times 10^{35} T\, D^{10.4} \exp\left(-\frac{29781}{T}\right) \qquad \text{(V-27)}$$

Combining the two equations leads to:

$$t_m = 7.89 \times 10^{-33}\, T^{-0.83}\, D^{-8.64} \exp\left(\frac{24714}{T}\right) \qquad \text{(V-28)}$$

where T is in °K, D is in MPa and t_m is in minutes. 95% of the data fitted are within ±3.3X the actual t_m.

Alternatively, the "stress ratio method"

$$\dot{\varepsilon}_m = 3.46 \times 10^{-3} \left(\frac{D}{D_u}\right)^{0.53} \qquad \text{(V-29)}$$

combined with (V-27) leads to:

$$t_m = 0.174 \left(\frac{D}{D_u}\right)^{-7.91} \qquad \text{(V-30)}$$

where D_u is the ultimate strength as previously described. The results indicate that the fit is very well-centered, with 95% of the fitted t_m within ±2.5X of the actual t_m. Both equations (V-28) and (V-30) yield fairly good results, with the method based on the stress ratios yielding marginally less scatter.

The second method replaces the $\dot{\varepsilon}_m$ - t_m correlation with an estimate of the ε_m in terms of $\dot{\varepsilon}_m$, and the Singh-Mitchell creep model, which is then used in conjunction with an estimate of $\dot{\varepsilon}_m$ as a function of stress and temperature to predict the time to minimum strain rate. However, this

method, while fundamentally pleasing, yielded fits which were slightly inferior to those with the $\dot{\varepsilon}_m$ - t_m correlation. Consequently, this method is not considered to be useful from an engineering viewpoint.

The use of the log $\dot{\varepsilon}_m$ - log t_m correlation as a predictive tool was examined using the same portion of the data set as before for 40% S_i 55% D_r MFS. Using the results from only eight constant load creep tests and numerous strength tests, the RPT-based and stress ratio-based predictors for $\dot{\varepsilon}_m$ and the log $\dot{\varepsilon}_m$ - log t_m correlation were determined. Then, these methods were used to predict the time to minimum strain rate, t_m, the results of which are plotted in Fig. V-11. As can be seen, both yield predictions of t_m which have 95% of the predicted t_m within ±3.7X of the actual values.

Based on this presentation, the following may be stated concerning the fitting/prediction of $\dot{\varepsilon}_m$ and t_m:

(1) Rate Process Theory (RPT), as written in equation (V-11), is entirely inadequate for describing the $\dot{\varepsilon}_m$ data for frozen MFS:

(2) The use of a pseudo-RPT equation of a form similar to (V-16), using a power function for describing the stress dependence and a constant apparent activation energy, is adequate for fitting the single stage $\dot{\varepsilon}_m$ creep data at varying stresses, temperatures, degrees of ice saturation and relative density;

(3) the parameters for this equation may be reliably determined in a manner indicated in Table V-4 from a relatively small number of tests, depending on overall sample and data reproducibility;

(4) the use of stress ratios with ultimate strengths based upon the ductile-to-brittle transition point as described in Section IV-D yields mathematically simple expressions for $\dot{\varepsilon}_m$, such as equation (V-23), which can fit and predict the data in a manner comparable to the modified RPT equation (V-16); this method requires data from both creep tests and strength tests, as outlined in Table V-4;

(5) for t_m fitting and prediction, the combination of linear log $\dot{\varepsilon}_m$ - log t_m correlation with an $\dot{\varepsilon}_m$ fitting/prediction model such as the modified RPT (equation V-16) or stress-ratio (equation V-23) methods seem to yield reliable results with a minimum of effort.

While a comparison of the $\dot{\varepsilon}_m$ and t_m values fitted and predicted by these models with the actual data indicate a considerable scatter (typically between ±2 to ±4 times the actual data), this scatter is no doubt due primarily to variability in the experimental test data, rather than in deficiencies in the mathematical models presented.

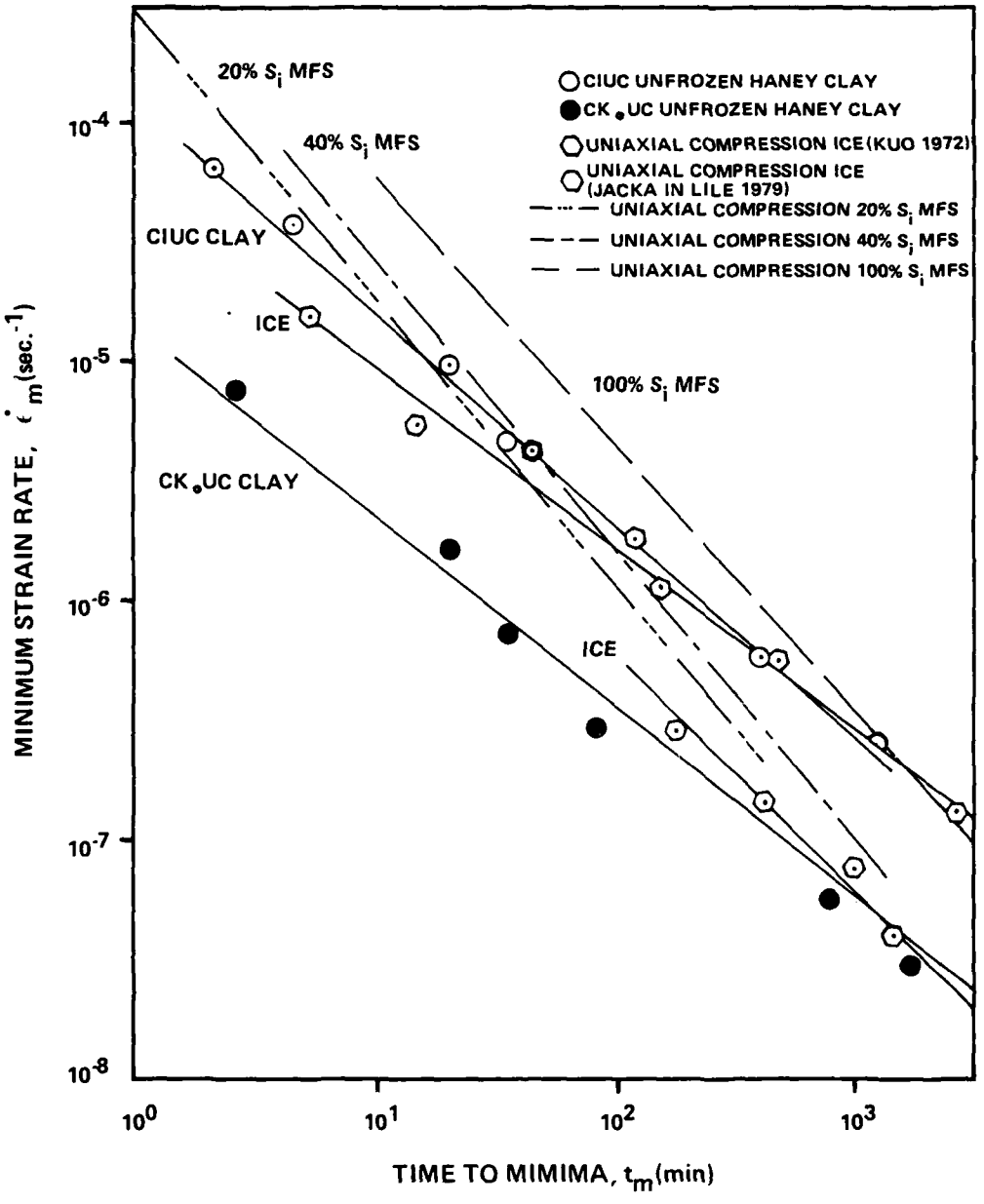

Fig. V-1 Minimum Strain Rate-Time to Minima Correlations for Frozen and Unfrozen Materials

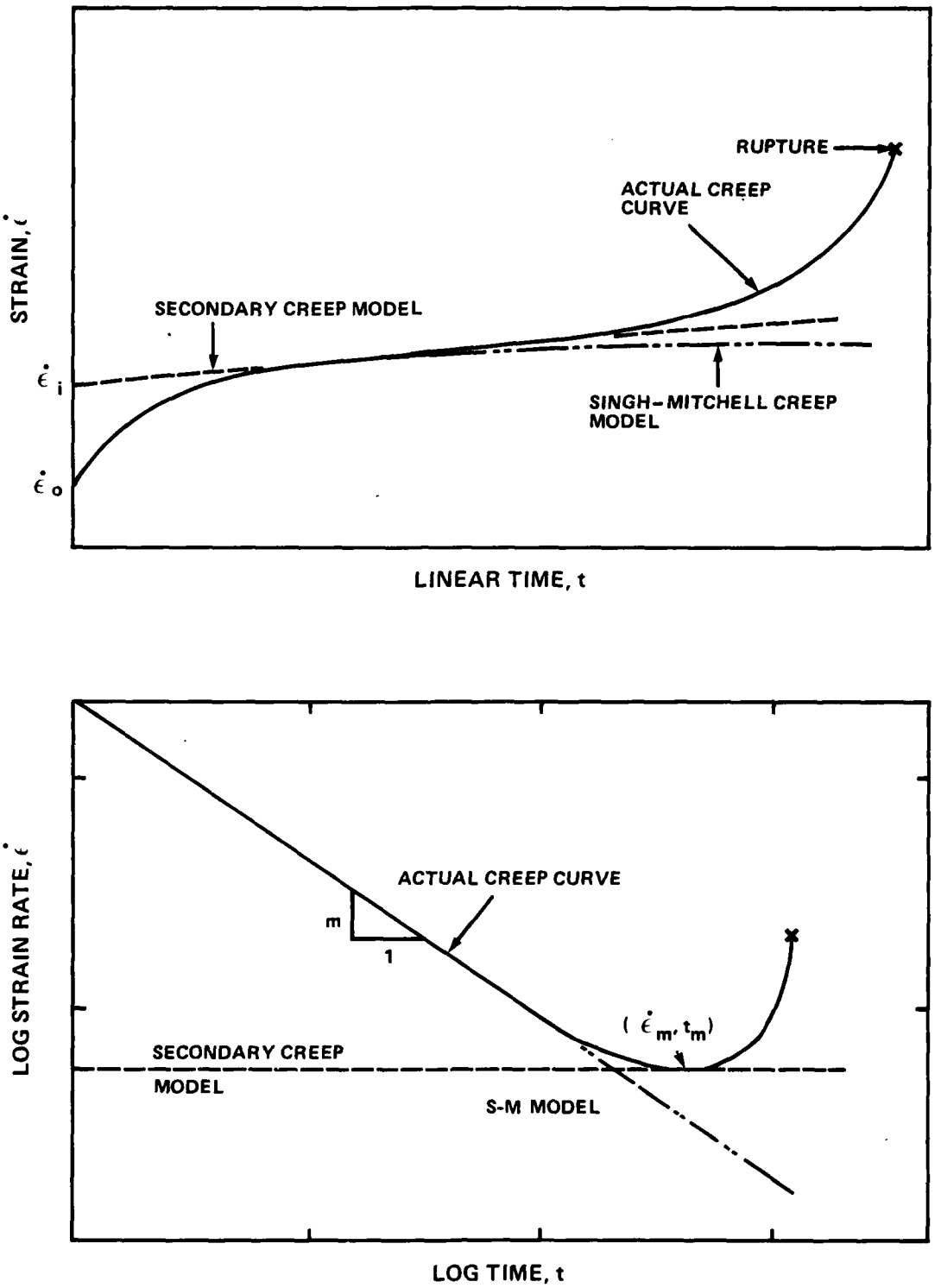

Fig. V-2 Comparison of Creep Models to Actual Creep Data

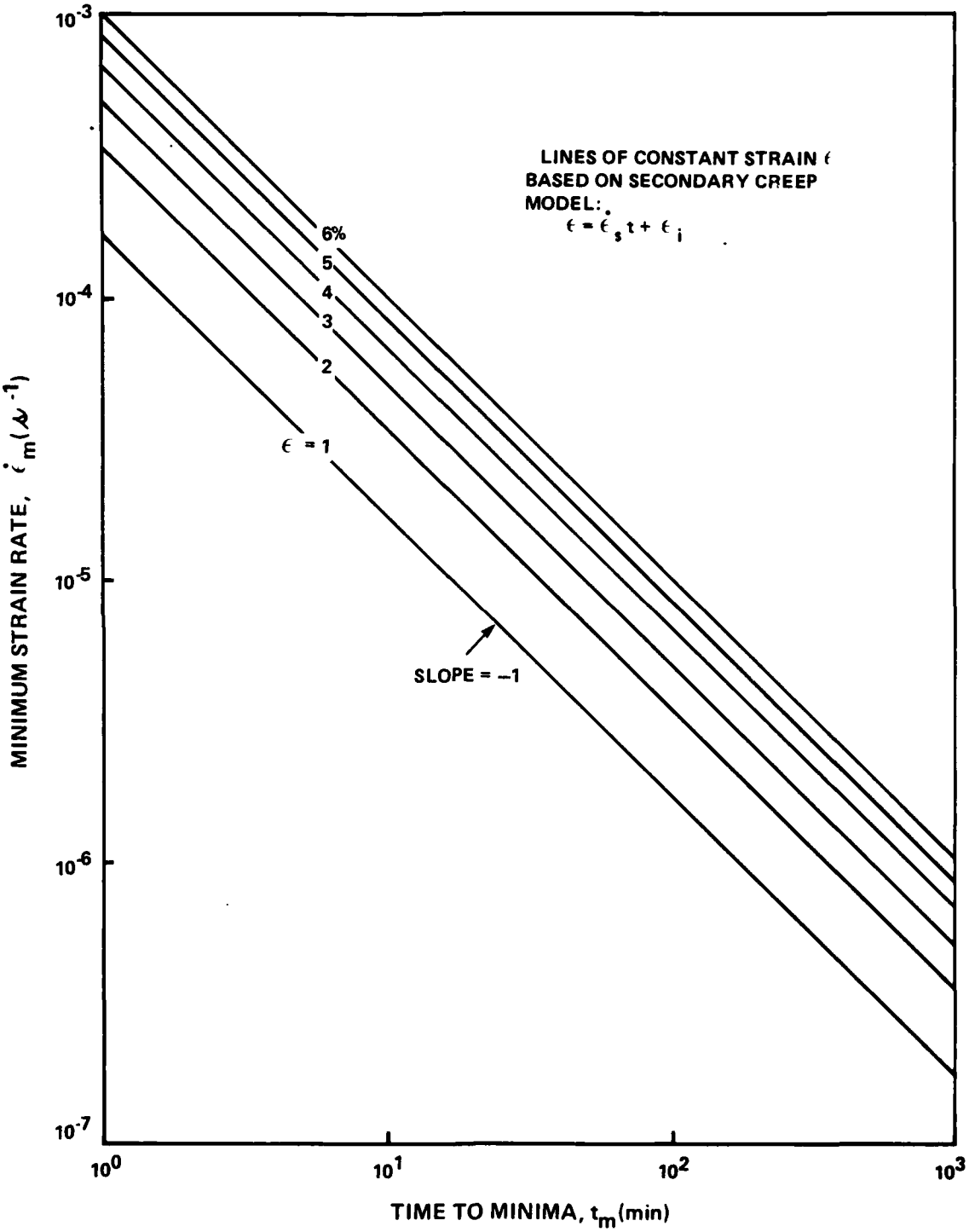

Fig. V-3 Constant Strain Contours on $\dot{\epsilon}_m$-t_m Plot using Secondary Creep Model

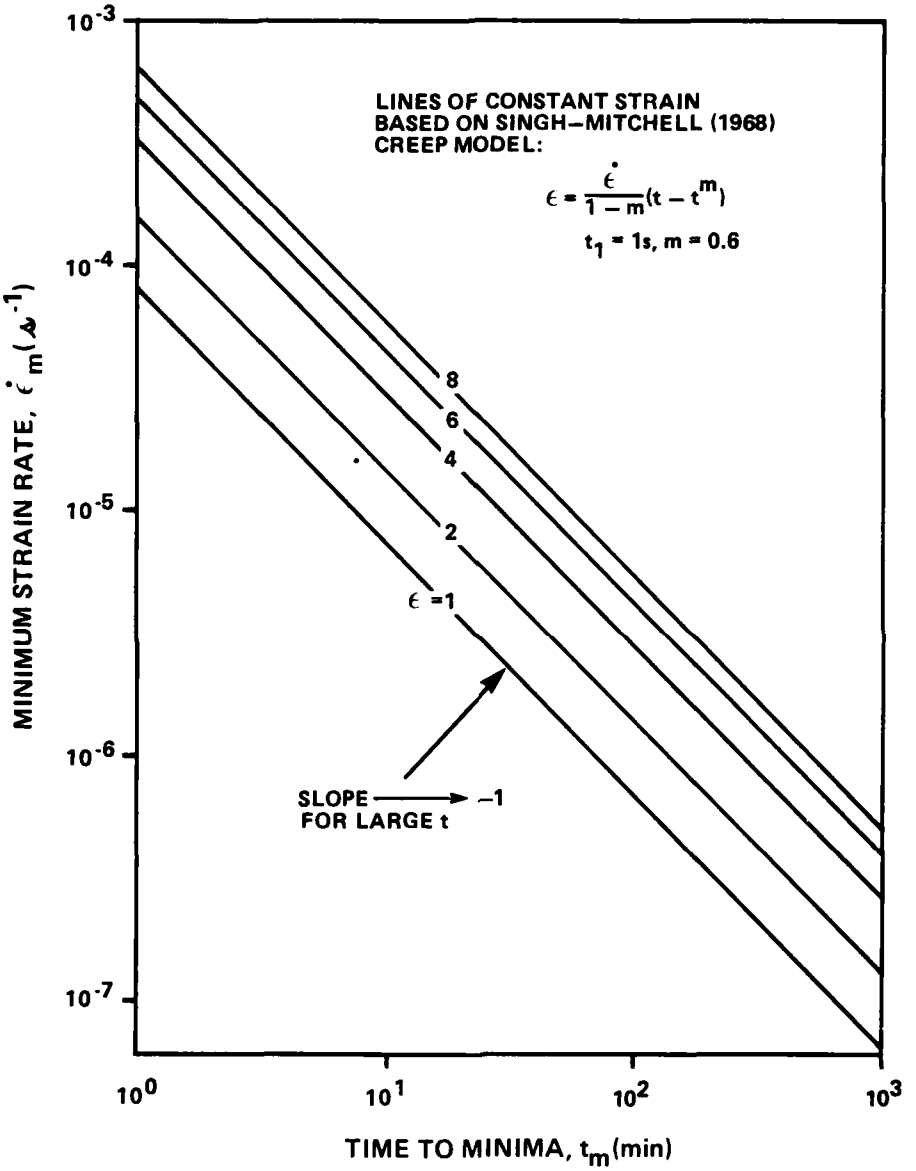

Fig. V-4 Constant Strain Coutours on $\dot{\epsilon}_m$-t_m Plot using Singh-Mitchell Model (1968)

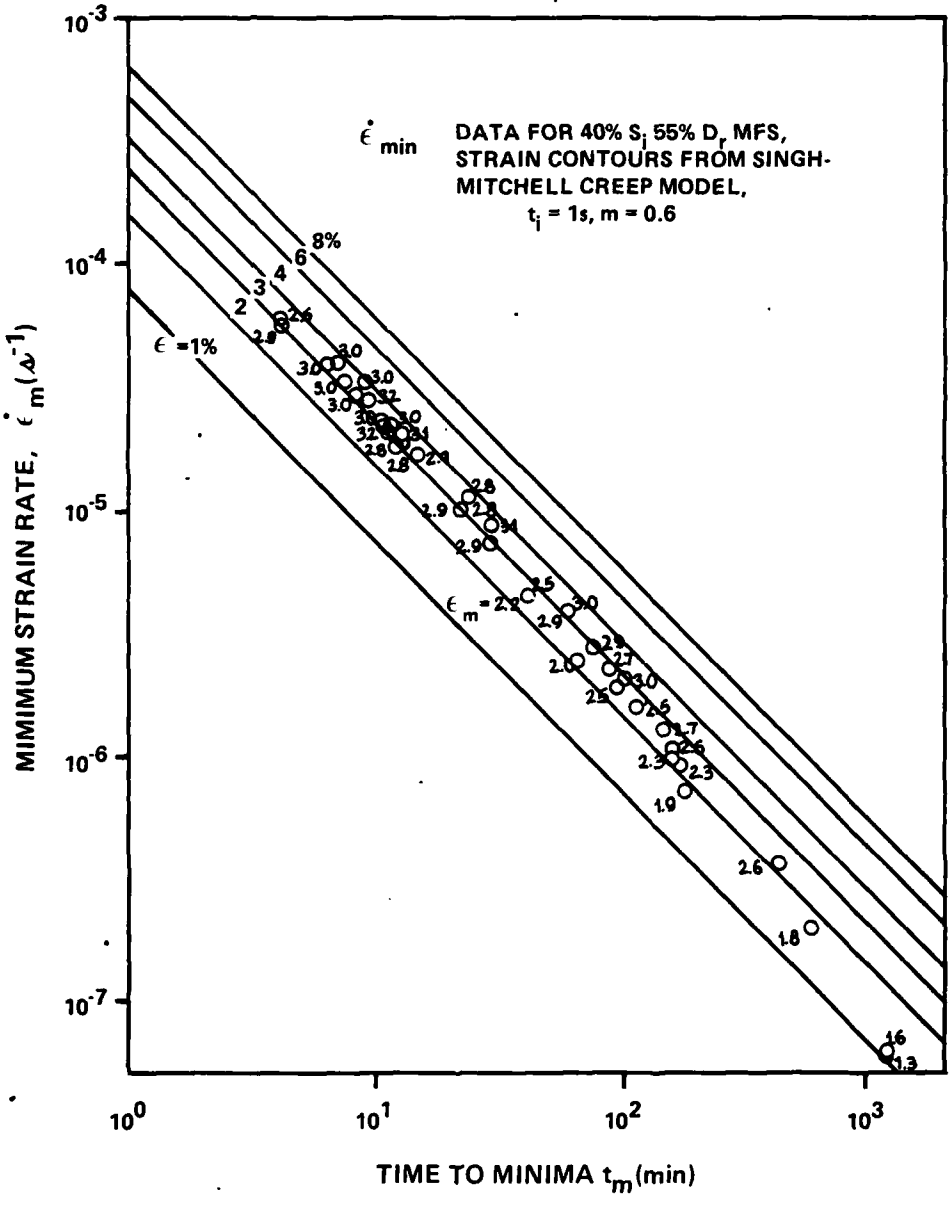

Fig. V-5 MFS Data plotted on Singh-Mitchell Model Plot

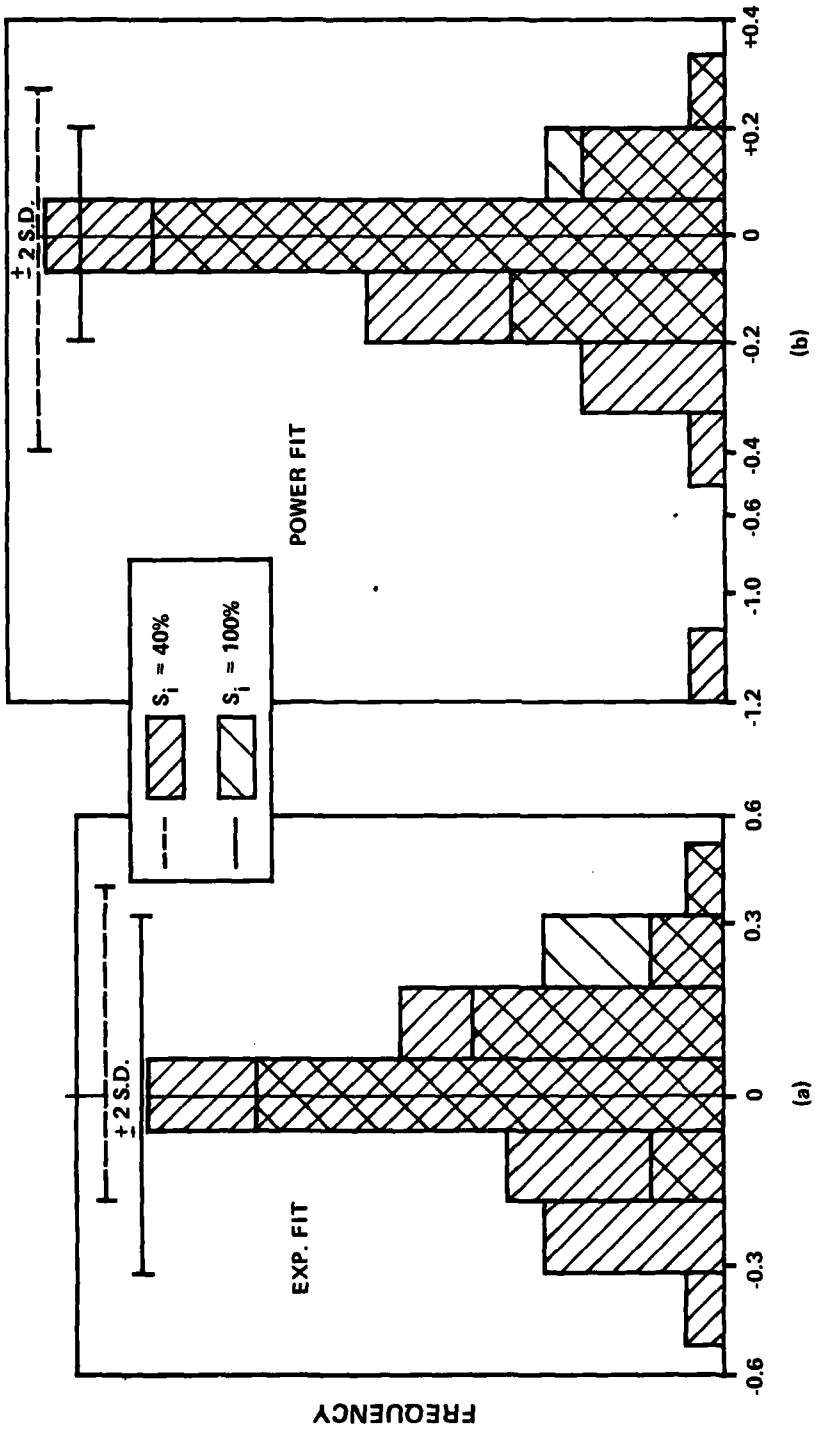

Fig. V-6 Frequency Histograms of Data Fits for 55%D_r MFS using Pseudo RPT (Eq. V-15 and Eq. V-16)

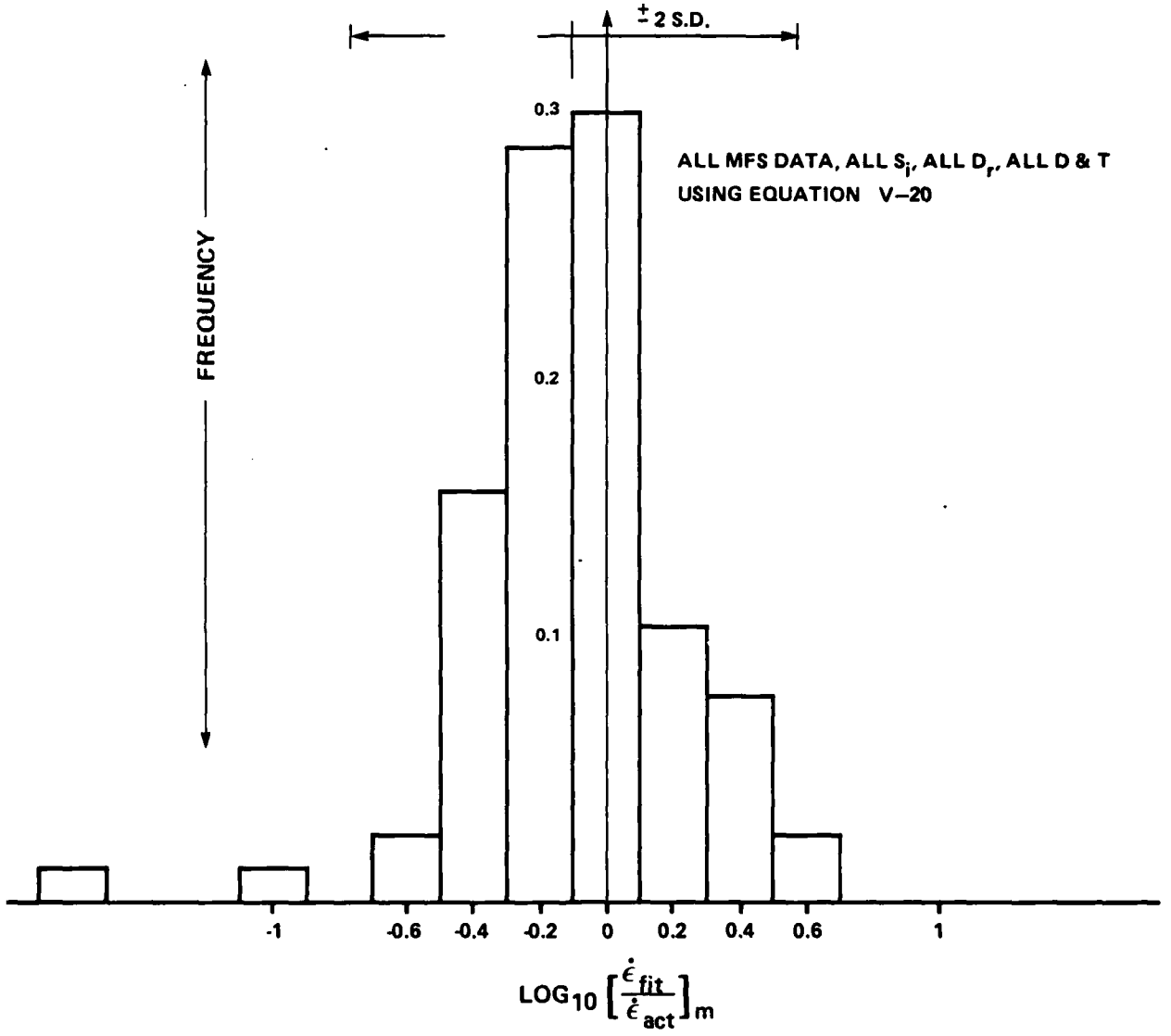

Fig. V-7 Frequency Histogram for All MFS Data using Eq. V-20

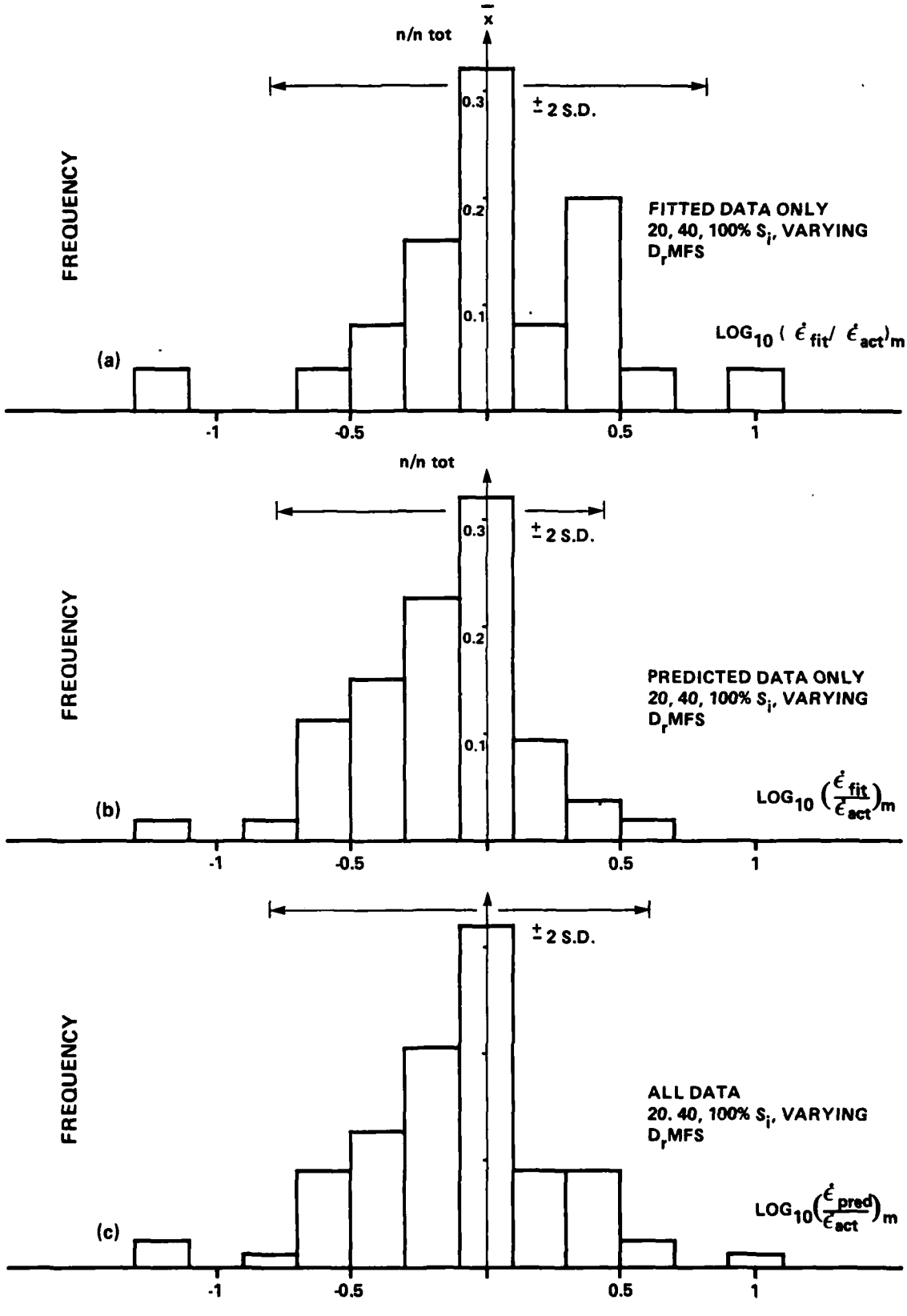

Fig. V-8 Frequency Histograms of $\dot{\epsilon}_m$ Predictions using One Third of Data to Precict all Data

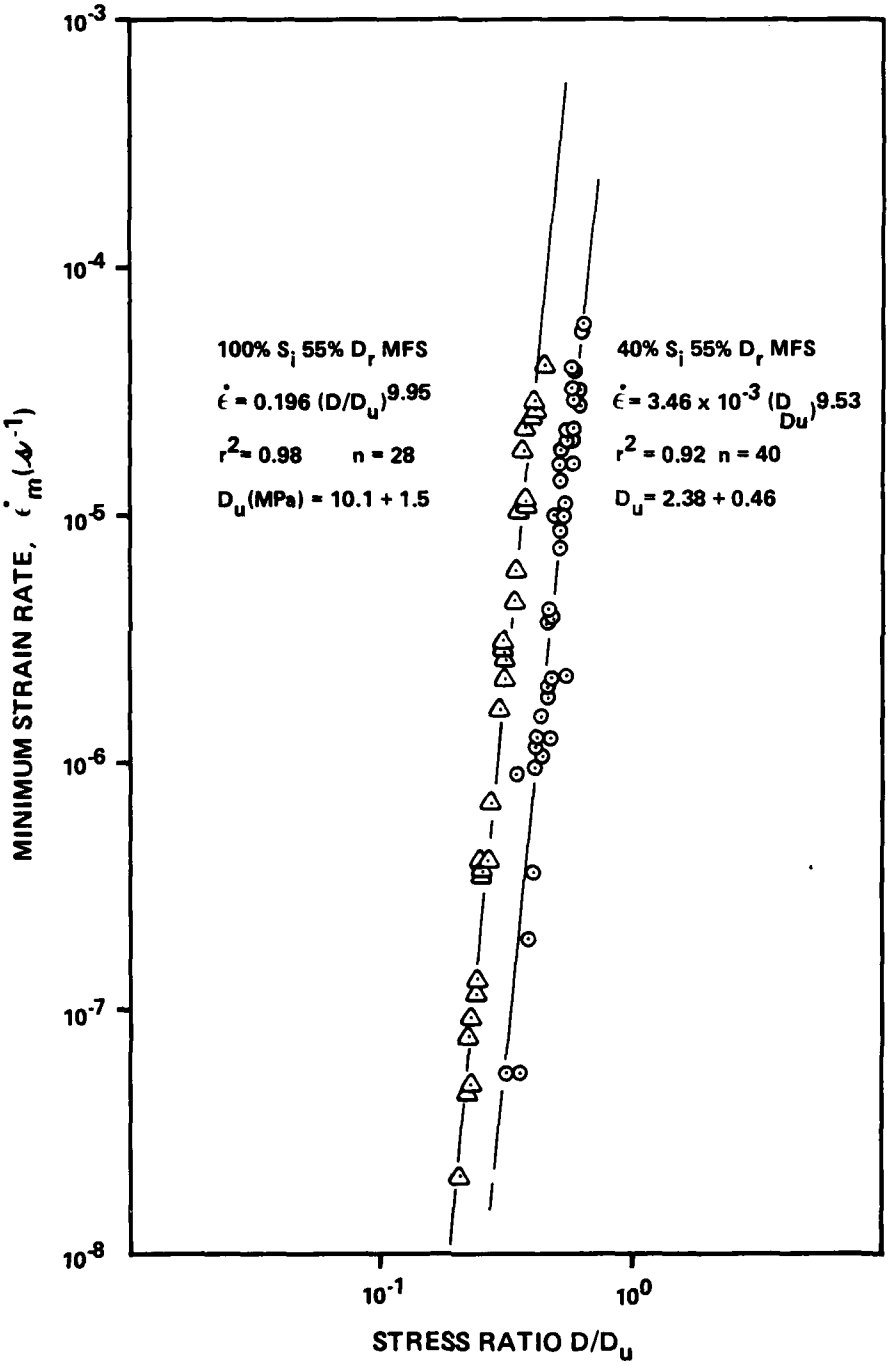

Fig. V-9 Minimum Strain Rate vs. Stress Ratio for MFS

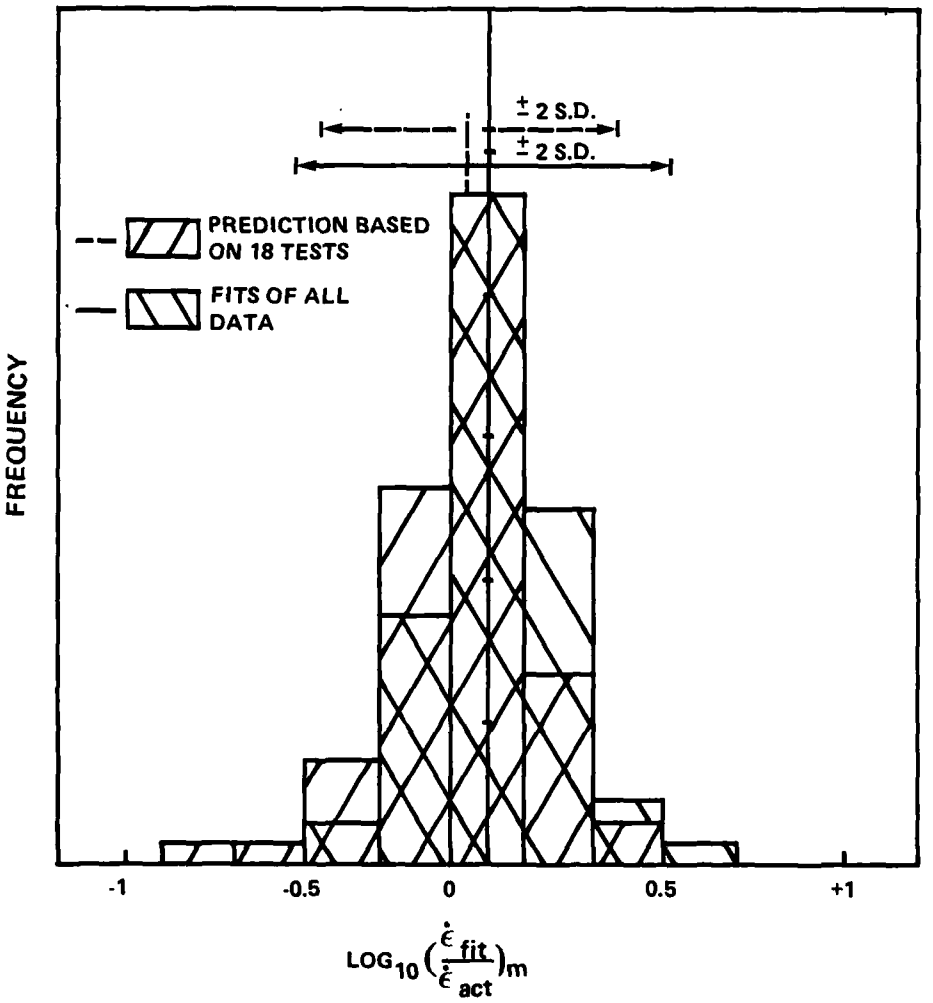

Fig. V-10 Frequency Histograms of $\dot{\epsilon}_m$ Fit and Prediction using Stress Ratio Method

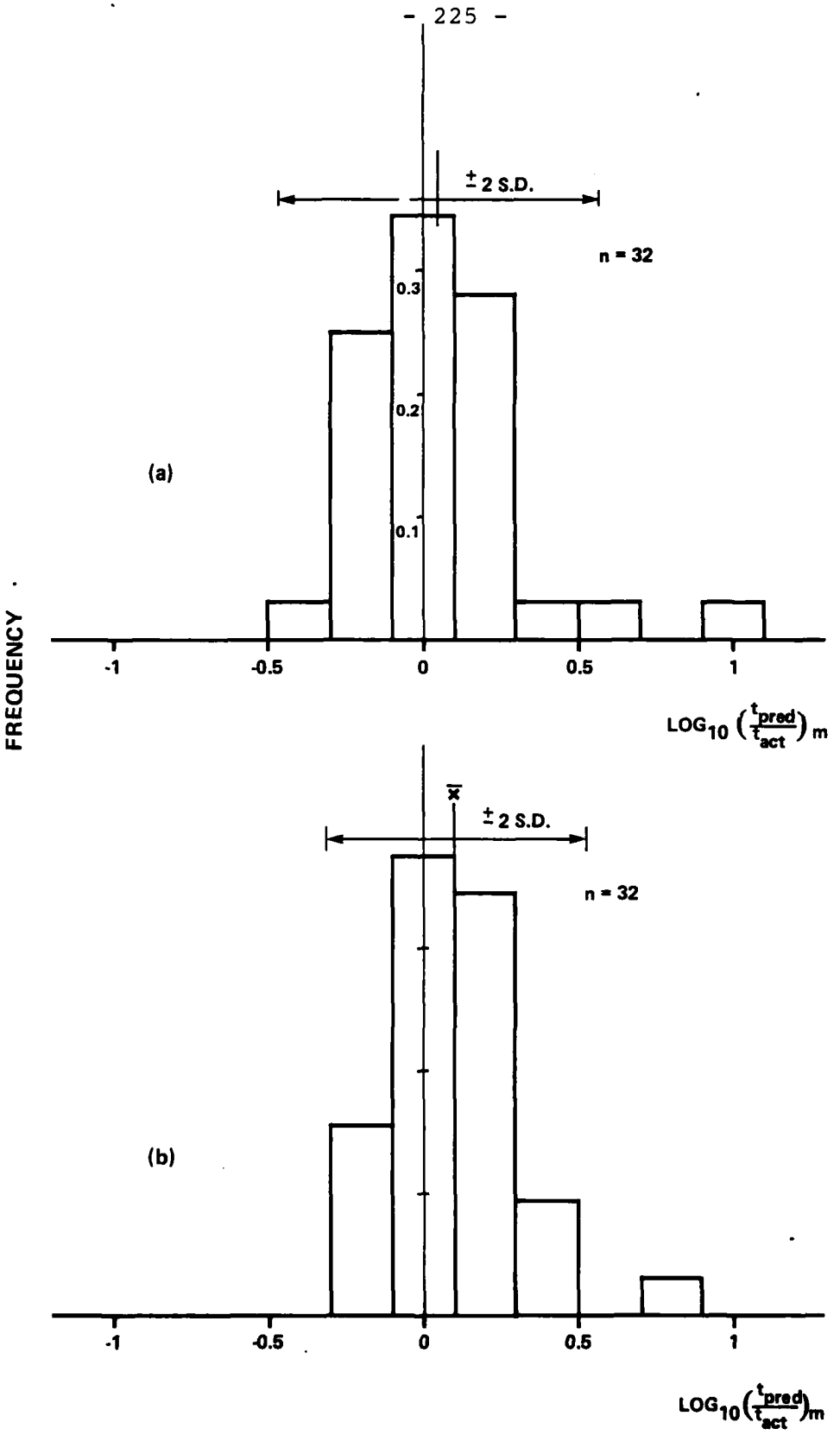

Fig. V-11 Frequency Histograms t_m Predictions using Eight Creep Tests to Predict Others:
a) Pseudo RPT Method, b) Stress Ratio Method

V-1

Rate Process Parameters ΔF and β at Constant X.

Frozen MFS	log X*	ΔF (kJ/mol)	$\beta \times 10^{-3}$ (m^3/mol)
w = 10 %	8	204	+13.5
	15	364	+38
	27	240	+4.9
w = 25 %	10	148	+0.9
	15	248	+8.0
	19	162	-2.9
	25	202	-1.8
	28	237	+1.0

* Given X constant to log X ± 1

Table V-2

Parameters for Equation V-16 for 55% D_r MFS
Using All Data: $\dot{\varepsilon}_m = ATD^n \exp(-Q/T)$

S_i (%)	$A(s^{-1})$	n	Q(°K)	Avg. $\log(\frac{\dot{\varepsilon}_{fit}}{\dot{\varepsilon}_{act}})_m$	S.D. $\log(\frac{\dot{\varepsilon}_{fit}}{\dot{\varepsilon}_{act}})_m$	No. of Tests
20	1.79×10^{-47}	9.2	34358	-0.09	0.45	6
40	2.03×10^{35}	10.4	29781	-0.11	0.26	40
100	1.09×10^{25}	10.0	25690	0.00	0.15	28

Table V-3

"A" Parameters for Equation V-16
for 55% D_r MFS Using Common n=10, Q=30,000

S_i (%)	A (s^{-1})
20	1.38×10^{39}
40	9.38×10^{35}
100	2.55×10^{32}

Method	Modified RPT	Stress Ratio
Generalized equation	$\dot{\varepsilon}_m = Ae^{\gamma D_r} e^{\frac{\beta}{S_i+\alpha}} TD^n e^{-\frac{Q}{T}}$	$\dot{\varepsilon}_m = Ae^{\alpha S_i} (\frac{D}{D_u})^n$
Test parameters	D, T, D_r, S_i	$D_u = f(S_i, T)$ D, T, S_i
Minimum tests required for one soil condition	3 creep	2 creep, 3-5 strength
Test conditions	(D_1,T_1) (D_1,T_2), (D_2,T_1)	creep: $(D/D_u)_1$, $(D/D_u)_2$ strength: vary $\dot{\varepsilon}$ to determine ductile to brittle transition, vary T to determine dependence of $D_u(T)$
number of tests required for reliable prediction, 1 soil condition	8 ± 2	4 creep, 6-8 strength
quality of fit for one soil condition	±2 to 4x actual, approx. centered fit	±2 to 3x actual, exactly centered fit
procedures for evaluating parameters	- plot $\dot{\varepsilon}_m/T$ vs 1/T to determine Q - choose central T, get fitted $\dot{\varepsilon}_m$ vs D - determine n from $\dot{\varepsilon}_m$-D - choose central D,T,$\dot{\varepsilon}_m$ for A - for varying S_i, use avg. n, E, -refit $\dot{\varepsilon}_m$ for new $A(S_i)$ -iterate for D - for varying D_r, compute avg. $\frac{\partial \ln \dot{\varepsilon}_m}{\partial D_r}$ to fit new A.	- correlate $\dot{\varepsilon}$ with D/D_u - for varying S_i, use avg n, - establish general $D_u = f(T,S_i)$ - recompute $A(S_i)$

TABLE V-4

Summary of $\dot{\varepsilon}_m$ Prediction Methods

VI. CONCLUSIONS

1. The linearity of the plot log minimum strain rate, $\dot{\varepsilon}_m$, vs. log time to minima, t_m, for frozen Manchester Fine Sand is completely consistent with the Singh-Mitchell model for creep of unfrozen soils.

2. The total strain at $\dot{\varepsilon}_m$ changes very slowly with applied stress and/or temperature which is completely consistent with the Singh-Mitchell creep model.

3. Creep data for ice monocrystals show excellent agreement with rate process theory, RPT.
   a) The free energy of activation obtained from RPT equals the self diffusion energy for a water molecule in ice.
   b) The number of bonds, S, computed from α exactly equals the number of bonds computed from β. NOTE: β is obtained from the results of change in temperature and α from change in stress.

4. RPT applied to creep data for polycrystalline ice showed that:
   a) ΔF increased 50% over that for ice monocrystal, and
   b) $S_\alpha \neq S_\beta$.

5. RPT applied to creep data for frozen MFS showed that:
   a) ΔF to be very high, about that of silicon-oxygen bond energy.

b) The number of bonds calculated from β was about ten times the number of bonds calculated from α.

6. The operational equations used to express RPT do not work for frozen sand but do work exceedingly well for ice monocrystals.

7. Prediction of time to creep rupture was obtained from creep test data and a pseudo RPT equation. Predicted failure times were within a factor of 2 to 4 the observed failures times.

RECOMMENDATIONS

Testing should be undertaken to establish the validity of the correspondence-principle; that is, whether or not the peak stress in a constant strain rate test equals the minimum strain rate obtained if a stress equal to the above peak stress was applied in a creep test. Further tests are needed regarding sample size effects on observed slip-stick observations in creep rate.

VII. REFERENCES

Reference Code:

ASCE JSMFD - American Society of Civil Engineers, Journal of Soil Mechanics and Foundation Engineering

1st ICP - First Permafrost Conference, Lafayette, Indiana, U.S.A.

2nd ICP - Second International Permafrost Conference, Yakutsk, U.S.S.R.

3rd ICP - Third International Permafrost Conference, Edmonton, Alberta, Canada

Physics of Ice - From the International Symposium on the Physics of Ice, Munich, Germany, Edited by N. Riehl, B. Bullener and H. Englehard, Plenum Press, N.Y.

Physics and Chemistry of Ice - From the International Symposium on the Physics and Chemistry of Ice, Ottawa, Canada, Edited by E. Whalley, S.J. Jones and L.W. Gold, Royal Society of Canada

CRREL - U.S. Army, Cold Regions Research and Engineering Laboratory

SIPRE - U.S. Army, Snow Ice and Permafrost Research Establishment

Andersland, O.B. and I. AlNouri (1970), Time Dependent Strength Behavior of Frozen Soil, ASCE, JSMFD, V. 96, p. 1249-1265.

Andersland, O.B. and D.M. Anderson (1978), Geotechnical Engineering for Cold Regions, McGraw-Hill, N.Y.

Andersland, O.B. and A.G. Douglas (1970), Soil Deformation Rates and Activation Energies, Geotechnique, V. 20, p. 1-16.

Assur, A. (1979), Some Promising Trends in Ice Mechanics, Proc. IUTAM Symposium, Copenhagen.

Baker, R.W. (1978), The Influence of Ice-Crystal Size on Creep, Journal of Glaciology, V. 21, p. 485-500.

Barnes, P., D. Tabor, and J. Walker (1971), The Friction and Creep of Polycrystalline Ice, Proc. Royal Society of London, V. A324, p. 127-154.

Campanella, R.G. and V.P. Vaid (1974), Triaxial and Plane Strain Creep Rupture of an Undisturbed Clay, Canadian Geotechnical Journal, V. 11, p. 1-10.

Chamberlain, E., C. Groves, and R. Perham (1972), the Mechanical Behavior of Frozen Earth Materials under High Pressure Triaxial Conditions, Geotechnique, V. 22, p. 469-483.

Cole, D.M. (1979), Preparation of Polycrystalline Ice Specimens for Laboratory Experiments, Cold Regions Science and Technology, V. 1, p. 153-159.

Glen, J.W. (1955), The Creep of Polycrystalline Ice, Proc. Royal Society of London, V. A228, p. 519-538.

Gold, L.W. (1962), Deformation Mechanisms in Ice, Ice and Snow, Conference Proceedings, M.I.T., Cambridge, Mass., p. 8-27.

Gold, L.W. (1966), Dependence of Crack Formation on Crystallographic Orientation of Ice, Canadian Journal of Physics, V. 44, p. 2757-2764.

Gold, L.W. (1973), Activation Energy for Creep of Columnar-Grained Ice, Physics and Chemistry of Ice, p. 362-364.

Goodman, D.J. (1977), Creep and Fracture of Ice and Surface Strain Measurements on Glaciers and Sea Ice, also in discussion to Baker (1978), Ph.D. Dissertation, Univ. of Cambridge.

Goughnour, R.R. and O.B. Andersland (1968), Mechanical Properties of a Sand-Ice System, ASCE JSMFD, V. 94, p. 923-950.

Gow, A.J. (1975), Application of Thin Section Techniques to Studies of the Internal Structure of Frozen Silts, CRREL, Technical Notes.

Haynes, F.D., J.A. Karalius and J. Kalafut (1975), Strain Rate Effect on the Strength of Frozen Silt, CRREL Research Report #350.

Haynes, F.D. Carbee, and D. Van Pelt (1981), Thermal Diffusivity of Frozen Soil, CRREL Special Report 80-38.

Higashi, A. (1969), Mechanical Properties of Ice Single Crystals, Physics of Ice, p. 197-222.

Hofmann, U. (1952), Neue erkenntnisse auf dem gebiete der thixotroppe insbesondere bei tonhaltigen gelen, Kolloid-Zeitschsift, V. 125, p. 86-99.

Homer, D.R. and J.W. Glen (1978), The Creep Activation Energies of Ice, Journal of Glaciology, V. 21, p. 429-444.

Holser, C.L., D.C. Jensen and L. Goldshlak (1957), On the Aggregation of Ice Crystals to Form Snow, Journal of Meterology, V. 44, p. 415-420.

Hult, J.A.H. (1966), Creep in Engineering Structures, Blaisdell Publ. Co., Waltham, MA.

Jellinek, H.H.G. (1957), Adhesive Properties of Ice: Part 1, SIPRE Research Report 38.

Jellinek, H.H.G. (1960), Adhesive Properties of Ice: Part 2, SIPRE Research Report 62.

Jellinek, H.H.G. (1962), Ice Adhesion, Canadian Journal of Physics, V. 40, p. 1294-1309.

Jones, S.J. (1978), Triaxial Testing of Polycrystalline Ice, 3rd ICP, p. 671-694.

Kay, G.D. and J.B. Goit (1975), Temperature Dependent Specific Heats of Dry Soil Materials, Canadian Geotechnical Journal, V. 12, p. 209-212.

Kuo, S.S. (1972), Stress and Time Effect on the Creep Rate of Polycrystalline Ice, Ph. D. Dissertation, Michigan State University, Lansing, Michigan.

Langdon, T.G. (1973), Creep Mechanisms in Ice, Physics and Chemistry of Ice, p. 356-361.

Ladanyi, B. (1972), An Engineering Theory of Crrep of Frozen Soils, Canadian Geotechnical Journal, V. 9, p. 63-80.

Lee, K.L. and H.B. Seed (1967), Drained Strength Characteristics of Sands, ASCE JSMFD, V. 23, p. 117-123.

Lile, R.C. (1979), Rheology of Polycrystalline Ice, Ph.D. Dissertation, University of Melbourne, Melbourne, Australia.

Mahmood, A. (1973), Fabric-Mechanical Property Relationships in Fine Grained Soils, Ph.D. Dissertation, University of California, Berkeley, California.

Martin, R.T., F.H. Sayles and J.M. Ting (1980), M.I.T. Creep Data on Manchester Fine Sand, CRREL Internal Report 627.

Mellor, M. and J.H. Smith (1966), Creep of Snow and Ice, CRREL Research Report 220.

Mitchell, J.K., R.G. Campanella and A. Singh (1968), Soil Creep as a Rate Process, ASCE JSMFD, V. 94, p. 231-253.

Mitchell, J.K. (1976), Fundamentals of Soil Behavior, J. Wiley & Sons, New York, N.Y.

Nakano, Y., R.J. Martin and M. Smith (1972), Ultrasonic Velocities of Dilational and Shear Waves in Frozen Soil, Water Resources Research, V. 8, p. 1024-1020.

Oda, M. (1972), Initial Fabrics and Their Relations to Mechanical Properties of Granular Material, Soils and Foundations, V. 12, p. 17-36.

Perkins, T.K. and R.A. Ruedrich (1973), The Mechanical Behavior of Synthetic Permafrost, Society Petroleum Engineers Journal, V. 12, p. 211-220.

Ramseier, R.O. (1971), Growth and Mechanical Properties of River and Lake Ice, Ph.D. Dissertation, Laval University, Quebec.

Roggensack, W.D. and N.R. Morgenstern (1978), Direct Shear Tests on Natural Fine Grained Permafrost Soils, 3rd ICP, p. 729-735.

Rowe, P.W. (1962), The Stress Dilatancy Relation for Static Equilibrium of an Assembly of Particles in Contact, Proc. Royal Society of London, V. A269, p. 500-527.

Sayles, R.H. (1968), The Creep of Frozen Sands, CRREL Technical Report 190.

Sayles, R.H. (1973), Triaxial and Creep Tests on Frozen Ottawa Sand, 2nd ICP, p. 384-931.

Sayles, F.H. (1974), Triaxial Constant Strain Rate Tests and Triaxial Creep Tests on Frozen Ottawa Sand, CRREL Technical Report 253.

Sayles, F.H. and D. Haines (1974), Creep of Frozen Silt and Clay, CRREL Technical Report 252.

Shoji, H. and A. Higashi (1978), A Deformation Mechanism Map of Ice, Journal of Glaciology, V. 21, p. 419-427.

Silver, M.L. (1976), Laboratory Triaxial Testing Procedures to Determine the Cyclic Strength of Soils, U.S. Nuclear Regulatory Commission, Report NU Reg.-31.

Singh, A. and J.K. Mitchell (1968), General Stress-Strain-Time Function for Soils, ASCE JSMFD, V. 94, p. 21-46.

Skinner, A.E. (1969), A Note on the Influence of Interparticle Friction on the Shearing Strength of a Random Assembly of Spherical Particles, Geotechnique, V. 19, p. 150-157.

Smith, L.L. and J.B. Cheatham (1975), Plasticity of Ice and Sand-Ice Systems, Journal of Engineering for Industry, V. 97, p. 479-484.

Steinfink, H. and J.E. Gebhart (1962), Compression Apparatus for Powder X-ray Diffractometry, Review of Scientific Instruments, V. 33, p. 542-544.

Tice, A.R., C.M. Burrows, and D.M. Anderson (1978), Determination of Unfrozen Water in Frozen Soil by Pulsed Nuclear Magnetic Resonance, 3rd ICP, p. 150-155.

Tietz, T.E. and J.E. Dorn (1956), Creep of Copper at Intermediate Temperatures, Trans. Am. Inst. of Mining, Metallurgical, and Petroleum Engineers, V. 206, p. 156-162.

Ting, J.M. (1981a), The Creep of Frozen Sands: Qualitative and Quantitative Models, Sc.D. Dissertation, Dept. of Civil Engineering, M.I.T., Cambridge, Mass.

Ting, J.M. (1981b), The Mechanisms of Frozen Soil: A Review, CRREL, in press.

Tsytovich, N.A. (1975), Mechanics of Frozen Ground, McGraw-Hill, New York, N.Y.

Van Olphen, H. (1963), An Introduction to Clay Colloid Chemistry, Interscience Publ., New York, N.Y.

Vyalov, S.S. (1959), Rheological Properties and Bearing Capacity of Frozen Soils, CRREL Translation 74.

Vyalov, S.S. (1962), Strength and Creep of Frozen Soils and Calculations in Ice-Soil Retaining Structures, CRREL Translation 76.

Vyalov, S.S., (1963), Rheology of Frozen Soils, 1st ICP, p. 332-342.

Vyalov, S.S., (1973), Long Term Rupture of Frozen Soil as a Thermally Activated Process, 2nd ICP, p. 222-228.

Weeks, W.F.and A. Assur (1969), Fracture of Lake and Sea Ice, CRREL Research Report 269.

Weertman, J. (1973), Creep of Ice, Physics and Chemistry of Ice, p. 320-337.

Whitman, R.V., (1979), Personal Communication.